2571991

CATALOGED BY ASTIA
AS AD No. ______

EXPERIMENTAL AND THEORETICAL STUDY OF LOCAL INDUCED VELOCITIES OVER A ROTOR DISC FOR ANALYTICAL EVALUATION OF THE PRIMARY LOADS ACTING ON HELICOPTER ROTOR BLADES

565000

EUROPEAN RESEARCH OFFICE
US. DEPARTMENT OF THE ARMY
CONTRACT No. DA-91-591-EUC-1165

Report No. DE.2012
15 October 1960

ASTIA

61-3-4 NOX

$ 17.50

Engineering Division GIRAVIONS DORAND Co.
PARIS

EXPERIMENTAL AND THEORETICAL STUDY OF LOCAL INDUCED VELOCITIES OVER A ROTOR DISC FOR ANALYTICAL EVALUATION OF THE PRIMARY LOADS ACTING ON HELICOPTER ROTOR BLADES

EUROPEAN RESEARCH OFFICE

US. DEPARTMENT OF THE ARMY

CONTRACT No.DA-91-591-EUC-1165

Report No. DE.2012

15 October 1960

Assistant Engineer:

Mrs. M.DELEST
Aero.Engineer

Principal Investigator:

S.TARGRINE
Head Engineer

Engineering Division GIRAVIONS DORAND Co.

PARIS

F R A N C E

Table of Contents

(Page numbering: Text pages are numbered from A.1 to A.123
Figure pages, at end of text, are numbered from B.1 to B.144)

/.

ABSTRACT

One of the main problems connected with the analytical evaluation of primary loads and transient control effects on helicopter rotors consists in the assumption of the local induced velocities over the rotor disc.

This problem has attracted the attention of many engineers all over the world but, up to now, no satisfactory engineering solution was found and though the mean value of the induced velocity, in hovering and forward flight conditions, is well known, thus permitting a fairly good evaluation of the helicopter general performance characteristics, lack of knowledge of the actual vortex structure, which gives rise to the local blade induced velocities, explains the poor agreement between analytical and experimental results, mainly in blade stress problems and those connected with the transient effects in rotor control and stability studies.

The solution of this problem by analytical methods alone leads to practically insoluble difficulties and for this reason an experimental method consisting in visualizing the vortices by smoke emission on model rotors, operated in a wind tunnel, was used to help to build-up a reasonable and intentionally simplified (for mathematical accessibility) canevas for the rotor vortex system.

As a result of this study engineering methods are proposed for the analytical evaluation, with a satisfactory degree of approximation, of the local instantaneous induced velocities over a rotor disc, in various helicopter flight conditions, as a function of the rotor characteristics.

Some of these methods are immediately applicable, others need numerical function tables which remain to be established.

LIST OF SYMBOLS

R	Rotor radius, measured from center of rotation	(m)
r	distance of a blade section to center of rotation	(m)
$\bar{r} = \frac{r}{R}$, $\bar{\bar{r}} = \frac{r_o}{R - r_o}$		
r_o	distance of inner end of blade to center of rotation	(m)
r_1	dummy variable of blade element	(m)
c	blade section chord	(m)
a	distance of flapping hinge to center of rotation	(m)
"	constant coefficient	
b	number of blades	
A	rotor disc aera	(sq.m.)
θ_c	blade section pitch angle	
θ_1, θ_2	cyclic pitch angles	
θ_t	blade twist angle	
i	blade section angle of attack	
ψ	blade azimuth angle	
α	rotor-shaft tilting angle (positive nose down unless otherwise indicated in text. See paragr.3.24)	
"	angle of rotation of airfoil section	
β	blade flapping angle	
a_n, b_n	flapping Fourier series coefficients	
σ	rotor solidity	

/.

T	period of rotation
Γ	blade circulation
γ	blade Lock's constant
L	blade aerodynamic lift
F_N	rotor thrust
C_L	Section lift coefficient
f_N	rotor thrust coefficient $\left(f_N = \frac{F_N}{\frac{1}{2}\rho A U^2} = 2C_T \right)$
$T_{0,s}$	rotor drag
ω	rotor angular velocity (rad/sec)
V	forward speed, wind speed
U	blade tip speed $U = \omega R$
μ	advance ratio $\mu = \frac{V}{\omega R}$
V_i	induced velocity on the blade element
V_f, V_{i_z}	induced flow (beneath rotor disc)
ρ	mass density of air ($Kg.m^{-4}.sec^2$)
B	blade tip loss factor
$E\,I$	blade flexural rigidity
ν	blade natural frequency
G_n	blade shape parameter

$$G_n = \int_0^{BR} \frac{\rho}{2} c \frac{dC_L}{d\alpha} r^n dr$$

I_0	Moment of inertia of blade about flapping hinge

All other particular symbols used are explained in the text.

EXPERIMENTAL AND THEORETICAL STUDY OF LOCAL INDUCED VELOCITIES OVER A ROTOR DISC FOR ANALYTICAL EVALUATION OF PRIMARY LOADS ON HELICOPTER ROTOR BLADES .-

INTRODUCTION

The purpose of this study is to make available to engineers a method of evaluating, with a satisfactory degree of approximation, the aerodynamic loads distributed over the blades of a helicopter rotor.

Two main effects were introduced :

- velocity induced by the free vortices,
- non stationary regime.

This document is divided into two parts :

- an experimental part,
- an analytical part.

In the experimental part, an attempt was made to situate in space the free vortices issuing from the rotor for different helicopter flight configurations. Indeed, in the case of fixed wings, the location of the free vortices is known, whereas it is difficult to define theoretically the location of such vortices beneath the rotor disc in the case of helicopter rotors; it was therefore decided to resort to experiment, which consisted in visualizing the vortices by means of smoke, on model rotors operated in a wind tunnel.

In the analytical part, the proposed method is set out and illustrated with numerical examples.

The method is an approximate one only. Wherever possible conventional calculation methods have been used.-

1 - WIND-TUNNEL VISUALIZATION TEST PROCEDURE

1.1 - Description of method

The visualizations were made in order to locate the free vortices streaming from the blades.

/.

A double visualization was performed :

- First, the smoke jet was emitted upstream and above the swept disc. These locations were chosen so that the jet touched the tip of the blade for a given azimuthal position (see photographs Fig. 3 through 10). This provided section views of the vortex.

- Second, the smoke was emitted either at the two blade tips or at the root, thereby showing up the vortices in continuous fashion (see photographs Fig.11 through 16).

The lift, the flapping and the drag were recorded in each case.

For the dynamic regimes, the input force was also recorded, but on the other hand the drag measurement was suppressed.

The tests were performed at the wind-tunnel of the INSTITUT DE MECANIQUE DES FLUIDES at MARSEILLES, under the direction of Professor VALENSI.

1.2 - Description of Rotor

1.21 - Definition of Blades

1.211 - Basic Characteristics (See tables 1.1, 1.2 and 1.3)

In order to facilitate data processing and interpretation the blades were of rectangular plan form (constant chord), without twist. The airfoil adopted was the NACA 0018. Rotor radius was R = 0.75m(2.46 ft).

From the structural standpoint, the blades comprised a massive leading edge spar (see Figure 47) and two shells in thick plate.

It was sought to make the blades rigid in bending and torsion (see table 1.3) to avoid introducing the bending and pitch distorsions in the calculations.

To avoid loads on the controls and a parasite cyclic pitch $\delta\theta$, the C.G. line was brought as close as possible to the feathering axis. Blade No. 5 deviates most from this condition (see Table I.1).

1.212 - Specific Test Requirements

To permit photographing to take place, it was necessary for the rotor to be able to rotate in both directions. This was possible by reversing the blades, due to the fact that they were symmetrical (NACA 0018 airfoil, with no twist).

/.

For the smoke emissions from the blade tips, a stainless steel tube was incorporated in the blade (Fig.47).

The blades were balanced statically and dynamically.

1.213 - Variation of Solidity Ratio and of Lock's Constant

The different sets of conditions were achieved with the five sets of blades :

Group 1 (blades 1, 2, 3) { solidity $\sigma = \frac{bcR}{\pi R^2}$ = Constant
{ Lock's constant: variable.

Group 2 (blades 1, 4, 5) { solidity variable
{ γ constant.

1.214 - Blade Resonance

Blades were designed in such a way that their natural torsional and bending frequencies were widely distinct in order to obviate bending/torsion couplings.

These frequencies were also compared to the frequencies of the aerodynamic forces (up to 10ω) so that there should be no resonance at the chosen rotational speed (133 rad/sec). (See Figures 48 through 52).

Taking into account the fact that the blades were heavy and that it was also necessary to insure c.g. requirements, good torsional rigidity and constancy of γ, the problem was obviously a tricky one.

1.215 - Shape Parameters

The blade was defined by shape parameters of the Glauert form (table 1.2)

$$G_n = \int_0^{BR} \frac{\rho}{2} \frac{dC_L}{di} c\, r^n \, dr \qquad n = 0, 1, 2, 3.$$

and

$$\overline{G}_n = \frac{G_n}{\frac{\rho}{2} \frac{dC_L}{di} c_{0,7} R^{n+1}}$$

/.

For a rectangular blade :

$$\bar{G}_0 \approx 1$$

$$\bar{G}_1 \approx 1/2$$

$$\bar{G}_2 \approx 1/3 \quad \text{if} \quad B = 1$$

$$\bar{G}_3 \approx 1/4$$

1.22 - Rotor - Hub - Controls

1.221 - The rotor was mounted on the end of the balance arm (photographs Fig.1 and 2) provided with cyclic pitch (θ_1 θ_2) and collective pitch (θ_c) controls capable of remote control. It was also possible to tilt the rotor in pitch (α) by remote control.

The rotor was driven by an asynchronous motor.

The shaft passed through the balance arm.

Smoke was delivered to the blades through the center of the hub.

1.222 - Balancing - Resonance

All rotating control masses (levers and swashplate) had to be very carefully balanced statically and dynamically.

The natural frequencies of the drive shaft and of the tunnel balance were compared to those of the blades (Fig.53).

1.3 - Test Program

The tests were divided into three groups :

Group A : $0.10 < \mu < 0.20$

Group B : $0 < \mu < 0.05$

Group C : dynamic tests.

Photographs and recordings were made for groups A and B.

Films and recordings were made for group C.

1.31 - Groups A and B

1.311. Flight Parameters

It was desirable to cover different flight conditions in order to be able to locate the vortices for each different configuration. To this end, the following were made to vary :

/.

Blade definition

Table 1.1

R = 0.75 m
= 2.47 ft

Rectangular blade   Naca 0018 Airfoil

Blade length : r = 0.596 m = 1.95 ft U = 100 m/s ω = 133 rad/sec

Blade n°		1	2	3	4	5
c	m	0.095	0.095	0.095	0.118	0.1415
	ft	0.312	0.312	0.312	0.387	0.465
σ		0.08	0.08	0.08	0.10	0.12
γ		0.36	0.422	0.264	0.36	0.36
Weight of blade alone	Kg	1.435	1.118	1.845	1.740	2.115
	lb.	3.17	2.46	4.07	3.84	4.66
C.G. % of c from leading edge		25.3	27.4	26.2	27	30.6
I (1)	Kgm sec^2	0.0297	0.0254	0.0406	0.03713	0.0445
F (2)	Kg	1080	882	1440	1310	1630
	lb.	2380	1945	3180	2900	3600
Position of feathering axis (% of c from leading edge)		24.6	25.2	25.3	25.4	26.4

(1) Moment of inertia relative to flapping hinge
(2) Centrifugal force

Table 1.2

Blade Shape Parameters

Rectangular blade $\frac{dC_L}{di_*} = 5.73$ $\rho = \frac{1}{8}$ R = 0.75 m

B	0.94					0.96					0.98				
Blade n°	G_0 10^3	G_1 10^3	G_2 10^3	G_3 10^3	$\frac{G_3}{I_P}$	G_0 10^3	G_1 10^3	G_2 10^3	G_3 10^3	$\frac{G_3}{I_P}$	G_0 10^3	G_1 10^3	G_2 10^3	G_3 10^3	$\frac{G_3}{I_P}$
	$kgm^{-2}s^2$	$kgm^{-1}s^2$	$kg\,s^2$	$kgm\,s^2$	0	$kgm^{-2}s^2$	$kgm^{-1}s^2$	kg^2	$kgm\,s^2$	0	$kgm^{-2}s^2$	$kgm^{-1}s^2$	$kg\,s^2$	$kgm\,s^2$	0
1	24	8.45	3.96	2.1	0.071	24.4	8.8	4.22	2.29	0.077	25	9.19	4.49	2.49	0.084
2	24	8.45	3.96	2.11	0.083	24.4	8.8	4.22	2.29	0.09	25	9.19	4.49	2.49	0.098
3	24	8.45	3.96	2.11	0.052	24.4	8.8	4.22	2.29	0.0563	25	9.19	4.49	2.49	0.615
4	29.8	10.49	4.93	2.61	0.705	30.4	10.91	5.24	2.84	0.0766	31	11.39	5.57	3.08	0.083
5	35.7	12.55	5.9	3.12	0.07	36.4	13.1	6.3	3.4	0.0765	37.2	13.6	6.6	3.69	0.083

Table 1,3

Torsional Rigidity

Flexural Rigidity

Blade n°	1	2	3	4	5
Torsion θ ° for $F_N = 20$ Kg.	20/100	20/100	15/100	20/100	13/100
Bending $E.I_{mean}$ (Kg. m^2)	87,2	80	113	140	329

- the collective pitch θ_c
- the cyclic pitch θ_1 , θ_2

$$\theta = \theta_c + \theta_1 \cos \Psi + \theta_2 \sin \Psi$$

- the inclination of the rotor shaft
- the solidity σ
- Lock's constant γ

The values of these parameters and their variations were determined so as to fulfil both mechanical and photographic requirements.

This was important because, from the standpoints of processing and visualization, any two values of a given parameter had to differ sufficiently from each other so that "a priori" the effects should also be different and the vortices distinct from each other.

Blade No. 4 (c= 0.118 m or 0.39 ft) was chosen as the basic blade for the tests as it best satisfied the rigidity, C.G. and weight requirements.

1.312 - **Test Phases**

Tables 1.4 and 1.5 (pages A.10 through A.16) indicate the test programm for these two groups.

Each individual case was itself divided into several groups of photographs. It is proposed to examine one specific case in detail.

External Smoke Emission (Photographs 3 through 10)

The ejection of the smoke was studied so that the tip of the blade cut through the smoke at different azimuth angles Ψ . We called for 24 values of Ψ .

Due to the fact that the balance arm hindered passage of the smoke for the obtainment of $0 < \Psi < 360°$, the direction of rotation was changed every 12 positions and noted as follows :

+ rotation : $180° < \Psi < 360°$

- rotation : $0 < \Psi < 180°$ (see photographs 4 and 8)

Internal Smoke Emission (Photographs 11 through 16)

This form of emission enabled several Ψ positions to be grouped on a single photograph.

./.

It may be noted (and there will be further reference to this when discussing the data processing method) that any one photograph made during, say a + rotation, does not give all the azimuths. Indeed it can be seen from Figure 54 that a number of blind angles arise from the position of the cameras, examples in + rotation being $340° < \Psi < 360°$ and $160° < \Psi < 180°$. The cameras were therefore moved and further photographs made to supplement the results. An example of this on an induced velocity curve is provided in Section 1.5 (cameras at C_2 and C_3).

The instantaneous position of the blade was also varied. In general , photographs were taken of the center-plane, advancing-blade and retreating-blade positions.

Smoke Emission Through the Hub (Photographs 17 through 20)

A central smoke emission was also made for two instantaneous blade positions.

In all cases and for each form of smoke emission considered above, the photographs were taken from vertical and horizontal viewpoints respectively. There will be further occasion to discuss the difference between these photographs when the data processing method is dealt with.

In each case a recording was made of the lift, the flapping and the drag.

1.32 - Group C (Figures 45 and 46)

In group C only films and recordings were made.

The tests were called for on blade No.4 for the reasons stated previously ; however, this blade was corroded by the smoke from the preceding tests and was therefore replaced by the lighter blade No.2 (c = 0.095 m, or 0.312 ft).

The conditions of determination of the different parameters were more rigid than precedingly, because the variations of the input variables were obtained by means of came, and thus effected with a high precision.

The input variables were, the same as for groups A and B, plus the tip speed U, the wind velocity V_0. Two extra acceleration tests were also performed.

Table 1.6 lists the test program.

Smoke emissions were of the internal variety only and only one case of rotation was called for. However, both the vertical and plan views were retained.

Each test was accompanied by flapping and lift recordings.

/.

TABLE 1.4

INDUCED VELOCITY - GROUP A

Case Nb	θ_c degrees	μ 0	V_0 with U=100 m/s m/sec	α degrees	θ_1 degrees	θ_2 degrees	Blade Nb			REMARKS	
1	6	0.10	1.0	3	0	0	4				
2	6	0.15	15	3	0	0	4				
3	6	0.20	20	3	0	0	4				
4	8	0.10	10	3	0	0	4				
5	8	0.15	15	3	0	0	4				
6	8	0.20	20	3	0	0	4			Effect of θ_c	
7	10	0.10	10	3	0	0	4				
8	10	0.15	15	3	0	0	4				
9	10	0.20	20	3	0	0	4				
10	12	0.10	10	3	0	0	4				
11	12	0.15	15	3	0	0	4				
12	12	0.20	20	3	0	0	4				
13	6	0.10	10	0	0	0	4				
14	6	0.15	15	0	0	0	4				
15	6	0.20	20	0	0	0	4				
16	12	0.10	10	0	0	0	4				
17	12	0.15	15	0	0	0	4				
18	12	0.20	20	0	0	0	4			Effect of α	
19	6	0.10	10	7	0	0	4				
20	6	0.15	15	7	0	0	4				
21	6	0.20	20	7	0	0	4				
22	12	0.10	10	7	0	0	4				
23	12	0.15	15	7	0	0	4				

TABLE 1.4 (Continued)

INDUCED VELOCITY GROUP A

Case No	θ_c degrees	μ_0	V_0 with U_0=100 m/s m/sec	α degrees	θ_1 degrees	θ_2 degrees	Blade No	REMARKS
24	12	0.20	20	7	0	0	4	
25	6	0.10	10	11	0	0	4	
26	6	0.15	15	11	0	0	4	
27	6	0.20	20	11	0	0	4	
28	12	0.10	10	11	0	0	4	
29	12	0.15	15	11	0	0	4	
30	12	0.20	20	11	0	0	4	Effect of α
31	6	0.10	10	15	0	0	4	
32	6	0.15	15	15	0	0	4	
33	6	0.20	20	15	0	0	4	
34	12	0.10	10	15	0	0	4	
35	12	0.15	15	15	0	0	4	
36	12	0.20	20	15	0	0	4	
37	6	0.10	10	3	0	-3	4	
38	6	0.15	15	3	0	-3	4	
39	6	0.20	20	3	0	-3	4	
40	12	0.10	10	3	0	-3	4	
41	12	0.15	15	3	0	-3	4	Effect of θ_2
42	12	0.20	20	3	0	-3	4	
43	6	0.10	10	3	0	-10	4	
44	6	0.15	15	3	0	-10	4	
45	6	0.20	20	3	0	-10	4	
46	12	0.10	10	3	0	-10	4	

TABLE 1.4 (Continued)

INDUCED VELOCITY. GROUP A

Case Nb.	θ_c degrees	μ 0	V_0 with $U = 100$ m/s m/sec	α degrees	θ_1 degrees	θ_2 degrees	Blade Nb.			REMARKS
47	12	0.15	15	3	0	-10	4			Effect of θ_2
48	12	0.20	20	3	0	-10	4			
49	6	0.10	10	3	3	0	4			
50	6	0.15	15	3	3	0	4			
51	6	0.20	20	3	3	0	4			
52	12	0.10	10	3	3	0	4			
53	12	0.15	15	3	3	0	4			
54	12	0.20	20	3	3	0	4			Effect of θ_1
55	6	0.10	10	7	7	0	4			
56	6	0.15	15	7	7	0	4			
57	6	0.20	20	7	7	0	4			
58	12	0.10	10	7	7	0	4			
59	12	0.15	15	7	7	0	4			
60	12	0.20	20	7	7	0	4			
61	6	0.10	10	3	0	0	5 (σ = 12/100			
62	6	0.15	15	3	0	0	5			
63	6	0.20	20	3	0	0	5			
64	12	0.10	10	3	0	0	5			
65	12	0.15	15	3	0	0	5			Effect of σ and α
66	12	0.20	20	3	0	0	5			
67	6	0.10	10	12	0	0	5			
68	6	0.15	15	12	0	0	5			
69	6	0.20	20	12	0	0	5			

TABLE 1.4 (Continued)

INDUCED VELOCITY. GROUP A										
Case Nb	θ_c degrees	μ 0	V_o with U=100 m/s m/sec	α degrees	θ_1 degrees	θ_2 degrees	Blade Nb			REMARKS
70	12	0.10	10	12	0	0	5			Effect of σ and α (cases 70–84)
71	12	0.15	15	12	0	0	5			
72	12	0.20	20	12	0	0	5			
73	6	0.10	10	3	0	0	1	$\sigma = 8/100$		
74	6	0.15	15	3	0	0	1			
75	6	0.20	20	3	0	0	1			
76	12	0.10	10	3	0	0	1			
77	12	0.15	15	3	0	0	1			
78	12	0.20	20	3	0	0	1			
79	6	0.10	10	12	0	0	1			
80	6	0.15	15	12	0	0	1			
81	6	0.20	20	12	0	0	1			
82	12	0.10	10	12	0	0	1			
83	12	0.15	15	12	0	0	1			
84	12	0.20	20	12	0	0	1			
85	12	0.10	10	3	0	0	2	$\gamma = 0.42$		Effect of γ (cases 85–87)
86	12	0.15	15	3	0	0	2			
87	12	0.20	20	3	0	0	2			
88	12	0.10	10	3	0	0	3	$\gamma = 0.25$		Effect of γ (cases 88–90)
89	12	0.15	15	3	0	0	3			
90	12	0.	0	3	0	0	3			

TABLE 1.4 (Concluded)

INDUCED VELOCITY. GROUP A

Case Nb	θ_c degrees	μ 0	V_0 with U = 100 m/s m/sec	α degrees	θ_1 degrees	θ_2 degrees	Blade Nb			REMARKS
91	12	0.15	15	3	0	-3	2 (γ = 0.42)			Effect of γ and θ_2
92	12	0.15	15	3	0	-10				
93	12	0.15	15	3	0	-3	3 (γ = 0.25)			
94	12	0.15	15	3	0	-10				

TABLE 1.5

INDUCED VELOCITY - GROUP B								
Case Nb	θ_c degrees	μ o	V_o with U_ι=100 m/s m/sec	α degrees	θ_1 degrees	θ_2 degrees	Blade Nb	REMARKS
1	6°	0	0	0	0	0	4	
2	8	0	0	0	0	0	4	θ_c in hovering
3	10	0	0	0	0	0	4	
4	12	0	0	0	0	0	4	
5	6	0,05	5	3	0	0	4	
6	8	0.05	5	3	0	0	4	Effect of θ_c with μ = 0,5
7	10	0.05	5	3	0	0	4	
8	12	0.05	5	3	0	0	4	
9	6	0.05	5	0	0	0	4	
10	6	0.05	5	7	0	0	4	Effect of α; θ_c = 6°
11	6	0.05	5	11	0	0	4	
12	6	0.05	5	15	0	0	4	
13	12	0.05	5	0	0	0	4	
14	12	0.05	5	7	2	0	4	Effect of α ; θ_c = 12
15	12	0.05	5	11	0	0	4	
16	12	0.05	5	15	0	0	4	
17	6	0.05	5	3	0	-3	4	
18	6	0.05	5	3	0	-10	4	Effect of θ_2
19	12	0.05	5	3	0	-3	4	
20	12	0.05	5	3	0	-10	4	
21	6	0.05	5	3	3	0	4	
22	6	0.05	5	3	7	0	4	Effect of θ_1
23	12	0.05	5	3	3	0	4	

TABLE 1.5 (Concluded)

INDUCED VELOCITY GROUP B								REMARKS
Case Nb	θ_c degrees	μ 0	V_o with U. m/sec.	α points degrees	θ_1 degrees	θ_2 degrees	Blade Nb	
24	12°	0.05	5	3	7	1	4	Effect of θ_1
25	6	0.05	5	3	0	0	5	
26	6	0.05	5	12	0	0	5	
27	12	0.05	5	3	0	0	5	
28	12	0.05	5	12	0	0	5	Effect of σ
29	6	0.05	5	3	0	0	1	
30	6	0.05	5	12	0	0	1	
31	12	0.05	5	3	0	0	1	
32	12	0.05	5	12	0	0	1	
33	12	0.05	5	3	0	0	2	Effect of γ
34	12	0.05	5	3	0	0	3	
35	12	0.05	5	3	0	-3	2	
36	12	0.05	5	3	0	-10	2	Effect of γ and of θ_2
37	12	0.05	5	3	0	-3	3	
38	12	0.05	5	3	0	-10	3	

INDUCED VELOCITY

TABLE 1.6	INITIAL STATE						GROUP C			Definition of the variation (Input)				
Case Nb	θ_c degrees	μ 0	V_0 m/sec	α degrees	θ_1 degrees	θ_2 degrees	Blade Nb.		Variable	Δ Difference	Final state / Initial state		$\frac{\partial}{\partial t}\Delta$ Velocity	Step or Frequency
1	8	0	$V_0 = 0$	0	0	0	4		θ_c	2	8	10	came 1	Step
2	8	0	U=100m/s	0	0	0	4		"	2	8	10	came 2	
3	8	0	"	0	0	0	4		"	2	8	10	came 3	
4	8	0	"	0	0	0	4		"	2	10	12	came 4	
5	10	0	"	0	0	0	4		"	2	10	12	came 1	
6	10	0	"	0	0	0	4		"	2	10	12	came 2	
7	10	0	"	0	0	0	4		"	2	10	12	came 3'	
8	10	0	"	0	0	0	4		"	2	10	12	came 4	
9	10	0	"	0	0	0	4		"	2	10	12	Frequency 0.5 CPS	
10	10	0	"	0	0	0	4		"	2	10	12	Frequency 1.3 CPS	
11	10	0	"	0	0	0	4		"	2	10	12	Frequency 2.2 CPS	
12	10	0	"	0	0	0	4			2	10	12	Frequency 3.5 CPS	
13	10	0	"	0	0	0	1			2	10	12	came 1	Step
14	10	0	"	0	0	0	2			2	10	12	came 1	
15	10	0	"	0	0	0	3			2	10	12	came 1	
16	10	0	"	0	0	0	5			2	10	12	came 1	
17	12	0	U=90 m/s w=120 m/s	0	0	0	1			10 m/sec	90 w=120	100 w=133	came 1	Step
18	12	0	U=90	0	0	0	1			10	90	100	came 2	
19	12	0	U=90	0	0	0	2			10	90	100	came 1	
20	12	0	U=90	0	0	0	2			10	90	100	came 2	
21	12	0	"	0	0	0	3			10	90	100	came 1	
22	12	0	"	0	0	0	3			10	90	100	came 2	
23	12	0	"	0	0	0	4			10	90	100	came 1	

INDUCED VELOCITY

TABLE 1.6 (Continued) INITIAL STATE GROUP C

Case Nb	θ_c degrees	μ 0	V_0 m/sec	α degrees	θ_1 degrees	θ_2 degrees	Blade Nb.		Variable	Δ Difference	Final state	Initial state	$\frac{\partial}{\partial t}\Delta$ Velocity	Step or frequency
24	12	0	U=90m/s	0	0	0	4		U	10 m/s	90	100	came 2	
25	12	0	ω=120r/s	0	0	0	5		U	10	90	100	came 1	
26	12	0	"	0	0	0	5		θ_2	10	90	100	came 2	
27	12	0	U=100 m/s	0	0	0	4		θ_2	3	0	-3	Freq. 3.4 CPS	
28	12	0	"	0	0	0	4		θ_2	3	0	-3	Freq. 2.3 CPS	
29	12	0	"	0	0	0	4		θ_2	3	0	-3	Freq. 1.5 CPS	
30	12	0	"	0	0	0	4		θ_2	3	0	-3	Freq. 0.7 CPS	
31	10	0.10	"	3	0	0	4		θ_c	2	10	12	F. 3.5 CPS	$\Psi=0$
32	10	0.10	"	3	0	0	4		θ_c	2	10	12	$\Psi=45°$	
33	10	0.10	"	3	0	0	4		θ_c	2	10	12	$\Psi=90°$	
34	10	0.10	"	3	0	0	4		θ_c	2	10	12	$\Psi=135°$	
35	12	0.10	"	3	0	0	4		θ_2	3	0	-3	F. 3.5 CPS	$\Psi=0$
36	12	0.10	"	3	0	0	4		θ_2	3	0	-3		$\Psi=90$
37	12	0.10	"	3	0	0	4		θ_2	3	0	-3	F. 1.5 CPS $\Psi=0$	
38	12	0.10	"	3	0	0	4		θ_2	3	0	-3	$\Psi=90$	
39	12	0.10	"	3	0	-3	4		θ_2	3	-3	-6	F. 3.5 CPS	$\Psi=0$
40	12	0.10	"	3	0	-3	4		θ_2	3	-3	-6	$\Psi=90$	
41	12	0.10	"	3	0	-3	4		θ_2	3	-3	-6	F. 1.5 CPS $\Psi=0$	
42	12	0.10	"	3	0	-3	4		θ_2	3	-3	-6	$\Psi=90$	
43	12	0.10	"	3	0	0	4		θ_1	3	0	3	F. 3.5 CPS $\Psi=0$	
44	12	0.10	"	3	0	0	4		θ_1	3	0	3	$\Psi=90°$	
45	12	0.10	"	3	0	0	4		θ_1	3	0	3	F. 1.5 CPS $\Psi=0$	
46	12	0.10	"	3	0	0	4		θ_1	3	0	3	$\Psi=90$	

INDUCED VELOCITY

TABLE 1.6 (Continued) INITIAL STATE GROUP C

Case Nb	θ_c degrees	μ 0	V_0 m/sec	α degrees	θ_1 degrees	θ_2 degrees	Blade Nb		Variable	Δ Difference	Initial state	Final state	$\frac{\partial}{\partial t}\Delta$ Velocity	Step or Frequency
47	12	0.05	5 (U=100m/s)	3	0	0	4		V_0	5m/s	5	10		
48	12	0.10	10	3	0	0	4		V_0	5	10	15		
49	12	0.15	15	3	0	0	4		V_0	5	15	20		
50	12	0.05	5 (U=100m/s)	7	0	0	4		α	4	7	11	Freq. 0.7 CPS $\Psi=0$	
51	12	0.05	5	7	0	0	4		α	4	7	11	Freq. 0.7 CPS $\Psi=45°$	
52	12	0.05	5	7	0	0	4		α	4	7	11	Freq. 0.7 CPS $\Psi=135°$	
53	12	0.05	5	7	0	0	4		α	4	7	11	Freq. 1 CPS $\Psi=0$	
54	12	0.05	5	7	0	0	4		α	4	7	11	Freq. 1 CPS $\Psi=45°$	
55	12	0.05	5	7	0	0	4		α	4	7	11	Freq. 1 CPS $\Psi=135°$	
56	12	0.05	5	7	0	0	4		α	4	7	11	Freq. 1.5 CPS $\Psi=0$	
57	12	0.05	5	7	0	0	4		α	4	7	11	Freq. 1.5 CPS $\Psi=45°$	
58	12	0.05	5	7	0	0	4		α	4	7	11	Freq. 1.5 CPS $\Psi=135°$	
59	12	0.05	5	7	0	0	4		α	4	7	11	Freq. 2 CPS $\Psi=0$	
60	12	0.05	5	7	0	0	4		α	4	7	11	Freq. 2 CPS $\Psi=45°$	
61	12	0.05	5	7	0	0	4		α	4	7	11	Freq. 2 CPS $\Psi=135°$	
62	12	0.10	10	7	0	0	4		α	4	7	11	Freq. 0.7 CPS $\Psi=0$	
63	12	0.10	10	7	0	0	4		α	4	7	11	Freq. 0.7 CPS $\Psi=45°$	
64	12	0.10	10	7	0	0	4		α	4	7	11	Freq. 0.7 CPS $\Psi=135°$	
65	12	0.10	10	7	0	0	4		α	4	7	11	Freq. 1 CPS $\Psi=0$	
66	12	0.10	10	7	0	0	4		α	4	7	11	Freq. 1 CPS $\Psi=45°$	
67	12	0.10	10	7	0	0	4		α	4	7	11	Freq. 1 CPS $\Psi=135°$	
68	12	0.10	10	7	0	0	4		α	4	7	11	Freq. 1.5 CPS $\Psi=0$	
69	12	0.10	10	7	0	0	4		α	4	7	11	Freq. 1.5 CPS $\Psi=45°$	

INDUCED VELOCITY

TABLE 1.6 (Concluded) INITIAL STATE							GROUP C		Definition of the variation (Input)				
case Nb	θ_c degrees	μ 0	V_0 m/sec	α degrees	θ_1 degrees	θ_2 degrees	Blade Nb		Variable	Δ Differance	Final state Initial state	$\frac{\partial}{\partial t}\Delta$ Velocity	Slap or frequency
70	12	0.10	10	7	0	0	4		α	4	7 11	Freq 15 CPS	$\psi = 135°$
71	12	0.10	10	7	0	0	4		α	4	7 11	Freq 2 CPS	$\psi = 0°$
72	12	0.10	10	7	0	0	4		α	4	7 11	Freq 2 CPS	$\psi = 45°$
73	12	0.10	10	7	0	0	4		α	4	7 11	Freq 2 CPS	$\psi = 135°$
74	12	$\mu = 0 \rightarrow 0.10$	$V_0 = 100$ m/s	3	0	0	4		θ_2	4	0 −3	Slowly	
75	12	$\mu = 0 \rightarrow 0.10$		3	0	−3	4		θ_2	4	−3 −6	$\mu = 0 \rightarrow \mu = 0.10$	

1.4 - Data Processing Method

The processing of these visualizations having for its object to determine the velocity induced over the disc at different azimuth angles Ψ , use was made of the photographs of groups A and B, in a different manner according to the form of emission.

1.41 - Principle Underlying the Method

The principle however is identical in both cases.

Let us consider two vortices (Figure 55a) formed at the same place at a given Ψ by each blade in turn one at an instant τ , the other at $\frac{T}{2} + \tau$.

Let these vortices be designated by A and B respectively.

Relative to the plane of the rotor, vortex B will have been carried along by a horizontal velocity V and by a vertical velocity $V_{i_{z_1}}$. $V_{i_{z_1}}$ will be neither the induced velocity at B nor the induced velocity in the swept disc plane, but a mean induced velocity beneath the disc. Vortex A will have sustained a same entrainment, but during a very short time only; furthermore it will have sustained only a mean vertical effect $V_{i_{z_2}}$ close to the disc and of lesser magnitude than $V_{i_{z_1}}$.

If we now consider A and B relative to each other, we may postulate that the distance AB is projected horizontally and vertically to give

$$AA' = V_t$$

$$AA'' = V_{i_z} t$$

respectively, where t is the time elapsing between the generation of A and B. Since A and B are formed by each of the blades and result from the same Ψ , then $t = \frac{T}{2}$.

The horizontal velocity V will represent the sum of the wind velocity V_0 and of a velocity V_{i_x} (this was determined at each processing performed).

Once this principle is established, only the modes of applying it will differ according as to whether the emissions were internal or external. These differences will in fact arise especially from determination of the angle Ψ.

1.42 - External Emission

Figure 55 groups together the determination of Ψ (Figure 55b, horizontal photograph) and the determination of V_i (Figure 55a, vertical photograph), as discussed previously.

Vortex A was formed τ seconds before by the blade A, and was formed when that blade out through the smoke fillet. Let A' be the position of the blade at the instant of generation of the vortex and ψ its azimuth.

1.43 - Internal Emission

Contrarily to the previous case, we shall choose here the angles ψ in order to locate the vortices upon their locus (smoke fillet). Processing of these photographs is somewhat tricky , as they overlap to some extent thereby entailing numerous correction factors regarding the respective positions of the cameras (Figure 56).

Photograph 56b

We determine the angles ψ ((1) (2) (3)) along the trace of the swept circle. Neglecting the effect of V_y , we will therefore have, on each vortex fillet, the position of the vortices generated at (1) (2) (3), say (4) (5) (6) for blade B and (4') (5') (6') for blade A.

Photograph 56a

V_{i_z} and V_{i_x} will be determined from this photograph, on which it will suffice to locate the points (4) (5) (6) and (4') (5') (6'). Figure 56 shows the construction used for the purpose, the processing taking place in accordance with the principle indicated previously .

In both processings , and as regards the corrections to be made, account was taken of the respective positions of the photographed object and the camera, the latter having in all cases been focused on the hub.

Figure 54 gives a schematic diagram of the relative locations of the cameras.

1.5 - Test Results

From a study of these tests it was possible to deduce the following fundamental results :

- the evolution of the mean induced velocity beneath the disc, in terms of the flight parameters (photographs),
- the experimental lift, drag and flapping values (recordings),
- the assigning of circles as substitutes for the helix vortices.

1.51 - Evolution of the Mean Induced Velocity

Figures 57 through 60 give the rough experimental results

/.

for two selected test cases computed from the various types of visualization defined previously.

These results concern the V_{iz} and V_{ix} values respectively. The following flight parameter assumptions were made for these selected test cases :

$$\mu = 0.05 \quad \theta_c = 12° \quad \alpha = 3° \quad \theta_1 = 7° \quad \theta_2 = 0$$

and

$$\mu = 0.10 \quad \theta_c = 12° \quad \alpha = 3° \quad \theta_1 = 0 \quad \theta_2 = -3°.$$

Figures 60 through 64 represent these same tests, except that the curves have been made somewhat smoother.

The evolution of V_{ix} has not been given for all the visualization cases, for it was found that for $\mu > 0.10$, $V_{ix\ mean} = 0$.

In all the test cases we find evolutions, in the case of V_{iz}, similar to that of Figures 61 through 63, with, in particular, a drop in V_{iz} for the retreating blade. Figures 65 through 97 give the processed results for various flight parameters.

An 8-point Fourier analysis on the "typical" V_{iz} curve showed that the third harmonic is sufficient to provide a good approximation (Figures 98, 99) and enabled a $V_{iz\,mean}$ to be calculated. This V_{izm} curve is drawn for different flight conditions (Figures 100 through 106), as is also the non-dimensional ratio $\frac{V_{iz}}{V_{io}}$ (Figures 107 through 113) in terms of $\mu = \frac{V_0}{\omega R}$ with $V_{io} = \sqrt{\frac{F_N}{2\rho A}}$, where $A = \pi R^2$ and $\rho = \frac{1}{8}$ and where F_N is the lift given by the recordings.

The following equations were found for V_{iz} :

- $\mu = 0.05,\ \theta_c = 12°,\ \alpha = 3°,\ \theta_1 = 7°,\ \theta_2 = 0.$

$$V_{iz} = 6.95 + 0.47 \sin\Psi - 0.461 \sin 2\Psi - 0.557 \sin 3\Psi$$
$$+ 0.745 \cos\Psi + 1.21 \cos 2\Psi + 0.055 \cos 3\Psi \text{ (in m/sec)}$$

- $\mu = 0.10,\ \theta_c = 12°,\ \alpha = 3°,\ \theta_1 = 0,\ \theta_2 = 3°$

$$V_{iz} = 6.15 + 1.74 \cos\Psi + 1.37 \cos 2\Psi - 0.593 \cos 3\Psi$$
$$- 0.5 \sin 2\Psi - 1.2 \sin 3\Psi \qquad \text{(in m/sec)}$$

In these two test cases, the V_{izm} values are 6.95 m/s and 6.15 m/s respectively.

These values of V_{izm} are useful, particularly for situating the vortex circles.

/.

1.52 - Experimental Lift. Drag and Flapping Values

The conventional processing performed on the recordings in each test case enabled the lift, drag and flapping to be defined from their fundamental, first and second harmonics.

In Table 1.8 the values of F_{N_0} , F_{N_1} , T_0 , T_1 , T_1' and a_0, a_1, a_2 are given. Also added is a Table 1,9 giving the rotor lift in non-dimensional $\frac{f_N}{\sigma}$ with $\sigma = \frac{bcR}{\pi R^2}$

1.53 - Situating the vortex Circles

The purpose here was to replace the vortex lines (1) (2) (3) (Figure 114) by mean circles parallel to the plane of the swept disc.

It was therefore necessary to determine the distance between the circles, also their centers and their radii.

1.531 - Distance between circles

In the case of the first fillet (1) which is distant, in time , by $\frac{T}{4}$ from the swept disc, a good approximation can be obtained by regarding it as lying within the swept disc.

We have already seen that the fillets, which are produced in alternation by each blade, are separated from one another by a time $\frac{T}{2}$. This is equally valid for the circles. Since (1) and (2) are distant by $\frac{T}{2}$ from each other, then if (1) is located upon the swept disc, the distance between (2) and the swept disk is, in mean value, of $\frac{3\ T}{4}$. But, at the tip of the blade, this distance is equal to $\frac{T}{2}$. The distance, between the others fillets, (2) and (3).. , must be taken as $\frac{T}{2}$.

1.532 - Circle Centers

All the circle centers are remote from the disc plane; we determined this experimentally from photographs.

These centers (Figure 114) are aligned upon a straight line A B C such that $O\ A = V_0 \frac{T}{8}$, where V_0 is the relative wind velocity. The straight line A B C makes an angle δ with the disc diameter lying in the center plane ($\Psi = 0$, $\Psi = 180°$). We first determined δ experimentally (Tables I.10, I.11); we then compared it to angles δ' such that $\tan \delta' = \frac{V_{izm} + V_0 \sin\alpha}{V_0 \cos\alpha}$ From tables I.10 and I.11 it may be noted that $\delta \simeq \delta'$. This result is logical enough, for the straight line A B C is located at the center of the helix and is not subjected to disturbance by vortices whose locus is the helix, or, if it is, the disturbances caused are symmetrical and cancel one another. Hence ,

$$\tan \delta = \frac{V_{izm} + V_0 \sin\alpha}{V_0 \cos\alpha}$$

/.

TABLE 1.7

FOURIER ANALYSIS OF THE EXPERIMENTAL ROTOR LIFT ROTOR DRAG AND BLADE FLAPPING GROUP A

						LIFT			ROTOR DRAG			BLADE FLAPPING			
CASE	μ	θ_c	α	θ_1	θ_2	F_{H_0} kg	F_{H_1} kg	F_{H_1}' kg	T_0 kg	T_1 kg	T_1' kg	a_0 deg	a_1 deg	b_1 deg	REMARKS
1	0.10	6	3	0	0	10.3	1.1	1	-1.4	2	3.91	00785	1.065	-0.355	BLADE No 4 Effect of θ_c
2	0.15	6	3	0	0	12.1	1.4	1.5	-3.65	-1.6	6.05	0.06	1.97	0.299	
3	0.20	6	3	0	0	12.2	1.9	1.25	-4.95	-0.75	10.65	0.42	2.08	0.77	
4	0.10	8	3	0	0	14.8	2.35	0.35	-2.98	-0.97	-1.69	0.63	1.62	-0.48	
5	0.15	8	3	0	0	16	1.05	1.45	-3.08	-2.1	-2.1	0.09	1.98	-0.48	
6	0.20	8	3	0	0	16.45	2.2	1.25	-3.53	-0.16	-1.21	0.57	2.82	0.6	
7	0.10	10	3	0	0	17.55	2.2	0.15	0.9	-1.615	-2.395	0.18	1.92	-0.36	
8	0.15	10	3	0	0	18.2	1.8	0.8	1.6	-2.9	-2.255	0.48	2.82	-0.42	
9	0.20	10	3	0	0	19.1	0.55	0.4	1.55	-0.8	-1.935	0.422	3.91	0.06	
10	0.10	12	3	0	0	20	-0.35	1.45	2.36	-2.56	-3.5	0.180	2.75	-0.67	
11	0.15	12	3	0	0	23	0.2	1.45	1.56	-2.55	-4.16	0.154	3.61	-0.61	
12	0.20	12	3	0	0	23.9	-0.9	0.5	1.65	-2.72	-2.56	0.308	4.84	0.305	
13	0.10	6	0	0	0	9.1	1.9	1.1	-0.36	-1.68	-2.4	0.324	1.16	-0.129	BLADE No 4 Effect of α
14	0.15	6	0	0	0	10.55	1.3	1.05	0.88	-1.2	-1.36	0.547	1.48	-0.0355	
15	0.20	6	0	0	0	11.42	1.6	0.85	3.12	-2.71	-0.96	0.321	2	-0.32	
16	0.10	12	0	0	0	20.1	1.6	-1.2	1.84	-2.875	-3.30	0.547	2.52	-1.87	
17	0.15	12	0	0	0	23.6	1.3	-0.1	2.36	-2.24	-3.6	0.246	3.61	-1.037	
18	0.20	12	0	0	0	24.6	1.46	-1.85	4.65	-3.36	-2.40	0.125	4.96	-0.55	
19	0.10	6	7	0	0	10.1	1.85	1.3	-1	-1.6	0.08	0.158	0.937	0.296	
20	0.15	6	7	0	0	11	2.15	0.7	-5.15	-2.85	2.56	0.508	1.31	0.535	
21	0.20	6	7	0	0	10.55	1.9	1.3	-5.95	-1.65	1.95	0.655	2.18	0.595	
22	0.10	12	7	0	0	20	1.1	1.1	0.42	-2.88	-3.2	0.246	2.63	-0.305	
23	0.15	12	7	0	0	21.6	1.3	2.35	-0.08	-2.4	-4.01	0.215	3.55	0.55	
24	0.20	12	7	0	0	22.2	-0.15	1.35	-1.04	-3.20	-3.51	0.208	4.58	0.439	
25	0.10	6	11	0	0	8.32	1.55	1.3	-1.58	-1.76	0.92	0.139	0.949	-0.435	
26	0.15	6	11	0	0	8.62	2.2	0.25	-3.4	-0.3	1.45	0.539	1.37	0.657	
27	0.20	6	11	0	0	8.05	1.75	1.75	-7.00	-1.0	3.50	0.566	1.79	1.37	
28	0.10	12	11	0	0	18.7	0.4	1.6	0.26	-3.36	-3.04	0.364	2.38	-0.678	

TABLE 1.7 (continued)

CASE	μ	θ_c deg	α deg	θ_1 deg	θ_2 deg	LIFT F_{H_0} kg	F_{H_1} kg	F_{H_1}' kg	ROTOR DRAG T_0 kg	T_1 kg	T_1' kg	BLADE FLAPPING a_0 deg	a_1 deg	b_1 deg	REMARKS
29	0.15	12	11	0	0	19.3	1.15	2.05	-0.08	-2.24	-3.91	0.242	3.36	-0.182	No 4 Effect of α
30	0.20	12	11	0	0	18.9	0.75	1.15	-0.69	-2.24	-4.08	0.21	4.46	1.22	
31	0.10	6	15	0	0	5.55	2.05	1.11	-0.8	-0.48	-2.24	0.4	0.874	0.903	
32	0.15	6	15	0	0	4.2	1.1	1.8	-1.44	-1.68	-1.44	0.316	1.033	1.45	
33	0.20	6	15	0	0	2.65	1.35	1.35	-1.54	-1.445	-2.32	0.484	1.03	2.13	
34	0.10	12	15	0	0	18.3	0.95	0.95	0.08	-2.4	-3.64	0.397	2.32	-0.306	
35	0.15	12	15	0	0	18.2	1.75	0.8	0.92	-2.56	-4.8	0.276	3.05	1.527	
36	0.20	12	15	0	0	15.95	1.1	-0.15	0.51	-2.56	-2.4	0.308	3.98	1.525	
37	0.10	6	3	0	-3	8.31	0.2	0.95	0.77	-1.695	-0.32	0.615	0.18	-0.15	BLADE No 4 Effect of θ_2
38	0.15	6	3	0	-3	8.2	1.1	0	0.24	-2.75	-0.65	0.57	0.36	0.3	
39	0.20	6	3	0	-3	8.6	1.75	0.85	0.41	-1.96	-0.97	0.54	0.54	0.481	
40	0.10	12	3	0	-3	19.5	0.65	0.90	1	-3.07	0.80	0.358	0.415	-0.9	
41	0.15	12	3	0	-3	20.6	0.25	1.05	2	-1.77	0.325	0.335	0.24	-0.66	
42	0.20	12	3	0	-3	21.4	1.85	1.1	4.6	-2.095	-0.805	0.267	3.36	-0.9	
43	0.10	6	3	0	-10	6.48	2.05	0	-1.98	-0.97	-1.45	0.45	-2.04	-0.66	
44	0.15	6	3	0	-10	5.8	1.25	0.25	-1.31	-3.235	-0.97	0.48	-1.22	-0.84	
45	0.20	6	3	0	-10	4.85	1.85	0.55	-1.62	-2.43	-2.1	0.57	-1.56	-1.02	
46	0.10	12	3	0	-10	20	-9.8	4	0.29	-0.97	-0.97	0.28	-2.02	-0.66	
47	0.15	12	3	0	-10	21	-7.6	6.7	-1.63	-0.77	0	0.3	-1.02	-0.30	
48	0.20	12	3	0	-10	19.15	-7	2.4	-0.09	-0.81	-0.325	0.195	0.36	0.15	
49	0.10	6	3	3	0	8.3	1.125	1.115	-1.66	-1.375	4.11	0.5	1.13	0.267	No 4 Effect of θ_1
50	0.15	6	3	3	0	8.9	2.58	0.325	-4.27	-0.195	4.16	0.534	1.66	0.2	
51	0.20	6	3	3	0	9.75	2.4	0.655	-6.36	-1.375	6.09	0.5	2.47	0	
52	0.10	12	3	3	0	20	1.31	2.05	-1.53	-0.35	-0.147	0.293	2.19	2.53	
53	0.15	12	3	3	0	21.6	0.9	1.525	-5.545	-1.18	3.06	0.248	2.6	3.6	
54	0.20	12	3	3	0	23.9	1.49	0.95	-5.575	-0.59	4.52	0.0475	4.58	2.8	
55	0.10	6	3	7	0	11.31	1.45	0.9	-3.945	-1.765	-1.38	0.73	1.93	0.066	
56	0.15	6	3	7	0	12.85	0.75	1.15	-5.35	-2.25	0.59	0.632	3.27	0.067	
57	0.20	6	3	7	0	12.8	0.55	1.15	-6.55	-1.57	2.36	0.6	3.33	0.133	
58	0.10	12	3	7	0	23.6	0.9	1.85	-3.16	-0.393	-0.685	0.3	2.76	1.53	
59	0.15	12	3	7	0	25.2	0.95	1.50	-4.17	0	2.36	0.432	4.06	1.063	
60	0.20	12	3	7	0	26.2	0.35	2.55	-5.575	0.195	4.13	0.168	5.19	2.195	

TABLE 1.7 (Concluded)

CASE	μ	θ_c deg	α deg	θ_1 deg	θ_2 deg	LIFT F_{H_0} kg	LIFT F_{H_1} kg	LIFT $F_{H_1'}$ kg	ROTOR DRAG T_0 kg	ROTOR DRAG T_1 kg	ROTOR DRAG T_1' kg	BLADE FLAPPING a_0 deg	BLADE FLAPPING a_1 deg	BLADE FLAPPING b_1 deg	REMARKS
61	0.10	6	3	0	0	10.40	-0.1	-0.25	-2.685	0.75	0.325	1.23	0.54	1	BLADE N°5 · Effect of σ and γ
62	0.15	6	3	0	0	11.15	0.25	-0.85	-5.91	0	0.125	1.25	0.77	1.27	
63	0.20	6	3	0	0	11.4	-0.9	0.1	-5.95	0.75	-1.25	1.41	1.39	1.2	
64	0.10	12	3	0	0	26	0.8	-1.05	-4.88	-1	-0.25	1.62	0.38	2.85	
65	0.15	12	3	0	0	27.0	0.1	0	-3.97	0.25	0	1.85	1.15	3.32	
66	0.20	12	3	0	0	29.8	-1.25	-0.25	-11.9	0.25	-0.38	1.77	1.85	4.15	
67	0.15	6	12	0	0	8.2	-0.25	-0.25	-2.68	-0.325	0	1.29	0.85	0.62	
68	0.15	6	12	0	0	7.45	-0.5	0	-5.34	0.75	0	1.35	1.69	0.54	
69	0.20	6	12	0	0	4.65	-0.8	0.5	-9.32	-1.375	-0.125	1.08	2.11	0.77	
70	0.10	12	12	0	0	21	0.6	-0.8	-2	0.20	0.75	1.51	0.62	2.23	
71	0.15	12	12	0	0	21.2	0.5	-0.75	-5.48	-0.825	-1.375	1.62	2.23	3	
72	0.20	12	12	0	0	19.45	1.55	-0.75	-9.51	0.625	-0.25	1.47	2.93	3.4	
73	0.10	6	3	0	0	12.9	1.5	1.2	0.38	-0.105	-0.265	1.5	-0.62	0.2	BLADE N°1 Effect of σ and γ
74	0.15	6	3	0	0	11.3	1.2	1.3	-0.34	-0.265	-0.545	1.46	-1.15	0.05	
75	0.20	6	3	0	0	10.3	1.2	1	-1.48	-0.32	-1.065	1.58	-1.54	-0.8	
76	0.10	12	3	0	0	17.2	0.2	0.5	1.28	-1.06	-2.65	1.8	-1.25	0.43	
77	0.15	12	3	0	0	18.4	-0.65	0.5	2.1	-1.92	-2.115	2.5	-2.86	0.91	
78	0.20	12	3	0	0	18.5	0.85	0.2	2.11	-1.8	-1.91	2.87	-4.06	-0.28	
79	0.10	6	12	0	0	11.05	-0.25	-0.5	3.06	0.27	-0.585	1.49	-0.725	-0.435	
80	0.15	6	12	0	0	7.9	-0.65	-0.2	2.09	-0.32	-0.375	1.39	-0.96	-0.77	
81	0.20	6	12	0	0	6.9	1.7	0.95	0.91	0	-0.35	1.37	-1.44	-1.10	
82	0.10	12	12	0	0	16	0.15	0.8	-0.15	-1.165	-1.22	2.59	-1.75	0.35	
83	0.15	12	12	0	0	15.3	0	0	-0.41	0.16	-0.765	3.18	-1.47	-0.7	
84	0.20	12	12	0	0	14.5	0.75	0.15	-2.6	0.105	-1.7	3.08	-2.79	-0.42	
85	0.10	12	3	0	0	18.15	1.0	-1.75	-1	-1.035	1.72	0.20	1.54	2.43	N°2 Effect of γ
86	0.15	12	3	0	0	19.9	6.2	-1.6	-1.36	-0.345	1.245	0.15	2.76	2.78	
87	0.20	12	3	0	0	20.5	1.0	-2	-0.54	1.275	-0.095	0.09	4.69	2.77	
88	0.10	12	3	0	0	16.5	1.1	-0.4	0.87	0.15	0.075	0.83	-1.62	2.41	N°3
89	0.15	12	3	0	0	21.8	0.8	-0.35	0.88	-0.15	1.43	0.49	-1.75	3.68	
90	0.20	12	3	0	0	22.3	1.2	0.2	-1.43	0.535	1.07	2.94	-1.5	0.33	
91	0.15	12	3	0	-3	20.6	0.4	-1.6	0	-0.17	0.865	0.03	1.66	2.09	
92	0.15	12	3	0	-10	1.9	1	-0.2	-1.22	-0.52	0.86	0.09	-0.61	0.305	
93	0.15	12	3	0	-3	20.2	0.25	2.35	-0.68	0.27	-1.07	0.78	-0.78	2.6	
94	0.15	12	3	0	-10	18	-0.85	1.05	-0.40	1.075	1.43	0.571	0.22	-4.19	

TABLE 1.8

TEST GROUP B

Case	μ	θ_c deg	α deg	θ_1 deg	θ_2 deg	LIFT F_{N_0}	LIFT F_{H_1} kg	LIFT F_{H_1}' kg	ROTOR DRAG T_0 kg	ROTOR DRAG T_1 kg	ROTOR DRAG T_1' kg	BLADE FLAPPING a_0 deg	BLADE FLAPPING a_1 deg	BLADE FLAPPING b_1 deg	REMARKS
1	0	6	0	0	0	8	1.75	1.1	-1.84	-1.92	-0.8	0.5	0.258	0.158	4 Effect θ_c
2	0	8	0	0	0	11.9	1.25	0.35	0.805	-3.23	-2.58	0.48	0.15	0.33	
3	0	10	0	0	0	15.6	2.4	0.35	0.485	-1.66	-2.905	0.51	0.36	0.3	
4	0	12	0	0	0	17.5	2.05	0.55	-1.2	0.64	-5.28	0.45	0.328	0.452	
5	0.05	6	3	0	0	7.9	0.5	-0.1	2.96	-1.2	-2.4	0.019	0.79	-0.56	4 Effect θ_c
6	0.05	8	3	0	0	13.45	1.7	0.9	-1.59	-0.325	-1.66	0.54	1.02	-0.66	
7	0.05	10	3	0	0	15.95	1.7	0.85	0.564	-1.66	-2.1	0.37	1.29	-0.72	
8	0.05	12	3	0	0	20.4	2.25	1.8	-1.92	-2.56	-3.20	0.24	1.52	-0.55	
9	0.05	6	0	0	0	7.7	1.1	0.4	-0.28	-2.08	-2.32	0.324	0.77	0.32	BLADE No 4 Effect of α
10	0.05	6	7	0	0	9.05	1.55	0.6	-1.6	-1.96	-0.08	0.188	0.77	-0.356	
11	0.05	6	11	0	0	7.55	1.35	0.7	0.4	-1.12	0.36	0.198	0.71	-0.163	
12	0.05	6	15	0	0	6.52	1.35	0.7	-1.12	-0.32	-1.28	0.45	0.575	0.114	
13	0.05	12	0	0	0	17.05	1.75	0	0.68	-2.88	-4.08	0.389	1.68	-0.387	
14	0.05	12	7	0	0	20	1.45	1.45	0.56	-3.2	-3.36	0.307	1.59	-0.122	
15	0.05	12	11	0	0	18.7	0	1.85	0.64	-2.4	-3.68	0.305	1.46	-0.245	
16	0.05	12	15	0	0	18.6	0.8	1	-1.6	-2.4	-3.36	0.335	1.40	-0.245	
17	0.05	6	3	0	-3	6.84	0	0.85	0.809	-2.42	-0.81	0.54	-0.06	-0.54	4 Effect θ_2
18	0.05	6	3	0	-10	3.98	1.3	0.15	-0.717	-2.26	-1.13	0.54	-2.52	-0.24	
19	0.05	12	3	0	-3	17.2	0	1.3	0.809	-2.74	-1.13	0.45	0.36	-0.66	
20	0.05	12	3	0	-10	18	-5.1	0	-0.252	-0.805	0.4	0.3	-2.7	-0.3	
21	0.05	6	3	3	0	3.95	0.74	0	3.09	-1.57	-0.885	0.467	0.73	0.2	4 Effect θ_1
22	0.05	6	3	7	0	9.7	2.4	0.35	-2.16	-2.55	-1.775	0.334	1.33	0.667	
23	0.05	12	3	3	0	18.9	0.55	1.65	0.397	-1.76	-0.59	0.265	1.46	1.06	
24	0.05	12	3	7	0	21.2	0.4	0.6	0.195	-2.55	0.59	0.242	2.31	0.66	
33	0.05	12	3	0	0	17.55	0.7	-2	-1.012	-1.38	-1.53	0.275	2.67	1.45	2 μ
34	0.05	12	3	0	0	18.4	0.7	-1.05	1.47	0.175	-1.165	0.68	-1.36	1.04	3
35	0.05	12	3	0	-3	17.7	0.6	-1.6	0.43	0	0.86	0.245	-0.30	1.04	2 μ
36	0.05	12	3	0	-10	16.55	0	0.4	0.085	-0.35	-1.2	0.122	-2.84	-0.24	
37	0.05	12	3	0	-3	18.9	1	2.25	0.98	0.535	-1.42	0.715	-1.3	0.26	5 θ_2
38	0.05	12	3	0	-10	15.4	0.4	0.45	0.629	-0.89	-0.715	0.272	1.10	-2.41	

TABLE 1.9

NON DIMENSIONAL ROTOR LIFT $\frac{f_N}{\sigma}$

$$\sigma = \frac{bcR}{A}$$

Case group B	μ	θ_c deg	α deg	θ_1 deg	θ_2 deg	$\frac{f_{H_0}}{\sigma}$	$\frac{f_{H_1}}{\sigma}$	$\frac{f'_{H_1}}{\sigma}$
1	0	6	0	0	0	0.073	0.0159	0.01
2	0	8	0	0	0	0.108	0.0113	0.00318
3	0	10	0	0	0	0.142	0.0218	0.0031
4	0	12	0	0	0	0.159	0.0186	0.005
5	0.05	6	3	0	0	0.0719	0.0045	-0.00091
6	0.05	8	3	0	0	0.122	0.0154	0.0082
7	0.05	10	3	0	0	0145	0.0154	0.00775
8	0.05	12	3	0	0	0.185	0.0204	0.0164
9	0.05	6	0	0	0	0.07	0.010	0.00364
10	0.05	6	7	0	0	0.0825	00141	0.00545
11	0.05	6	11	0	0	0.0685	0.0122	0.00635
12	0.05	6	15	0	0	0.0594	00122	0.00635
13	0.05	12	0	0	0	0.155	0.0159	0
14	0.05	12	7	0	0	0.182	0.0132	0.0132
15	0.05	12	11	0	0	0.17	0	0.0168
16	0.05	12	15	0	0	0.169	0.00726	0.0091
17	0.05	6	3	0	-3	0.062	0	0.00775
18	0.05	6	3	0	-10	0.0362	0.0118	0.00177
19	0.05	12	3	0	-3	0.156	0	0.0118
20	0.05	12	3	0	-10	0.164	-0.0465	0
21	0.05	6	3	3	0	0.054	0.0067	0
22	0.05	6	3	7	0	0.088	0.0218	0.00318
23	0.05	12	3	3	0	0.172	0.005	0.015
24	0.05	12	3	7	0	0.193	0.0364	0.00545
33	0.05	12	3	0	0	0.199	0.00795	-0.0228
34	0.05	12	3	0	0	0.209	0.00795	-0.012
35	0.05	12	3	0	-3	0.201	0.0068	-0.0182
36	0.05	12	3	0	-10	0.188	0	0.0045
37	0.05	12	3	0	-3	0.143	0.0076	0.0171
38	0.05	12	3	0	-10	0.117	0.003	0.0034

TABLE 1.9 (Continued)

Case group A	μ	θ_c deg	α deg	θ_1 deg	θ_2 deg	$\frac{f_{H_0}}{\sigma}$	$\frac{f_{H_1}}{\sigma}$	$\frac{f'_{H_1}}{\sigma}$
1	0.10	6	3	0	0	0.093	0.01	0.0091
2	0.15	6	3	0	0	0.11	0.0127	0.0136
3	0.20	6	3	0	0	0.111	0.0173	0.0114
4	0.10	8	3	0	0	0.134	0.0214	0.0031
5	0.15	8	3	0	0	0.145	0.0095	0.0132
6	0.20	8	3	0	0	0.15	0.02	0.0113
7	0.10	10	3	0	0	0.16	0.02	0.00136
8	0.15	10	3	0	0	0.165	0.0164	0.0073
9	0.20	10	3	0	0	0.174	0.005	0.0036
10	0.10	12	3	0	0	0.182	- 0.0031	0.0132
11	0.15	12	3	0	0	0.21	0.0018	0.0132
12	0.20	12	3	0	0	0.217	- 0.0082	0.0045
13	0.10	6	0	0	0	0.083	0.0173	0.01
14	0.15	6	0	0	0	0.096	0.0117	0.0095
15	0.20	6	0	0	0	0.104	0.0145	0.0077
16	0.10	12	0	0	0	0.183	0.0145	-0.0109
17	0.15	12	0	0	0	0.214	0.0118	- 0.00091
18	0.20	12	0	0	0	0.224	0.0133	- 0.0168
19	0.10	6	7	0	0	0.092	0.0168	0.0118
20	0.15	6	7	0	0	0.10	0.0195	0.0063
21	0.20	6	7	0	0	0.096	0.0173	0.0118
22	0.10	12	7	0	0	0.182	0.010	0.010
23	0.15	12	7	0	0	0.196	0.0118	0.0214
24	0.20	12	7	0	0	0.202	- 0.00137	0.0123
25	0.10	6	11	0	0	0.076	0.0141	0.0118
26	0.15	6	11	0	0	0.0785	0.02	0.00227
27	0.20	6	11	0	0	0.073	0.0159	0.0159
28	0.10	12	11	0	0	0.17	0.0036	0.0145
29	0.15	12	11	0	0	0.175	0.0104	0.0180
30	0.20	12	11	0	0	0.172	0.0068	0.0104
31	0.10	6	15	0	0	0.0505	0.0186	0.0101
32	0.15	6	15	0	0	0.038	0.01	0.0164
33	0.20	6	15	0	0	0.024	0.0123	0.0123
34	0.10	12	15	0	0	0.166	0.0086	0.0086
35	0.15	12	15	0	0	0.166	0.0159	0.0072
36	0.20	12	15	0	0	0.145	0.010	- 0.00136
37	0.10	6	3	0	- 3	0.0755	0.0018	0.0086
38	0.15	6	3	0	- 3	0.0745	0.010	0
39	0.20	6	3	0	-3	0.078	0.0159	0.0077
40	0.10	12	3	0	- 3	0.177	0.0059	0.0082
41	0.15	12	3	0	-3	0.188	0.00228	0.0092
42	0.20	12	3	0	-3	0.194	0.0168	0.010
43	0.10	6	3	0	-10	0.059	0.0186	0
44	0.15	6	3	0	-10	0.0526	0.0114	0.00277
45	0.20	6	3	0	-10	0.044	0.0168	0.005
46	0.10	12	3	0	-10	0.182	- 0.089	0.0364
47	0.15	12	3	0	-10	0.191	- 0.069	0.061

Case group A	μ	θ_c deg	α deg	θ_1 deg	θ_2 deg	f_{N_0}/σ	f_{N_1}/σ	f'_{N_1}/σ
48	0.20	12	3	0	-10	0.174	-0.0635	0.0218
49	0.10	6	3	3	0	0.0755	0.0102	0.0101
50	0.15	6	3	3	0	0.081	0.0234	0.00296
51	0.20	6	3	3	0	0.0885	0.0218	0.006
52	0.10	12	3	3	0	0.182	0.0119	0.0188
53	0.15	12	3	3	0	0.197	0.0089	0.0138
54	0.20	12	3	3	0	0.218	0.0135	0.0086
55	0.10	6	3	7	0	0.103	0.0132	0.0089
56	0.15	6	3	7	0	0.117	0.0068	0.0105
57	0.20	6	3	7	0	0.116	0.005	0.0105
58	0.10	12	3	7	0	0.214	0.0082	0.0168
59	0.15	12	3	7	0	0.229	0.0086	0.0136
60	0.20	12	3	7	0	0.238	0.00318	0.0232
61	0.10	6	3	0	0	0.079	-0.00076	-0.00208
62	0.15	6	3	0	0	0.0845	0.00208	0.00645
63	0.20	6	3	0	0	0.086	-0.0068	0.0007
64	0.10	12	3	0	0	0.197	0.00605	-0.0079
65	0.15	12	3	0	0	0.204	0.0076	0
66	0.20	12	3	0	0	0.226	-0.0095	-0.0019
67	0.10	6	12	0	0	0.062	-0.0019	-0.0019
68	0.15	6	12	0	0	0.0565	-0.0037	0
69	0.20	6	12	0	0	0.0352	-0.00605	0.0037
70	0.10	12	12	0	0	0.159	0.0045	-0.00605
71	0.15	12	12	0	0	0.161	0.0037	-0.0057
72	0.20	12	12	0	0	0.147	0.0117	-0.0057
73	0.10	6	3	0	0	0.1465	0.0171	0.0135
74	0.15	6	3	0	0	0.128	0.0136	0.0148
75	0.20	6	3	0	0	0.117	0.0136	0.0114
76	0.10	12	3	0	0	0.195	0.00227	0.0057
77	0.15	12	3	0	0	0.209	-0.0074	0.0057
78	0.20	12	3	0	0	0.209	0.0096	0.0022
79	0.10	6	12	0	0	0.126	-0.0028	-0.0057
80	0.15	6	12	0	0	0.09	-0.0074	-0.0022
81	0.20	6	12	0	0	0.0785	0.0193	0.0108
82	0.10	12	12	0	0	0.182	0.0017	0.0091
83	0.15	12	12	0	0	0.174	0	0
84	0.20	12	12	0	0	0.165	0.0085	0.0017
85	0.10	12	3	0	0	0.206	0.0114	-0.02
86	0.15	12	3	0	0	0.226	0.00227	-0.0182
87	0.20	12	3	0	0	0.233	0.0114	-0.0277
88	0.10	12	3	0	0	0.187	0.0125	-0.0045
89	0.15	12	3	0	0	0.248	0.0091	-0.004
90	0.20	12	3	0	0	0.254	0.0137	0.00228
91	0.15	12	3	0	0	0.234	0.0045	-0.018
92	0.15	12	3	0	0	0.216	0.0113	0.0022
93	0.15	12	3	0	0	0.23	0.00284	0.0267
94	0.15	12	3	0	0	0.205	-0.00965	0.012

TABLE 1.9 (Concluded)

In order to be able to place circles in the horizontal plane we have defined the distance OB' (Figure 114b), where B" is the projection of the center of the first circle on the horizontal plane passing through the center of the swept disc.

$$O\,B'' = V_0 \frac{T}{8} + V_0\, \tau + V_{i_{zm}}\, \tau\, \frac{\sin\alpha}{\cos\alpha}$$

where $V_{i_{zm}} \tau$ is the distance between two circles

$$\tan \delta = \frac{V_{i_{zm}} + V_0 \sin\alpha}{V_0}$$

$$O\,B' = V_0 \frac{T}{8} \cos\alpha + V_0 \cos\alpha\,(nT)$$

1.533 - Circle Radii

It will be remembered that the circles are parallel to the swept disc, so that they form an angle α with the relative wind.

It now remains to determine their radii.

To this end we shall first determine experimentally the directions δ_1 and δ_2 defining a bounded zone containing the circles (Figure 114). In the zone $\Psi = 180°$, the direction δ_1 does not bear upon the blade tip , but is at a distance $O'A = V_0 \frac{T}{4}$.

From the photographs we found different values for $\delta_1, \delta_2, \delta_3$ for $0 < \mu < 0.05$. On the other hand, for $\mu \geqslant 0.10$, we have.

$$\delta = \delta_1 = \delta_2 = \ldots$$

The values $\delta_1 \neq \delta_2 \neq \delta$ are capable of explanation. Let us call $V_{i_{xm}}$ the mean horizontal induced velocity (Figure 114b). The vortex at E will be influenced by the V_{i_x} of the vortex E' and will be accelerated with respect to the relative wind. On the other hand, the vortex F will be retarded by the influence of F'.
We can therefore calculate δ_1 and δ_2 from the following:

$$\tan \delta_1 = \frac{V_{i_{zm}} + V_0 \sin\alpha}{V_0 + V_{i_{xm}}} \qquad \tan \delta_2 = \frac{V_{i_{zm}} + V_0 \sin\alpha}{V_0 - V_{i_{xm}}}$$

As already stated, $V_{i_{xm}}$ is defined from the data processing in each test case. Also, when V_0 becomes relatively large ($\mu > 0.10$), we obtain $V_{i_x} \approx 0$, which explains the equality between δ, δ_1, δ_2.

The radius of the circles is given by

/.

$$R = R_o - \frac{V_o \frac{T}{4} + V_{i_z}\,\tau \left(\frac{1}{\tan\delta_1} - \frac{1}{\tan\delta_2}\right)}{2}$$

$$V_o \frac{T}{4} = O'A'$$

where $V_{i_z}\,\tau$ is the distance between two circles

R_o is the radius of the swept disc and

$\tan\delta_1$ and $\tan\delta_2$ have been defined previously.

Let us take, for $0 < \mu < 0.05$,

$$R = R_o - \frac{V_o \frac{T}{4} + 2\,V_{ix_m}\tau}{2}$$

and for $0.10 < \mu < 0.20$

$$R = R_o - \frac{V_o}{2} \quad \frac{T}{4} \quad .$$

In Tables I.10 and I.11 we summarize , for different parameter values, the values of V_o, V_{iz_m} , $\frac{V_{iz_m}}{V_o}$, of δ calculated , of δ measured and of V_{ix_m} (for group B).

/.

Table 1.10

SITUATING THE CIRCLES

GROUP "B" $0 < \mu < 0.05$

$\delta_1, \delta_2, \delta$, are given relative to the plane of the swept disc

V_o		θ_c	α	θ_1	θ_2	$V_{i_{zm}}$	Blade	δ calcul	$\delta_{exp.}$	δ_1	δ_2	$V_{i_{xm}}$
m/s	ft/s	deg	deg	deg	deg	m/s	Nb	deg	deg	deg	deg	m/s
5	0	6	0	0	0	4.85	4	90	90	80	100	0.85
0	0	8	0	0	0	5	4	90	90	80	100	0.88
0	0	10	0	0	0	6.6	4	90	90	80	100	1.16
0	0	12	0	0	0	7	4	90	90	80	100	1.23
5	16.4	6	3	0	0	5	4	48	45	40	50	0.9
5	16.4	8	3	0	0	5.4	4	50	47	43	51	1.78
5	16.4	10	3	0	0	6.6	4	55	52	48	56	0.74
5	16.4	12	3	0	0	6.9	4	57	55	50	60	0.895
5	16.4	6	0	0	0	5.3	4	46	45	40	50	0.955
5	16.4	6	7	0	0	4.5	4	49	45	40	50	0.81
5	16.4	6	11	0	0	4	4	49	45	40	50	0.72

GROUP "B"

Table 1.10 (Concluded)

V_0		θ_c	α	θ_1	θ_2	$V_{i_{zm}}$	Blade	δ calculated	$\delta_{exp.}$	δ_1	δ_2	$V_{i_{xm}}$
m/s	ft/s	deg	deg	deg	deg	m/s	Nb	deg	deg	deg	deg	m/s
5	16.4	6	15	0	0	3.7	4	51	45	40	50	0.665
5	16.4	12	0	0	0	7.5	4	56	60	50	70	1.78
5	16.4	12	7	0	0	7	4	61	60	50	70	1.66
5	16.4	12	11	0	0	6.6	4	63	60	50	70	1.57
5	16.4	12	15	0	0	6.1	4	65	60	50	70	1.45
5	16.4	6	3	0	-3	4.6	4	45	47	30	45	1.68
5	16.4	6	3	0	-10	4.6	4	45	47	30	45	1.68
5	16.4	6	3	3	0	4.6	4	45	47	30	45	1.68
5	16.4	6	3	7	0	4.8	4	47	47	30	45	1.75
5	16.4	12	3	7	0	7	4	57	60	50	70	1.66
5	16.4	12	3	0	0	7.3	2	58	60	50	70	1.73
5	16.4	12	3	0	0	6.8	3	56	60	50	70	1.61

$\delta_1 = \delta_2 = \delta$ GROUP "A" $0.10 < \mu < 0.20$ $V1x_m = 0$ Table 1.11

V_o		θ_c	α	θ_1	θ_2	Vi_{z_m}	δ Calculated	$\delta_{2\,exp.}$	Blade
m/s	ft/s	deg	deg	deg	deg	m/s	deg	deg	Nb
10	32.8	6	3	0	0	4.2	25	25	4
15	49.2	6	3	0	0	2.8	13	15	4
20	65.5	6	3	0	0	2.3	9	10	4
10	32.8	8	3	0	0	5.2	30	25	4
15	49.2	8	3	0	0	4	17	20	4
20	65.5	8	3	0	0	3.3	12	15	4
10	32.8	10	3	0	0	5.8	33	30	4
15	49.2	10	3	0	0	4.9	21	20	4
20	65.5	10	3	0	0	4	14	17	4
10	32.8	12	3	0	0	6.7	37	30	4
15	49.2	12	3	0	0	5.3	22	20	4
20	65.5	12	3	0	0	4.5	15	15	4
10	32.8	6	0	0	0	3.7	20	25	4
15	49.2	6	0	0	0	2.8	10	15	4
20	65.5	6	0	0	0	2.55	10	10	4

GROUP. "A"

Table 1.11 (continued)

V_0 m/s	V_0 ft/s	θ_c deg	α deg	θ_1 deg	θ_2 deg	$V_{i_{3m}}$ m/s	δ Calculated deg	$\delta_{2exp.}$ deg	Blade Nb.
10	32.8	12	0	0	0	6.9	34	35	4
15	49.2	12	0	0	0	5.8	21	21	4
20	65.5	12	0	0	0	4.9	13	15	4
10	32.8	6	7	0	0	3.4	25	25	4
15	49.2	6	7	0	0	2.5	16	15	4
20	65.5	6	7	0	0	2.25	13	11	4
10	32.8	12	7	0	0	5.8	37	35	4
15	49.2	12	7	0	0	4.9	25	25	4
20	65.5	12	7	0	0	4.5	19	19	4
10	32.8	6	11	0	0	3.1	28	25	4
15	49.2	6	11	0	0	2.3	19	15	4
20	65.5	6	11	0	0	2	16	11	4
10	32.8	12	11	0	0	5.6	31	35	4
15	49.2	12	11	0	0	4.7	28	25	4
20	65.5	12	11	0	0	4.3	23	20	4

GROUP "A" Table 1.11 (continued)

V_o		θ_c	α	θ_1	θ_2	$V_{i_{\mathcal{Z}m}}$	δ Calculated	$\delta_{2\,exp.}$	Blade
m/s	ft/s	deg	deg	deg	deg	m/s	deg	deg	Nb.
10	32.8	6	15	0	0	2.9	31	30	4
15	49.2	6	15	0	0	2.2	23	20	4
20	65.5	6	15	0	0	1.8	18	15	4
10	32.8	12	15	0	0	5.2	42	40	4
15	49.2	12	15	0	0	4.5	31	30	4
20	65.5	12	15	0	0	4.1	26	20	4
10	32.8	6	3	0	-3	3.9	24	20	4
15	49.2	6	3	0	-3	2.8	13	15	4
20	85.5	6	3	0	-3	2.6	10	11	4
10	32.8	12	3	0	-3	6	34	30	4
10	32.8	6	3	0	-10	3	19	15	4
15	49.2	6	3	0	-10	1.9	10	12	4
20	65.5	6	3	0	-10	1.7	8	10	4
10	32.8	6	3	3	0	3.6	22	20	4
15	49.2	6	3	3	0	2.8	13	12	4
20	65.5	6	3	3	0	2.2	9	10	4

Table 1.11 (continued)

GROUP "A"

V_o		θ_c	α	θ_1	θ_2	V_{izm}	δ Calculated	$\delta_{2\,exp.}$	Blade
m/s	ft/m	deg	deg	deg	deg	m/s	deg	deg	Nb.
10	32.8	6	3	7	0	4.4	26	25	4
15	49.2	6	3	7	0	3.7	16	15	4
20	65.5	6	3	7	0	2.9	11	10	4
10	32.8	6	3	0	0	3.6	22	25	5
15	49.2	6	3	0	0	2.8	13	15	5
20	65.5	6	3	0	0	2.6	10	10	5
10	32.8	12	3	0	0	6.6	36	35	5
15	49.2	12	3	0	0	5	21	25	5
20	65.5	12	3	0	0	4.5	15	15	5
10	32.8	6	3	0	0	3.5	22	25	1
15	49.2	6	3	0	0	2.6	12	15	1
20	65.5	6	3	0	0	2.3	9	10	1
10	32.8	12	3	0	0	6.3	35	35	2
15	49.2	12	3	0	0	4.8	21	25	2
20	65.5	12	3	0	0	4.2	15	15	2

GROUP "A"

Table 1.11 (Concluded)

V_0 (m/s)	V_0 (ft/s)	θ_c (deg)	α (deg)	θ_1 (deg)	θ_2 (deg)	$V_{i_{3m}}$ (m/s)	δ Calculated (deg)	$\delta_{2\,exp.}$ (deg)	Blade Nb.
10	32.8	12	3	0	0	5.9	33	35	3
15	49.2	12	3	0	0	4.6	20	25	3
20	55.5	12	3	0	0	3.8	13	15	3

2 - BASICS FOR THE ESTABLISHMENT OF AN ANALYTICAL METHOD OF EVALUATING AERODYNAMIC LOADS

2.1 - Causes of a discrepancy between the predicted lift and the actual lift of a blade element

2.11 - The local lift dL of a blade element c dr (see Figure 115) is usually calculated from the following formula:

$$\frac{dL}{dr} = \frac{1}{2}\rho(\omega r + V\sin\Psi)^2 c \frac{dC_L}{di}\left[\theta_c + \theta_1\cos\Psi + \theta_2\sin\Psi - \frac{V_i + V\sin\alpha + r\frac{d\beta}{dt} + V\beta\cos\Psi}{\omega r + \sin\Psi}\right] \tag{II.1.1}$$

The values of the flapping coefficients:

$$\beta = a_0(t) - a_1(t)\cos\Psi - a_2(t)\cos 2\Psi - a_3(t)\cos 3\Psi - b_1(t)\sin\Psi - b_2(t)\sin 2\Psi - b_3(t)\sin 3\Psi \tag{II.1.2}$$

are calculated (hinged blade) from the equation :

$$I_o\omega^2\beta + I_o\frac{d^2\beta}{dt^2} = \int\frac{dL}{dr}\,r\,dr \tag{II.1.3}$$

The induced velocity V_i is in general defined by overall formulae. The simplest of these is :

$$V_i = \frac{K F_M}{2\rho A\sqrt{V^2 + V_i^2}} \tag{II.1.4}$$

Discrepancies can arise for a variety of reasons.

2.12 - Simplification of the formulae

In actual fact, the local lift should be expressed by :

$$\frac{dL}{dr} = \frac{1}{2}\rho\, V_R^2\, c\, C_L(i) \tag{II.1.5}$$

There is an error in the velocity :

$$V_R^2 = (\omega r + V\sin\Psi)^2 + \left(V_i + V\sin\alpha + r\frac{d\beta}{dt} + V\beta\cos\Psi\right)^2$$

(the second square term is often neglected).

/.

There is an error in the evaluation of the angle of incidence :

(II.1.6) $$i = \theta - \varphi$$

(II.1.7) $$\theta = \theta_c + \theta_1 \cos\Psi + \theta_2 \sin\Psi$$

(II.1.8) $$\varphi = \operatorname{arc tan.} \frac{V_i + V\sin\alpha + r\frac{d\beta}{dt} + V\cos\alpha\,\beta.\cos\Psi}{\omega r + V\sin\Psi}$$

The tangent arc and the angle are taken to be one and the same.

This gives rise to an error of non-linearity; if the angle of incidence i becomes too large it is no longer possible to replace C_L by $\frac{dC_L}{di}(\theta - \varphi)$.

If one confines oneself to low advance ratios

$$\mu = \frac{V}{\omega R} \leqslant 0.2$$

and if one avoids over-accentuated stalls, one may retain the formulae (II.1.1) and (II.1.3).

2.13 - Blade rigidity

Blades are usually flexible in bending and sometimes also not very rigid in torsion.

For a flexible blade β no longer has any physical significance. If y (r,t) be the distortion of the blade (see Figure 116) the expression for β must be replaced by the following expressions :

$$\beta \text{ by } \frac{\partial}{\partial r} y$$

$$r\frac{d\beta}{dt} \text{ by } \frac{\partial}{\partial t} y$$

$$r\frac{d^2\beta}{dt^2} \text{ by } \frac{\partial^2}{\partial t^2} y$$

The blades in the five sets built were made very rigid in order to avoid the y distortions at low frequencies.

A parasite rotation $\delta\theta$ of the blade can also take place if the blade distorts in torsion or if the pitch controls are "mushy".

The blades built for the tests were torsionally rigid.

/.

The CG's of the various blade sections were located upon the feathering axis.

On the other hand, the controls were light enough to permit remote control and to introduce unit-step harmonic forces.

It is considered that the parasite $\delta\theta$ effects from the inserted blade-roots were small.

Consequently* the expressions (II.1.1) and (II.1.2) remain valid.

2.14 - Induced velocity and blade flapping

A priori, the only doubtful terms in equation (II.1.1) are :

$$V_i, \quad r\frac{d\beta}{dt} \quad \text{and } \beta$$

The induced velocity V_i is generated by the free vortices escaping from the b rotor blades (b = 2).

As long as the free vortex is remote from the blade (at a distance of about 3 to 4 chords) it produces, on the straight section of the airfoil, a constant velocity distribution that generates an ordinary type of circulation (see below): hence the blade can be reduced to a line and the velocity V_i sought at that point.

When the vortex is close to the blade (at a distance of less than 3 chords), the blade can no longer be reduced to a straight line because the distribution of the velocity induced by the vortex on the airfoil varies too much, thereby causing inertia forces to be set up in addition to the circulations.

The variation through time of the circulation about the blade causes free vortices to escape from the trailing edge.

These two latter free vortex effects produce dynamic (non-stationary) regimes that must be taken into account. These will be examined again later. As a result, the lift $d_{L\,stat.}$ may sustain amplitude modifications as well as an out-phasing.

The static lift $d_{L\,stat.}$ given by formula (II.1.1) consequently becomes a dynamic (non-stationary) lift $d_{L\,dyn.}$

(II.1.9) $$\left(\frac{dL}{dr}\right)_{dyn.} = \square_1\left(\frac{dL}{dr}\right)_{stat.}$$

where $\square_1$ designates an operator, i.e. a mathematical

/.

transformation of the static lift, which takes into account the amplitude and phase modifications.

The blade flapping value β is consequently modified:

$$\text{(II.1.3)'}\quad I_0\omega^2\beta + I_0\frac{d^2\beta}{dt^2} - \int\left(\frac{dL}{dr}\right)_{dyn.} r\,dr = \Box_1 \int\left(\frac{dL}{dr}\right)_{stat.} r\,dr$$

2.15 - In what follows, it is proposed to attempt to show how Vi and the operator $\Box_1$ can be calculated.

2.2 - Description of vortex model

2.21 - General

Before proposing a calculation method, a vortex model will be described and the orders of magnitude of the various phenomena estimated so as to permit simplification of the mathematical equations.

In the case of an aircraft fixed wing (in a compressible medium), the whole set of phenomena is known. On the other hand whereas the phenomena are similar in the case of a helicopter rotor, expressing them mathematically is a complex business; an attempt will therefore be made to find approximations for these mathematical expressions, by introducing the phenomena in rough form only.

The vortex visualizations obtained by means of smoke emissions proved of great help in achieving these approximations and especially as a means of insuring that all effects had been accounted for.

2.22 - Helix vortices and radial vortices

The free vortices are generated on the blade and are of two kinds.

Any change in the circulation $\Gamma(r,t)$ around the blade :

$$\text{(II.2.1)}\qquad dL = \rho\, V_{Res.}\, \Gamma\, dr$$

gives rise to a streaming of free vortices.

2.221 - First, the circulation Γ can vary along the span : $\frac{d\Gamma}{dr}$

These free vortices locate themselves along the flow streamlines if they are referred to axes linked to the blades

(V . rotation V = 0)

/.

These will be termed helix vortices (Figure 117).

Let us now calculate a point of such an helix vortex (Figure 118).

Let us consider the blade at the instant $t = t_1$ and a system of coordinates $0\ x\ y\ z$ linked to the blade, and let M be a point on the blade from which is detached an helix vortex of intensity $\frac{d\Gamma}{dr}(t_1)$.

The coordinates of the point M are :

$$\text{(II.2.2)}\quad \begin{cases} r \\ \psi(t_1) \\ \beta(t_1) \end{cases} \quad \begin{cases} x_M = -r\cos\omega t_1 \\ y_M = r\sin\omega t_1 \\ z_M = -r\beta(t_1) \end{cases}$$

Let us now find the location of the helix vortex element formed τ seconds before, i.e. at the instant $t_1 - \tau$.

τ seconds before, the center 0 of the rotor was at $0_{1,2}$.

$$\overrightarrow{0\ 0_{1,2}} = \overrightarrow{V_0}\ \tau$$

τ seconds before, the point M was at M_2, such that:

$$\text{(II.2.3)}\quad \begin{cases} x_{M_2} = -r\cos\omega(t_1-\tau) - V\cos\alpha\,\tau \\ y_{M_2} = r\sin\omega(t_1-\tau) \\ z_{M_2} = -r\beta(t_1-\tau) - V\sin\alpha\,\tau \end{cases}$$

At that instant $(t_1 - \tau)$ a free vortex element became detached at M_2 .

During the time taken for the blade $0_2\ M_2$ to reach 0 M (viz. two seconds) this vortex element was entrained from the point M_2 to the point H by the velocities induced by all the free and connected vortices :

$$\text{(II.2.4)}\quad \begin{array}{l} V_{ix}\ (x, y, z, t) \\ V_{iy}\ (x, y, z, t) \\ V_{iz}\ (x, y, z, t) \end{array}$$

The coordinates of H are therefore :

$$\text{(II.2.5)}\quad \begin{aligned} x_H &= -r\cos\omega(t_1-\tau) - V\cos\alpha\,\tau + \oint_0^\tau V_{ix}\,d\tau \\ y_H &= r\sin\omega(t_1-\tau) + \oint_0^\tau V_{iy}\,d\tau \\ z_H &= -r\beta(t_1-\tau) + V\sin\alpha\,\tau + \oint_0^\tau V_{iz}\,d\tau \end{aligned}$$

The slope of the vortex line at H is consequently:

(II.2.6)
$$\begin{cases} \dfrac{dx_H}{d\tau} = -r\omega \sin \omega(t_1 - \tau) - V\cos\alpha + V_{ix} \\ \dfrac{dy_H}{d\tau} = -r\omega \cos \omega(t_1 - \tau) + V_{iy} \\ \dfrac{dz_H}{d\tau} = r\dfrac{d\beta}{d\tau}(t_1 - \tau) + V\sin\alpha + V_{iz} \end{cases}$$

Let us consider the difference with an aircraft fixed wing.

In the case of fixed wings it is customary to cancel out V_{ix}, V_{iy}, V_{iz} in the wake, since their values are small compared with the flying speed V_0.

From this it may be asserted that the free vortices remain at the place (referred to space coordinates) where they were formed (M_2).

This is not always true in the case of a helicopter.

The helix vortex is tangential to the streamline at that point.

Determination of V_{ix}, V_{iy} and of V_{iz} is a difficult problem. The visualization tests made have nevertheless enabled valid approximations to be made.

2.222 - Second, the circulation Γ may vary at a point r on the blade in terms of time, as follows :

$$\frac{\partial \Gamma}{\partial t}$$

When that is the case, a vortex will stream from the trailing edge. Such a vortex will be termed a radial vortex (Figure 119) and its intensity will be equal to :

$$-\frac{\partial \Gamma}{\partial t}$$

since it is opposite to the intensity which generates it (conservation of the circulation).

This radial vortex is orthogonal to the streamlines defined above

$$(V \cdot \text{rot.}\ V = \text{maximum}) \qquad \alpha = \frac{\pi}{2}$$

The coordinates at the instant $t = t_1$ of a radial vortex /.

element formed τ seconds before, i.e. at the instant $t_1 - \tau$, are :

(II.2.7)
$$x_T = -r\cos\omega(t_1-\tau) - V\cos\alpha\,\tau + \oint_0^\tau V_{ix}\,d\tau$$
$$y_T = r\sin\omega(t_1-\tau) + \oint_0^\tau V_{iy}\,d\tau$$
$$z_T = -r\beta(t_1-\tau) + V\sin\alpha\,\tau + \int_0^\tau V_{iz}\,d\tau$$

The tangent to the radial vortex line is defined by :

(II.2.8)
$$\frac{\partial x_T}{\partial r} = -\cos\omega(t_1-\tau) + \frac{\partial}{\partial r}\oint_0^\tau V_{ix}\,d\tau$$
$$\frac{\partial y_T}{\partial r} = \sin\omega(t_1-\tau) + \frac{\partial}{\partial r}\int_0^\tau V_{iy}\,d\tau$$
$$\frac{\partial z_T}{\partial r} = -\beta(t_1-\tau) + \frac{\partial}{\partial r}\oint_0^\tau V_{iz}\,d\tau$$

The orthogonality of the radial vortices and of the helix vortices can be expressed by :

$$\frac{\partial x_T}{\partial r}\cdot\frac{\partial x_H}{\partial \tau} + \frac{\partial y_T}{\partial r}\cdot\frac{\partial y_H}{\partial \tau} + \frac{\partial z_T}{\partial r}\cdot\frac{\partial z_H}{\partial \tau} = 0$$

2.23 - <u>Conservation of circulation</u>

2.231 - The complete system of free and connected vortices constitutes a system of closed curves of elemental intensity (Figure 121):

$$\frac{\partial^2 \Gamma}{\partial r\,\partial \tau}$$

Each elemental closed curve consists of connected vortex section ($\alpha\beta$), an helix vortex section ($\beta\gamma$), a radial vortex section ($\gamma\delta$) and a further helix vortex section ($\delta\alpha$).
The free vortex, viz. $\gamma\delta\alpha$ ($\alpha\beta$ excluded) may assume a wide variety of configurations and change its location periodically in response to the velocity field (depending on whther operation takes place as a helicopter, a gyrodyne, or in autorotating descent); the total circulation will consequently by zero. It is proposed to consider only helicopter configurations here.

/.

For long-established hovering ($\tau \to \infty$), the radial vortex $\gamma\delta$ is thrown back to downstream infinity ($\int_0^\infty V_{i_z}\, \partial\tau$) and the helix vortices $\beta\gamma$ and $\delta\alpha$ are of infinite length.

2.232 - The connected circulation produces the local lift:

$$\rho V_{Res.} \Gamma(r,t)$$

Since the lift cancels out at the two ends of a blade (at the root (V_0) and at the tip (R) (see Figure 120)), we have :

$$\Gamma(r_0,t) = 0$$

$$\Gamma(R,t) = 0$$

The conservation of circulation gives :

(II.2.9) $$\int_{r_0}^{R} \frac{\partial\Gamma}{\partial r}(r,t)\, dr = \Gamma(R) - \Gamma(r_0) = 0$$

Whence :

$$\Gamma(r) = \int_{r_0}^{r} \frac{\partial\Gamma}{\partial r}(r,t)\, dr = -\int_{r}^{R} \frac{\partial\Gamma}{\partial r}(r,t)\, dr$$

The circulation at a point in the helix vortex is :

$$\frac{\partial\Gamma}{\partial r}(r,t) = \int_0^{\tau} \frac{\partial^2\Gamma}{\partial r\,\partial\tau}\, d\tau$$

The circulation at a point in the radial vortex is :

$$-\frac{\partial\Gamma}{\partial t} = -\int_0^{r} \frac{\partial^2\Gamma}{\partial r\,\partial\tau}\, dr$$

2.233 - <u>Experimental orders of magnitude</u>

In order to estimate the values of :

$$\Gamma(r,\psi), \quad \frac{d\Gamma}{\partial r}(r,\psi) \text{ and } \frac{d\Gamma}{d\psi}(r,\psi)$$

these will be calculated from the experimental lift dis-
/.

tribution values $\frac{dL}{dr}$ (Lb/in), based on the tests carried out by John Meyer Jr. and Gaetano Falabella (see reference .4.).

Two cases will be considered : hovering flight ($\mu = 0$) and forward flight ($\mu \neq 0$). The rotor characteristics are given by Table 2.13 and the circulation Γ is obtained from :

$$\bar{\Gamma} = \frac{1}{\bar{r} + \mu \sin \Psi} \frac{dL}{dr}$$

The points in the neighborhood of $r = R$ and $r = r_o$ are somewhat uncertain.

The variations of Γ in terms of $\bar{r}$ are given by the graphs in Figures 122, 123, 124.

The maximum value of Γ is situated in the vicinity of $\bar{r} = 0.8$, for $\mu = 0.2$ and $\bar{r} = 0.9$ for $\mu = 0$.

The values

$$\Gamma(\bar{r} = 0.5, \Psi) \quad \text{and} \quad \Gamma(\bar{r} = 0.8, \Psi)$$

have been broken down into a Fourier series (Runge's 12-point method) for forward flight ($\mu = 0.20$).

The expressions for $\frac{\Gamma}{\Gamma_o}$ are given by Table 2.12).

(II.2.10) $$\Gamma = \Gamma_o - \sum_{n=1}^{\infty} \left[\Gamma_n \cos n\Psi + \Gamma_1^{*} \sin n\Psi \right]$$

As a first approximation, we may write :

$$\frac{\Gamma}{\Gamma} = 1 - \frac{\Gamma_1^{*}}{\Gamma_o} \sin \Psi .$$

This result bears a relation to that found by Meijer Drees (see reference .15.).

If it is assumed that the circulation $\Gamma(r)$ is constant over the span, so that :

$$\frac{\partial \Gamma}{\partial r} = 0$$

then the blade flapping equation :

(II.2.11) $$(aA + I_o)\, \omega^2 \beta + I_o \ddot{\beta} = M_{Ae}$$

developed in cosine and sine form gives the following two simple relations :

$$\begin{cases} \dfrac{\partial A}{I_o\omega^2}\, a_1 = \dfrac{\rho R^3 U}{3\, I_o\omega^2}\left[\Gamma_1 + \dfrac{3}{4}\mu\,\Gamma_2^x\right] \simeq 0 \\[2ex] \dfrac{\partial A}{I_o\omega^2}\, b_1 = \dfrac{\rho R^3 U}{3\, I_o\omega^2}\left[\Gamma_1^x - \dfrac{3}{2}\mu\,\Gamma_o - \dfrac{3}{4}\mu\,\Gamma_2\right] \simeq 0 \end{cases}$$

If the hinge is a central one $(a = 0)$ then we have :

$$\frac{\Gamma_1^x}{\Gamma_o} = \frac{3}{2}\mu - \frac{3}{4}\mu\,\Gamma_2$$

and

$$\frac{\Gamma_1}{\Gamma_2^x} = -\frac{3}{4}\mu$$

Using the local values for Γ given by Table 2.12, it will be seen that the second relation :

$$\frac{\Gamma_1}{\Gamma_2^x} = -\ 0.15$$

is true neither in sign nor in magnitude, for :

$$\frac{\Gamma_1}{\Gamma_2^x} = \begin{cases} +\ 1.47 \text{ for } \bar{r} = 0.5 \\ +\ 1.52 \text{ for } \bar{r} = 0.8. \end{cases}$$

On the other hand, the first relation :

$$\frac{\Gamma_1^x}{\Gamma_o} = 0.30 - 0.15\,\frac{\Gamma_2}{\Gamma_o}$$

gives 0.415 and 0.245 for $\frac{\Gamma_1^x}{\Gamma_o}$, with $\frac{\Gamma_2}{\Gamma_o}$ negligible.

From this it emerges that the hypothesis of constant circulation is untrue for cos ψ and sine 2ψ frequencies and that it would provide an approximation for the 0 and $\sin\psi$ frequencies, unless the blade flapping equation (II.2.11) is incomplete.

$\frac{d\Gamma}{d\bar{r}}$ was calculated by deriving the curve $\Gamma(r)$ graphically. This graphical derivation was performed as follows :

a) A protractor was used to measure the slope of the tangent in degrees.

b) A curve was drawn to represent the values of the angles found; this curve was then 'smoothed out' /.

Table 2.12

Harmonic Analysis of the Circulation around a Blade at $\bar{r}$ = 0.5 and $\bar{r}$ = 0.8 for μ = 0.20 (See Reference ...)

		$\frac{\Gamma}{\Gamma_0}$ (0.5 ψ)	$\frac{\Gamma}{\Gamma_0}$ (0.8 ψ)
C^{te}	$\frac{\Gamma_0}{\Gamma_0}$	- 1	- 1
Cos ψ	$-\frac{\Gamma_1}{\Gamma_0}$	0.069	0.0514
Cos 2ψ	$-\frac{\Gamma_2}{\Gamma_0}$	0.1142	0.056
Cos 3ψ	$-\frac{\Gamma_3}{\Gamma_0}$	+ 0.032	+ 0.0316
Cos 4ψ	$-\frac{\Gamma_4}{\Gamma_0}$	+ 0.025	- 0.02
Cos 5ψ	$-\frac{\Gamma_5}{\Gamma_0}$	- 0.002	- 0.0114
Cos 6ψ	$-\frac{\Gamma_6}{\Gamma_0}$	+ 0.0073	+ 0.0114
Sine ψ	$-\frac{\Gamma_1^x}{\Gamma_0}$	0.415	0.245
Sine 2ψ	$-\frac{\Gamma_2^x}{\Gamma_0}$	- 0.047	- 0.0338
Sine 3ψ	$-\frac{\Gamma_3^x}{\Gamma_0}$	+ 0.05	+ 0.01
Sine 4ψ	$-\frac{\Gamma_4^x}{\Gamma_0}$	- 0.0107	- 0.009
Sine 5ψ	$-\frac{\Gamma_5^x}{\Gamma_0}$	- 0.025	+ 0.0

and checked against the measurements obtained under a) above.

c) The angles were converted into trigonometry tangents, thus enabling the derivatives to be obtained.

The variations $\frac{d\Gamma}{dr}(r, \Psi)$ are shown by the graphs in Figures 124,125 and 126.

The area comprised between the curve and the x-axis must be zero :

$$\int_{r=r_o}^{r=R} \frac{\partial \Gamma}{\partial r}\, dt = 0$$

Although the value $\frac{\partial \Gamma}{\partial r}$ appears to tend towards infinity (∞) as $r \rightarrow R$ and $r \rightarrow r_o$, the area bounded by the curve and the r axis between

$$r = r_m$$

$$\frac{\partial \Gamma}{\partial r}(r = r_m, t) = 0$$

and R, must have a finite value :

$$\int_{r=r_m}^{r \rightarrow R} \frac{\partial \Gamma}{\partial r}(r, \Psi)\, dr = \Gamma_{max}$$

2.234 - Determination of the induced velocity as a complementary term.

If it is assumed that the local circulation is expressed by:

$$\frac{dL}{dr} = \rho(\omega r + V\sin\Psi)\,\Gamma$$

$$\Gamma = \frac{1}{2}c(\omega r + V\sin\Psi)\left[\frac{dC_L}{di}\right]\left[\theta - \frac{V_i + r\frac{d\beta}{dt} + V\cos\Psi\beta + V\sin\alpha}{\omega r + V\sin\Psi}\right]$$

then the induced velocity V_i will be equal to :

(II-2.12) $$V_i = U\left[\bar{r} + \mu\sin\Psi\right]\theta - \left[r\frac{d\beta}{dt} + V\cos\Psi\beta + V\sin\alpha\right] - \frac{\Gamma}{\frac{1}{2}c\frac{dC_L}{di}}$$

In the case of the Meyer-Falabella tests (see reference ... and Table 2.13) all the terms on the right-hand side of the equation being known, it was possible to calculate the induced velocity required to balance the equation. Evidently, all errors and parasite effects are included.

The V_i curves (r, Ψ) are given in Figures 124, 127, and 128 for hovering flight and also for forward flight ($\mu = 0.20$).

These curves were compared to the mean induced velocities:

(II.2.13)
$$V_i = \sqrt{\frac{F_N}{2\rho \pi R^2}} \qquad \text{for } \mu = 0$$

$$V_i = \frac{F_N}{2\rho \pi R^2 \sqrt{V_0^2 + V_i^2}} \qquad \text{for } \mu = 0.2$$

These calculations call for the following observations :

1) In forward flight ($\mu \neq 0$), the induced velocity is not just an indirect measurement of the lift. For $\Psi = 90°$, due account was taken of a possible error in θ of 0.5° (dotted curve); however, it does not account for the possibility of the negative induced velocity. The latter is presumably due to the free vortices of the second blade, which are located beneath the rotor disc (see visualization photographs).

2) This way of determining the induced velocity, from the Meyer-Falabella results, is not physically correct. For it is not the incidence but the chord which cancels out at the blade tip, thereby giving rise to a large increase in the circulation derivative.

/.

Table 2.13

Data Concerning the Meyer-Falabella Rotor

Diameter	$2R = 5$ ft
Airfoil	NACA 0015 $\frac{dC_L}{di} = 5.7$
Chord	$c = 3$ inches
RPM	$N = 800$
Angular velocity	$\omega = 83.8$ rad/sec
Central hinge	$\varepsilon = 0$

Hovering flight $\mu = 0$

$\theta_c = 8°$

$T = 7.6$ lbs

Forward flight $\mu = 0.22$

$\theta_c = 8°$

$\beta = 0°5 - 4°6 \cos\psi - 2° \sin\psi$

$\frac{c_T}{\sigma} = 0.083$

$\alpha = -5°$

2.24 - Vortex visualization

- The accompanying photographs taken at the Marseilles Wind-Tunnel show:

  - the extreme marginal vortex and
  - the vortex at the blade root.

- The vortex at the blade tip is clearly localized: it is also more marked (sharper photographs) for blades located between azimuth angles $\psi = 180°$ and $360°$ (retreating blades) than for blades located at $0 < \psi < 180°$ (advancing blades)(photographs markedly less contrasted).

- There is a single core only in the case of a steady periodic regime. According to a film which was taken, if sudden collective pitch changes are made, small cores may appear which, after a certain time has elapsed, are sucked in by the main core.

- The vortex at the root is much less intense and difficult to place in evidence. The spirals correspond to a high local μ ($r = 0.2$).

2.25 - Calculated orders of magnitude

2.251 - Application to the two-blade rotor

In a manner somewhat analogous to the theory of fixed wings, it is necessary, in order to calculate the lift at a point M on a blade A, to know the velocities induced there by the free vortices and the connected vortices.

It is therefore necessary to know both the location and the intensity of the vortices. Visualizations permit a simplification of the problem of situating these vortices.

Let M be a point where we wish to know the velocity induced by the vortices :

(II.2.14)
$$x_M = - r \cos \Phi$$
$$y_M = + r \sin \Phi$$
$$z_M = - r \beta_M$$

To calculate the induced velocities, use will be made of the Biot and Savart formula written in Cartesian coordinates (Figure 129).

This point M will be on blade A if

$$\Phi = \psi_1$$
$$\beta_M = \beta(t_1)$$

/.

It will be on blade B if

$$\Phi = \Psi_1 + \pi .$$

$\beta_M = \beta\,(t_1 + T)$ where T=period of rotation.

2.252 - The coordinates of a point H in the helix vortex are known in terms of the auxiliary variable (see Eq.II.2.5).

Formula II.2.16 given on the following page permits calculation of the velocity induced at a point M by the helix vortex (τ varies between 0 and ∞).

Since it was necessary to make approximations, a number of numerical applications were made by graphical integration.

2.253 - Helix vortex in hovering flight

The velocity induced at a point r = 0.5 R on the blade A by an helix vortex of intensity Γ streaming from the point r_1 = 0.8 R with :

$$U = \omega R = 100 \text{ m/sec}$$

$$R = 0.75 \text{ m}$$

$$V_i = 4.55 \text{ m/sec,}$$

is given by : $V_i = \dfrac{\Gamma}{4\pi} A^*$

(II.2.15) $$A^* = \int_0^{\omega\tau} \frac{(r_1^2 - r_1 r \cos\omega\tau)\, d(\omega\tau)}{\left[r_1^2 + r^2 - 2 r r_1 \cos\omega\tau + \left(\frac{V_i}{\omega R}\right)^2 (\omega\tau)^2\right]^{3/2}}$$

The integration is performed graphically for the following three cases (Figure 130) :

1) For the helix (V_i = 4.55 m/s $\quad 0 \leqslant \omega\tau \leqslant 2n$)

2) For a circle (V_i = 0) contained in the plane of the disc and acting as a substitue for the helix.

3) For a circle located half a period beneath the disc, i.e.

$$\left(\frac{V_i}{\omega R}\right)^2 (\omega\tau)^2 = \left(\frac{V_i}{\omega R}\right)^2 \pi^2 \qquad (V_i = 4.55 \text{ m/sec})$$

/.

FORMULA II.2.16 - INDUCED VELOCITY AT A POINT M (r, Φ, β_M)
BY AN HELIX VORTEX ISSUING FROM A BLADE AT (r_1, Ψ_1)

$$(II.2.16) \qquad \frac{dV_{iz}}{dr_1} = \frac{1}{4\pi} \int_{\tau=\infty}^{\tau=0} \frac{\partial \Gamma}{\partial r_1}\left[r_1, (t_1-\tau)\right] \frac{n}{\left[d^2\right]^{3/2}} \, d\tau.$$

$$\begin{aligned}
d^2 = {} & r^2 + r_1^2 - 2 r r_1 \cos\left[\Psi_1 - \omega\tau - \Phi\right] + \left[V\cos\alpha\,\tau - \int_0^\tau V_{ix}\, d\tau\right]^2 + \left[V\sin\alpha\,\tau + \int_0^\tau V_{iy}\, d\tau\right]^2 \\
& + 2\left[r_1 \cos(\Psi_1 - \omega\tau) - r\cos\Phi\right]\left[V\cos\alpha\,\tau - \int_0^\tau V_{ix}\, d\tau\right] \\
& + 2\left[r_1 \sin(\Psi_1 - \omega\tau) - r\sin\Phi\right]\left[\int_0^\tau V_{iz}\, d\tau\right] \\
& + \left[r\beta_M - r_1\beta(t_1-\tau)\right]^2 + \left[r\beta_M - r_1\beta(t_1-\tau)\right]\left[V\sin\alpha\,\tau + \int_0^\tau V_{iz}\, d\tau\right]
\end{aligned}$$

$$\begin{aligned}
n = {} & r r_1 \omega \cos\left[\Psi_1 - \omega\tau - \Phi\right] - r_1^2\omega - r_1\omega\cos(\Psi_1 - \omega\tau)\left[V\cos\alpha\,\tau - \int_0^\tau V_{ix}\, d\tau\right] \\
& + r_1 \cos(\Psi_1 - \omega\tau) V_{iy} - r_1 \sin(\Psi_1 - \omega\tau)\left[\omega \int_0^\tau V_{iy}\, d\tau + V\cos\alpha - V_{ix}\right] \\
& + r\sin\Phi\left[V\cos\alpha - V_{ix}\right] + r\cos\Phi\, V_{iy} + V_{iy} V\cos\alpha\,\tau - V_{iy}\int_0^\tau V_{ix}\, d\tau + V_{ix}\int_0^\tau V_{iy}\, d\tau
\end{aligned}$$

For a whole period, i.e. for one complete loop, the following values are respectively obtained for A $\left(\frac{1}{\text{meter}}\right)$

	A . $\frac{1}{\text{meter}}$	error for one period	
1	9.05	0	0 %
2	10.7	+ 1.65	18 %
3	9.7	+ 0.65	7 %

For a quarter-period , i.e. for the first quarter-loop , we have

	A. $\frac{1}{\text{meter}}$	error for the first 1/4	
1	4.5	0	0
2	4.5	0	0
3	4.0	- 0.5	- 12 %

If the quarter helix be replaced by a straight line half-vortex issuing from the same point (0.8 R) and having the same intensity, we have

$$V_i = \frac{\Gamma}{4\pi} \cdot \frac{1}{(0.8-0.5)R} \left[\cos\varphi\right]$$

$$\varphi \longrightarrow 0$$

The value of A' then becomes :

$$A' = 4.45 \text{ m}^{-1}$$

From the calculations it can be asserted that :

a) The effect of a quarter helix upon its own blade can be replaced either by a quarter circle contained in the plane of the disc or by a straight half-vortex (Figure 131b).

b) The effect of a complete helix loop can be replaced by a circle located beneath the swept disc, one-half period from it . From the processing made of the visualizations, one is led to situating the circles in the manner indicated below, in order to take into account the deformation sustained by the vortices :

/...

- When calculating the effects of the helix vortices on the blade A, the effect of the latter's marginal helix vortex can be replaced by that of a circle located a quarter period beneath the disc.

- To study the effect of the first half of the loop, the half-loop in question can be replaced by a semi-circle situated in the plane of the disc. This gives a good approximation.

- To study the effect of the helix vortex of blade B on blade A, the effect of the first loop can be replaced by that of a circle located $\frac{3}{4}T$ beneath the swept disc (Figure 131a).

The effect of the remaining helix loops can be replaced by circles located at distances measured in half-periods..

2.254 - Velocity induced on the blade A by the first loops of the marginal helix vortices from blade A and blade B.

The circulation of these vortices is constant. The graphical integration was performed for forward flight ($\mu = 0.20$) in the following two cases :

Case (a) : Blade A is in the position $\psi = 0$ and the induced velocity is calculated spanwise.

Case (b) : Blade A occupies different azimuthal positions, the induced velocity being calculated for a fixed point P ($r = 0.75\ R$).

Characteristics are as follows:

$b =$ 2 blades

$R = 0.746$ meter

$\omega = 111$ rad/sec

$\mu = 0.2$

$\Gamma_o = 0.927$ sq.m/sec

$$\lambda = \frac{V_i}{\omega R} = 0.0765$$

$\alpha = 0$

$U = \omega R = 83$ m/s

/.

Case (a)

The induced velocity at the point $\Psi = 0$ is given by the table below :

Table 2.14

$\bar{r} = \frac{r}{R}$	ΔVi_A	ΔVi_B	Total Vi
-	m/s	m/s	m/s
0	0	0.4	1.0
0.75	0.625	0.555	1.18
0.95	2.0	3.0	5.0

It may be noted that the effects arising from the two blades are substantially be same ($\Psi = 0$).

Case (b)

Velocity induced at the point r = 0.75 R with Ψ assuming 16 different positions.

The result is given in the table on the following page and is illustrated graphically in Figure 132.

It may be noted that the constant -circulation helix give variable induced velocities.

The effect produced by the helix of blade A is always sizeable.

The effect of the helix from blade B is particularly marked in the second rear half of the swept circle.

2.255 - Practical estimation of infinity

Number of helix periods necessary. This study was made for the following case :

$b = 2$

$\Gamma_o = 0.927$ sq.m/sec (constant)

$R = 0.746$ m

$\mu = 0.2$

$\omega = 111$ rad/sec

$\lambda = 0.0763$

$\alpha = 0$

Table 2.15

ψ	ΔV_i (A)	ΔV_i (B)	V_i total
rad	m/s	m/s	m/s
0	0.625	0.555	1.18
$\frac{\pi}{6}$	0.92	0.43	1.35
$\frac{\pi}{4}$	0.895	0.55	1.45
$\frac{\pi}{3}$	0.72	0.78	1.5
$\frac{\pi}{2}$	0.288	0.752	1.04
$\frac{2\pi}{3}$	0.35	- 0.10	0.25
$\frac{3\pi}{4}$	0.316	- 0.086	0.23
$\frac{5\pi}{6}$	0.41	- 0.116	0.294
π	0.485	- 0.033	0.452
$\frac{7\pi}{6}$	0.465	- 0.007	0.458
$\frac{5\pi}{4}$	0.59	- 0.05	0.531
$\frac{4\pi}{3}$	0.595	0.035	0.63
$\frac{3\pi}{2}$	0.70	0.035	0.735
$\frac{5\pi}{3}$	0.73	0.6	1.33
$\frac{7\pi}{4}$	0.73	0.697	1.425
$\frac{11\pi}{6}$	0.72	0.74	1.46
2π	0.625	0.555	1.18

A graphical calculation was made of the velocity induced at the point r = 0.75 and $\Psi = 0$ by the helix vortices up to the second loop; beyond this, the asymptotic formula deduced from the formula (II.2.16) given previously was adopted.

$$V_i = \frac{\Gamma_0}{4\pi R} \frac{2}{(\mu^2 + \lambda^2)^{3/2}} \int_{\omega\tau \to \infty}^{\omega\tau = 6\pi} \frac{\lambda - \frac{3}{2} \frac{\mu^2}{\mu^2+\lambda^2} \cos^2 \omega\tau \, d(\omega\tau)}{(\omega\tau)^3}$$

The numerical results obtained are given in the following table 2.16.

Table 2.16

	Helix A V_i m/s	Helix B V_i m/s	Total V_i m/s	%
First period	0.625	0.555	1.1800	77.5
Second "	0.108	0.17	0.2780	18.2
Other periods	0.033	0.033	0.0661	4.3
Total			1.5241	100

The first two periods give the induced velocity with an approximation of 4 %.

Let us now seek the location of the downstream infinity for $\mu = 0.2$.

The first period gives 77.5 % of the total induced velocity.

The first two periods give the induced velocity at 4 % near of the total induced velocity.

Therefore the second loop must be located at a distance (Figure 131c) :

$$A_0 A_2 = V_0 \times 2T$$

where T is the period.

We have :

$$\mu = \frac{V \cos\alpha}{\omega R} = 0.2 \qquad T = \frac{2\pi}{\omega}$$

whence:

$$A_0 \; A_2 = 1.5 \cdot 2 R$$

The practical infinity can consequently be defined as follows :

1) Depending on the value of the advance ratio and upon the disc loading λ , n helix periods will be taken such that :

$$n \geqslant \frac{3}{2\pi} \frac{1}{\sqrt{\mu^2 + \lambda^2}}$$

2) The practical downstream infinity is located at a distance of 1.5 times the rotor diameter.

This result can be compared either to half a straight line vortex (Figure 133) or to a solenoid.

2.26 - Conclusion

These basic considerations will be used in approximate methods of calculation exposed in the following chapter.

3 - PROPOSED METHOD OF EVALUATING THE AERODYNAMIC LIFT OF A HELICOPTER BLADE

3.1 - Hovering

3.11 - Setting in equation form

Taking the case of a two-bladed rotor, the local circulation Γ_A (r) at a given point on the blade A is provided by the expression

(III.1.17) $$\Gamma_{A(r)} = \frac{1}{2}\omega r c \frac{dC_L}{di}\left[\theta_c - \frac{V_{i_A}}{\omega r} - \frac{V_{i_B}}{\omega r}\right]$$

where V_{i_A} and V_{i_B} are the velocities induced on a station point of blade A by the free vortices issuing from blade A and blade B.

The velocities V_{i_A} and V_{i_B} are normal to the blade, no account having been taken of the radial induced velocities.

The expressions for the induced velocities V_{i_A} and V_{i_B} are computed from a helix vortex having issued from a point r_1 on the blade (A or B) τ seconds before (see Figure 134 , formulae III.1.18 and III.1.19).

The variables $\omega\tau$, τ , and r_1 are integration variables. V_f designates the vertical velocity of the flow beneath the disc, generated by the free and connected vortices.

Equation (III.1.17) may then be written :

(III.1.20) $$\Gamma_A(r) = \frac{1}{2}c\frac{dC_L}{di}\omega r\theta_c - \frac{c}{2}\frac{dC_L}{di}\int_{r_0}^{R}\frac{\partial\Gamma_A}{\partial r_1}H_A(r,r_1)dr_1 - \frac{c}{2}\frac{dC_L}{di}\int_{r_0}^{R}\frac{\partial\Gamma_B}{\partial r_1}H_B(r,r_1)dr_1$$

In theory, to resolve this equation, one may postulate:

$$\Gamma(r) = \sum_{n=1}^{n} \gamma_n \varphi_n(r)$$

$$\varphi_n(r_0) = \varphi(R) = 0$$

where φ_n (r) is a sequence of known functions which satisfy the limit conditions, and

γ_n are unknown constant coefficients to be determined.

To this end, n points

$$r = r_j \ldots\ldots \quad (j = 1, \ldots\ldots n)$$

are taken on the blade, writing that equation III.1.20

/.

is satisfied at those n points, which in turn gives n linear relations containing $\gamma_1 \ldots\ldots \gamma_n$ as unknowns.

This method would call for the calculation of 2 n^2 double integrals ($\omega\tau$ and r_1).

These are the integrals of (III.1.18), in which $\frac{\partial \Gamma}{\partial r_1}$ is replaced by n φ_n (r_1) functions. These integrals contain a fixed parameter $V_f T$ such that $(V_f T/R)^2 = 4\pi^2 F_M / 2\rho A U^2$ and n parameters $r = r_j$ with (j = 1 ----- n).

A good approximation with this method gives n equal to 5 or 6, which in turn leads to research for an approximating method.

3.12 - Approximate expressions for the cores N_A and N_B

The core N_A reveals the discontinuity for

$$r = r_1$$
$$\omega\tau \longrightarrow 0$$

To isolate this discontinuity, the first half helixes of the vortex $0 \leqslant \omega\tau \leqslant \pi$ must be separated from the core N_A.

(III.1.21) $$N_A = \Big[N_{A_0} \Big]_{\omega\tau = 0}^{\omega\tau = \pi} + \Big[N'_A \Big]_{\omega\tau = \pi}^{\omega\tau \to \infty}$$

Let us replace these first half-helixes by semi-circles ($0 \leqslant \omega\tau \leqslant \pi$ and $V_f = 0$) located in the plane of the swept disc.

The expression for the velocity induced by a vortex circle has been given by Lamb. Castles and Deleew have tabulated this velocity numerically.

In connection with the method under discussion, the following approximate numerical expression has been established for a vortex semi-circle :

(III.1.22) $$N_{A_0}\Big|_0^{\pi} = \frac{1}{5.7} \left[\frac{0.5}{r - r_1} - \frac{0.5}{r - r_1} - \frac{r_1}{r^2 + 2.35\, r_1^2} \right]$$

Here, the first term predominates. The first two terms can be interpreted as two half-straight-line vortices, i.e:

/.

(III.1.23) $$\frac{1}{4\pi}\left[\frac{1}{r-r_1} - \frac{1}{r+r_1}\right].$$

It is to be noted that the discontinuity is of the same nature as for a fixed wing.

The remaining core N'_A and the core N_D will now be dealt with simultaneously.

These cores are double integrals with respect to r_1 and τ.

Proceeding now with this double integration, that with respect to r_1 can be performed by applying the theorem of averages :

$$\int_a^b f(u)\,\varphi(u)\,du = f(x)\int_a^b \varphi(u)\,du$$

$$x = a + \theta\,(b-a) \qquad 0 \leqslant \theta \leqslant 1$$

thereby enabling the marginal vortices observed in the wind-tunnel to be introduced.

The integration with respect to τ is performed by replacing the single variable τ by two independent variables : a linear variable $z = V_f\,\tau$, and an angular one $\omega\tau$. This method entails replacing the helixes by a circle and a solenoid.

Integrating with respect to r_1 by applying the theorem of averages , we have :

(III.1.24) $$\left\{\begin{array}{l} \displaystyle\int_{r_0}^{R} \frac{\partial\Gamma}{\partial r_1}(r_1)\,N(r,r_1)\,dr_1 = \int_{r_0}^{r_M} + \int_{r_M}^{R} \\ \displaystyle\int_{r_0}^{r_M} \frac{\partial\Gamma}{\partial r_1}(r_1)\,N(r,r_1)\,dr_1 = N(r,r_1)\int_{r_0}^{r_M} \frac{\partial M}{\partial r_1}(r_1)\,dr_1 \\ \displaystyle\int_{r_M}^{R} \frac{\partial\Gamma}{\partial r_1}(r_1)\,N(r,r_1)\,dr_1 = N(r,r_1)\int_{r_M}^{R} \frac{\partial\Gamma}{\partial r_1}(r_1)\,dr_1 \end{array}\right.$$

whence, since $\Gamma_{(o)} = \Gamma_{(R)} = 0$ we have

/.

$$\int_{r_0}^{r_M} \frac{\partial \Gamma}{\partial r_1}(r_1)\, N(r, r_1)\, dr_1 = N(r, x_1)\, \Gamma_M(r_M)$$

(III.1.25) $$\int \frac{\partial \Gamma}{\partial r_1}(r_1)\, N(r, r_1)\, dr_1 = -N(r, x_2)\, \Gamma_M(r_M)$$

$$\begin{cases} x_1 = r_0 + \varepsilon_1 (r_M - r_0) & 0 < \varepsilon_1 < 1 \\ x_2 = r_M + \varepsilon_2 (R - r_M) & 0 < \varepsilon_2 < 1 \end{cases}$$

The equations require elucidation of the following three unknowns:

1) - Γ_M : value of the maximum circulation intensity

2) - $x_1(\varepsilon_1)$

3) - $x_2(\varepsilon_2)$

Knowledge of r_M is not necessary.

Γ_M and r_M can only be estimated, so that one must proceed by successive approximations.

Though no proof can be offered, it will be assumed that the abscissae x_1 and x_2 correspond to the marginal vortices observed in the wind tunnel.

- Integrating with respect to $\omega\tau$. The expressions for the cores N'_A and N_B contain terms in $V_f\,\tau$ and in cos $\omega\tau$, sin $\omega\tau$, thereby excluding the use of the usual simple functions. $V_f\,\tau$ and $\omega\tau$ will be treated as two independent variables.

  The first helix loop of the vortex, issuing from B ($0 \leqslant \omega\tau \leqslant 2\pi$) (see III.1.18) will be replaced by a circle in a horizontal plane located beneath the blade A, at a distance equal to $V_f\ T/2$. The first helix loop of the vortex issuing from A, i.e.

$$\pi \leqslant \omega\tau \leqslant 3\pi$$

  will be replaced by a circle in a horizontal plane located beneath the blade A, at a distance equal to $V_f T$. These vortex circles as a whole will be termed "recent vortices". The velocity induced by these circles is given in the tables compiled by Castles and De Leew.

- The other helix vortices :

Vortices A $3\pi \leqslant \omega\tau \to \infty$

Vortices B $2\pi \leqslant \omega\tau \to \infty$

will be treated as solenoids.

Let

$$\frac{\partial \Gamma}{\partial r_1}(r_1) \tag{III.1.26}$$

be replaced by $\frac{\partial}{\partial z}\frac{\partial \Gamma}{\partial r_1} dz$ (see equation III.1.18) by postulating :

$$\frac{\partial}{\partial z}\frac{\partial \Gamma}{\partial r_1} = \frac{1}{V_f T}\frac{\partial \Gamma}{\partial r_1} \quad \text{and} \quad dz = d(V_f \tau)$$

This amounts to saying that a helix (or circle) $\frac{\partial \Gamma}{\partial r_1}$ has been distributed in uniform fashion over a cylindrical surface of height $V_f T$ (1/2 $V_f T$ on either side of the initial helix).

The integration limits are then as follows :

for $\omega\tau$: 0 and 2π

for $z = V_f\tau$: (given in table below).

TABLE 3.18

Vortex	$(V_f\tau)_1$	$(V_f\tau)_2$
A	$2V_fT = \frac{3}{2}V_fT + \frac{1}{2}V_fT$	∞
B	$\frac{3}{2}V_fT = V_fT + \frac{1}{2}V_fT$	∞

Integration is now possible and has already been performed by Callaghan and Maslen. Equations 10, 11 and 12 in their study, transposed into the annotations used here, give the following :

$$\int_{r_0}^{R}\frac{\partial \Gamma}{\partial r_1} H(r,r_1)\,dr_1 = -\int_{r_0}^{R}\frac{\partial \Gamma}{\partial r}\frac{dr_1}{4V_fT}\left[\frac{(V_f\tau)k}{\pi\sqrt{r\,r_1}}K(k)\frac{(r_1-r)V_f\frac{3}{2}T}{|(r_1-r)V_f\frac{3}{2}T|}\lambda_0(\varphi,k)\right]_{V_f\tau_1}^{V_f\tau_2} \tag{III.1.27}$$

where K is a complete elliptical integral of the first species, the modulus of which is :

(III.1.28) $$k^2 = \frac{4 r r_1}{(V_f \tau)^2 + (r+r_1)^2}$$

The approximate value of K for k values in the region of unity is :

$$K(k) \sim L_n \frac{4}{k'} \qquad (k'^2 = 1 - k^2)$$

(Tables are available).

$\lambda_0(\varphi, k)$ is the Heuman function (Byrd's table).

For k = 0, this reduces to sin φ , and for k = 1 to $\frac{2}{\pi}\varphi$.

The argument φ is given by :

(III.1.29) $$\tan\varphi = \frac{V_f \tau}{r_1 - r}$$

The equation for the circulation Γ_A (III.1.17) then becomes :

(III.1.30) $$\Gamma_A(r) = \frac{1}{2} c \frac{dC_L}{di} \omega r \theta_c - \frac{1}{2} c \frac{dC_L}{di} \left[V_{CA} + V_{CB} + V_{SA} + V_{SB}\right]$$
$$- \frac{1}{2} c \frac{dC_L}{di} \int_{r_0}^{R} \frac{\partial \Gamma}{\partial r_1} \left[\frac{dr_1}{11.4}\right] \left[\frac{1}{r - r_1} - \frac{1}{r + r_1} - \frac{2 r_1}{r^2 + 2.35 r_1^2}\right]$$

where V_{CA} and V_{CB} are velocities induced by the four recent vortex circles issuing from blades A and B (outer and inner), and V_{SA} and V_{SB} are the velocities induced by the four solenoids.

Let $$\Gamma_M C(r_1, x, z)$$

designate the velocity induced at a point ($r, z = 0$) on the blade A by a vortex circle of intensity Γ_M .

The radius of the vortex circle is x ($x = x_1$ and x_2), located at a distance z beneath the swept disc such that .

$$z = V_f \frac{T}{2} \text{ for } \Gamma_B \quad \text{and} \quad V_f T \text{ for } \Gamma_A$$

The function C is equal to the quotient of a function ./.

tabulated by Castles and De Leew $(\frac{rV_z}{\Gamma})$ divided by the radius x (x_1 and x_2) of the vortex circle.

The table below shows the difference between the annotations used here and those used by Castles and De Leew:

TABLE 3.19

Designation	Present Text	Castles and De Leew
Radius of vortex circle	$x = x_1$ or x_2 .	r
Vertical distance of a point (P) from vortex circle	$Z = V_f \frac{n}{2} T$	z_r
Horizontal distance of a point (P) from vortex circle	r	x_r
Velocity induced at a point (P) by a vortex circle of intensity	$\Gamma_M \, C\,(r, x, z)$	V_z
Induced velicity referred to vortex intensity	$C\,(r, x, z)$	$\frac{V_z}{\Gamma}$
Formula of Castles and De Leew	$x\,C\,(r, x, z)$	$\frac{rV_z}{\Gamma}$

In this case, the velocities V_{CA} and V_{CB} are expressed by :

(III.1.31)
$$V_{CA} = \Gamma_M \left[C\,(r, x_2, V_f \tfrac{T}{2}) - C\,(r, x_1, V_f \tfrac{T}{2}) \right]$$
$$V_{CB} = \Gamma_M \left[C\,(r, x_2, V_f T) - C\,(r, x_1, V_f T) \right]$$

Let S_∞ and S_z be taken to designate the velocities induced at a point on the blade A by a solenoid of radius x, the density of the vortex intensity of which is :

$$\frac{\Gamma_M}{V_f T} = 1$$

S_∞ extends from the swept disc to upstream infinity

/.

S_z extends downwards from the swept disc over a distance z .

In the case of the infinite solenoid, we have :

$$S_\infty = \begin{cases} -\frac{1}{2} \text{ if } r < x \\ 0 \text{ if } r > x \end{cases}$$

In the case of the finite solenoid, the Callaghan and Maslen result is obtained :

(III.1.32)
$$\begin{cases} k^2 = \dfrac{4xr}{(\frac{n}{2} V_f T)^2 + (x+r)^2} \\ S_z(r, x, \frac{n}{2} V_f T) - \frac{1}{4} \dfrac{V_f \frac{n}{2} T k}{\pi \sqrt{rx}} K(k) + \frac{1}{4} \dfrac{(x-r)\frac{n}{2} V_f T}{(x-r)\frac{n}{2} V_f T} \lambda_0(\varphi, k) \\ \tan\varphi = \dfrac{\frac{n}{2} V_f T}{(x-r)} \end{cases}$$

Whence, the velocities V_{SA} and V_{SB} are given by :

(III.1.33)
$$\begin{cases} V_{SA} = \dfrac{\Gamma_M}{V_f T} \Big[\big[S_\infty(r, x_2) - S(r, x_2, V_f T) \big] \\ \qquad - \big[S_\infty(r, x_1) - S(r, x_1, V_f T) \big] \Big] \\ V_{SB} = \dfrac{\Gamma_M}{V_f T} \Big[\big[S_\infty(r, x_1) - S(r, x_2, \frac{n}{2} V_f T) \big] \\ \qquad - \big| S_\infty(r, x_1) - S(r, x_1, \frac{n}{2} V_f T) \big] \Big] \end{cases}$$

The functions K and λ_0 (φ, k) exist in tabulated form.

3.13 - Estimation of V_f , Γ_M , r_M , x_1 and x_2

In the visualization tests, the basic length used was

$$V_f \quad T \quad .$$

$T = \dfrac{2\pi}{\omega}$ is the period of rotation, and

V_f the mean induced velocity, given by :

$$V_f = \sqrt{\frac{F_H}{2\rho A}}$$

F_H was measured during the tests and was therefore known at all times.

/.

In applying the calculation method, recourse may be had to the momentum theorem:

$$4\pi r V_f^2 = \frac{b.C}{2} (\omega r)^2 \frac{dC_L}{di} \left(\theta - \frac{V_f}{\omega r}\right) \qquad \text{(III.1.35)}$$

on the assumption that V_f is being calculated for $r = 0.5\ R$.

Estimation of Γ_M (r_M). The position of the circulation maximum must be calculated by successive approximations when applying the method. To this end, a first approximation is necessary, and it will suffice to take the circulation at r = 0.9 R on the basis of the momentum equation.

A knowledge of r_M is not essential.

Estimation of x_2 . Beneath the blade, the outer marginal helix reveals a marked contraction which is a function of the load on the disc. To simplify calculations, one may take x = R for the outer circles and solenoids (A and B).

Estimation of x_1 . The inner circles and solenoids (A and B) can be located in the following manner : in the case of the solenoid, the radius of the marginal inner helix increases markedly below the disc. In view of the variation in the circulation (see Section 2), it would be logical to estimate the radius as :

$$r = r_0 + \frac{r_M - r_0}{2}$$

i.e., halfway between the inner extremity of the blade and the point where circulation is at a maximum. For simplification purposes, the radius of the inner solenoid is taken as half that of the blade.

With regard to the inner circles, their radius is taken as :

$$r_0 + \frac{R/2 - r_0}{2}$$

3.14 - Application of the proposed method

It is now required to solve equation III.1.30.

Γ_A is the unknown function, while Γ_M is known approximately only. The remaining values are either known or estimated , as stated in the previous paragraph.

/.

Equation III.1.30 may be written in the following form :

$$\Gamma_{(r)} + \frac{1}{2} c \frac{dC_L}{di} \int_{r_0}^{R} \frac{\partial \Gamma}{\partial r_1}(r_1) \frac{dr_1}{4\pi(r-r_1)} = \left[T_1(r) + \Gamma_M T_2(r) \right] \frac{c_0}{2} \frac{dC_L}{di} \omega R \qquad \text{(III.1.36)}$$

The terms T_1 (r) and T_2 (r) are known.

For a given Γ_{M_0}, the function Γ (r) must be found. Having determined it, the Γ(r)curve is plotted and the Γ_{M_1} thus found compared with the previous Γ_{M_0}, thereby providing a better approximation Γ_{M_2}.

This process is pursued until a Γ_{M_n} is obtained which is little different from $\Gamma_{M_{n+1}}$.

It is now proposed to show how Γ(r) is found and how it is then modified.

- Resolution of the equation. Obtainment of Γ(r)

Changing the variable, we have :

$$\text{(III.1.37)} \qquad \begin{cases} r = r_0 + \frac{R - r_0}{r} (1 - \cos\varphi) \\ \varphi = 0 \qquad r = r_0 \\ \varphi = \pi \qquad r = R \end{cases}$$

The unknown circulation Γ_A takes the form :

$$\text{(III.1.38)} \qquad \begin{cases} \Gamma_A = \frac{1}{2} c_0 \frac{dC_L}{di} \omega R \sum_{n=1}^{n} \gamma_n \sin n\varphi \\ \varphi = 0 = \pi \qquad r = 0 \end{cases}$$

where c_0 is the reference chord, such that c_0= constant.

The unknowns are the dimensionless coefficients γ_n.

Performing the change of variable in equation III.1.36, integration can be carried out easily by using the well known relation :

$$\int_0^{\pi} \frac{\cos n\varphi_1 \, d\varphi}{\cos\varphi_1 - \cos\varphi} = \pi \frac{\sin n\varphi}{\sin\varphi}$$

Dividing both sides of the equation by $\frac{1}{2} C_o \frac{dC_L}{di} \omega R$ we have :

$$\sum_{n=1}^{n} \gamma_n \sin n\varphi + \frac{1}{2} C \frac{dC_L}{di} \frac{\pi}{11.4} \sum_{n=1}^{n} \gamma_n \, n \, \frac{\sin n\varphi}{\sin \varphi}$$

(III.1.39)

$$= T_1 (\varphi) + \Gamma_M \, T_2 (\varphi) = E (\varphi)$$

n = 6 was chosen to represent the function Γ . One may therefore write that the equation is satisfied for the following values of φ.

φ = 30°, 36°, 45°, 60°, 72°, 108°,
120°, 135°, 144° and 150°

The next step is to calculate the values of the functions T_1 (φ) and T_2 (φ) for the ten values of the variable .

This gives 10 linear equations in γ_n (n = 1 ------ 6).

A number of elementary transformations lead to a simple system of equations, given in table 3.20.

Should it be desired to modify Γ_M , the expressions T_1 (φ) and T_2 (φ) do not change; only E (φ) varies, but resolution of the system III.1.41 can be accomplished quickly.

The major part of the labor resides in calculating T_1 (φ) and T_2 (φ). Tables would undoubtedly facilitate this work.

The expressions for the lift and the aerodynamic moment at the blade root (a = 0) are given by the following expressions :

$$\begin{cases} \dfrac{dL}{dr} = \rho \omega r \Gamma \\[2ex] \qquad = \dfrac{\rho}{2} C_o \dfrac{dC_L}{di} (\omega R) \left(\dfrac{R - r_o}{2} \right) \omega \displaystyle\sum_{n=1}^{n} \gamma_n \sin n\varphi \, (1 + 2 \bar{\bar{r}}_o - \cos\varphi) \\[2ex] \dfrac{dM}{dr} = \dfrac{\rho}{2} C_o \dfrac{dC_L}{di} (\omega R) \left(\dfrac{R - r_o}{2} \right)^2 \omega \displaystyle\sum_{n=1}^{n} \gamma_n \sin n\varphi \, (1 - 2 \bar{\bar{r}}_o - \cos\varphi) \end{cases}$$

$$r = r_o + \frac{R - r_o}{2} \; (1 - \cos\varphi)$$

$$dr = \frac{R - r_o}{2} \sin\varphi \, d\varphi$$

$$\bar{\bar{r}}_o = \frac{r_o}{R - r_o}$$

Integrating, we have :

$$L = \frac{\rho}{2} c_o \frac{dC_L}{di} (\omega R)^2 R \left(\frac{R - r_o}{2R}\right)^2 \frac{\pi}{2} \left[\left(1 + \frac{2 r_o}{R - r_o}\right) \gamma_1 - \frac{1}{2} \gamma_2 \right]$$

(III.1.40)

$$M = \frac{\rho}{2} c_o \frac{dC_L}{di} (\omega R)^2 R^2 \left(\frac{R - r_o}{2R}\right)^3 \frac{\pi}{2} \left\{ \gamma_1 \left[\left(1 + \frac{2 r_o}{R - r_o}\right)^2 + \frac{1}{4} \right] - \right.$$

$$\left. - \gamma_2 \left(1 + \frac{2 r_o}{R - r_o}\right) + \frac{\gamma_3}{4} \right\}$$

/.

TABLE 3.20

RESOLUTION OF EQUATION (III.1.39)

The unknowns are γ_1 ---------------- γ_6

(III.1.41)

$$\gamma_1 0.58779 \left[1^{(\circ)} + \frac{k}{0.58779}\right] + \gamma_3 0.95106 \left[1 + \frac{3k}{0.58779}\right] = \frac{E(36) + E(144)}{2}$$

$$\gamma_1 0.95106 \left[1 + \frac{k}{0.95106}\right] - \gamma_3 0.58779 \left[1 + \frac{3k}{0.95106}\right] = \frac{E(72) + E(108)}{2}$$

$$\gamma_1 0.866 \left[1 + \frac{k}{0.866}\right] - \gamma_5 0.866 \left[1 + \frac{5k}{0.866}\right] = \frac{E(60) + E(120)}{2}$$

$$\gamma_2 0.866 \left[1 + \frac{2k}{0.5}\right] + \gamma_4 0.866 \left[1 + \frac{4k}{0.5}\right] = \frac{E(30) - E(150)}{2}$$

$$\gamma_2 0.866 \left[1 + \frac{2k}{0.866}\right] - \gamma_4 0.866 \left[1 + \frac{4k}{0.866}\right] = \frac{E(60) + E(120)}{2}$$

$$\gamma_2 \left[1 + \frac{2k}{0.707}\right] - \gamma_6 \left[1 + \frac{6k}{0.866}\right] = \frac{E(45) - E(135)}{2}$$

$$k(\varphi) = \frac{1}{2} c \frac{d C_L}{di} \cdot \frac{r}{R - r_o} \cdot \frac{\pi}{11.4}$$

(°) Note : For simplified methods, 1 must be replaced by $1 + \frac{1}{2} c \frac{dC_L}{di} \frac{1}{V_f T}$

3.15 - Example of numerical application

3.151-The general equation III.1.30 will now be verified by comparing the experimental results of John P. Rabbott (see references) to the theoretic data resulting from this equation, rotor characteristics being the same in both cases.

The general equation, as indicated before, is as follows:

(III.1.30) (see page 69)

$$\left\{\begin{aligned} \Gamma_A(r) &= \frac{1}{2}c\frac{dC_L}{di}\omega r\theta_c - \frac{1}{2}c\frac{dC_L}{di}\left(V_{CA}+V_{CB}+V_{SA}+V_{SB}\right) \\ &- \frac{1}{2}c\frac{dC_L}{di}\int_{r_0}^{R}\frac{\partial\Gamma}{\partial r_1}\left(\frac{dr_1}{11.4}\right)\left(\frac{1}{r-r_1}-\frac{1}{r+r_1}-\frac{2r_1}{r^2+2.35\,r_1^2}\right)\end{aligned}\right.$$

The numerical calculation of the different terms of this equation shows that the terms in $1/r+r_1$ and $\frac{2r_1}{r^2+2.35\,r_1^2}$ may be neglected being indeed ten times smaller than the term in $1/r-r_1$ when connected whith sin φ and hardly reaching $\frac{1}{10000}$ of its value when connected with sin 3φ, 4φ - - - 6φ.

Equation III.1.30 may then be written as follows :

$$\Gamma_A(r) = \frac{1}{2}c\frac{dC_L}{di}\omega r\theta_c - \frac{1}{2}c\frac{dC_L}{di}\left(V_{CA}+V_{CB}+V_{SA}+V_{SB}\right) - \frac{1}{2}c\frac{dC_L}{di}\int_{r_0}^{R}\frac{\partial\Gamma}{\partial r_1}\cdot\frac{dr_1}{11.4}\cdot\frac{1}{r-r_0}$$

Its resolution will be made with the help of equations III.1.41.

J. Rabbott's curve $\frac{dL}{dr} = f(\bar{r})$ was transformed in a curve $\Gamma = f(\varphi)$, φ being our variable in the Γ equation.

The expressions permitting this transformation are :

$$\frac{dL}{dr} = \rho\omega r\Gamma \qquad \text{and}$$

$$\bar{r} = \bar{r}_0 + \frac{1-\bar{r}_0}{2}(1-\cos\varphi) \qquad \text{with } \bar{r}_0 = 0.18.$$

/.

The transformation of J. Rabbott's curve in curve $\Gamma = f(\varphi)$, which will be our reference of comparison, is given in Table 3.22 . See also Fig.135.

3.152 - Equation resolution hypotheses

The characteristics of the rotor experimented by J. Rabbott are given in Table 3.21.

These same characteristics will be introduced in the considered equations.

Flow velocity V_f, the knowledge of which is necessary for computation of V_{CA} , V_{CB}, V_{SA} and V_{SB}, is given by the momentum equation $V_f = f(\bar{r})$, at $\bar{r} = 0.5$ (fig.136).

The vortices are located, as indicated in paragraph 3.14, as follows :

$$x_2 = R$$

$x_1 = 0.36\ R$ for V_{CA} and V_{CB} and

$x_1 = 0.5\ R$ for V_{SA} and V_{SB} .

For a first approximation it is necessary to know an order of magnitude of Γ_M .

In the considered case $\Gamma_M = 11$ sq.m/sec will be selected , this being the value of the momentum equation for $\bar{r} = 0.9$ (see FIG.136).

3.153 - Equation computation

Using Castles and De Leew Tables for computing V_{CA} and V_{CB} and Byrd Tables for computing V_{SA} and V_{SB} it is possible to determine the second member of the general equation III.1.41.

Values of $\bar{r}\theta_c$, $\frac{V_{SA}}{\Gamma_M}$, $\frac{V_{SB}}{\Gamma_M}$, $\frac{V_{CA}}{\Gamma_M}$ and $\frac{V_{CB}}{\Gamma_M}$ are given in Table 3.23.

These values make it possible to determine E (φ) and E ($\pi - \varphi$) such as :

$$E(\varphi) = T_1(\varphi) - |\Gamma_M|\ T_2(\varphi)$$

with $T_1(\varphi) = \bar{r}\theta_c$ and

$$T_2(\varphi) = \frac{1}{\omega R} \frac{(V_{SA} + V_{SB} + V_{CA} + V_{CB})}{\Gamma_M}$$

./.

TABLE 3.21

Characteristics of rotor experimented by J.Rabbott

Item	Dimension or magnitude
Blade radius	$R = 2.30$ m = 7.5 ft.
Blade tip speed	$\omega R = 151$ m/sec = 496 ft/sec.
Rotor angular velocity	$\omega = 65.5$ rad/sec.
Rotor Solidity	$\sigma = 0.097$
Blade chord	$c = 0.35$ m = 14 inches
Thrust coefficient	$C_T = 0.00518$
Blade coefficient pitch angle	$\theta_c = 9°2 = 0.161$ rad.

TABLE 3.22

$\bar{r}$	$\frac{dL}{dr}$ lb/inch	$\frac{dL}{dr}$ Kg/m	Γ sq.m/sec	φ degree
0.18	0	0	0	0
0.30	0.9	16.1	2.84	45
0.56	2.6	46.5	4.40	85
0.75	4.8	86	6.10	113
0.85	7	125	7.80	129
0.90	8.1	145	8.50	139
0.95	7.1	127	7.1	151
1.00	0	0	0	180

/.

Each term such as V_{SA}------etc---- is decomposed into inner and outer V_{SA}, say, along x_1 and x_2 .

In Table 3.24 are given the values of equations second members, that is $E(\varphi) \pm E(\pi - \varphi)$ and in Table 3.25 the derived equations, in a form still admitting Γ_M as parameter.

The k coefficient of III.1.41 equations is equal to 0.287

$$k = \frac{c}{R - r_0} \quad \frac{dC_L}{di} \quad \frac{\pi}{11.4} = 0.287$$

In figures 137 and 138 are indicated the variations of V_{CA}, V_{CB}, V_{SA} and V_{SB}, versus φ .

In Table 3.26 are given the values of γ_1------ γ_6 as a function of Γ_M .

3.154 - Determining $\Gamma = \frac{1}{2} c \, \frac{dC_L}{di} \, \omega R \sum_{n=1}^{n=6} \gamma_n \sin n\varphi$

It is only necessary to replace, in the equations of Table 3.26, Γ_M as given by the momentum equation for $\bar{r} = 0.9$, that is : $\Gamma_M = 11$ sq.m/sec.

This first approximation gives γ_1 --------- γ_6 and leads to the following equation :

(III.1.42)
$$\Gamma_{(sq.m/sec)} = 4.19 \sin\varphi - 3.81 \sin 2\varphi + 1.835 \sin 3\varphi - 0.219 \sin 4\varphi + 0.118 \sin 5\varphi - 0.191 \sin 6\varphi$$

Starting from this equation we can draw the curve $\Gamma = f(\varphi)$. See Fig.139.

The Γ_M of this curve does not correspond to the selected Γ_M and it is thus necessary to begin again the calculations with a new Γ_M , taken as a mean value between the two previous values, and this as long as the Γ_M introduced into the calculations and the Γ_M given by the derived curve are not practically identical.

The convergence is rapid as shown by Table 3.27 where are indicated the various results of the computing process.

Fig.139 gives the variations of $\Gamma = f(\varphi)$ for the different approximations.

The equation giving the circulation is thus finally obtained : /.

TABLE 3.23

θ_c = 9°2 = 0,161 rad   outer x_2 = R

V_f = 7,7 m/sec   inner x_1 = (0.5 R (V_S)
(0.36 R (V_C)

$\bar{r}$	φ	$\bar{r}\,\theta_c$	$\frac{V_{CB}}{\Gamma_M}$ outer	$\frac{V_{CB}}{\Gamma_M}$ inner	$\frac{V_{CA}}{\Gamma_M}$ outer	$\frac{V_{CA}}{\Gamma_M}$ inner	$\frac{V_{SB}}{\Gamma_M}$ outer	$\frac{V_{SB}}{\Gamma_M}$ inner	$\frac{V_{SA}}{\Gamma_M}$ outer	$\frac{V_{SA}}{\Gamma_M}$ inner
0	deg	0	m^{-1}							
0.235	30	0.0378	0.2165	- 0.436	0.190	- 0.191	0.491	- 0.275	0.416	- 0.185
0.26	36	0.0419	0.218	- 0.411	0.191	- 0.1755	0.488	- 0.269	0.411	- 0.18
0.30	45	0.0484	0.2205	- 0.342	0.192	- 0.149	0.482	- 0.25	0.405	- 0.176
0.385	60	0.062	0.2305	- 0.105	0.196	- 0.088	0.468	- 0.22	0.391	- 0.154
0.465	72	0.075	0.242	0.0349	0.20	- 0.0388	0.455	- 0.184	0.374	- 0.134
0.715	108	0.115	0.304	0.0374	0.2075	0.0104	0.383	- 0.079	0.306	- 0.0745
0.795	120	0.128	0.3315	0.027	0.199	0.011	0.345	- 0.059	0.275	- 0.0605
0.88	135	0.142	0.33	0.0204	0.166	0.0106	0.301	- 0.045	0.245	- 0.0494
0.925	144	0.149	0.272	0.0177	0.145	0.01	0.272	- 0.037	0.225	- 0.0435
0.95	150	0.153	0.216	0.0166	0.119	0.0094	0.260	- 0.033	0.21	- 0.0396

TABLE 3.24

φ deg	$E(\varphi)$
30	$E(30) = 0.0378 - 0.000837\ \Gamma_M$
36	$E(36) = 0.0419 - 0.00181\ \Gamma_M$
45	$E(45) = 0.0484 - 0.00252\ \Gamma_M$
60	$E(60) = 0.062 - 0.00474\ \Gamma_M$
72	$E(72) = 0.075 - 0.00627\ \Gamma_M$
108	$E(108) = 0.115 - 0.00725\ \Gamma_M$
120	$E(120) = 0.128 - 0.00702\ \Gamma_M$
135	$E(135) = 0.142 - 0.00646\ \Gamma_M$
144	$E(144) = 0.149 - 0.0057\ \Gamma_M$
150	$E(150) = 0.153 - 0.00501\ \Gamma_M$

TABLE 3.25

System of equations to be solved, with Γ_M as parameter

(1)	$1.86\,\gamma_2 + 2.85\,\gamma_u$		$= -\,0.0576$	$+\,0.002086\,\Gamma_M$
(2)	$1.441\,\gamma_2 - 2.01\,\gamma_4$		$= -\,0.033$	$+\,0.00114\,\Gamma_M$
(3)	$1.812\,\gamma_2$	$-\,3.44\,\gamma_6$	$= -\,0.0468$	$+\,0.00197\,\Gamma_M$
(1)'	$1.151\,\gamma_1$	$-\,2.3\,\gamma_5$	$=\ 0.095$	$-\,0.00588\,\Gamma_M$
(2)'	$0.874\,\gamma_1 + 2.345\,\gamma_3$		$= 0.09502$	$-\,0.003755\,\Gamma_M$
(3)'	$1.24\,\gamma_1 - 1.12\,\gamma_3$		$= 0.095$	$-\,0.00676\,\Gamma_M$

TABLE 3.26

Determining γ_n versus Γ_M

(The values of γ_n are dimensionless, Γ_M being given in sq.m/sec.)

$$\gamma_1 = 0.0849 - 0.00515\,\Gamma_M$$
$$\gamma_2 = -0.0268 + 0.00095\,\Gamma_M$$
$$\gamma_3 = 0.00891 + 0.000318\,\Gamma_M$$
$$\gamma_4 = -0.0027 + 0.000111\,\Gamma_M$$
$$\gamma_5 = 0.00113 - 0.0000304\,\Gamma_M$$
$$\gamma_6 = -0.000495 - 0.0000728\,\Gamma_M$$

$$\Gamma_{(sq.m/sec)} = 6.275 \sin \varphi - 2.804 \sin 2\varphi$$

(III.1.43) $$+ 1.708 \sin 3\varphi - 0.2637 \sin 4\varphi + 0.130 \sin 5\varphi - 0.162 \sin 6\varphi$$

It is now possible to compare this curve $\Gamma = f(\varphi)$, as given by equation III.1.43, with the curve obtained by J.Rabbott. (See Fig.135 and 140).

In the same way as previously the curve $\Gamma = f(\varphi)$ may be transformed backwards into $\frac{dL}{dr} = f(\bar{r})$ and compared to the original J. Rabbott's curve. See Fig.141.

It may be seen that the comparison of the two curves is quite satisfactory.

In Fig.142 is given the final curve $\Gamma = f(\varphi)$.

This Fig. shows also all the components of Γ as indicated by equation III.1.30.

3.16 - Attempts to use simplified methods

In this section are analysed simplified methods, the objective of which is to reduce the number of terms of the equation giving the circulation.

First simplified method.

(III.1.44) $$\Gamma_A = \frac{1}{2} c \frac{dC_L}{di} \omega r \theta_c - \frac{1}{2} c \frac{dC_L}{di} \frac{1}{11.4} \int_{r_0}^{R} \frac{\partial \Gamma_A}{\partial r_1}(r_1) \frac{dr_1}{r - r_1}$$

$$+ \frac{1}{2} c \frac{dC_L}{di} \cdot \frac{1}{2} \int_{r}^{R} \left(\frac{\partial \Gamma_A}{\partial r_1} + \frac{\partial \Gamma}{\partial r_1} \right) \frac{dr_1}{V_f T}$$

The first two terms of the second member of this equation are the same as previously.

The last integral means that to the helix vortices located under the swept disc has been substituted an infinity of elemental solenoids (A and B) whose number of turns per unit coil length is :

$$\frac{1}{V_f T} \frac{\partial \Gamma}{\partial r_1}$$

It may be noted that the lower limit of the last integral is r instead of r_0 because inside the solenoid the

/.

TABLE 3.27

$$\Gamma = \sum_{n=1}^{n=6} A_n \sin n\varphi$$

Γ_M initial	γ_n	A_n	$\Gamma = \sum A_n \sin n\varphi$	Γ_M final (read on curve)
sq.m/sec.	0	sq.m/sec	sq.m/sec.	sq.m/sec.
11	$\gamma_1 = 0.0283$ $\gamma_2 = -0.02576$ $\gamma_3 = 0.0124$ $\gamma_4 = -0.00148$ $\gamma_5 = 0.000796$ $\gamma_6 = -0.00129$	4.19 - 3.81 1.835 - 0.219 0.118 - 0.191	$\Gamma = 4.19 \sin\varphi - 3.81 \sin 2\varphi +$ $+ 1.835 \sin 3\varphi - 0.219 \sin 4\varphi$ $+ 0.118 \sin 5\varphi - 0.191 \sin 6\varphi$	7.9
9.45	$\gamma_1 = 0.03625$ $\gamma_2 = -0.01782$ $\gamma_3 = 0.01191$ $\gamma_4 = -0.001651$ $\gamma_5 = 0.000843$ $\gamma_6 = -0.001183$	5.365 - 2.637 1.7626 - 0.244 0.1247 - 0.175	$\Gamma = 5.365 \sin\varphi - 2.637 \sin 2\varphi +$ $+ 1.762 \sin 3\varphi - 0.244 \sin 4\varphi$ $+ 0.1247 \sin 5\varphi - 0.175 \sin 6\varphi$	7.5

TABLE 3.27 (Continued)

$\Gamma_{M\,initial}$	γ_n	A_n	$\Gamma = \sum A_n \sin n\varphi$	Γ_M final
sq.m/sec.	0	sq.m/sec.	sq.m/sec.	sq.m/sec.
8.5	$\gamma_1 = 0.04113$ $\gamma_2 = -0.01873$ $\gamma_3 = 0.01161$ $\gamma_4 = -0.001757$ $\gamma_5 = 0.000872$ $\gamma_6 = -0.001113$	6.087 - 2.772 1.718 - 0.26 0.129 - 0.1647	$\Gamma = 6.087 \sin\varphi - 2.772 \sin 2\varphi +$ $+ 1.718 \sin 3\varphi - 0.26 \sin 4\varphi$ $+ 0.129 \sin 5\varphi - 0.1647 \sin 6\varphi$	8.04
8.25	$\gamma_1 = 0.0423$ $\gamma_2 = -0.01895$ $\gamma_3 = 0.01154$ $\gamma_4 = -0.00178$ $\gamma_5 = 0.000879$ $\gamma_6 = -0.001097$	6.275 - 2.8046 1.708 - 0.2637 0.13 - 0.162	$\Gamma = 6.275 \sin\varphi - 2.8046 \sin 2\varphi +$ $+ 1.708 \sin 3\varphi - 0.2637 \sin 4\varphi$ $+ 0.13 \sin 5\varphi - 0.162 \sin 6\varphi$	8.25

axial magnetic field is constant and it is null outside the solenoid.

Let us perform the transformation already indicated :

$$r = r_0 + \frac{R - r_0}{2}(1 - \cos\varphi)$$

$$\Gamma = \sum_{n=1}^{n} A_n \sin n\varphi$$

The above equation may then be written as follows :

$$\text{(III.1.45)} \quad \sum_{n=1}^{n} A_n \sin n\varphi \left(1 + \frac{1}{2} c \frac{dC_L}{di} \frac{1}{V_f T} + \frac{1}{2} c \frac{dC_L}{di} \frac{2}{R - r_0} \frac{\pi}{11.4} \frac{n}{\sin\varphi}\right) = \frac{1}{2} c \frac{dC_L}{di} \omega r \theta_c$$

The system of equations III.1.24 is still valid if 1 (°) is replaced by ($1 + \frac{1}{2} c \cdot \frac{dC_L}{di} \cdot \frac{1}{V_f T}$) and if $E(\varphi) = \frac{1}{2} c \frac{dC_L}{di} \omega r \theta_c$.

For the numerical application selected previously (J.Rabbot's rotor) and using the metric system, the following results are obtained :

$$\begin{cases} \frac{1}{2} c \frac{dC_L}{di} \omega R \bar{r} \theta_c = 23.75 & (\theta_c = 9°2) \\ \frac{1}{2} c \frac{dC_L}{di} \frac{2}{R - r_0} = 1.04 & V_f T = 0.74 \\ \frac{1}{2} c \frac{dC_L}{di} \cdot \frac{2}{R - r_0} \cdot \frac{\pi}{11.4} = 0.287 & \\ 1 + \frac{1}{2} c \frac{dC_L}{di} \frac{1}{V_f T} = 2.325 & \end{cases}$$

The values of $E(\varphi) = \frac{1}{2} c \frac{dC_L}{di} \omega r \theta_c$ are given by Table 3.28

/.

TABLE 3.28

$$E(\varphi) = \frac{1}{2} c \frac{dC_L}{di} \omega r \theta_c$$

φ	30	36	45	60	72	108	120	135	144	150
E	5.57	6.125	7.12	9.15	14.5	16.85	18.9	20.9	21.9	22.4

The resolution of the system of equations gives :

$$\Gamma(\varphi) = 6.38 \sin\varphi - 2.34 \sin 2\varphi + 0.99 \sin 3\varphi$$
$$- 0.38 \sin 4\varphi + 0.189 \sin 5\varphi - 0.0812 \sin 6\varphi$$

The harmonic analysis 'Runge's method) of J.Rabbott's experimental curve gives :

$$\Gamma(\varphi) = 6.05 \sin\varphi - 2.46 \sin 2\varphi + 1.56 \sin 3\varphi$$
$$- 0.511 \sin 4\varphi + 0.192 \sin 5\varphi .$$

Fairly large discrepancies may be observed for the terms in sin φ , sin 3φ and sin 4φ though the sum of terms is practically the same : 7.61 against 7.59.

The corresponding curve is given in Fig.143.

Second simplified method

$$\Gamma_A = \frac{1}{2} c \frac{dC_L}{di} \omega r \theta_c - \frac{1}{2} c \frac{dC_L}{di} \frac{1}{4\pi} \int_{r_0}^{R} \frac{\partial \Gamma}{\partial r_1} \frac{dr_1}{r - r_1}$$

(III.1.46)

$$- \frac{1}{2} c \frac{dC_L}{di} \bar{V}_f$$

$$4 \pi r \bar{V}_f^2 = \omega r \frac{b}{2} c \frac{dC_L}{di} (\omega r \theta_c - \bar{V}_f)$$

The second expression is the momentum equation.

The successive transformations show a relationship with the equation of the infinite solenoid.

/.

$$\begin{cases} \Gamma_A - \Gamma_B = \frac{1}{2} bc \frac{dC_L}{di} (\omega r \theta_c - V_f) \\ 4\pi r \bar{V_f} \bar{V_f} = \omega r (\Gamma_A + \Gamma_B) \\ \omega = \frac{2\pi}{T} \\ V_f = \frac{2\pi r}{4\pi r \bar{V_f} T} (\Gamma_A + \Gamma_B) \\ V_f = \frac{1}{2 V_f T} (\Gamma_A + \Gamma_B = \frac{1}{\bar{V_f} T} \Gamma_A \\ \bar{V_f} \simeq \int_r^R \frac{\partial \Gamma}{\partial r} \frac{1}{\bar{V_f} T} dr_1 \end{cases}$$

The change of variable, from r to φ , leads to the following equation :

$$\Gamma = \sum_{n=1}^{n} A_n \sin n\varphi$$

(III.1.47) $$\sum_{n=1}^{n} A_n \sin n\varphi \left(1 + \frac{1}{2} c \frac{dC_L}{di} \frac{1}{4} \frac{n}{\sin\varphi}\right) = $$

$$= \frac{1}{2} c \frac{dC_L}{di} \omega r \theta_c - \frac{1}{2} c \frac{dC_L}{di} \bar{V_f}$$

The III.1.41 equations system remains valid if a substitution is made for :

$$E = \frac{1}{2} c \frac{dC_L}{di} \omega r \theta_c - \frac{1}{2} c \frac{dC_L}{di} \bar{V_f}$$

Taking again the previous numerical application , the following is obtained (metric system) :

/.

$$\frac{1}{2}\, c\, \frac{dC_L}{di}\, \frac{1}{4} = 0.245$$

$$\frac{1}{2}\, c\, \frac{dC_L}{di}\, \omega R \bar{r}\, \theta_c = 23.75\, r \qquad (\theta_c = 9^\circ\!.2)$$

$$\frac{1}{2}\, c\, \frac{dC_L}{di} = 0.98$$

TABLE 3.29

φ °	30	36	45	60	72	108	120	135	144	150
$\frac{1}{2} c \frac{dC_L}{di} \omega r \theta_c$	5.59	6.14	7.14	9.15	14.5	16.9	18.9	20.9	21.95	29.95
$\bar{V}_f$	4.61	4.95	5.5	6.5	8.7	9.6	10.3	11.1	11.3	11.5
$\frac{1}{2} c \frac{dC_L}{di} \bar{V}_f$	4.52	4.85	5.39	6.37	8.52	9.41	10.2	10.88	11.0	11.26
$E(\varphi)$	1.07	1.29	1.75	2.78	5.98	7.49	8.70	10.02	10.95	11.69

Resolution of type III.1.41 system of equations gives the following results :

$$\Gamma(\varphi) = 6.05 \sin \varphi - 2.62 \sin 2\varphi + 0.505 \sin 3\varphi$$
$$- 0.32 \sin 4\varphi + 0.469 \sin 4\varphi + 0.301 \sin 5\varphi$$

The corresponding curve is given in Fig.143.

In this Figure are grouped for comparison :

- the experimental J.Rabbott's curve,
- the curve derived from the complete theoretical method,
- the two curves derived from the simplified methods.

The proposed complete theoretical method shows to be far the best. It may be used to determine the loads acting on the blades.

The first simplified method is less good but it may be used, however, for overall performance calculations.
The proposed complete method may still be improved by taking into account the contraction of the outside helix.

3.2 - Problem of the non-stationary conditions applied to helicopter rotors.

Attempts to find an approximate solution.

3.21 - Objective

The local lift of a blade in non-stationary conditions may be considered a the sum of two effects :

- circulation due to a distribution of velocities, normal to the (thin) airfoil section ,
- impulsion of air on the airfoil due to accelerations (derivatives of those normal velocities).

Defining the circulation is difficult because of the presence of the free vortices escaping from the trailing edge (wake), the intensity of which must satisfy the vortex conservation law.

These free vortices (termed radial vortices, by opposition to helix vortices), after appearing at the trailing edge of blade A, move away from the latter during a half period (except in the inversion circle) then come back under the rotor disc and so forth.

Those of the radial vortices, which are formed less than half a period ago, will be termed recent vortices.

The totality of the radial vortices escaping from the blade trailing edge will then be separately considered according whether they are recent vortices or not.

The recent vortices will be considered as the vortices of the non-stationary wake.

The other radial vortices, whether they come from blade A or from blade B (in the case of a two bladed rotor) will be considered as inputs in the same way as the blade section pitch angle variations.

In this way it becomes possible to make use of number of results of the fixed wing non-stationary theory.

However, these results lead to expressions which are difficult to handle when applied to helicopter rotors, and for this reason approximate formulae will have to be derived.

In the first part of this section will be reminded some basics of the non-stationary theory.

In the second part will be exposed an approximate method used for fixed wings.

/.

In the last part these results will be applied to helicopter rotor blades.

3.22 - Basics

3.221 - It is not our intention to expose here the non-stationary theory of lifting wings* but merely to give some results which might be useful for a better comprehension of the following text.

The lift of a blade section dr, either in stationary or in non-stationary conditions, is due to a pressure difference between the upper and lower surfaces of the airfoil section. It may thus be obtained by integrating the pressure differences along the airfoil chord. We may write :

(III.2.48) $$\frac{dL}{dr} = \int_{-c/2}^{c/2} (p_2 - p_1)\, dx$$

p_2 and p_1 designate, respectively, the local pressures on the airfoil lower and upper surfaces (See Fig.144).

In Fig.145 are given characteristic pressure distributions, for stationary (a) and non-stationary (b) working conditions, in the case when the airfoil may be considered as a plane thin sheet.

Presence of large "bumps", in the rear part of the airfoil section (rigid and flapless) indicates rates of non-permanence of the motion.

Their absence indicates that the working condition is quasi stationary.

3.222 - The study of non-stationary conditions is made easier by substituting to the notion of section angle of attack a notion of distribution of the velocity V_z (x,t) normal to the airfoil. V_z varies along the chord (x) and with time (t).

The existence of two typical distributions of V_z (translation and rotation) gives rise to a circulation.

The existence of accelerations $\frac{\partial}{\partial t} V_z$ (x,t) gives rise to an impulsive lift, i.e. to the effect on the blade of the accelerated air surrounding it.

In stationary conditions, lift is due to the circulation Γ exclusively.

(III.2.49) $$\frac{dL}{dr} = \rho V_R \Gamma$$

/.

Circulation is kept up by the V_{z_0} component of the velocity, normal to the airfoil (see Fig.146). This velocity is constant in time $\left(\frac{\partial}{\partial t} V_{z_0} = 0\right)$ and along the chord $\left(\frac{\partial}{\partial x} V_{z_0} = 0\right)$.

All happens as if the airfoil section, placed in an air stream V_R, was translated with a speed V_{z_0}, relative to the surrounding air, in a direction normal to the chord.

(III.2.50)
$$\begin{cases} \Gamma = \frac{1}{2} c \frac{dC_L}{di} V_{z_0} = \frac{1}{2} c \frac{dC_L}{di} \frac{V_{z_0}}{V_R} V_R \\ i = \frac{V_{z_0}}{V_R} \end{cases}$$

We will say that the airfoil section placed in an air stream is a black box whose input is a translation velocity V_{z_0} and whose output is the circulation.

For a helicopter in hovering conditions :

$$V_{z_0} = \omega r \theta - V_i$$

The velocity $\omega r \theta$ is constant in time and along the chord.

The velocity V_i induced by the helix vortices is constant in time but not absolutely constant along the chord. In fact it is the velocity of the neutral rear point (located at three quarter chord from the leading edge).

As it has been said before, in non-stationary conditions lift is produced by a double effect :

- the circulation due to the $V_z\,(x,t)$ velocities,
- the impulsive force due to accelerations $\frac{\partial}{\partial t} V_z$.

Let us first examine the circulation .

It is convenient to write :

(III.2.51)
$$\begin{cases} x = \frac{c}{2} \cos\theta & & \\ x = -\frac{c}{2} & \theta = 0 & \text{leading edge} \\ x = +\frac{c}{2} & \theta = \pi & \text{trailing edge} \end{cases}$$

and to express $V_z\,(x,t) = V_z\,(\theta,t)$ in the form of a Fourier series (cosine series).

(III.2.52) $$V_z\,(\theta,t) = V_{z_0}\,(t) + \sum_{n=1}^{n} V_{z_n}\,(t) \cos n\theta$$

/.

The first term of the second member of this equation corresponds to a translation of the airfoil section along the normal to this section.

The second term :

$$V_{z_1}(t)\cos\theta = -\frac{V_{z_1}(t)}{c/2}\,x \quad .$$

represents a rotation of the airfoil section around a point located at half chord.

All the components of the V_z velocity give rise to a pressure distribution (Thin airfoil theory, by Munk-Glauert), but only the two first components, i.e :

$V_{z_0}(t)$ translation

$V_{z_1}(t)$ rotation

give rise to a circulation around the airfoil which generates lift.

For the other terms of V_{z_n}, such as $n > 1$, the (III.2.48) integral is equal to zero.

We may note that the translation velocity $V_{z_0}(t)$ is not a mean velocity along x :

$$V_{z_0}(t) \neq \frac{1}{c}\int_{c/2}^{c/2} V_z(x,t)\,dx$$

It is the constant term in the cosine series :

$$V_{z_0}(t) = \frac{1}{\pi}\int_{c/2}^{c/2} V_z(x,t)\,\frac{dx}{\sqrt{(\frac{c}{2})^2 - x^2}}$$

We will admit that the discrepancy is small between these two values.
The effect due to accelerations will be examined later.

3.223 - Schematic description of the circulation. Relative importance of translation and rotation motions.

Let us consider an airfoil section placed in a bi-dimensional flow, with a uniform wind $V_R(t)$ which may vary in time.

The possible inputs are :

a) a translation of the airfoil section along a direction /.

normal to this section : $z(t)$.

b) a rotation $\alpha(t)$ around a point located at half chord.

The $V_z\ (x,t)$ velocity is then :

(III.2.53) $$V_z(x,t) = \left[\dot{z}(t) + \frac{\partial}{\partial t}\left[V_R(t)\,\alpha\right]\right] + \dot{\alpha}(t)\,x$$

If no vortices existed at the trailing edge, the corresponding circulation would be :

(III.2.54) $$\Gamma^x(t) = \frac{1}{2}c\,\frac{dC_L}{di}\left[\dot{z}(t) + \frac{\partial}{dt}(V_R\,\alpha)\right] + \frac{1}{2}c\,\frac{dC_L}{di}\cdot\frac{1}{2}\frac{c}{2}\dot{\alpha}$$

As circulation varies in time, vortices having the same intensity and their signs opposed to the successive increases of circulation around the airfoil will, in fact, be escaping from the trailing edge, in virtue of the vortex conservation law.

These new free vortices, parallel to the trailing edge and orthogonal to the stream-lines, will induce a new distribution $\Delta V_z(x,t)$ around the airfoil which, in turn, will modify the circulation and give rise to a new departure of free vortices, and so forth......

If we consider again our image of the "black box", described previously, the input is the V_z given by equation (III.2.53) but the output, i.e. the circulation, is not Γ^x given by equation (III.2.54), but , given by :

(III.2.55) $$\Gamma = \square\,\Gamma^x$$

where $\square$ is an operator of Γ^x accounting for the passage through the black box.

A vortice - $d\Gamma$ (see Fig.148) which has escaped from the trailing edge τ seconds before the present time t, is located at a distance :

$$\xi\,\frac{c}{2} = \frac{c}{2} + \int_0^{\tau} V_R(t-\tau)\,d\tau$$

It induces at a point x of the airfoil a velocity V_z, such as :

/.

$$V_z(x,t) = -\frac{d\Gamma}{2\pi} \frac{1}{\xi\frac{c}{2} - x} = \frac{\Gamma}{c} \frac{1}{\xi + \cos\theta}$$

By braking down this expression into a Fourier harmonic series , we obtain:

$$V_z(x,t) = \frac{d\Gamma}{2\pi\frac{c}{2}} \left[\frac{1}{\sqrt{\xi^2 - 1}} + 2\sum_{n=1}^{n} (-1)^n \frac{(\xi - \sqrt{\xi^2 - 1})^n}{\sqrt{\xi^2 - 1}} \cos n\theta \right] \tag{III.2.56}$$

and using the transformation indicated by Rufus Isaacs:

$$\int_0^\pi \frac{\cos n\theta}{a - \cos\theta} d\theta = \pi \frac{(a - \sqrt{a^2 - 1})^n}{\sqrt{a^2 - 1}} \qquad a > 1$$

the local vortex distribution may be written :

$$g_B(\theta,t) \frac{d\Gamma}{2\pi\frac{c}{2}} \left[\frac{2}{\sqrt{\xi^2 - 1}} \operatorname{cotan}\frac{\theta}{2} - 4 \sum_{n=1}^{n} (-1)^n \frac{(\xi - \sqrt{\xi^2 - 1})^n}{\sqrt{\xi^2 - 1}} \sin n\theta \right]$$

Among other terms, we can recognise in (III.2.56) the presence of the translation and rotation terms.

As the total circulation around the airfoil is only due to the translation and rotation terms, the modification of the circulation around the airfoil by a wake free vortex, located at a distance $\xi\frac{c}{2}$ from the half chord, is :

$$\gamma = \frac{d\Gamma}{2\pi\frac{c}{2}} \left[\frac{2\pi}{\sqrt{\xi^2 - 1}} + \frac{2\pi(\xi - \sqrt{\xi^2 - 1})}{\sqrt{\xi^2 - 1}} \right] \tag{III.2.57}$$

or :

$$\gamma = \frac{2\,d\Gamma}{c} \left(\sqrt{\frac{\xi + 1}{\xi - 1}} - 1 \right)$$

This additional circulation, highly intensive at the trailing edge ($\xi = 1$), becomes very rapidly equal to zero, as the vortex moves away ($\xi \longrightarrow \infty$).

We may note that it is not only a function of the intensity of variation of the circulation $d\Gamma$ but also a /.

function of the velocity V_R, with which the free vortex is carried away by the air stream (see Table 3.30).

No great error would be made if the effect of the wake was modified or even suppressed beyond a distance of 4 to 5 chord lengths.

The circulation produced by the translation effect is always larger than the one produced by the rotation.

The ratio between those two effects, is as follows :

$$\frac{\gamma\ \text{translation}}{\gamma\ \text{rotation}} = \xi - \sqrt{\xi^2 - 1} \qquad \xi > 1$$

The values of this ratio, versus ξ, are given in Table 3.30.

ξ times the half chord length being the distance of the free vortex to the middle of the chord.

TABLE 3.30

ξ	1	2	4	5	10
$\sqrt{\frac{\xi+1}{\xi-1}} - 1$		0.73	0.29	0.22	0.11
$\xi - \sqrt{\xi^2-1}$	1	0.27	0.13	0.10	0.05

Figure 145 (b) gives (ref. Von Karman) the pressure distributions generated by the wake vortex, as a function of its distance to the airfoil.

We may note here that V_R (t) intervenes in two ways : on the one hand, it appears in the expression giving V_Z (see equation III.2.53), whence it plays the role of an input, and, on the other hand, it appears in ξ, which means that in the circulation black box it plays the role of an impedance having an influence on all the inputs.

/.

3.224 - Approximate configuration proposed for helicopter rotor blades.

In the case of a helicopter rotor blade the free radial vortices (wake) draw a spiral shaped surface. They first move away from the blade, during half a period (except in the inversion circle) then come back under the rotor disc, in the vicinity of the blade.

In order to make maximum use of the results available for fixed wings, the wake of the blade will be cut down into two parts.

To the first portion of the spiral shaped sheet, which was formed between half a period ago and the present time t, will be substituted a plane sheet moving away to infinity, because, as it has been said before, its influence after four or five chord lengths is small.

The other portion of the spiral shaped sheet, formed at an earlier time, will be regarded as an effect which would be foreign to the wake, comparable to a blade pitch angle variation.

3.225 - Accelerations effects

In the case of a two-dimensional flow (infinite aspect ratio) the lift generated by impulsion is equal to the inertia force of a mass of air whose volume is a cylinder having c for diameter and the wing span for height

The acceleration is :

$$\frac{\partial}{dt} V_z(t) = \frac{\partial}{\partial t} \dot{z}(t) + \frac{\partial}{\partial t}(V_R \alpha) \tag{III.2.58}$$

$$= \frac{\partial^2}{\partial t^2} z(t) + \alpha \frac{\partial^2 V_R}{\partial t^2} + 2\frac{\partial \alpha}{\partial t} \frac{\partial V_R}{\partial t} + V_R \frac{\partial^2 \alpha}{\partial t^2}$$

In the case of a wing having a finite aspect ratio the above force is to be multiplied by a coefficient which is the ratio between the span and the half perimeter of the wing.

In the case of a helicopter rotor this ratio will be taken equal to one .

3.23 - Approximate method used for fixed wings

3.231 - Objective. Limitative hypotheses.

The wing, placed in a wind V_R (t) is considered as an /.

impedance system Z (p) whose input is the velocity V_Z (x,t) normal to the airfoil (except in the zone of the trailing edge wake) and whose output is the circulation.

This system is generally governed by an integral equation.

It may be theoretically replaced by a system of an infinite number of differential equations.

A first approximation is thus made when this system is replaced by a single differential equation.

The second approximation comes from the non linearity.

If the airfoil is stalled the theory is not valid any more and another theory is necessary.

As mentioned previously, the velocity V_R (t) plays a double role in the circulation : firstly as an input, secondly as a wake. The influence of V_R on the impedance is thus a cause of non linearity.

It may be noted, however, that if the local advance ratio μ is small the error made in considering the system as linear is also small.

We will, therefore, hence consider the system as being linear.

In these conditions we are led to the following problem : we have to define the impedance of a system, by means of a linear differential equation, knowing the latter's response to :

- a sinusoddal input

- a unit step input.

3.232 - Determining an approximate solution

Let us consider a wing of aspect ratio Λ, placed in a wind speed V_R (t).

The input $\frac{V_{Z_0}(t)}{V_R(t)}$ is an unit step, i.e., being zero at time 0 it suddenly takes the value $\frac{V_{Z_0}(t)}{V_R(t)}$ then remains constant.

This case has been studied by Wagner for infinite aspect ratios and by Jones for aspect ratios of 6 to 3.

The approximate unit solutions given by Jones are :

$$(\text{III.2.59})\qquad \begin{cases} \left[1-R(s)\right]_{\Lambda=\infty} = 1-0.165\,e^{-0.0451} - 0.335\,e^{-0.3s} \\ \left[1-R(s)\right]_{\Lambda} = 1-R_o\,e^{-\delta s} \end{cases}$$

$$ds = \frac{2V_R\,dt}{c}$$

The values of R_o and δ, for $\Lambda = 3$ and $\Lambda = 6$, are given in Table 3.31

Λ	R_o	δ
3	0.283	0.540
6	0.361	0.381

The approximation made can only be estimated for $\Lambda = \infty$: the Laplace transform of the response to the unit step input is compared to Theodorsen's curve (see Fig.149).

We will admit that this approximation is valid for values of Λ such as 3 and 6.

For a helicopter rotor we will admit $\Lambda = 6$. In this way we will not only take into account the vortex parallel to the trailing edge but also portions of lateral helixes.

Formula III.2.5 for $\Lambda = 6$, may be construed as the solution of a differential equation. We obtain :

$$(\text{III.2.60})\qquad \frac{di}{ds} + \delta i = \frac{di^x}{ds}(1-R_o) + \delta i^x$$

i^x is the static angle of attack (similar to Γ^x)

i is the dynamic angle of attack (similar to Γ)

/.

It is to be noted that we may substitute to i, either

$$C_L = \frac{dC_L}{di}\, i \quad \text{or} \quad \frac{\Gamma}{V_R}$$

The equivalent expression may then be written as follows:

$$\text{(III.2.61)} \quad \begin{cases} \dfrac{c}{2V_R}\dfrac{di}{dt} + \delta i = \dfrac{c}{2V_R}\dfrac{di^x}{dt}(1-R_o) + \delta i^x \\[2ex] \dfrac{c}{2}\dfrac{d}{dt}\left(\dfrac{\Gamma}{V_R}\right) + \delta\Gamma = \dfrac{c}{2}\dfrac{d}{dt}\left(\dfrac{\Gamma^x}{V_R}\right)(1-R_o) + \delta\Gamma \\[2ex] \dfrac{d\Gamma}{dt} + \left(\dfrac{2\delta V_R}{c} - \dfrac{V'_R}{V_R}\right)\Gamma = (1-R_o)\dfrac{\partial\Gamma^x}{\partial t} + \left[\dfrac{2\delta V_R}{c} - (1-R_o)\dfrac{V'_R}{V_R}\right]\Gamma^x \\[2ex] V'_R = \dfrac{\partial}{\partial t} V_R(r,t) \end{cases}$$

If the derivative V'_R is considered as negligible and V_R considered as constant during a range of four chord lengths, it may be said that the wake vortices move with a constant speed.

This result is only valid for the translation motions. In order to introduce the rotation we will calculate an equivalent translation velocity ΔV_{Z_o} by means of the following formula :

$$\text{(III.2.62)} \quad \Delta V_Z = \dot{\alpha}\left(\frac{c}{4} - \frac{ac}{2}\right)$$

a.c defines the position of the center of rotation, taken as positive in the direction starting from the middle chord point towards the trailing edge.

If rotation takes place around the middle chord point then a = 0.

If rotation takes place around the forward neutral point (aerodynamic center) we obtain : $a = -\frac{1}{2}$ and $\frac{a\,c}{2} = -\frac{c}{4}$.

3.24 - Application to a two-blade helicopter rotor

3.241 - Disturbed working conditions

3.2411 - Definition

Let us consider that hovering conditions is the initial state of operation of the rotor and that small dis-

/.

turbances are then introduced.

These disturbances may be classified in two types:

- symmetric
- antisymmetric

(see Tables 3.32 and 3.33).

The symmetric perturbances increase rotor lift and modify the rotor conicity angle a_0.

The antisymmetric perturbances do not modify rotor lift but tilt the rotor

(III.2.63)
$$\begin{cases} \beta(t) = a_0(t) - a_1(t)\cos\Psi - b_1(t)\sin\Psi \ldots\ldots \\ I_0 \dfrac{d^2\beta}{dt^2} + I_0\omega^2\beta = M_0 + M_1\cos\Psi + M_2\sin\Psi \ldots\ldots \\ \dfrac{d^2 a_0}{dt^2} + \omega\dfrac{G_3}{I_0}\dfrac{da_0}{dt} + \omega^2 a_0 = \dfrac{M_0}{I}(t) \\ \ddot{a}_1 + \omega\dfrac{G_3}{I_0}\dot{a}_1 + 2\omega\dot{b}_1 + \omega^2\dfrac{G_3}{I_0} b_1 = -\dfrac{M_1}{I_0}(t) \\ 2\omega\dot{a}_1 + \omega^2\dfrac{G_3}{I_0} a_1 - \ddot{b}_1 - \omega\dfrac{G_3}{I_0}\dot{b}_1 = \dfrac{M_2}{I_0}(t) \\ G_n = \dfrac{1}{2}\rho\displaystyle\int_0^R c\,\dfrac{dC_L}{di}\,r^n\,dr \end{cases}$$

TABLE 3.32
Symmetric Disturbances

	Disturbance originated by :	Variable	Disturbed state
1	Collective pitch	θ_c	$\theta_c + \Delta\theta_c$
2	Rotational speed	ω	$\omega + \Delta\omega$
3	Ascensional velocity(°)	V_z	$\theta + \Delta V_z$

(°) not experimented.

TABLE 3.33

Antisymmetric - Disturbances

Disturbance originated by :	Variable	Disturbed state
4 Cyclic pitch	$\theta_2 \sin \Psi$	$0 + \Delta\theta_z$
5 Horizontal speed	V_0	$0 + \Delta V$
6 Rotor tilt or angle of attack	$\alpha\ (\dot{\alpha})$	$0 + \Delta\dot{\alpha}$

Every disturbance modifies the lift of a blade.

Let us assume that this modification consists in an increase of lift of blade A.

The increase which appears at the birth of the disturbance is attenuated by the blade's own recent wake effect and by the impulsion (τ_{o1}). As lift increases the hinged blade comes up (τ_{o2}) and this motion gives rise to a double effect :

a) the flapping velocity opposes lift,

b) as the blade comes up it gets away from the former helix vortices.

   This decreases their influence on the blade and , therefore, decreases blade's lift.

After approximately half a period (τ_{o3}) the influence of the radial vortices issued from blade B becomes effective on blade A, first giving rise to a decrease then to an increase of lift.

Finally intervene the marginal vortices.

The latter do not take their position immediately but the different helix portions get into place progressively as they are being reached by the disturbances or the vortices.

A movie film has been taken of this phenomenon (see reference 8), which illustrates what has been said above.

Let us compare now the time constants τ_o .
Account being taken of the wake and of the impulsion, /

the lift of blade A becomes established when the blade has travelled over a distance of n chord lengths (say , n = 4).

(III.2.64) $$\tau_{01} = \frac{nc}{\omega r} = \frac{2\pi}{\omega}\, n\, \frac{bc}{\pi R} \cdot \frac{1}{\bar{r}}\, \frac{1}{2b} \qquad (\bar{r} = \frac{r}{R})$$

For a two bladed rotor, having a solidity $\sigma = 0.10$, the time constant τ_{01} is :

$$\tau_{01} = T \cdot \frac{0{,}10}{\bar{r}} \qquad (T = \frac{2\pi}{\omega})$$

that is :

0.10 T for the blade tip,

0.133 T for the section at 0.75 R

0.20 T for the section at 0.50 R

and T for the section at 0.10 R.

In the case when the influence of lift on the flapping motion is to be calculated it may be taken that the non stationary effect is the one which concerns the section at 0.75 R.

When it is wanted to study lift distribution along the blade, the variation of the non stationary effect along the blade radius may be taken into account.

The flapping time constant τ (02) is as follows (see equation III.2.63):

(III.2.65) $$\tau_{02} = \frac{2I}{\omega G_3} = \frac{2\pi}{\omega}\left(\frac{1}{\pi}\, \frac{I_0}{G_3}\right) = T\, \frac{1}{\pi}\, \frac{I_0}{G_3}$$

For helicopter rotor blades the ordinary value of $\frac{G_3}{I_0}$ is comprised between 0.5 and 1.25.

Whence :

$$0.8 \leqslant \frac{I}{G_3} \leqslant 2.0$$

The value of τ_{02} is therefore comprised between a quarter and two third of a period (we leave out the case of Δ hinges).

The recent radial vortices, issued from blade B, become effective on blade A after a time τ_{03}, approximately equal to half a period.

/.

The same happens with the former radial vortices which follow with intervals of $\underline{T}$. The process is completed by the establishment of the final positionning of the helix vortices which also affects blade A approximately every half a period :

$$\tau_{04} \simeq \frac{T}{2}$$

During the visualization tests carried out for the study of non stationary conditions, very heavy blades were intentionally selected ($\frac{G_3}{I}$ = 0.10) in order to make appearant the aerodynamic process without too much blade flapping.

The disc loading was also high in order to avoid coupling and to obtain a better view of the helix vortices.

The pitch angle disturbance amplitude reached, during those tests, fifty per cent of the initial pitch angle.

The displacement of the marginal vortices, after one period time, is not visible too well on the films.

On the contrary, the displacement of the blade relatively to the marginal vortices is quite large if the rotor is tilted (α) . It is also noticeable in the case of cyclic pitch variation (θ_2), though at a smaller degree.

3.2412 - Let us examine the case where the whole rotor pitches nose-up, by an angle α (t), starting from hovering conditions, and let us determine the response to this motion in flapping.

The resulting normal blade section velocity (translation) and the acceleration are :

$$V_z = \dot{\alpha}\, r \cos\psi - r\,\frac{d\beta}{dt} - \Delta v_i$$

$$\dot{V}_z = \ddot{\alpha}\, r \cos\psi - \dot{\alpha}\,\omega\, r \sin\psi - r\,\frac{d^2\beta}{dt^2} - \frac{d}{dt}\,\Delta v_i$$

The local lift and the moment at the blade root due to the blade inertia forces and to the impulsion of air, are :

./.

$$\text{III.2.66}\quad\left\{\begin{aligned}
\frac{dL_1}{dr} &= \ddot{\alpha} r m' \cos\Psi - 2\dot{\alpha}\omega r m' \sin\Psi - m' r \frac{d^2\beta}{dt^2} \\
&- m' r \beta \omega^2 + \rho \frac{\pi c^2}{4}\left(\ddot{\alpha} r \cos\Psi - \dot{\alpha}\omega r \sin\Psi - r\frac{d^2\beta}{dt^2} - \frac{d}{dt}\Delta V_i\right) \\
M_1 &= \ddot{\alpha} I_0 \cos\Psi - 2\dot{\alpha}\omega I \sin\Psi - I_0 \frac{d^2\beta}{dt^2} - I_0 \beta \omega^2 \\
&+ \rho \frac{\pi c^2 R^3}{12}\left(\ddot{\alpha}\cos\Psi - \dot{\alpha}\omega \sin\Psi - \frac{d^2\beta}{dt^2}\right) - \rho \frac{c^2}{4}\int_{r_0}^{R} r \frac{d}{dt}\Delta V_i \, dr \\
\left(I_0 + \rho \frac{\pi c^2 R^3}{12}\right)\frac{d^2\beta}{dt^2} + I_0 \omega^2 \beta &= \int_{r_0}^{R} \rho r \omega r \Gamma \, dr + \\
&+ \ddot{\alpha}\cos\Psi\left(I_0 + \rho\frac{\pi c^2 R^3}{12}\right) - 2\dot{\alpha}\omega\sin\Psi\left(I_0 + \rho\frac{\pi c^2 R^3}{24}\right) - \rho\frac{c^2}{4}\int_{r_0}^{R} r\frac{d}{dt}\Delta V_i \, dr
\end{aligned}\right.$$

where $m' dr$ is the mass of the blade element dr and I the blade moment of inertia relative to the root.

Let us compare $\rho \dfrac{\pi c^2 R^3}{12}$ to G_3

$$\rho \frac{\pi c^2 R^3}{12 G_3} = \frac{\pi}{3b} \cdot \frac{bc}{\pi R} \sim \frac{\sigma}{b}$$

(b being the number of blades).

With a solidity $\sigma = 0.10$ this ratio is equal to 5 %, in the case of a two blade rotor, that is, 2.5 to 5 % of I for a conventional rotor.

We will, therefore, neglect $\rho \dfrac{\pi c^2 R^3}{12}$ (appearant mass effect) in front of I.

We will introduce now the effect of lift (due to circulation) on the flapping motion, by examining, first, simple cases, then, more complex ones.

Usually, the non stationary conditions and the free vortices being not taken into account, it may be written :

$$\text{(III.2.67)}\quad dL = \rho \omega r \Gamma = \frac{1}{2}\rho(\omega r)^2 c \frac{dC_L}{d\iota}\left(\frac{\dot{\alpha}}{\omega}\cos\Psi - \frac{r}{\omega r}\frac{d\beta}{dt}\right)$$

/.

The flapping equation is then, ($+\alpha(t)$ nose up) :

(III.2.68)
$$\begin{cases} \ddot{a}_1 + \omega \frac{G_3}{I_0} \dot{a}_1 + 2\omega b_1 + \omega^2 \frac{G_3}{I_0} b_1 = -\ddot{\alpha} - \alpha\omega \frac{G_3}{I_0} \\ 2\omega \dot{a}_1 + \omega^2 \frac{G_3}{I_0} a_1 - \ddot{b}_1 - \omega \frac{G_3}{I_0} \dot{b}_1 = -2\dot{\alpha}\omega \end{cases}$$

In practice, this system has a time constant $\frac{2 I_0}{\omega G_3}$ and a natural frequency ω .

Let us introduce the effect of the recent wake, belonging to the blade from which it is issued. This is the black-box system which has been described previously.

In stationary conditions we have :

(III.2.69)
$$\Gamma^{x} = \frac{1}{2} c \frac{dC_L}{di} \omega r \left(\frac{\dot{\alpha}}{\omega} \cos\Psi - \frac{r}{\omega r} \frac{d\beta}{dt} \right)$$

The true circulation, at the output of the black-box, is given by the equation which was indicated in paragraph 3.23 :

(III.2.70)
$$\frac{\partial \Gamma}{\partial t} + \frac{0.762}{c} \omega r \Gamma = \frac{\partial \Gamma^{x}}{\partial t} (0.639) + \frac{0.762}{c} \omega r \Gamma^{x}$$

For the calculation of the flapping motion we will assume ωr constant and equal to the one at $\bar{r} = 0.75$ R.

ωr is thus to be replaced by $\overline{\omega r} = 0.75\ \omega$ R.

Let us multiply the two members of equation III.2.70 by $\rho\omega r^2 dr$ and integrate from r_0 to R.

The flapping equations may then be written :

(III.2.71)
$$\begin{cases} M = \int_{r_0}^{R} \rho\omega r^2 \Gamma dr \qquad G_3 = \frac{1}{2}\rho \int_{r_0}^{BR} c \frac{dC_L}{di} r^3 dr \\ \ddot{\beta} + \omega^2 \beta - \frac{M}{I_0} = \ddot{\alpha}\cos\Psi - 2\dot{\alpha}\omega \sin\Psi \\ 0.639\,\omega G_3 \ddot{\beta} + \frac{0.762}{c} \overline{\omega r}\, \omega G_3 \beta + \frac{\partial}{\partial t} M + \frac{0.762}{c} \overline{\omega r} M = \\ = 0.639\,\omega G_3 (\ddot{\alpha}\cos\Psi + \dot{\alpha}\omega \sin\Psi) + \frac{0.762}{c} \overline{\omega r}\, \omega G_3 \dot{\alpha} \cos\Psi \end{cases}$$

It is known that, comparatively to the previous III.2.68 system, the black-box introduces a decrease of amplitude and a phase shift which does not exceed 15 degrees.

Let us examine the influence, on the disturbed motion, of the inner and outer marginal helix vortices.

Before the disturbance those helixes are defined by their circulation intensity and their pitch.
In the case of symmetric disturbances, when the final conditions are reached, the helices have a new circulation intensity and a new pitch.

In the case of antisymmetric disturbances, which is the case examined here, the helic is distorbed in a sinusoidal way, its pitch does not vary and its circulation intensity varies in azimuth (because of the radial vortices).

During the transient period a triple effect will be obtained (in differentiating with respect to three variables). First effect : the marginal helix vortices remain at their place and keep their pitch and their intensity. The blade undergoes a flapping motion and takes a position distant by Δ_z above its initial position. Originally blade A was located at a distance z_o above the inner and outer marginal vortices ($z_o = V_f \frac{T}{2}$).

At a time t during the disturbance, the distance z_e of the blade to the first outer helix is :

$$\Delta z_e = R\,(\beta - \alpha \cos\Psi)$$

$$z_e = z_o + \Delta z_e = V_f \frac{T}{2} + R\,(\beta - \alpha \cos\Psi)$$

and its distance z_i to the first inner helix is :

$$\Delta z_i = \frac{R}{2}\,(\beta - \alpha \cos\Psi$$

$$z_i = z_o + \Delta z_i = V_f \frac{T}{2} + \frac{R}{2}\,(\beta - \alpha \cos\Psi)$$

Let $\sum V_i\,(z_o, r)$ be the velocity induced by the helixes in hovering conditions and $\sum V_i(z_o + \Delta_z, r)$ the induced velocity when the blade is lifted by .

We have :

$$\sum \Delta V_i = \Delta_z \frac{\partial V_i}{\partial z}(z_o, r)$$

$$\text{If } \Delta_z > 0 \qquad \frac{\partial V_i}{\partial z}(z_o, r) < 0$$

/.

Hence, the new induced velocity variations.

$$\text{(III.2.72)} \quad \begin{cases} \Sigma \Delta V_{i_I} = \frac{R}{2} (\beta - \alpha \cos \Psi) \frac{\partial V_i}{\partial z} (z_o, r) \\ \Sigma \Delta V_{i_E} = R (\beta - \alpha \cos \Psi) \frac{\partial V_i}{\partial z} (z_o, r) \\ \delta V_i = - (\beta - \alpha \cos \Psi) k R = \Sigma V_{i_I} + \Sigma \Delta V_{i_E} \end{cases}$$

The expressions $\frac{\partial V_i}{\partial z} (Z_o, r)$ are derivatives of the elliptic integral K and of the Heuman's λ_o function (see hovering conditions).

Second effect. The intensity of the marginal vortices is constant and their distance $z_o \, V_f \, \frac{T}{2}$ to the blade remains the same. The pitch of the vortices,alone,varies in azimuth.

This term takes the following form :

$$\delta V_i = \frac{\Delta V_f (\Psi)}{V_f^2}$$

Third effect. The pitch and the distance z_o of the vortices are constant. The circulation varies in azimuth.

This term may be written :

$$\delta V_i = \frac{\Delta \Gamma}{\Gamma} V_i (z_o, r)$$

The disturbances being small, we will neglect the two last effects.

Let us introduce the first effect (III.2.72) into the III.2.71 system.

The circulation equation is modified as follows :

/.

$$(III.3.73)\quad \begin{cases} 0.639\, G_3 \omega G_3 \beta + (0.639\omega\, G_2\, R\, k + \frac{0.762}{c} \bar{\omega r} \omega G_3)\dot{\beta} \\ + \frac{0.762}{c} \bar{\omega r} \omega G_2\, R\, k\, \beta + \frac{\partial}{\partial t} M + \frac{0.762}{c} \bar{\omega r} \quad M \\ = 0.639\, \omega G_3\, \ddot{\alpha} \cos\Psi + 0.639\, \omega\, G_3\, \dot{\alpha}\omega \sin\Psi \\ + (\frac{0.762}{c} \bar{\omega r} \omega G_3 + 0.639\, \omega\, G_2\, R\, k)\, \dot{\alpha} \cos\Psi \\ - 0.639\, \omega\, G_2\, R\, k\, \alpha\omega \sin\Psi + \frac{0.762}{c} \bar{\omega r}\, \omega\, G_2\, R\, k\, \alpha \cos\Psi. \end{cases}$$

Introduction of the term III.2.72 in the conventional flapping equations (III.2.68) may have a double effect.

Firstly, the b_1 flapping term may be modified, secondly, there may be a slight α spring effect on the rotor. This latter effect improves stability in hovering.

The effect of the radial vortices located beneath the rotor disc has been studied by R. Loewy and also by R. Timman and A. Van de Vooren (Ref. 13 and 14).

As far as there is no resonnance this effect may be compared to a gain modification of the lift.

We have introduced in the calculations of the above paragraph the G_n expressions instead of the more accurate γ_n development terms (see hovering conditions). Account may be taken of this by introducing B R instead of R (with B < 1) in the higher limit of the integrals.

3.242 - Periodic working conditions

The circulation $\Gamma(r,t)$ may be expressed in a general way as follows :

$$\Gamma(r,t) = \Gamma(r,t) + \sum_{m=1}^{m} \left[\Gamma_m(r,t) \cos m\Psi + \Gamma_m^x(r,t) \sin m\Psi\right]$$

Only the first term, which is a function of r alone, exists in hovering.

Disturbed flight conditions, the knowledge of which is necessary for stability and control studies, may be writen in a linearized form as follows :

$$\delta\Gamma(r,t) = \delta\,\Gamma_0(r,t) + \delta\Gamma_1(r,t) \cos\Psi + \delta\Gamma_1^x(r,t) \sin\Psi$$

The expressions Γ_0, Γ_M and Γ_M^x are, in periodic working conditions, independant from time and functions of r alone.

This is the ideal case of a rotor in stabilized level flight (when the machine is stable or indifferent).

The phenomenon is periodic : the marginal helix vortices have reached their equilibrium location and perform only periodic displacements, when Ψ varies. Their distance z to the blade depends upon the azimuthal position of the latter. This distance z takes into account the flapping effect $r\beta$. There is no reason, therefore, to consider this effect separately, as this has been done in the previous paragraph for transient conditions.

The radial vortices, of the type studied by R. Loewy, form a steady surface which extends towards infinity. A theoretical problem arises concerning those vortices : what happens to them when the sheets of helix vortices coil up to form the marginal vortices ?

From a practical stand-point it may be noted that the intensity of the radial vortices is only high at the immediate vicinity of the blade. This remark permits approximations to be introduced.

3.25 - Conclusive remarks

The application of the non-stationary theory leads, for fixed wings and incompressible flow, to satisfactory results. This makes one believe that the results will also be good in the case of fairly high loaded helicopter rotors.

In the author's point of view, the primary effect of the introduction of non-stationary conditions concerns the flapping motion of the blades (in transient conditions as well as in the steady state) and rotor control performance.

The mathematical apparatus which was introduced in the calculations is of the same order as those normally used to handle such problems.

3.3 - Forward flight

(It is recommended to read first paragraph 3.1)

3.31 - Setting in equation form

Let us consider a two-blade rotor in forward flight. Let $\Gamma_A(r,\Psi)$ be the non-stationary circulation at a stand-point (r,Ψ) of blade A and $\Gamma_A^*(r,\Psi)$ the stationary circulation at the same stand-point.

We obtain :

/.

$$(\text{III.3.74}) \begin{cases} \Gamma_A^x(r,\Psi) = \frac{1}{2} c \frac{dC_L}{di}(\omega r + V\sin\Psi)(\theta_c + \theta_t + \theta_1\cos\Psi + \theta_2\sin\Psi) \\ \quad - \frac{1}{2} c \frac{dC_L}{di}\left(V\sin\alpha + r\frac{d\beta}{dt} + V\beta\cos\Psi\right) \\ \quad - \frac{1}{2} c \frac{dC_L}{di} \frac{1}{4\pi} \int_{r_0}^{R} \frac{\partial \Gamma_A}{\partial r_1} \frac{dr_1}{r - r_1} - \frac{1}{2} c \frac{dC_L}{di} \sum V_i \end{cases}$$

The integral term represents, in an approximate way, the half helix issued from blade A.

The relation between the stationary circulation and the non-stationary one, is given by :

$$(\text{III.3.75}) \quad \frac{\partial \Gamma}{\partial t} + \left[\frac{2\times 0.381\,(\omega r + V\sin\Psi)}{c} + \frac{V\omega\cos\Psi}{\omega r + V\sin\Psi}\right]\Gamma =$$

$$= 0.639\,\frac{\partial \Gamma^x}{\partial t} + \left[\frac{2\times 0.381}{c}(\omega r + V\sin\Psi) + 0.639\,\frac{V\omega\cos\Psi}{\omega r + V\sin\Psi}\right]\Gamma^x$$

For flapping, we will substitute to this equation the following one :

$$(\text{III.3.76}) \begin{cases} \frac{\partial \Gamma}{\partial t} + k\Gamma = 0.639\,\frac{\partial \Gamma^x}{\partial t} + k\Gamma^x \\ k = \frac{2\times 0.381}{c}\,\omega\,0.75R \end{cases}$$

The flapping equation may then be written : (central hinge)

$$(\text{III.3.77}) \quad I_o\ddot{\beta} + \omega^2 I_o\beta = \rho\int_{r_0}^{R} \Gamma(r,\Psi)\,\omega r^2\,dr$$

3.32 - <u>Defining vortex location</u>

As it has been said in the study of hovering conditions (paragr.3.1) two methods are proposed :

First method,

The first half-turns of the helixes, which are evenly

/.

distributed along the blade radius, are replaced by half straight lines.

$$\frac{1}{4\pi}\int_{r_0}^{R}\frac{\partial\Gamma}{\partial r_1}\quad\frac{dr_1}{r-r_1}$$

Then the helix vortices are grouped together in four marginal helixes :

- two outer marginal helixes (blades A and B)
- two inner marginal helixes (" " " ")

The circulations of the outer and inner helixes are opposed and equal to $\pm\ \Gamma_M\ (\Psi)$ which is the maximum circulation to be determined by successive approximations.

Each marginal helix is replaced by a circle (C^*) and a solenoid (S^*) the characteristics of which are summarized in tables 3.34 and 3.35.

TABLE 3.34

Vortex Circles

	A		B	
	Inner	Outer	Inner	Outer
Radius	$r_0+\frac{1}{2}(\frac{R}{2}-r_0)$	R	$r_0+\frac{1}{2}(\frac{R}{2}-r_0)$	R
z	$V_0 \sin\alpha + V_{iz}(\Psi)\quad T$		$V_0 \sin\alpha + V_{iz}(\Psi)\ \frac{T}{2}$	
Circulation	$+\Gamma_M\ (\Psi)$	$-\Gamma_M\ (\Psi)$	$+\Gamma_M\ (\Psi)$	$-\Gamma_M\ (\Psi)$
Circle center location O B' $\cos\alpha$	$\frac{V_0 T}{8} + (V_0 \quad \cos\alpha)\ T$		$\frac{V_0 T}{8} + (V_0 \cos\alpha)\frac{T}{2}$	

/.

TABLE 3.35

Vortex Solenoids

	A		B	
	Inner	Outer	Inner	Outer
Radius	$\frac{R}{2}$	R	$\frac{R}{2}$	R
Limits of integration z_s to ∞	$z_s = (V_0 \sin\alpha + Vi_z)\,\frac{3T}{2}$		$z_s = (V_0 \sin\alpha + Vi_z)\,T$	
Circulation	$\frac{+\Gamma_M}{(V_0 \sin\alpha + Vi_z)T}$	$\frac{-\Gamma_M}{(V_0 \sin\alpha + Vi_z)T}$	$\frac{+\Gamma_M}{(V_0 \sin\alpha + Vi_z)T}$	$\frac{-\Gamma_M}{(V_0 \sin\alpha + Vi_z)T}$
Direction of axis	$\frac{V_0 \sin\alpha_0 + Vi_{zm}}{V_0 \cos\alpha}$		$\frac{V_0 \sin\alpha_0 + Vi_{zm}}{V_0 \cos\alpha}$	
Displacement of solenoid axis O A (see Fig.114)	$\frac{V_0 T}{8}$		$\frac{V_0 T}{8}$	

The distances z of the tables are measured normally to the rotor disc, from blade A downwards.

The value of Vi_{zm} is given by :

$$Vi_{zm} = \frac{F_M}{2\rho A\sqrt{V_0^2 + Vi_{zm}^2}}$$

The values of Vi_z (Ψ) may be estimated with the help of curves of Figures 107 to 113.

The first value of Γ_M (Ψ)

(III.3.78)
$$\begin{cases} \Gamma_{MA} = \Gamma_{M_0} + \Gamma_{M_1} \sin\Psi \\ \Gamma_{MB} = \Gamma_{M_0} - \Gamma_{M_1} \sin\Psi \end{cases}$$

/.

may be taken, for the first approximation, from formula III.3.74 in which the induced velocity terms are replaced by the mean V_{izm}.

Γ_M will be computed for r = 0.9 and for ψ = 0, 90°, 180° and 270°.

It is important to take into account the circle (C*) center location. The solenoid axis displacement (OA) may be neglected.

The effect, on blade A, of the radial vortices issued from blade B will be introduced in the form of a corrective term, when the correct value for Γ_M will have been obtained.

The expression of this corrective term is given in the following paragraph.

Second method.

In the same way as previously the first half-turns of the helixes distributed along the blade radius will be replaced by half straight lines.

However, in order to avoid the successive approximation for Γ_M, the remaining helixes will no more be grouped, here, in marginal helixes but will be considered as sheets of oblique solenoids stretching from z = 0 to infinity.

The intensity of every elemental solenoid is unknown and may be written : :

$$\frac{\partial \Gamma}{\partial r_1}(r_1, \psi) \frac{1}{(V \sin\alpha + V_{iz})\, T}$$

The corrective term for the radial vortices issued from blade B will be maintained here.

3.33 - Calculation work up

Let us write :

/.

$$r = r_0 + \frac{R - r_0}{2} (1 - \cos \varphi)$$

$$0 \leq \varphi \leq \pi$$

(III.3.79)
$$\Gamma (\varphi, \psi) = \sum_{n=1}^{n=6} \gamma_n \sin n\varphi +$$

$$+ \sum_{n=1}^{n=6} \sum_{m=1}^{m=3} (C^*_{n,m} \cos m\psi + S^*_{n,m} \sin m\psi) \sin n\varphi$$

The circulation is defined by 42 coefficients.

This figure may seem very high, but it may be noted that this comes to calculate load distributions for seven azimuthal blade positions, which is quite usual in rotor calculations.

We may also note that flapping calculations, with the help of equation III.3.37, are simple and that use of equations of table 3.20 (still valid) does not raise any difficulty, these equations being solvable with variable parameters.

However, the calculations of the induced velocities for variable ψ values and stand-points (r) such as :

(III.3.80) $\varphi = 30°, 36°, 45°, 60°, 72°, 108°, 120°, 135°, 144°$ and $150°$.

are not practically feasible without availability of Tables of functions.

3.34 - Requirement of Tables of Functions

The objective is the calculation of the induced velocities, for different azimuthal positions, for φ values defined by III.3.80 and for the two parameters $\mu = \frac{V}{\omega R}$ and $\frac{V_{izm}}{\omega R}$

When use is made of the first method, one must compute :

- the velocities induced by an inner and an outer circles,
- the velocities induced by an inner and an outer solenoid,
- the velocities induced by the radial vortex corrective terms.

When use is made of the second method, one must compute:

- the velocities induced by the solenoid sheet,
- the velocities induced by the radial vortex corrective terms.

The typical formulae are given by equations III.3.81, in Table 3.36.

In order to render the method practically accessible to engineers, calculations should be carried out with the help of numerical Tables.

Digital computers should be used for the drawing up of such Tables.

3.35 - Flexible blades

It is possible, in the proposed method, to take into account blade flexibility.

To this end, the value of the flapping angle β must be replaced, in equation III.3.74, by the natural modes of a homogeneous blade.

The flapping equation III.3.76 is then replaced by a linear system which will define the new η_i coefficients substituted to the a_1 and b_1 flapping coefficients :

$$y_i = \sum \eta_i \, e^{i\omega t} \left(\sin \beta_i \frac{r}{R} - \operatorname{sh} \beta_i \frac{r}{R} \right)$$

$$\beta^2 = \frac{1}{R^2} \sqrt[2]{\frac{m^2 \nu_i^2}{EI}}$$

with :

ν = natural frequency of the blade

EI = flexural rigidity.

/.

TABLE 3.36

Equations III.3.81 - Forward flight

FIRST METHOD

- *de Laaw - Castles type Circles. Larger z distances. Γ variable with θ*
- *Solenoid.*

$$V_i = \frac{1}{4\pi T}\int_{\tau_1=nT}^{\infty}\int_{\theta=0}^{\theta=2\pi}\frac{\Gamma_M\left[\omega r r_1\cos\theta - r_1^2\omega + V_x r\sin\Psi - V_x r_1\sin(\Psi-\theta) - V_x\omega\tau r_1\cos(\Psi-\theta)\right]d\tau\, d\theta}{\left[r^2 + r_1^2 + (V_x^2+V_z^2)\tau^2 - 2rr_1\cos\theta - rV_x\tau\cos\Psi + rr_1V_x\tau\cos(\Psi-\theta)\right]^{3/2}}$$

$r_1 = R,\ \frac{R}{2}$; $V_x = V_o$; $V_z = V_o\sin\alpha + V_{i_z}$; $\Gamma_M = \Gamma_{M_o} + \Gamma_{M_1}\sin\Psi$; $\tau_1 = nT$

$\Gamma_M = c^{\frac{R}{2}}$

- *Radial vortices*

$$V_i = \frac{1}{4\pi}\int_{\omega\tau=0}^{\omega\tau=2\pi}\frac{\partial\Gamma}{\partial t}(\Psi-\omega\tau)\left[\frac{r\sin\omega\tau}{V_z^2 + r^2\sin^2\omega\tau}\right]\left[\frac{r\cos\omega\tau}{\sqrt{V_z^2+r^2}} + \frac{(R - r\cos\omega\tau)}{\sqrt{V_z^2 + R^2 + r^2 - 2rR\cos\omega\tau}}\right]d\omega\tau$$

SECOND METHOD

- *Solenoid*

$$V_i = \frac{1}{4\pi T}\int_{\tau=0}^{\tau=\infty}\int_{r_1=r_o}^{r_1=R}\int_{\theta=0}^{\theta=2\pi}\frac{\partial\Gamma}{\partial r_1}\frac{\left[\omega r r_1\cos\theta - r_1^2\omega + V_x r\sin\Psi - V_x r_1\sin(\Psi-\theta) - V_x\omega\tau r_1\cos(\Psi-\theta)\right]d\tau\, dr_1\, d\theta}{\left[r^2 + r_1^2 + (V_x^2+V_z^2)\tau^2 - 2rr_1\cos\theta - 2rV_x\tau\cos\Psi + rr_1V_x\tau\cos(\Psi-\theta)\right]^{3/2}}$$

$\Gamma = \Sigma\sin n\Psi$ $\qquad\qquad$ $\cos\Psi = \left(\frac{2}{R-r_o}\right)(r - r_o)$

4 - CONCLUSION

4.1 - The results of this study show that it is possible to substitute to the determination, by analysis, of a helicopter rotor vortex structure, an experimental method leading to a satisfactorily simple and general vortex architecture.

This experimental method consists in visualizing the vortices by smoke emission on model rotors operated in a wind tunnel.

The accuracy of this method is not very high but it proved to be quite satisfactory.

In order to avoid hasty generalizations of particular cases, a large number of operating conditions and of blade characteristics was experimented.

However, only "normal" flight conditions, such as :

- flight in established state,
- disturbances due to rotor control motions,
- fairly high disc loadings,

have been considered.

Peculiar cases such as rotor stall, blade flutter and aerodynamic resonances have been intentionally omitted.

4.2 - Confrontation of the vortex theory with test results was made in a way which is believed to be logical.

The introduction of inner marginal vortices (already brought to evidence by Robin Gray) was, in particular, considered as necessary as well from the theoretical point of view, as for the obtainement of more accurate load distributions over the blades.

The theoretical correlation of the mathematical vortices distributed along the blade to the marginal vortices observed in the wind tunnel was not established (same as for fixed wings).

It has not been possible to demonstrate with accuracy that the marginal vortices are to be considered as streamlines (in a co-ordinate system linked to the blade) and that the vortices which appear, at any modification of lift, are orthogonal to the latter.

Our conclusions refer to the fact that the marginal vortices do not give rise to any exchange of energy

($\vec{V} \cdot \overrightarrow{\text{rot } V} = 0$) while the radial vortices do give rise to such an exchange ($\vec{V} \cdot \overrightarrow{\text{rot } V} \neq 0$).

In the Rankine - Froude theory, the infinite down-stream flow velocity is twice the one at the rotor disc.

In the solenoid formulae which were used, flow velocity has not this double value.

It seems that a theoretical explanation may be found to this in the study performed by R. Hirsch (see Ref.11).

4.3 - The proposed vortex architecture is intentionally simplified.

We have sought to avoid, wherever possible, giving empirical, and so called "practical", formulae for situating the vortices.

We believe that such formulae lead to a delusive precision.

4.4 - Even when the vortex structure is available, the mathematical problems remain difficult to solve.

Every time it was possible complex functions were replaced by approximate expressions comprising polynomials and trigonometric functions.

Such a "slaughter" of "attractive formulae" is, however, not always possible.

Different methods were sometimes suggested for solving one same problem. They are generally subject to the difficulty to handle the mathematical apparatus.

4.5 - The object of this work was to make available to engineers a method, easy to work-up, for the evaluation of air loads acting on helicopter rotor blades.

We believe that this result has been achieved though a complementary work consisting in numerical calculations remains to be performed.

The distribution of the air loads acting on a rotor blade, in hovering conditions, such as obtained with the proposed method was compared to the available J. Rabbott's experimental results.

It may be seen that the agreement of the two curves is excellent, particularly at the blade tip.

Introduction of non stationary effects, for the stability and control calculations, leads to linearized equations similar to those normally used for such problems. Application of this method to forward flight conditions necessitates the use of numerical Functions Tables /.

which remain to be established.

The calculations of such Tables must be carried out with the help of digital computers;

Availability of these Tables would render the proposed method easy to work-up.

It would also be of interest to have, for further comparison, accurate experimental data of air load distributions along the blades, in forward flight, with account for non-stationary effects.

LIST OF REFERENCES

1 - Robin B.GRAY - "An aerodynamic analysis of a Single-bladed rotor in hovering and low-speed forward flight as determined from smoke studies of the vorticity distribution in the wake" (Aeronautical Engineering department. Report No.356, September 1956).

2 - Gaetano FALABELLA Jr. and John R.MEYER Jr. - "The determination of inflow distributions from experimental aerodynamic loading and blade motion data on a model helicopter rotor in hovering and forward flight" - Princeton University (Department of aeronautical engineering, Massachusetts Institute of Technology, June 1953).

3 - John R.RABBOTT Jr. - "Static-thrust measurements of the aerodynamic loading on a helicopter rotor blade". (NACA T.N.3688, July 1956).

4 - Edmund E. CALLAGHAN and Sthephen H.MASLEN - "The magnetic field of a finite solenoid" (NASA TM. D465. October 1960).

5 - LAMB - "Hydrodynamics" - DOVER 1923.

6 - CASTLES W. Jr. and DELEEW J.H. " The normal component of the induced velocity of a lifting rotor and some examples of its application (NACA TN.2912).

7 - ISAACS Rufus - "Airfoil theory for flows of variable velocity" JAS (Jan.1945) and (Apr.1946).

8 - REBONT - VALENSI - SOULEZ LARIVIERE - "Réponse d'un rotor d'hélicoptère à une augmentation du pas général dans le cas d'un vol vertical". (Technique et Science Aéronautique. Mai-Juin 1959).

9 - Dr. Eugene JAHNKE and Fritz EMDE "Tables of functions with formulae and curves" Dover Publications N.Y.

10 - P.CARPENTER and B.FRIDOWICH "Effect of a rapid blade pitch increase on the thrust and induced velocity response of a full scale helicopter rotor (NACA TN.3044.1958)

/.

11 - HIRSCH R. " Installation de la portance sur un profil muni d'une fente de soufflage au bord de fuite et correction due à l'envergure finie" Publications Scientifiques et Techniques du Ministère de l'Air - Série jaune n°69.

12 - Th. Von KARMAN et W.R.SEARS. "Théorie de l'Aile en mouvement non uniforme" (J.A.S. Août 1938).

13 - Robert G.LOEWY "A Two-dimensional approximation to the unsteady aerodynamics of Rotary wings" J.A.S. Feb. 1957

14 - R. TIMMAN and A.I.Van de VOOREN - "Flutter of a helicopter rotor rotating in its own wake" (JAS Sept.1957)

15 - MEIJER DREES J. "A theory of airflow through rotors and its application to some helicopter problems" J.Helicopt. Ass. G.B. 3, No.2 (July, Aug.Sept. 1949).

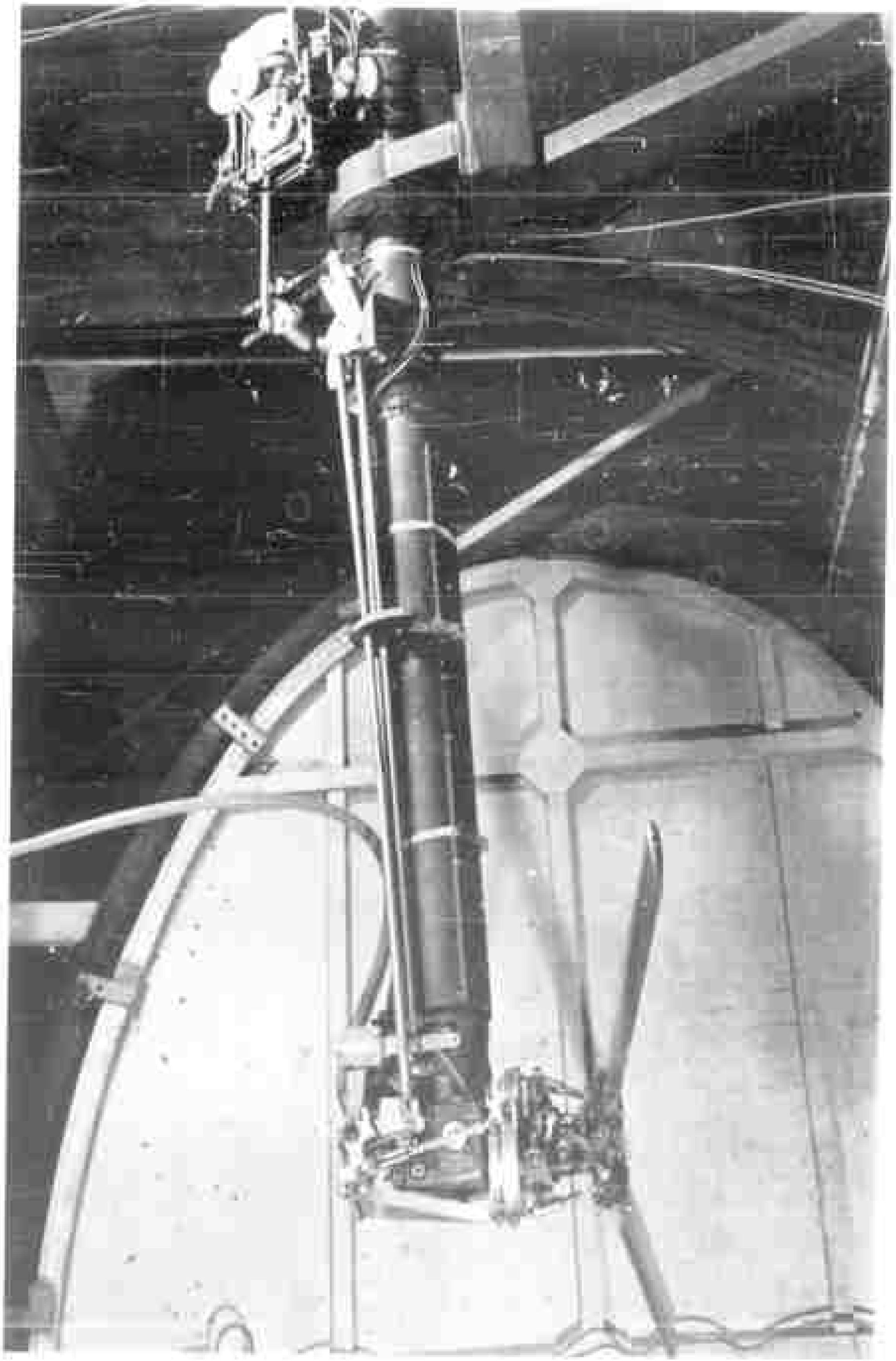

VIEW OF SET-UP IN WIND-TUNNEL

FIG. 1

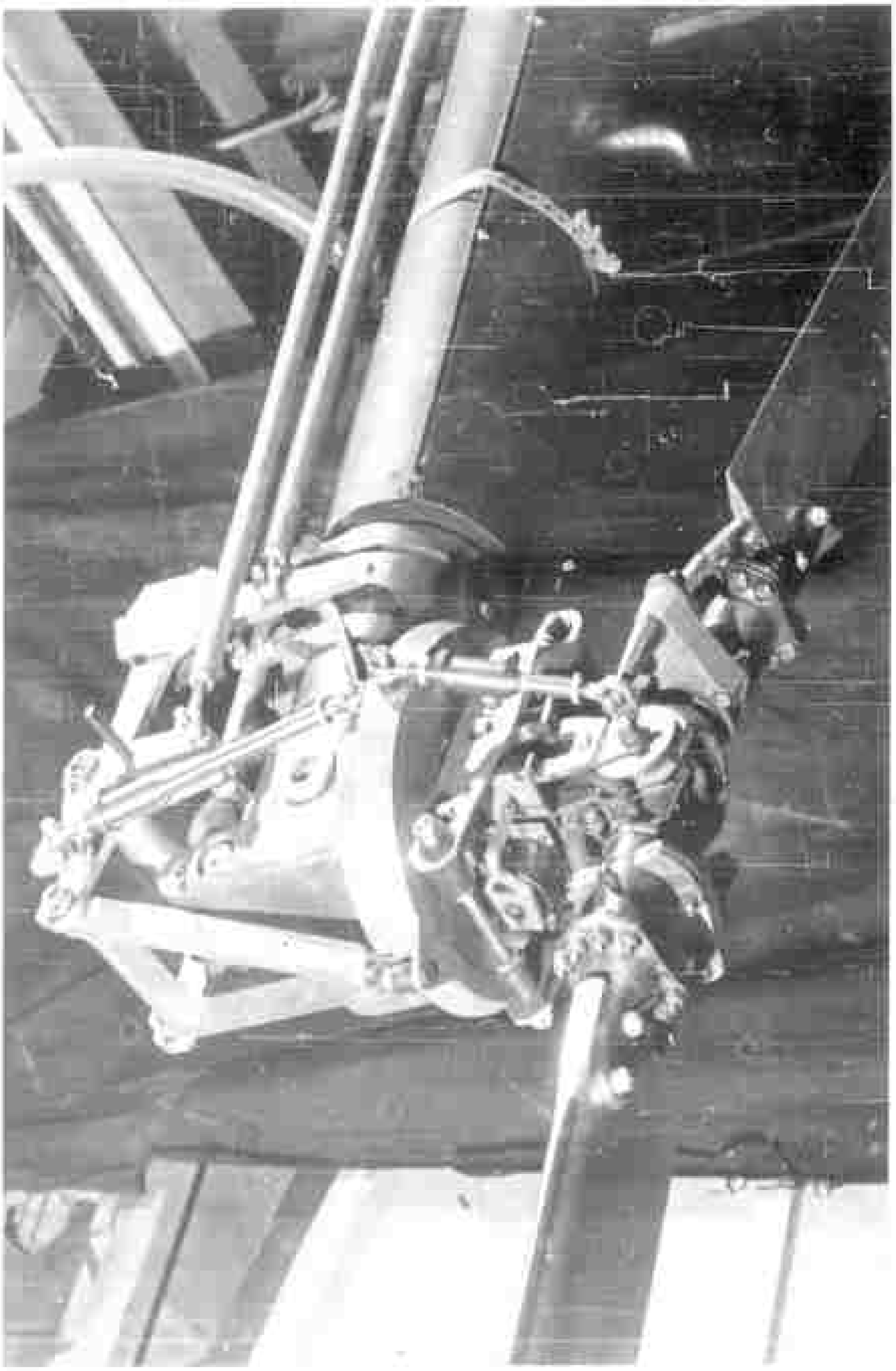

FIG. 2

CLOSE VIEW OF ROTOR-HEAD ON SUPPORTING ARM

ESTABLISHED STATE, EXTERNAL SMOKE EMISSION

FIG. 3

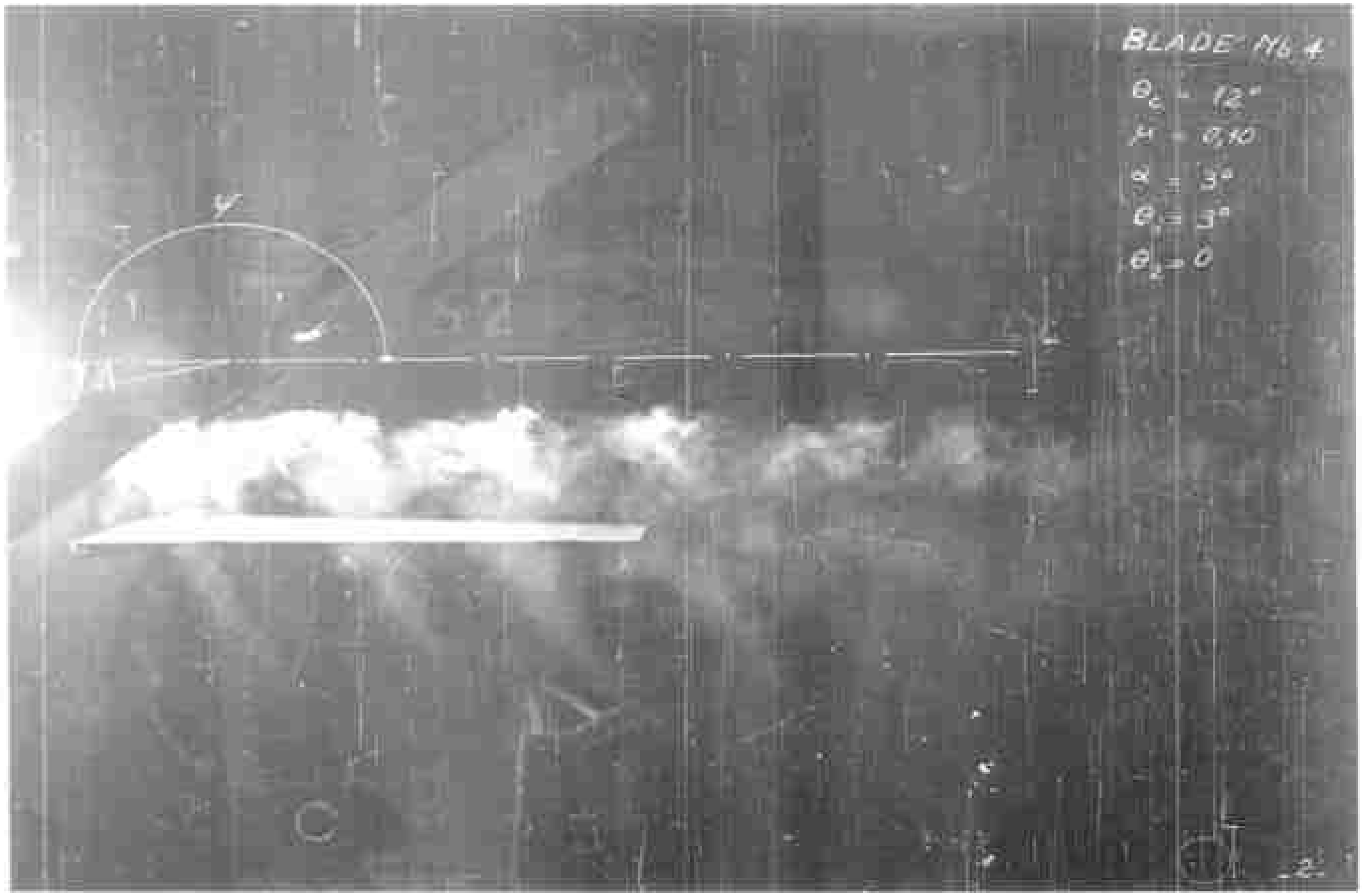

ESTABLISHED STATE. EXTERNAL SMOKE EMISSION

FIG. 4

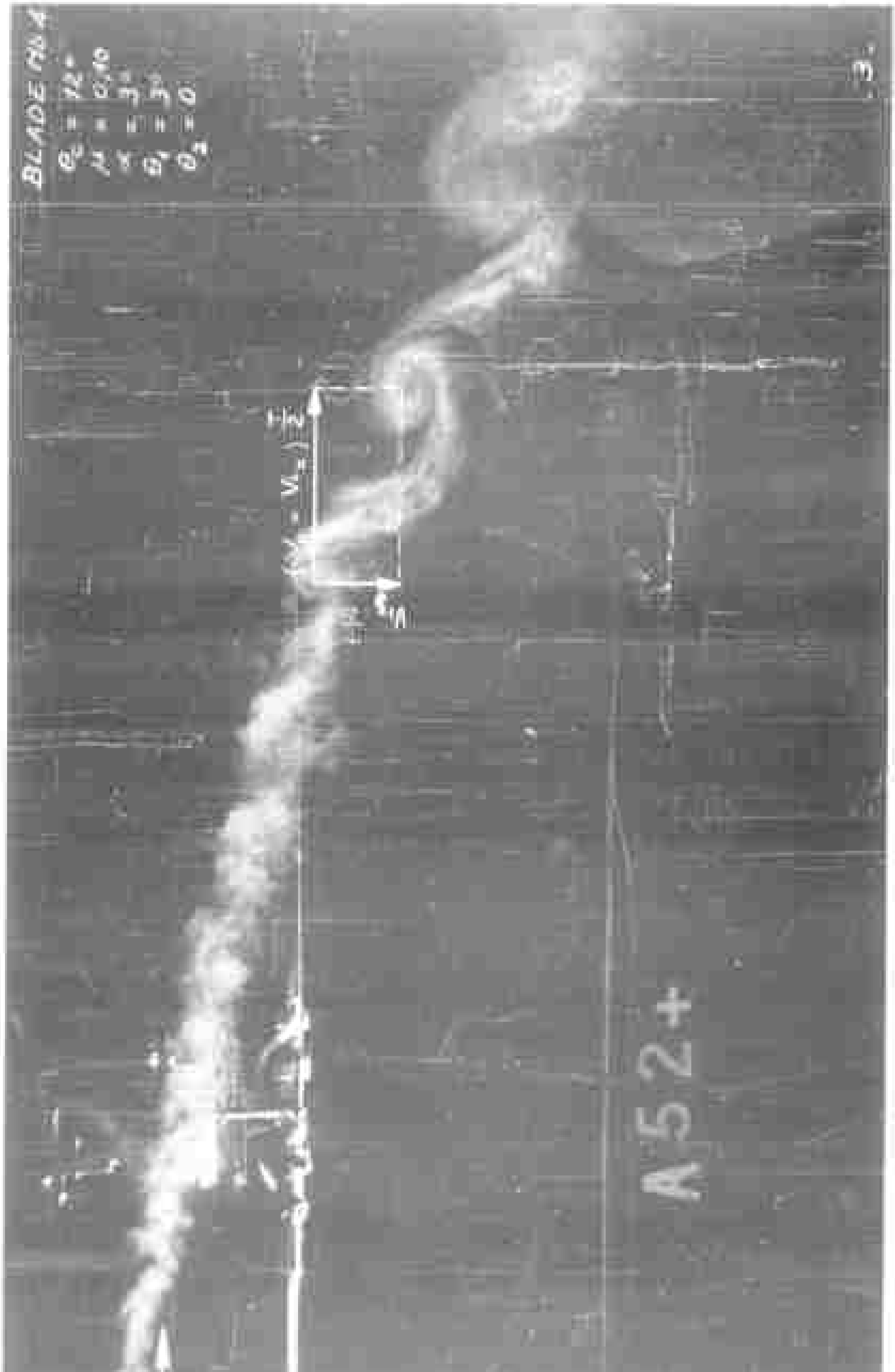

FIG. 5

ESTABLISHED STATE. EXTERNAL SMOKE EMISSION

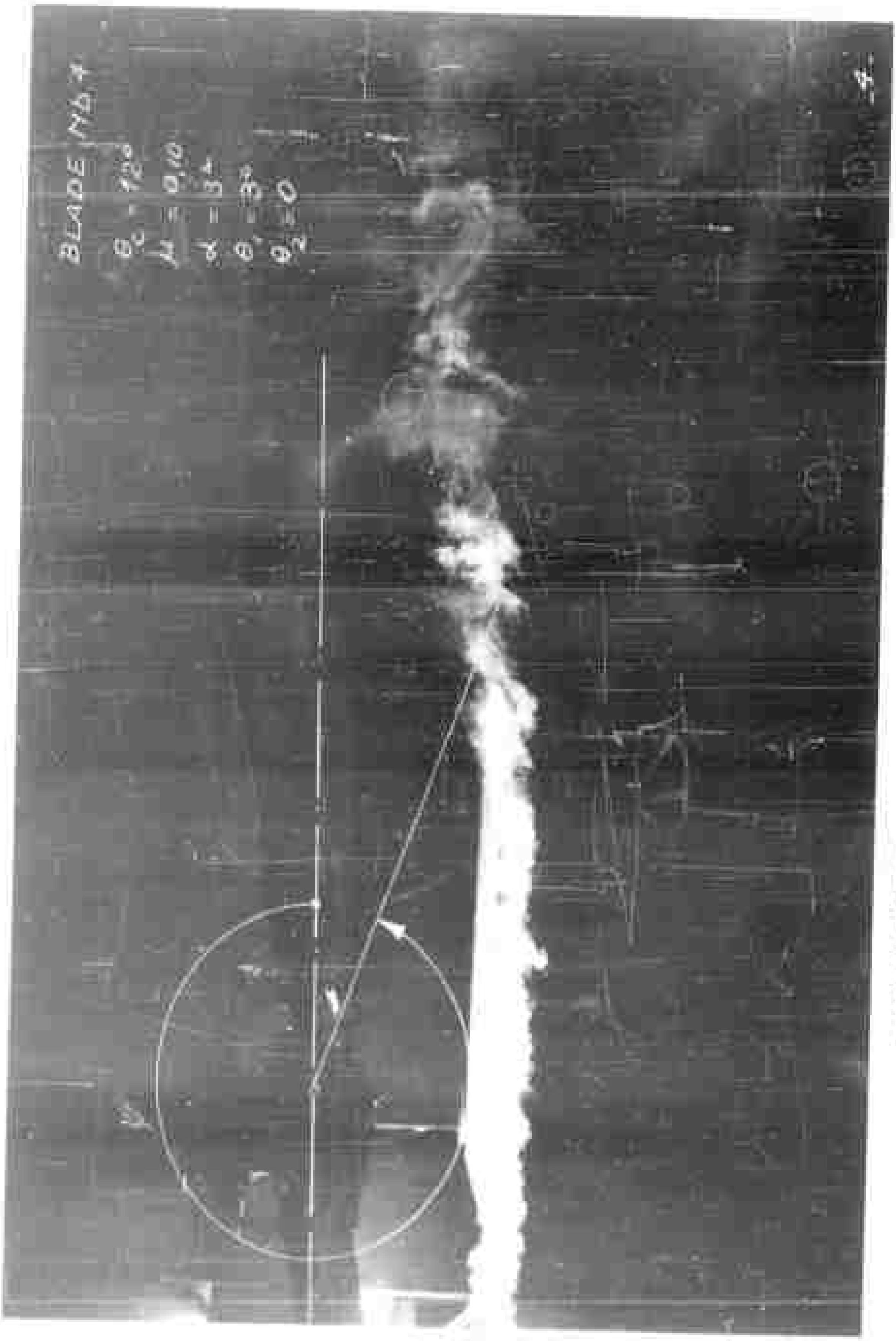

ESTABLISHED STATE, EXTERNAL SMOKE EMISSION

FIG. 6

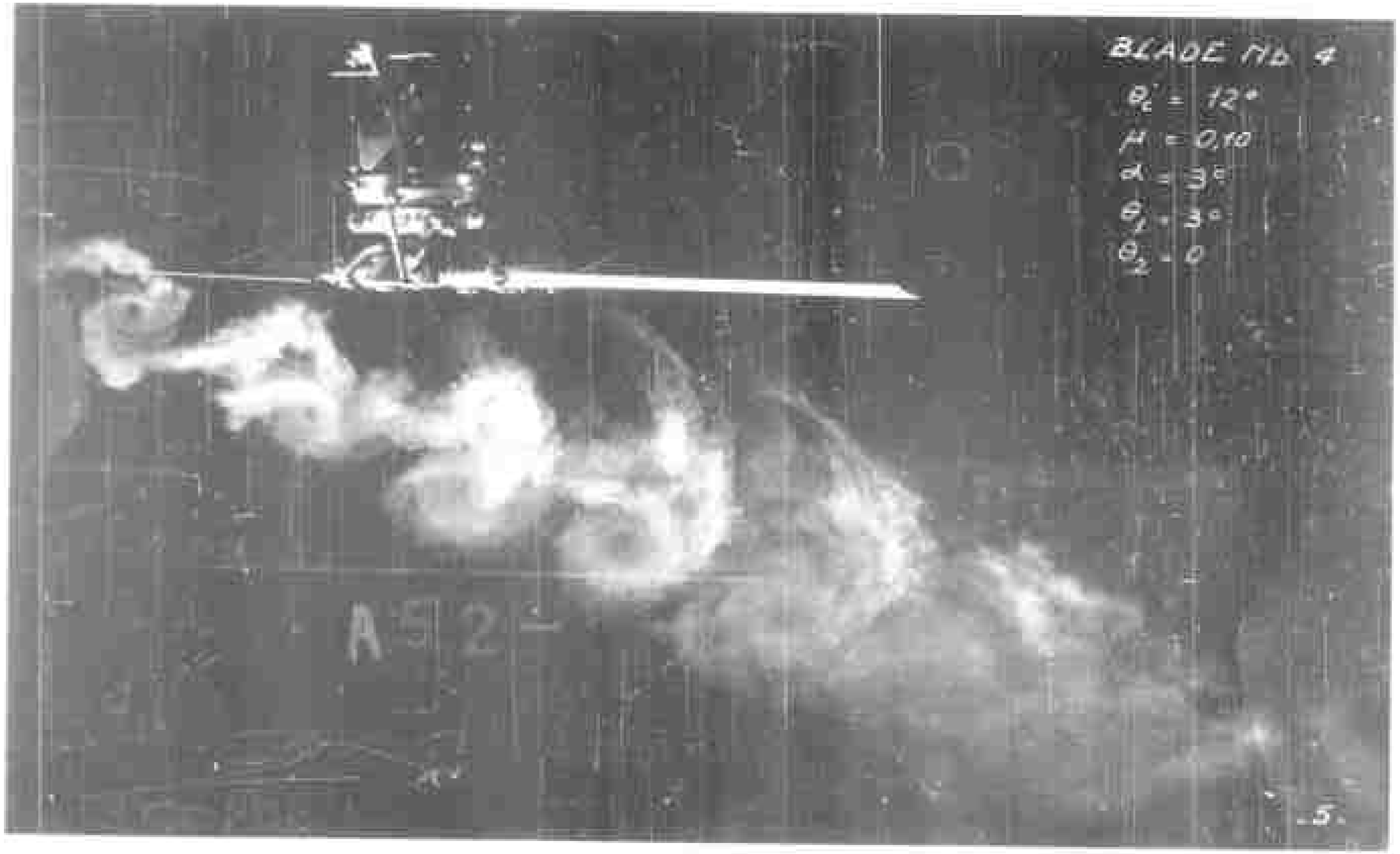

ESTABLISHED STATE. EXTERNAL SMOKE EMISSION

FIG. 7

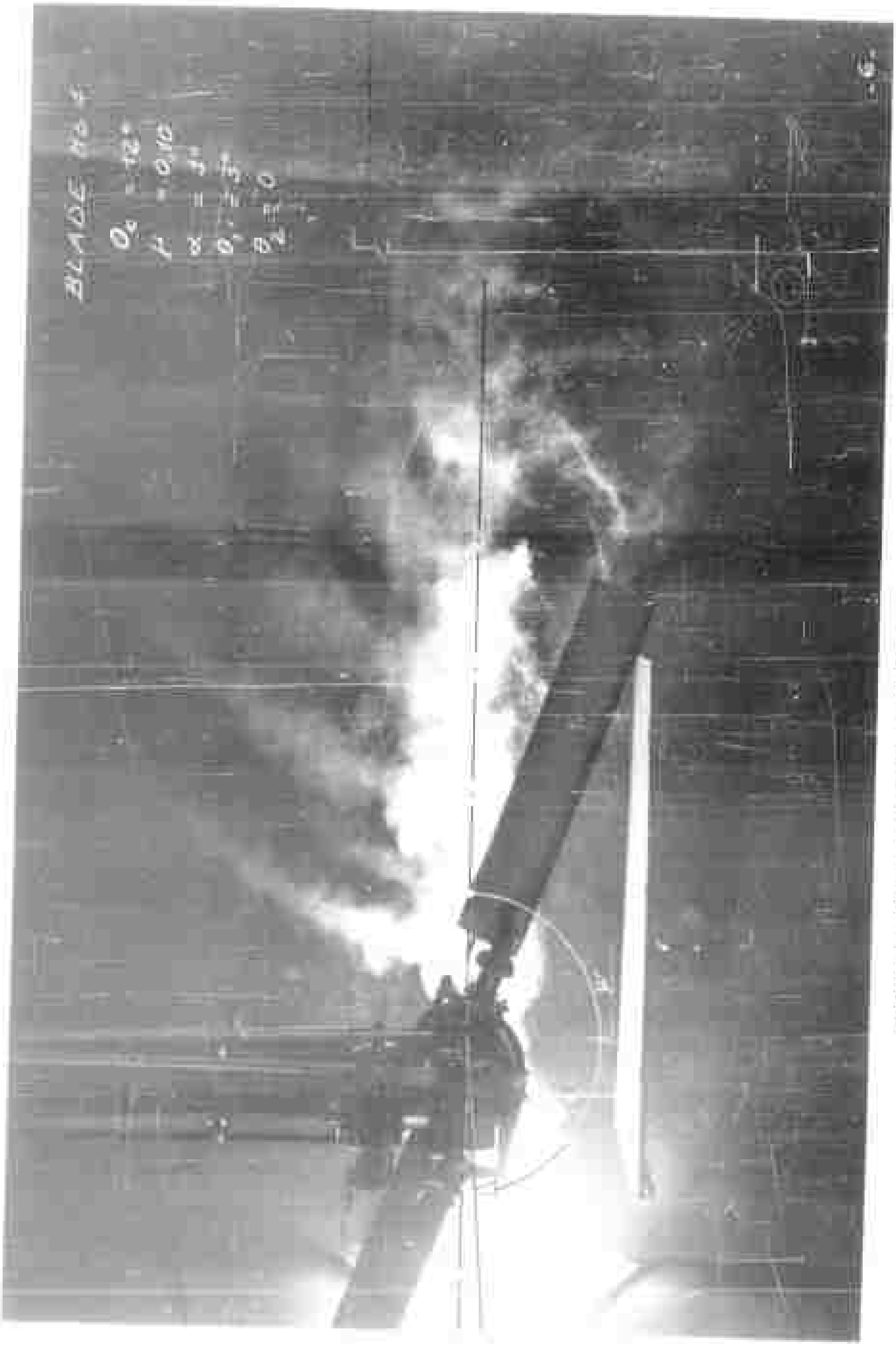

ESTABLISHED STATE, EXTERNAL SMOKE EMISSION

FIG. 8

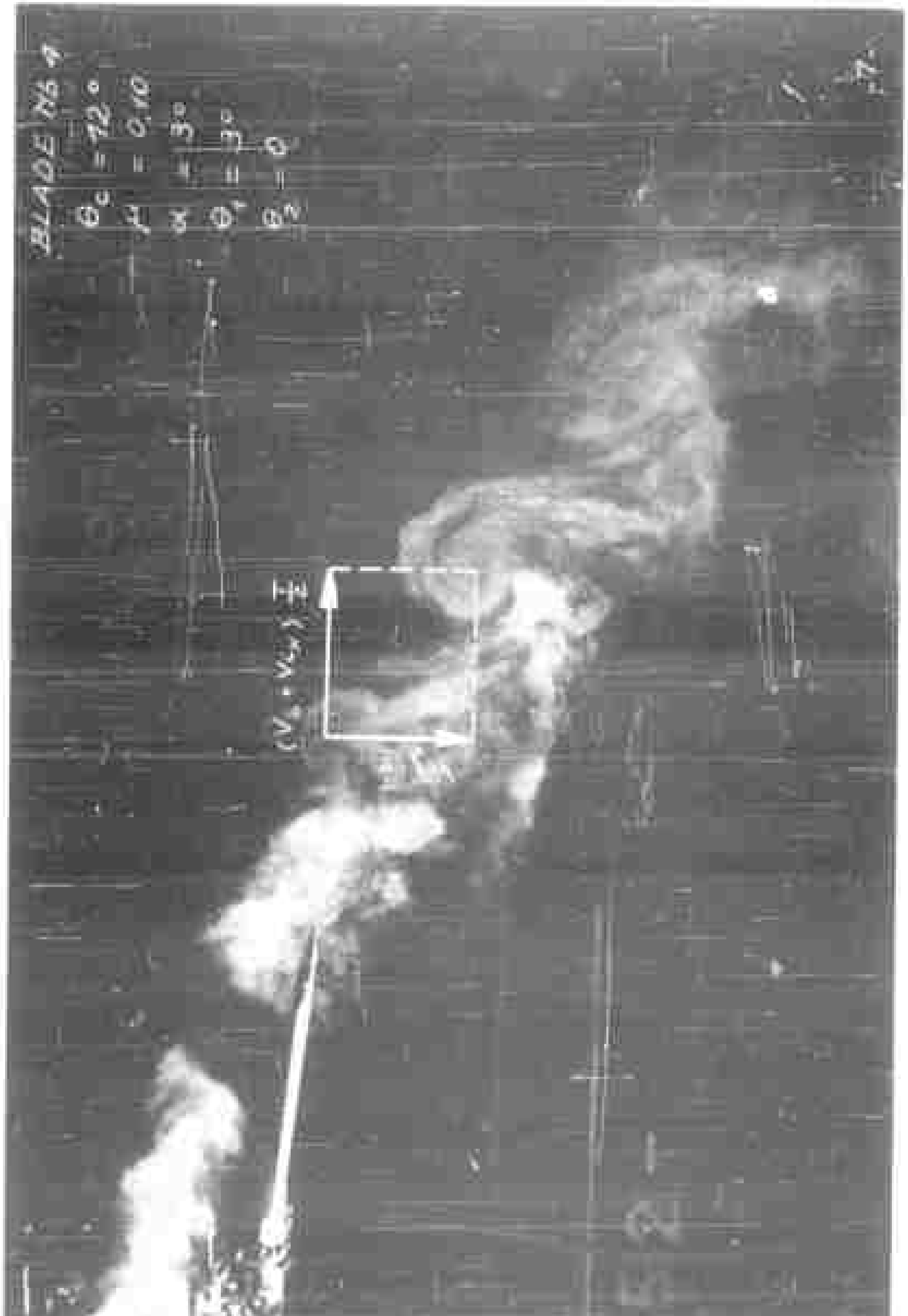

ESTABLISHED STATE. EXTERNAL SMOKE EMISSION

FIG. 9

FIG. 10

ESTABLISHED STATE. EXTERNAL SMOKE EMISSION

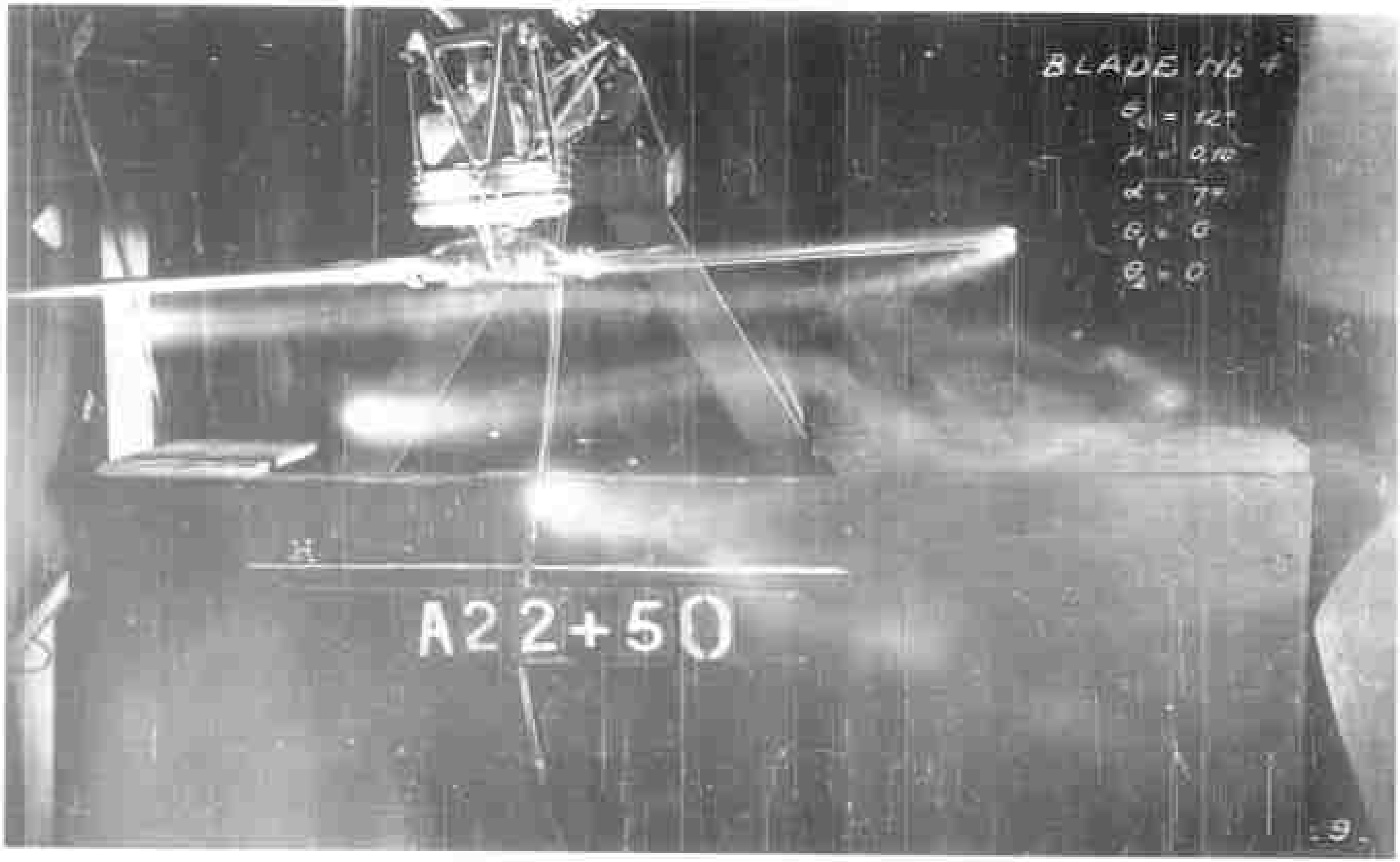

ESTABLISHED STATE. SMOKE EMISSION AT BLADE TIP

FIG. 11

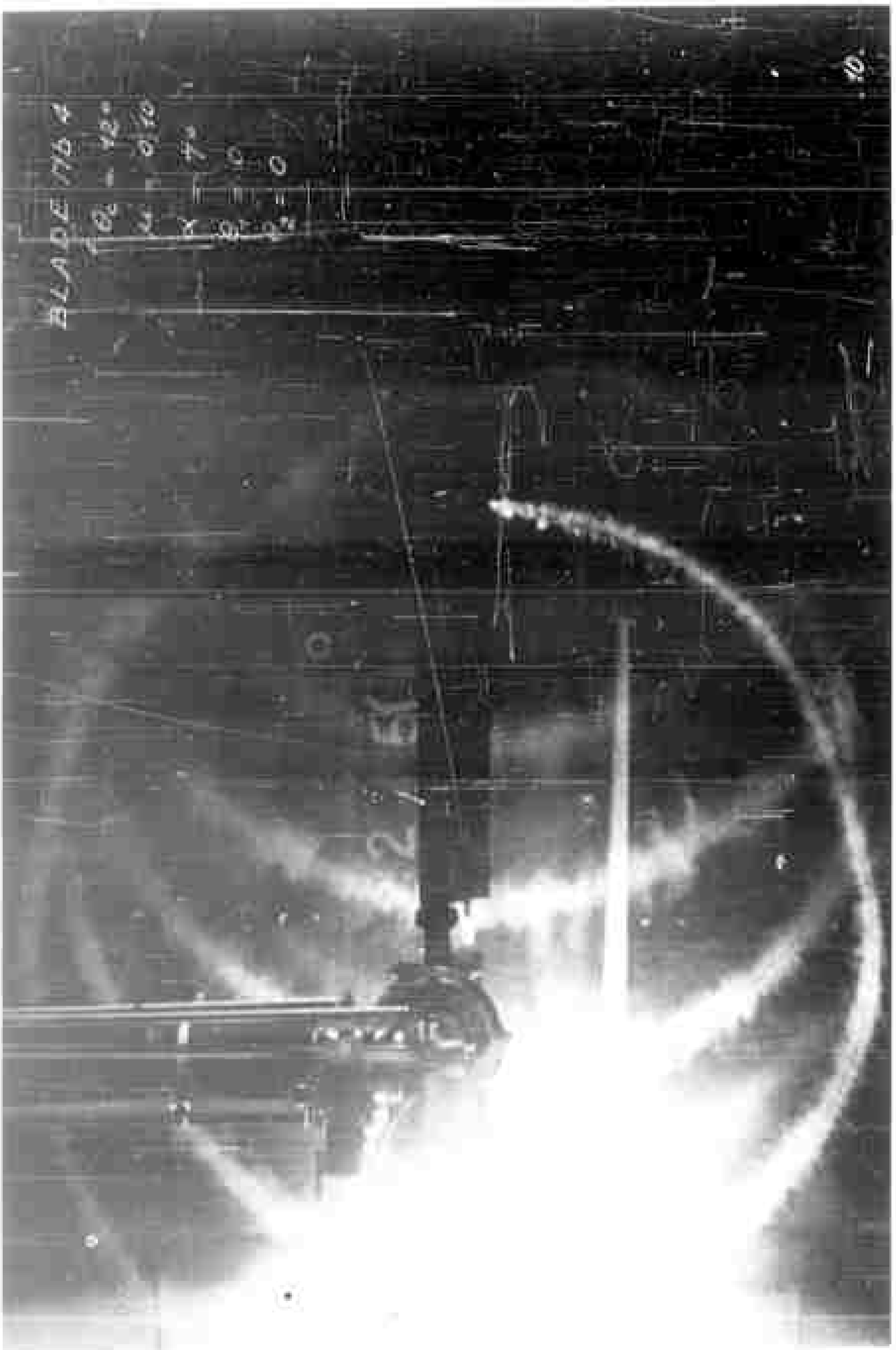

ESTABLISHED STATE. SMOKE EMISSION AT BLADE TIP

FIG. 12

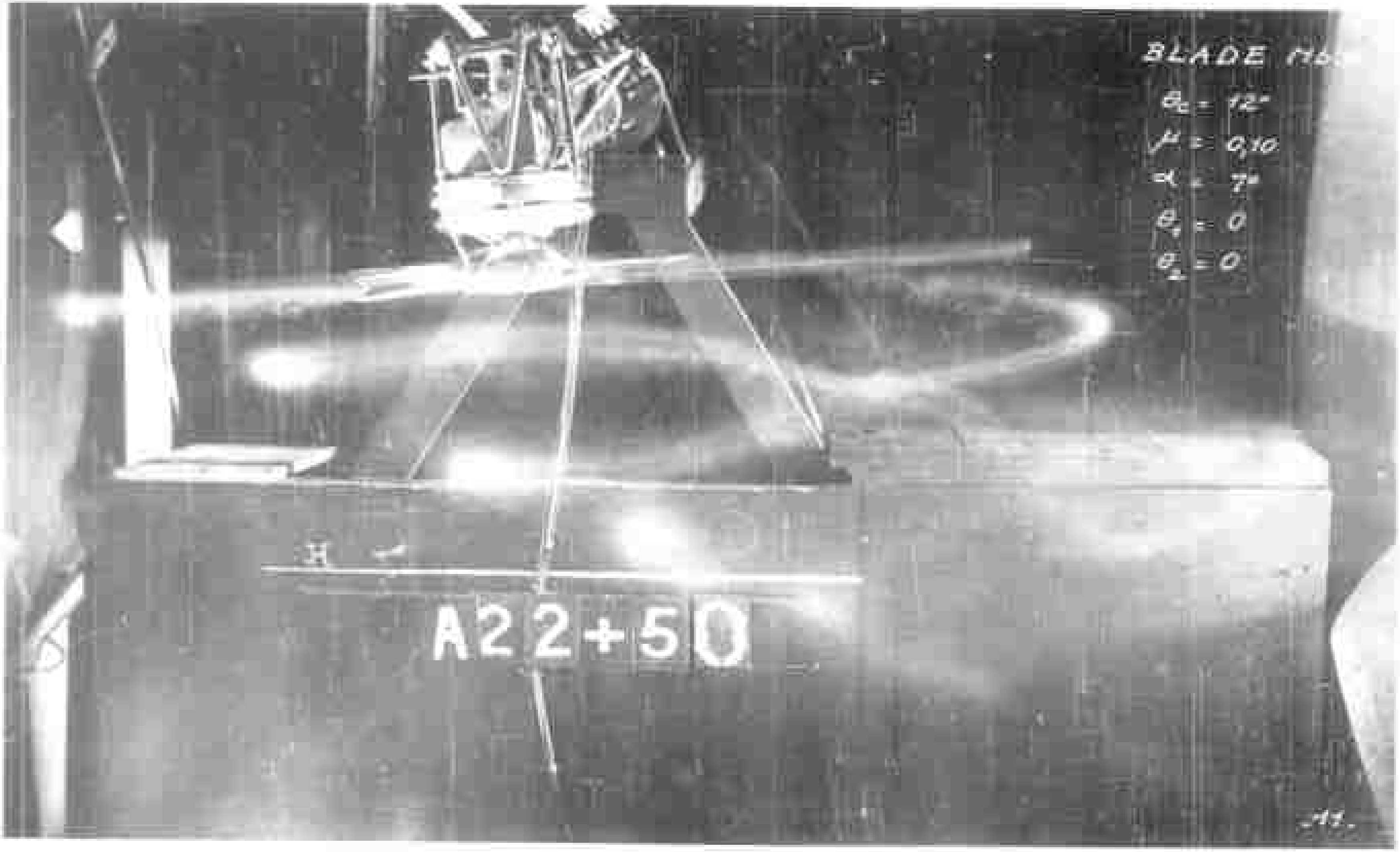

ESTABLISHED STATE. SMOKE EMISSION AT BLADE TIP

FIG. 13

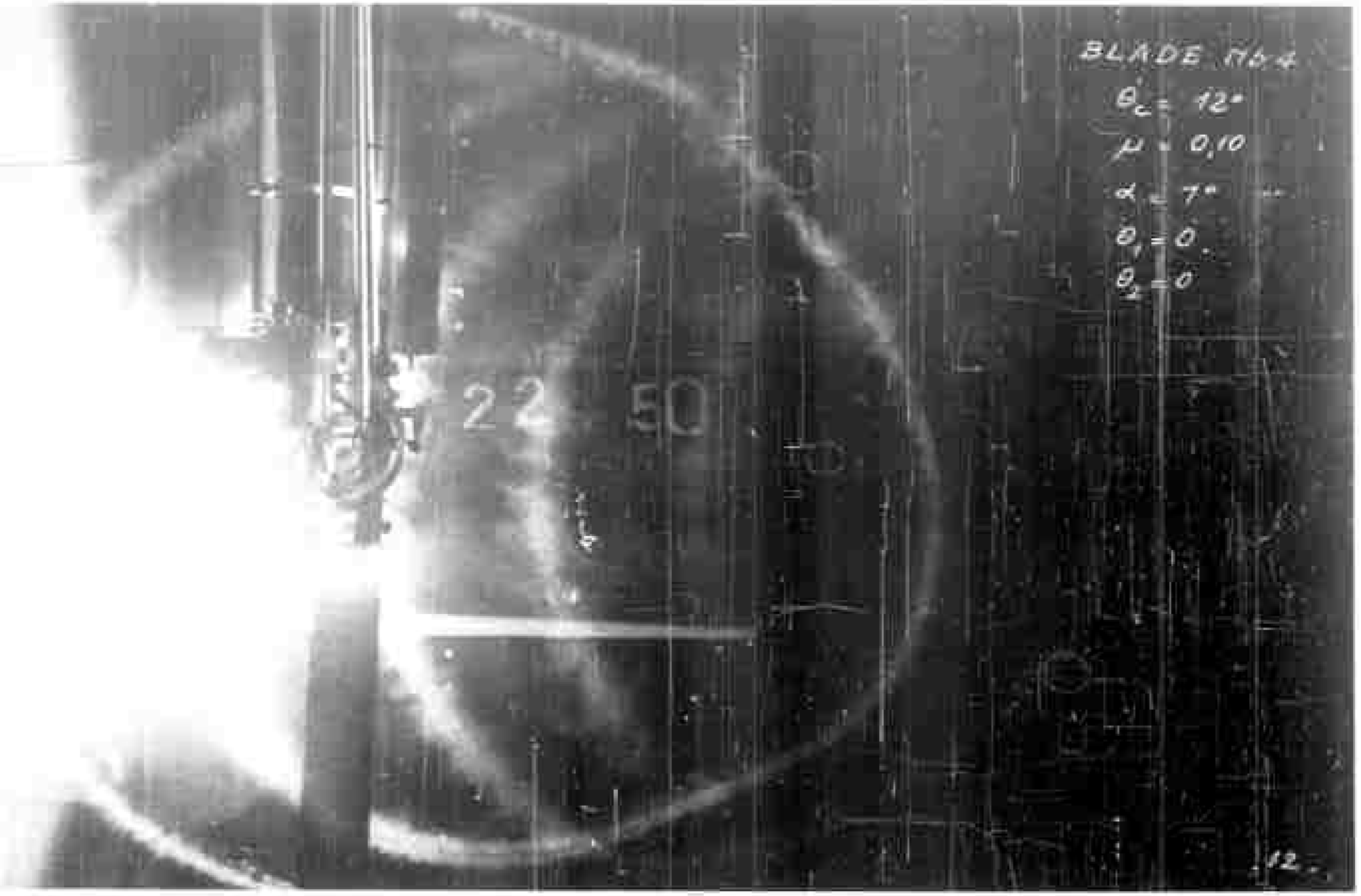

ESTABLISHED STATE. SMOKE EMISSION AT BLADE TIP

FIG. 14

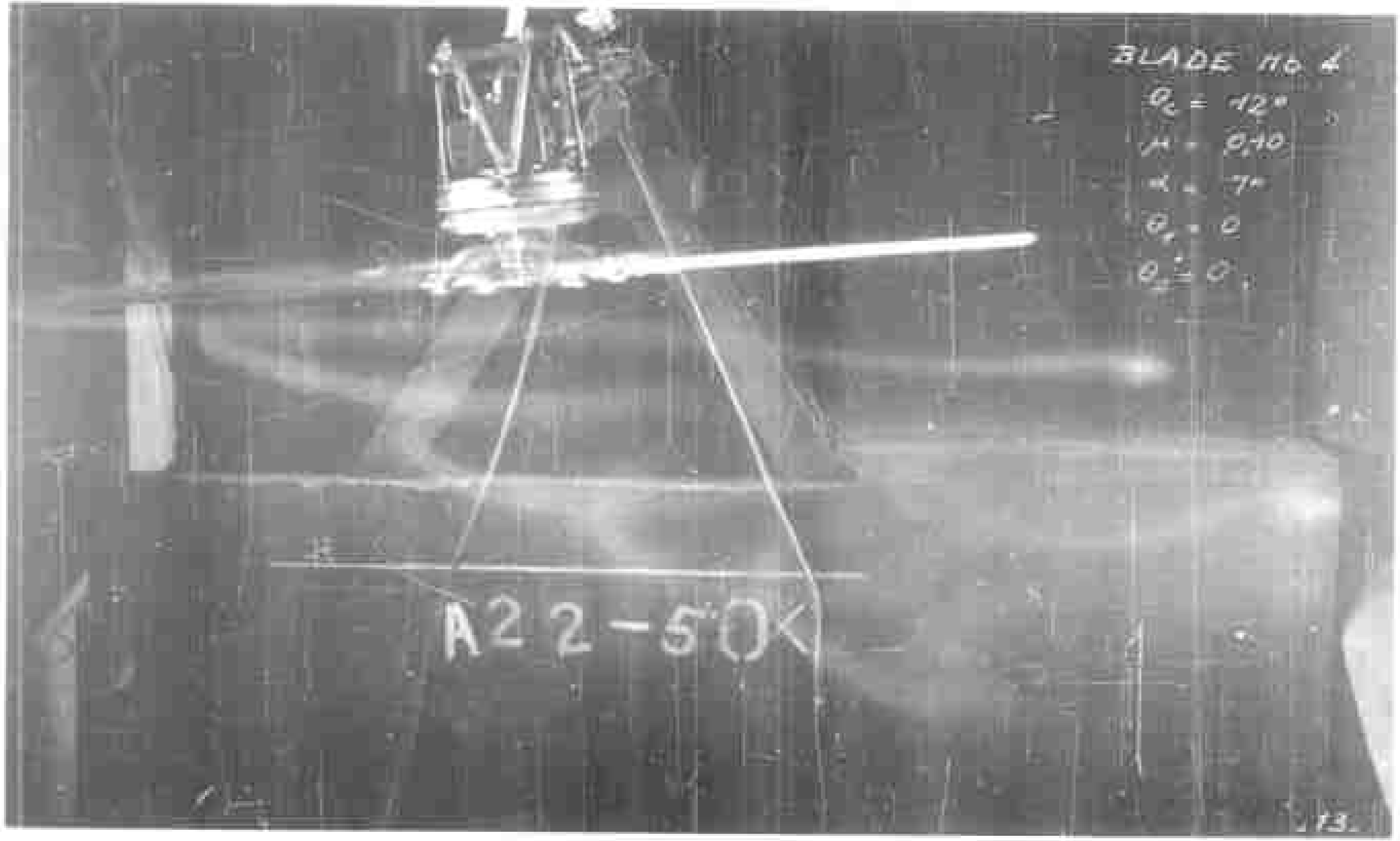

ESTABLISHED STATE. SMOKE EMISSION AT BLADE TIP

FIG. 15

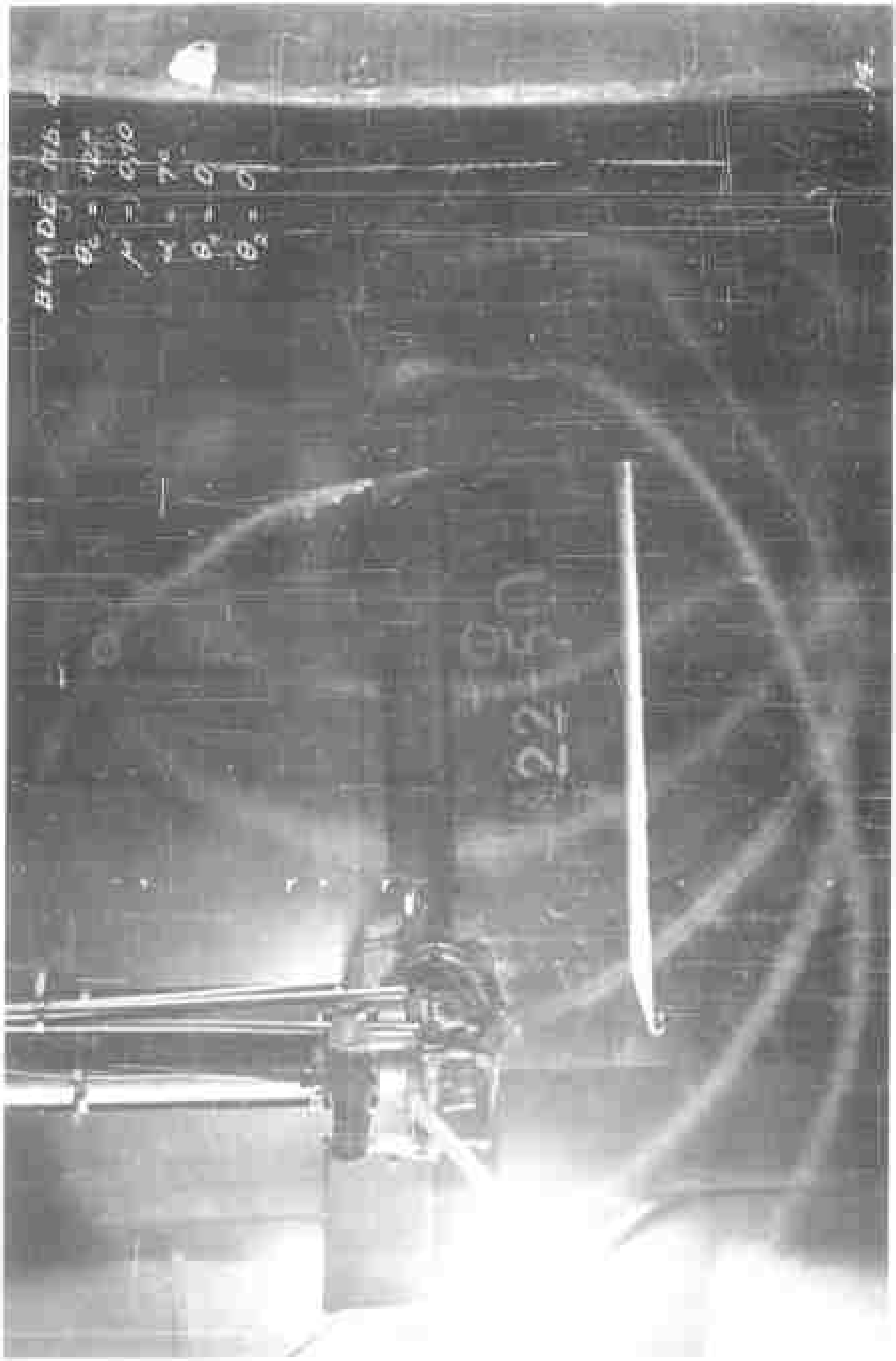

ESTABLISHED STATE. SMOKE EMISSION AT BLADE TIP

FIG. 16

ESTABLISHED STATE. SMOKE EMISSION AT BLADE ROOT

FIG. 17

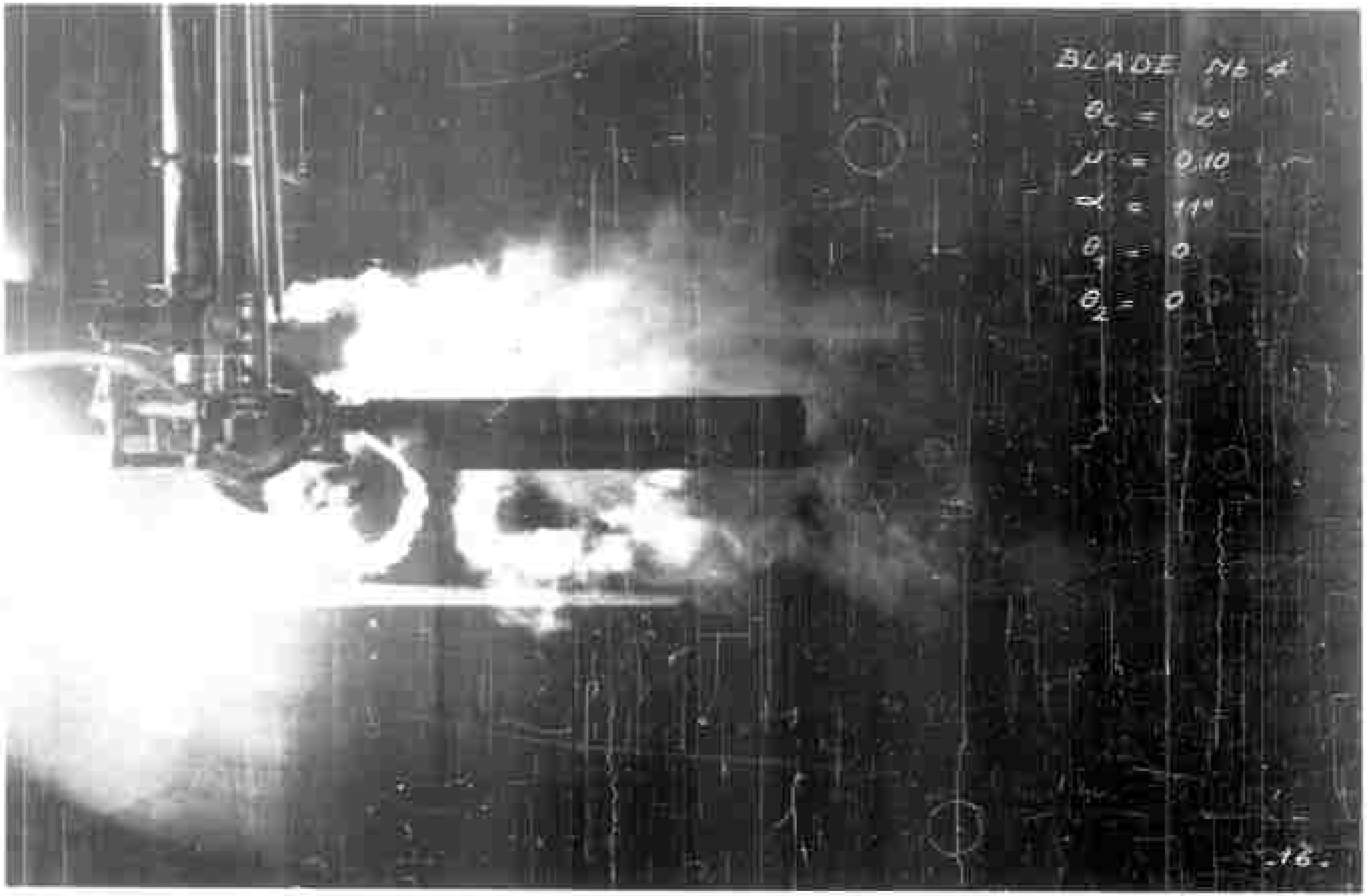

ESTABLISHED STATE, SMOKE EMISSION AT BLADE ROOT FIG. 18

ESTABLISHED STATE. SMOKE EMISSION AT BLADE ROOT

FIG. 19

ESTABLISHED STATE. SMOKE EMISSION AT BLADE ROOT FIG. 20

ESTABLISHED STATE. SMOKE EMISSION AT BLADE TIP FIG. 21

ESTABLISHED STATE. SMOKE EMISSION AT BLADE TIP

FIG. 22

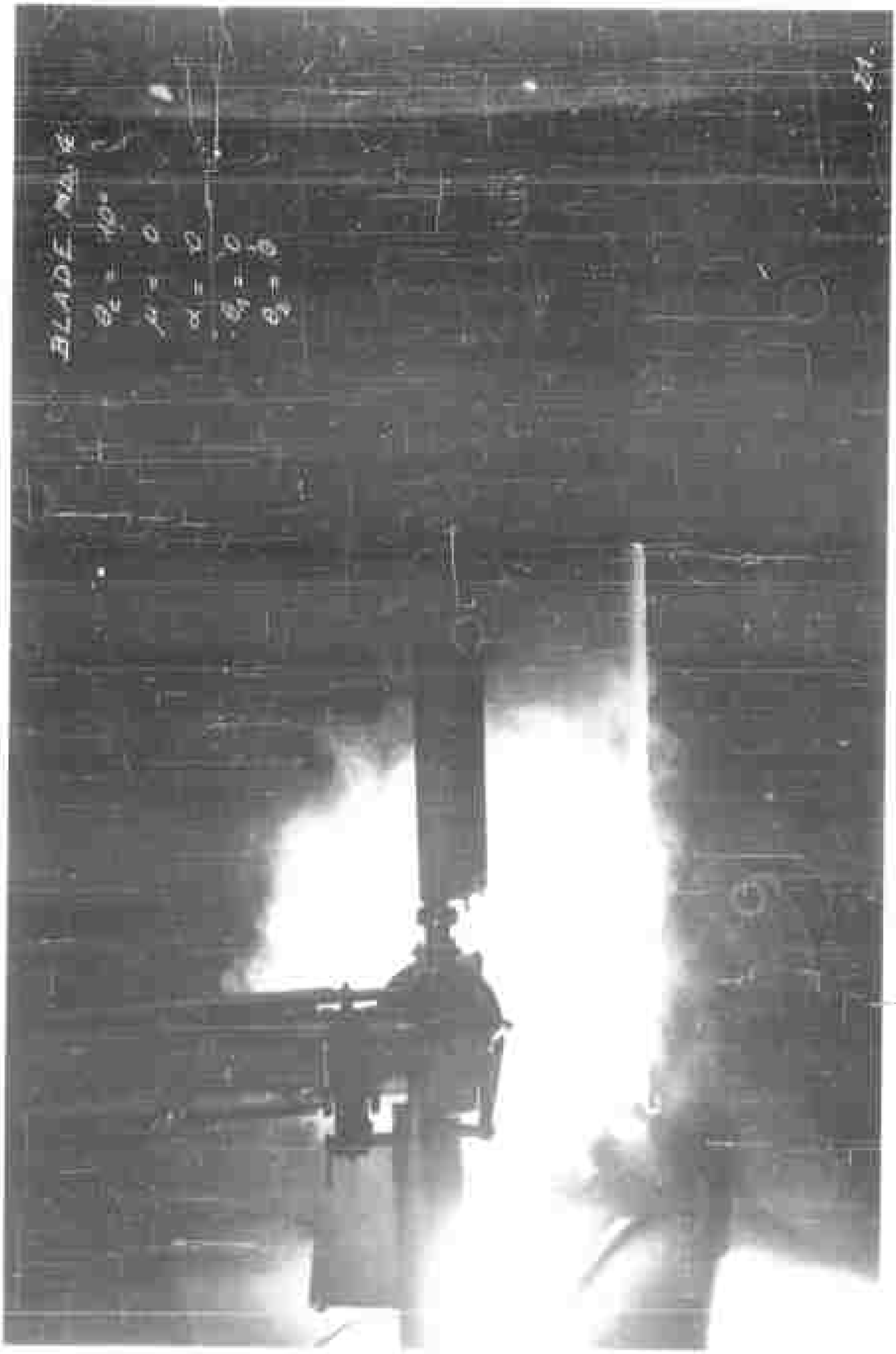

ESTABLISHED STATE. SMOKE EMISSION AT BLADE ROOT

FIG. 23

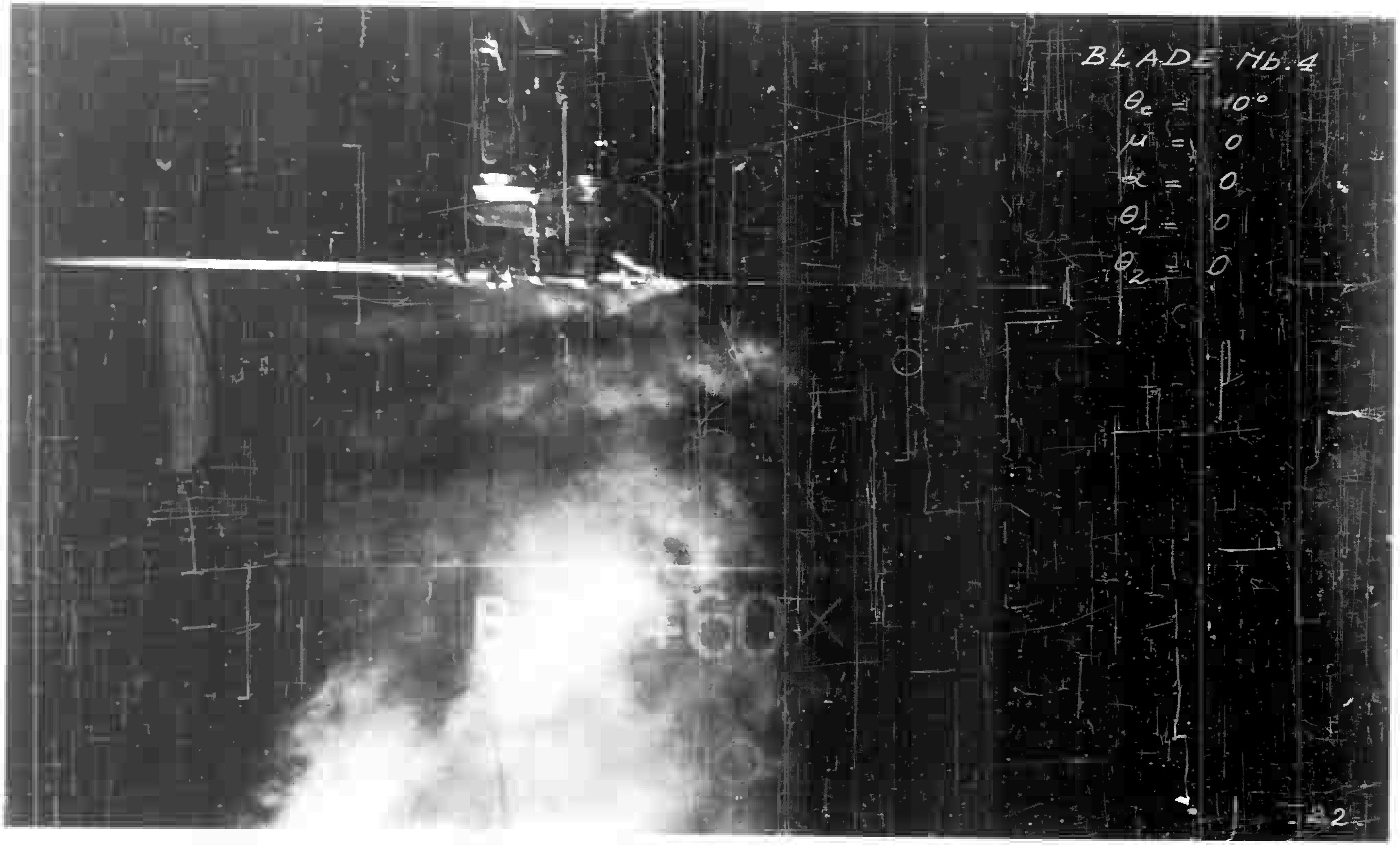

ESTABLISHED STATE. SMOKE EMISSION AT BLADE ROOT FIG. 24

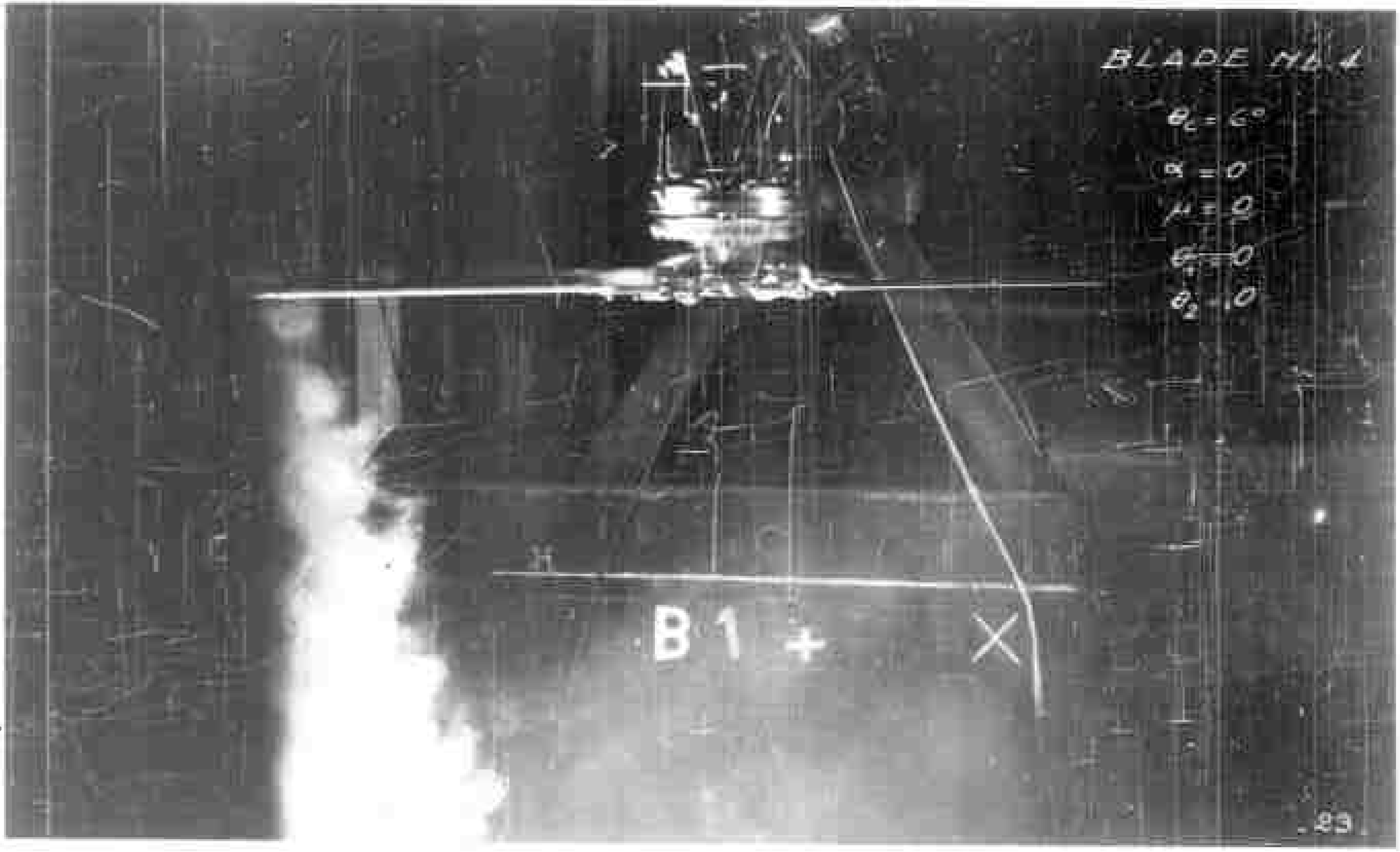

ESTABLISHED STATE. EXTERNAL SMOKE EMISSION

FIG. 25

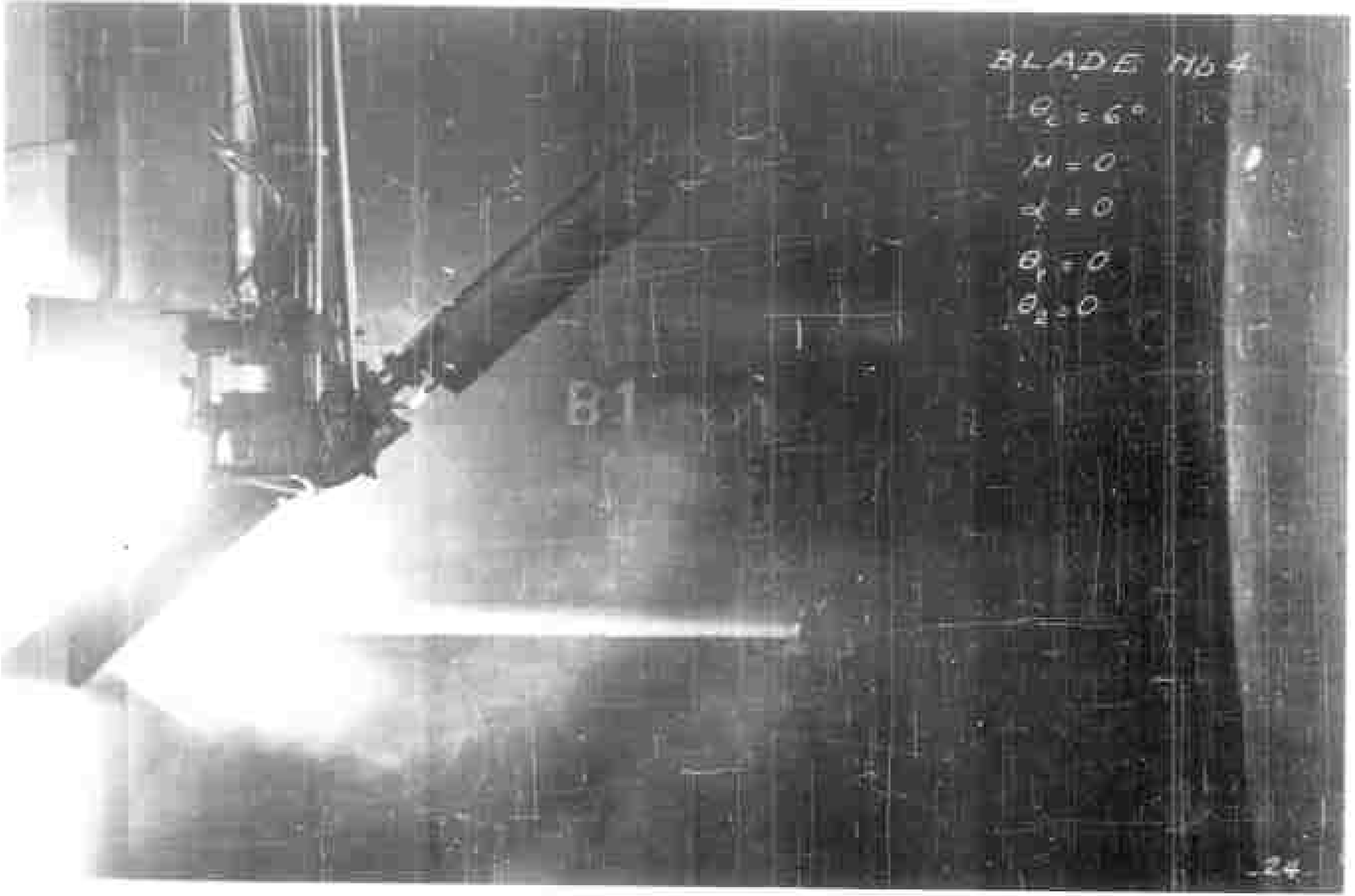

ESTABLISHED STATE. EXTERNAL SMOKE EMISSION

FIG. 26

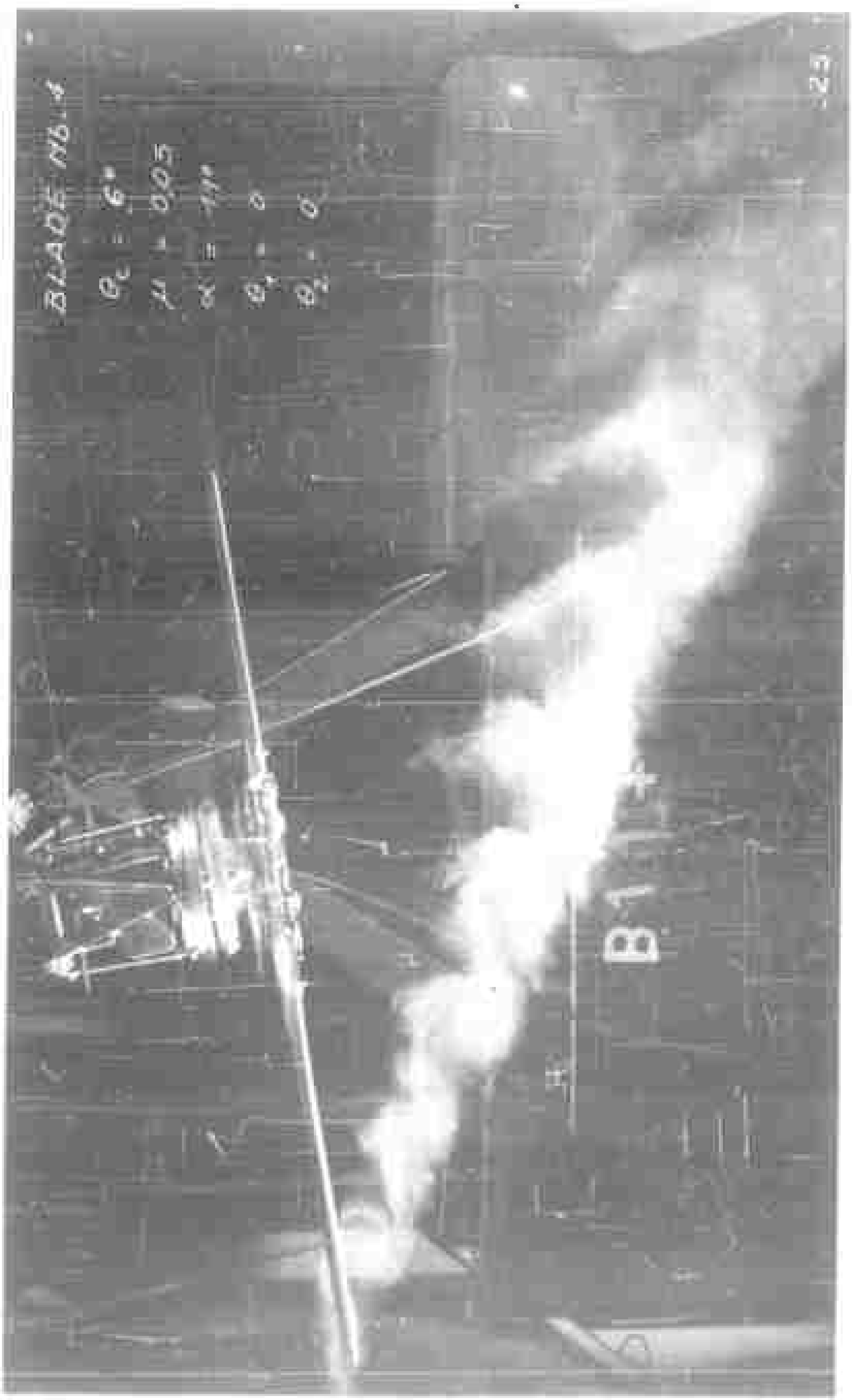

ESTABLISHED STATE. EXTERNAL SMOKE EMISSION

FIG. 27

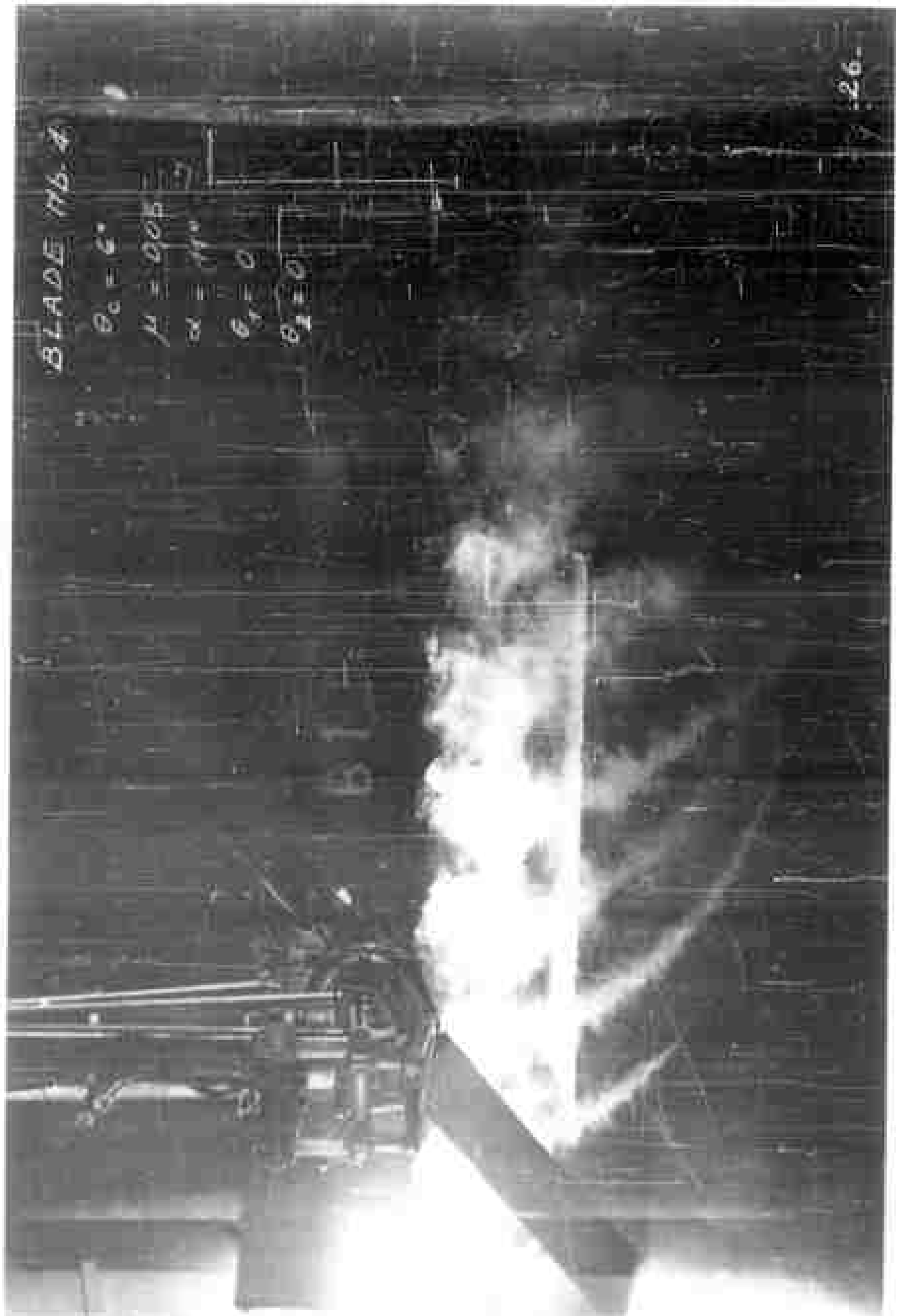

ESTABLISHED STATE. EXTERNAL SMOKE EMISSION

FIG. 28

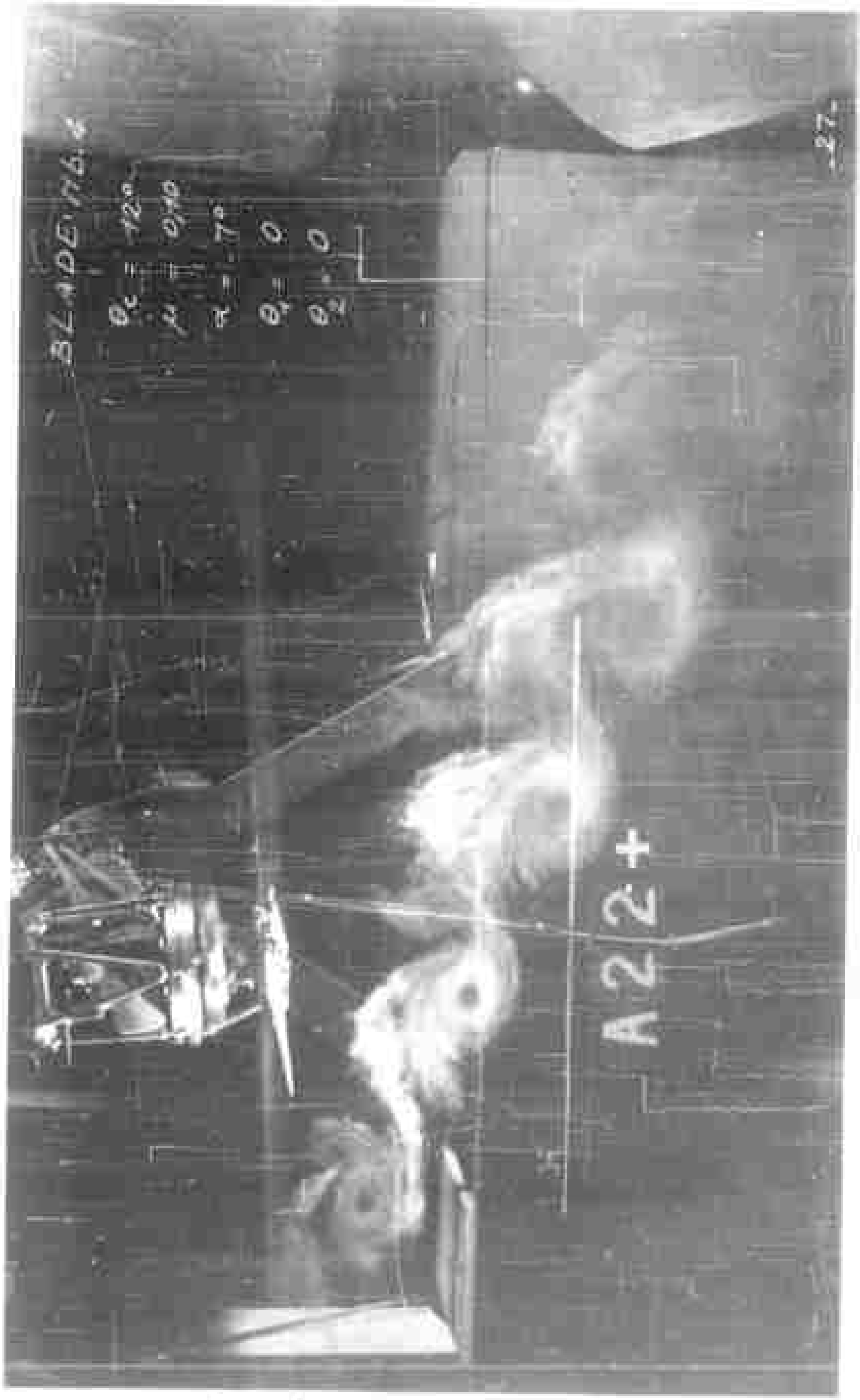

FIG. 29

ESTABLISHED STATE. EXTERNAL SMOKE EMISSION

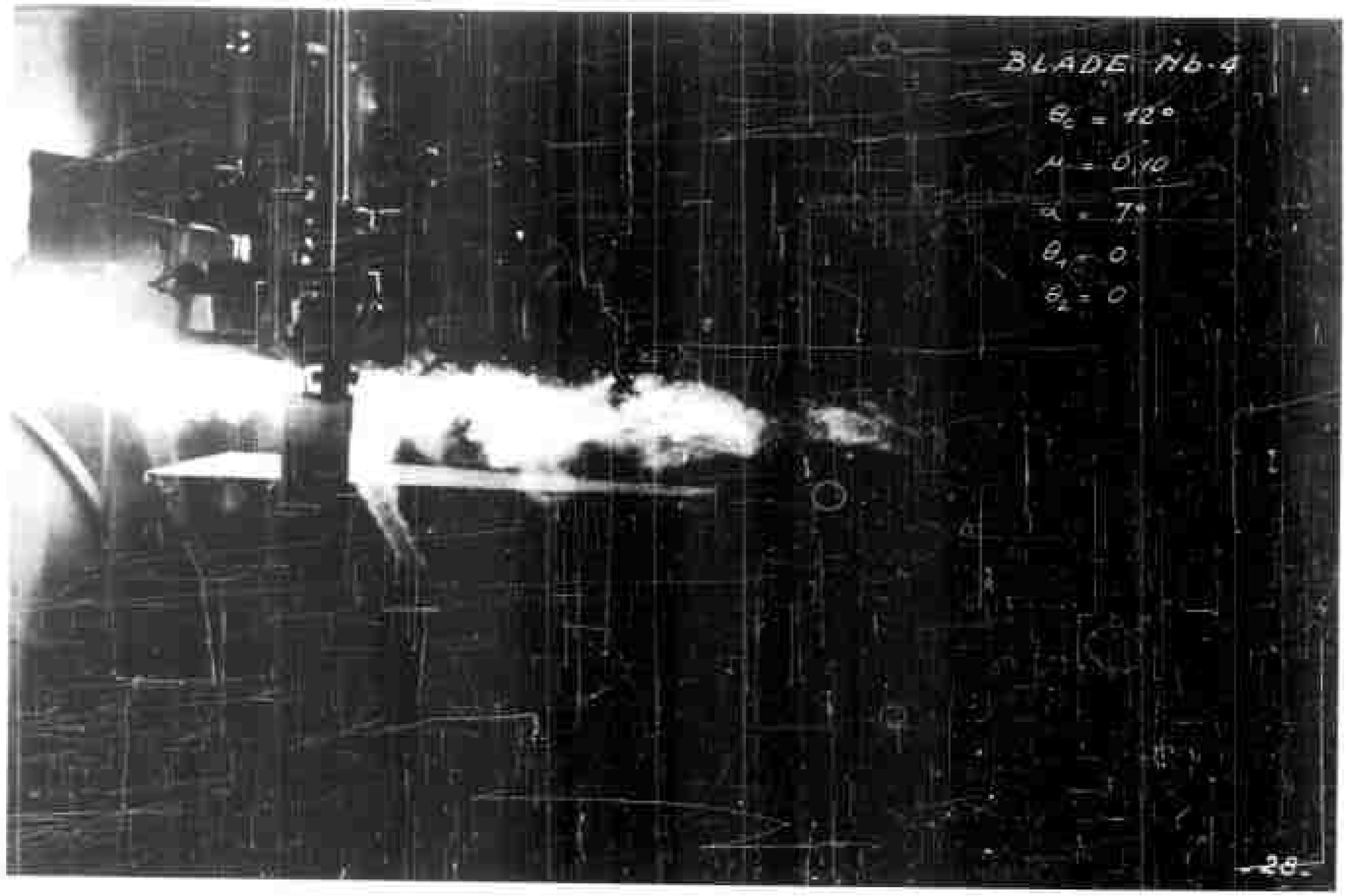

ESTABLISHED STATE. EXTERNAL SMOKE EMISSION

FIG. 30

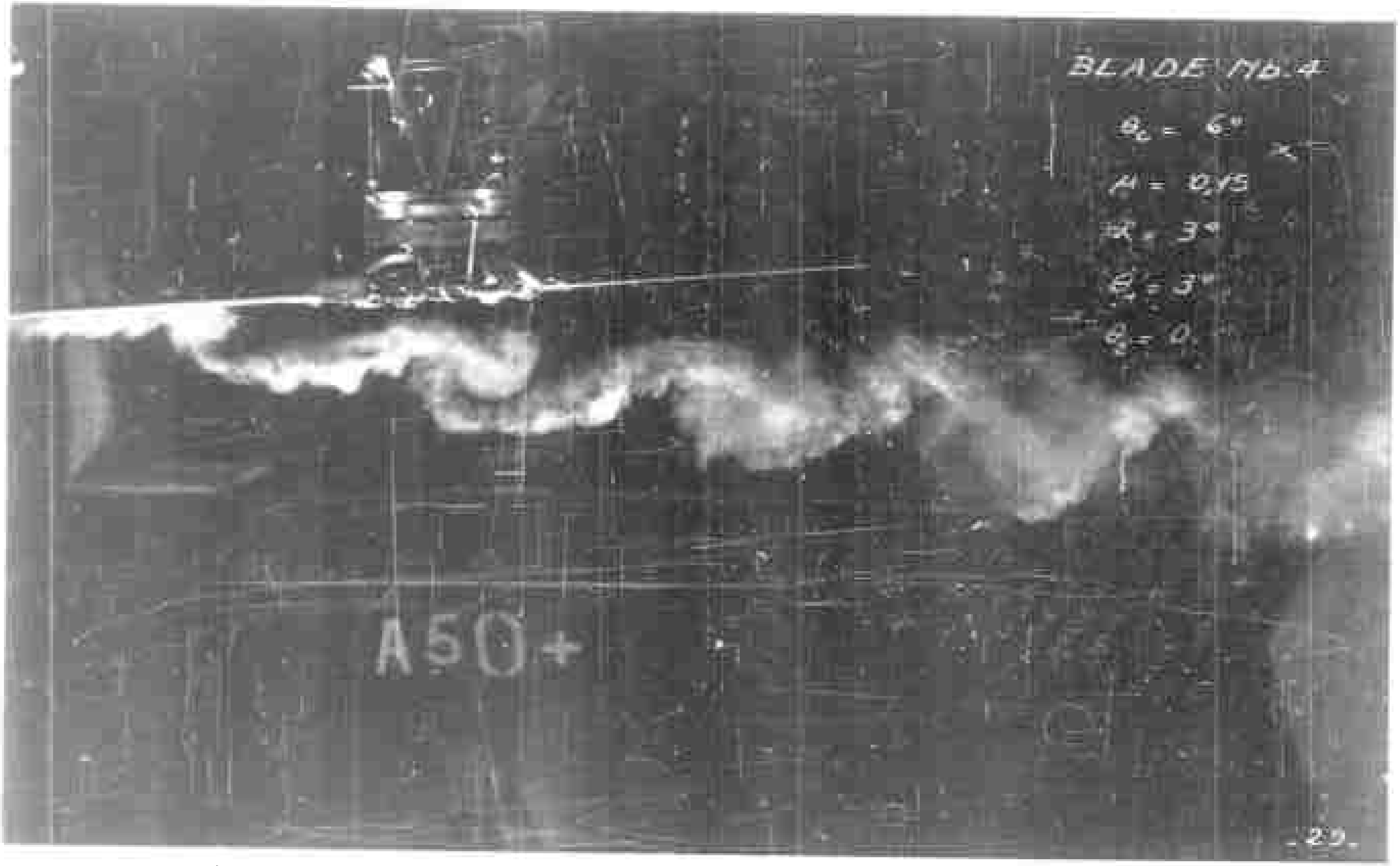

ESTABLISHED STATE. EXTERNAL SMOKE EMISSION

FIG. 31

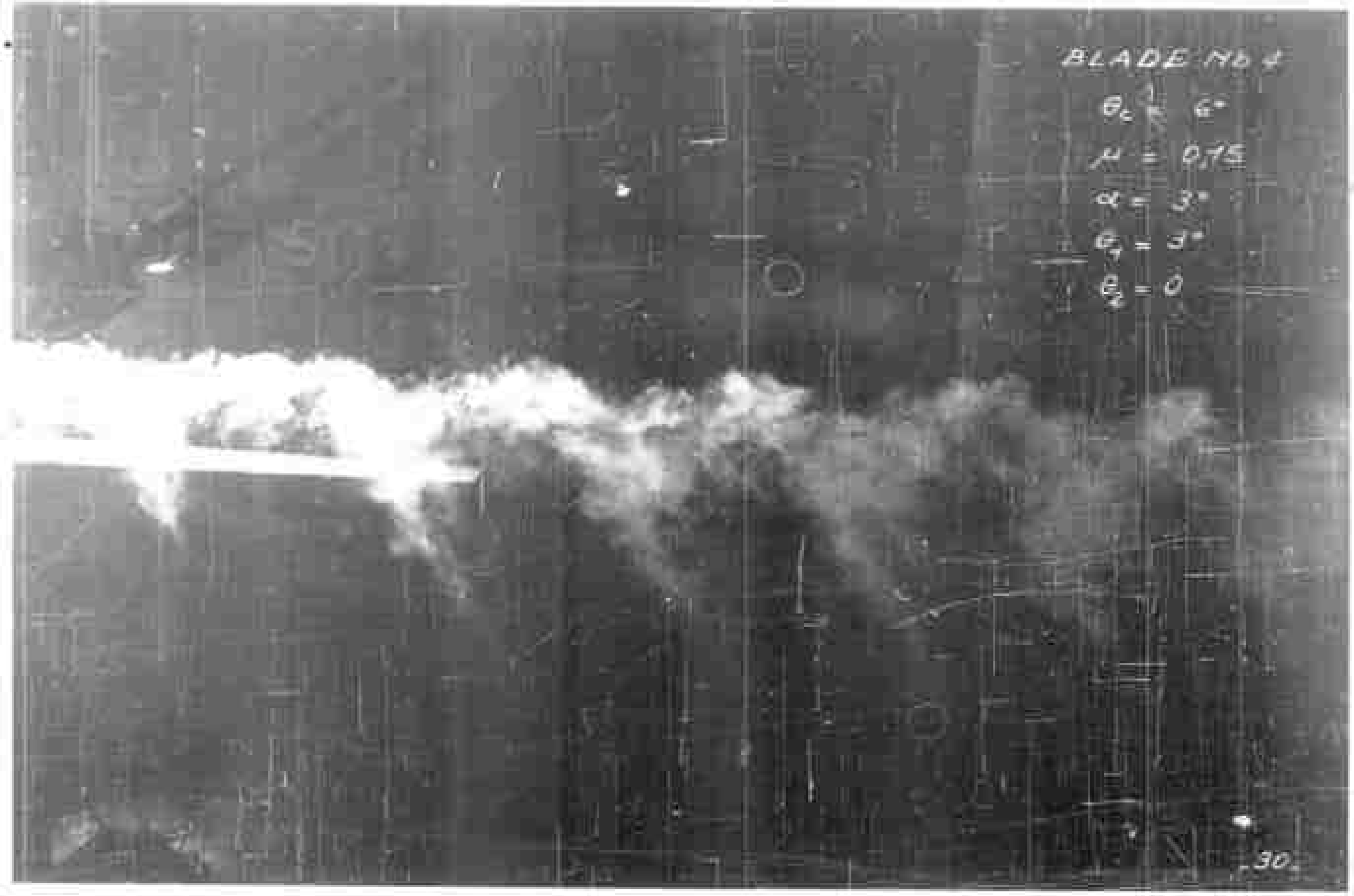

ESTABLISHED STATE. EXTERNAL SMOKE EMISSION

FIG. 32

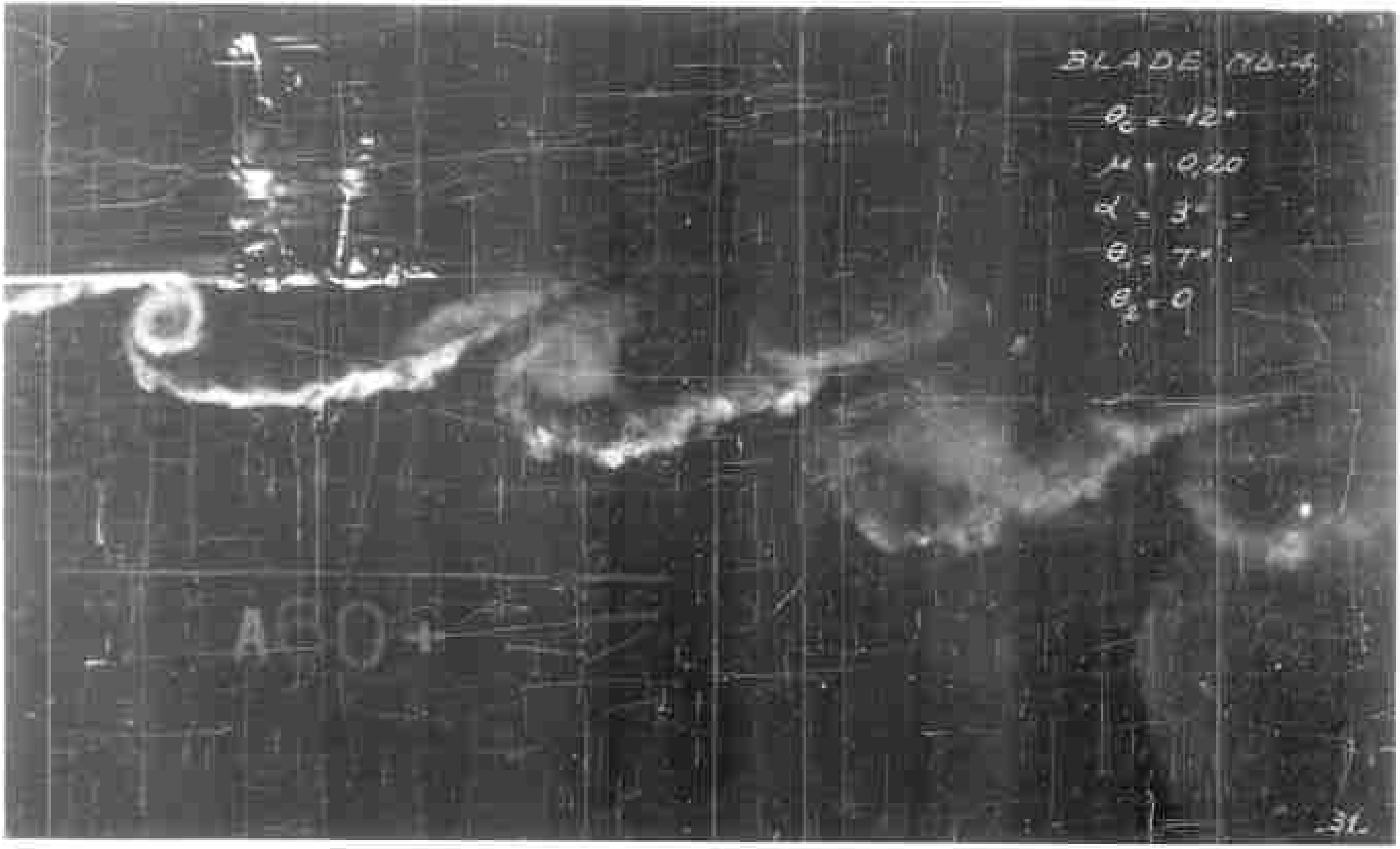

ESTABLISHED STATE. EXTERNAL SMOKE EMISSION

FIG. 33

FIG. 34

ESTABLISHED STATE. EXTERNAL SMOKE EMISSION

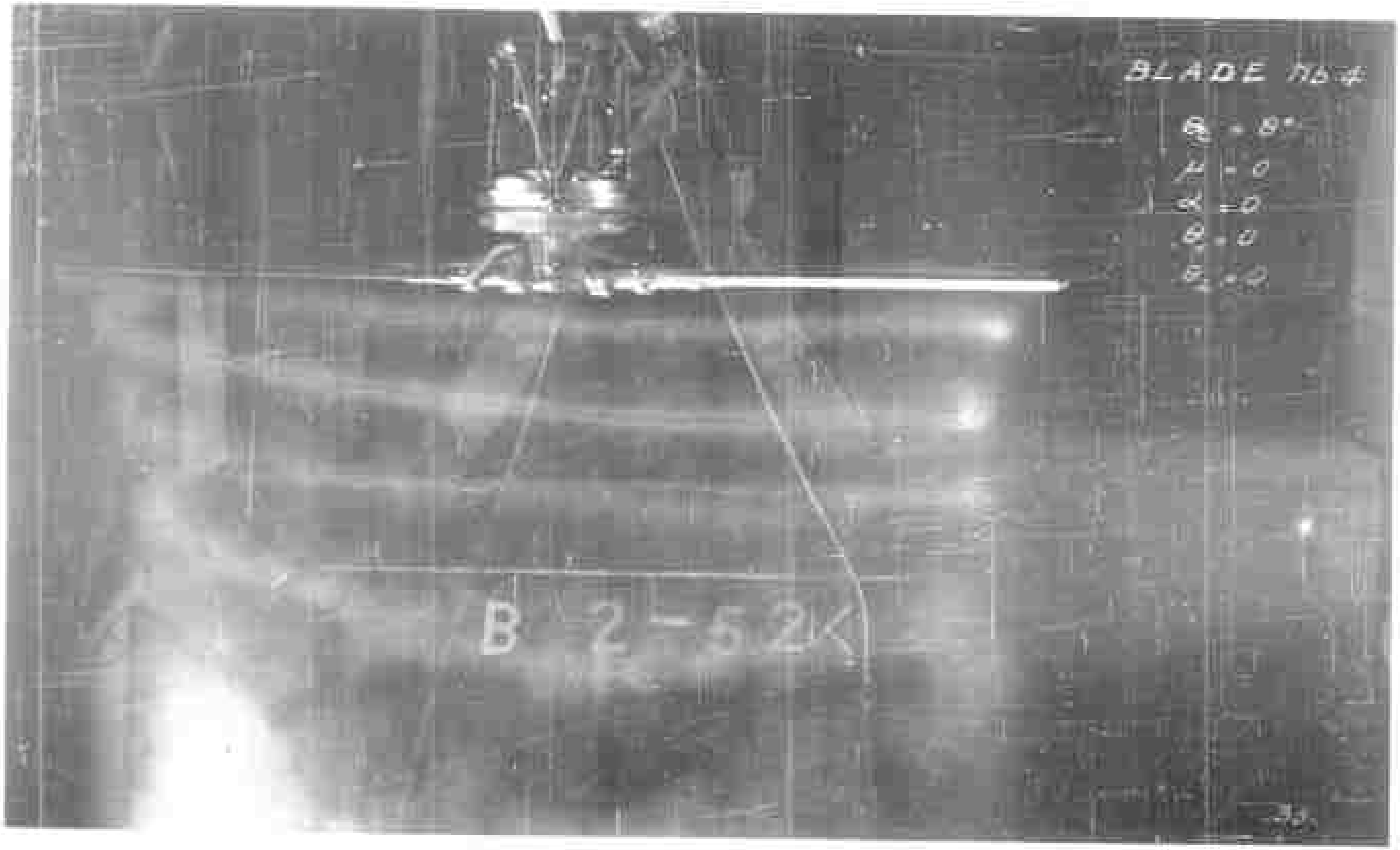

ESTABLISHED STATE. SMOKE EMISSION AT BLADE TIP

FIG. 35

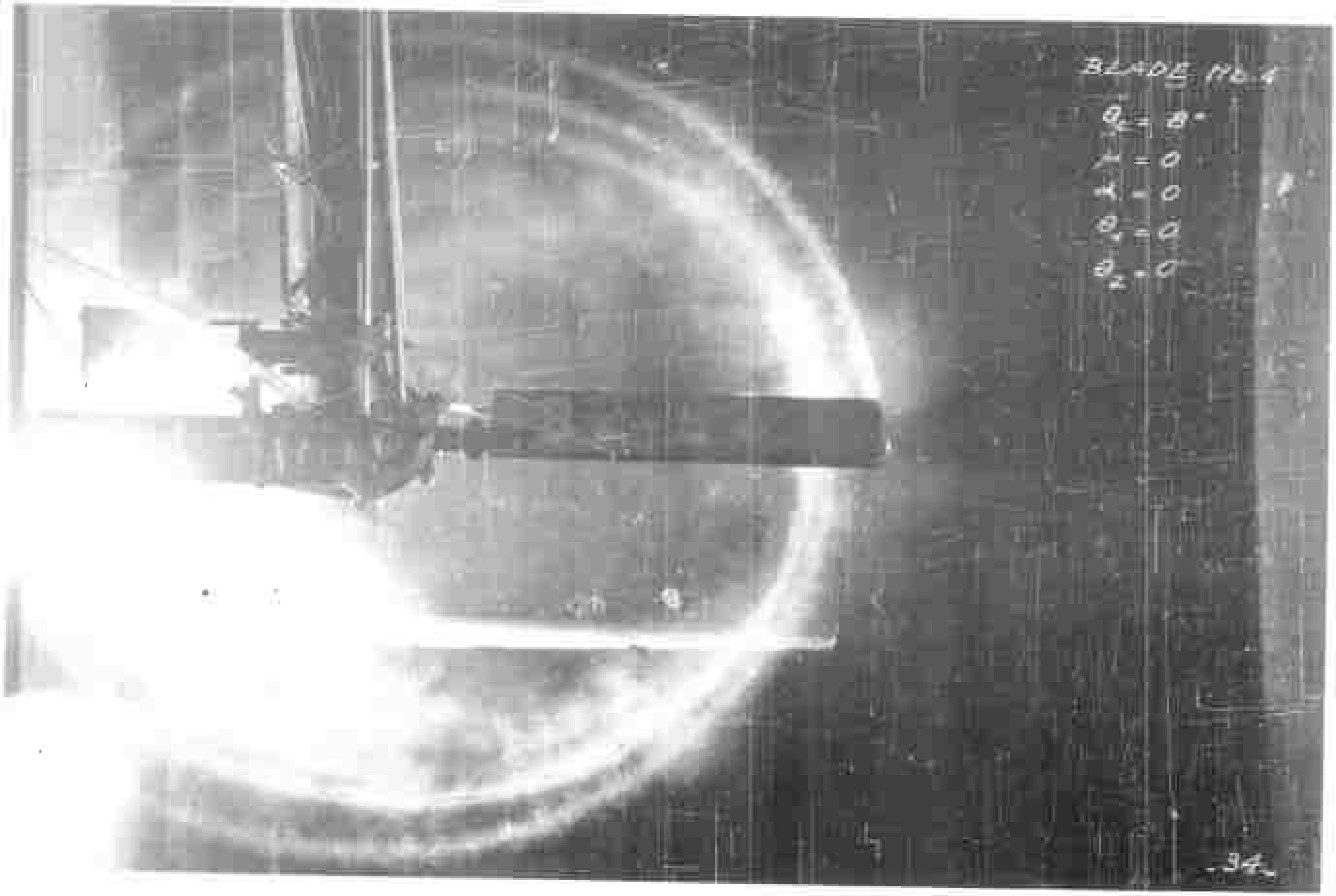

ESTABLISHED STATE. SMOKE EMISSION AT BLADE TIP

FIG. 36

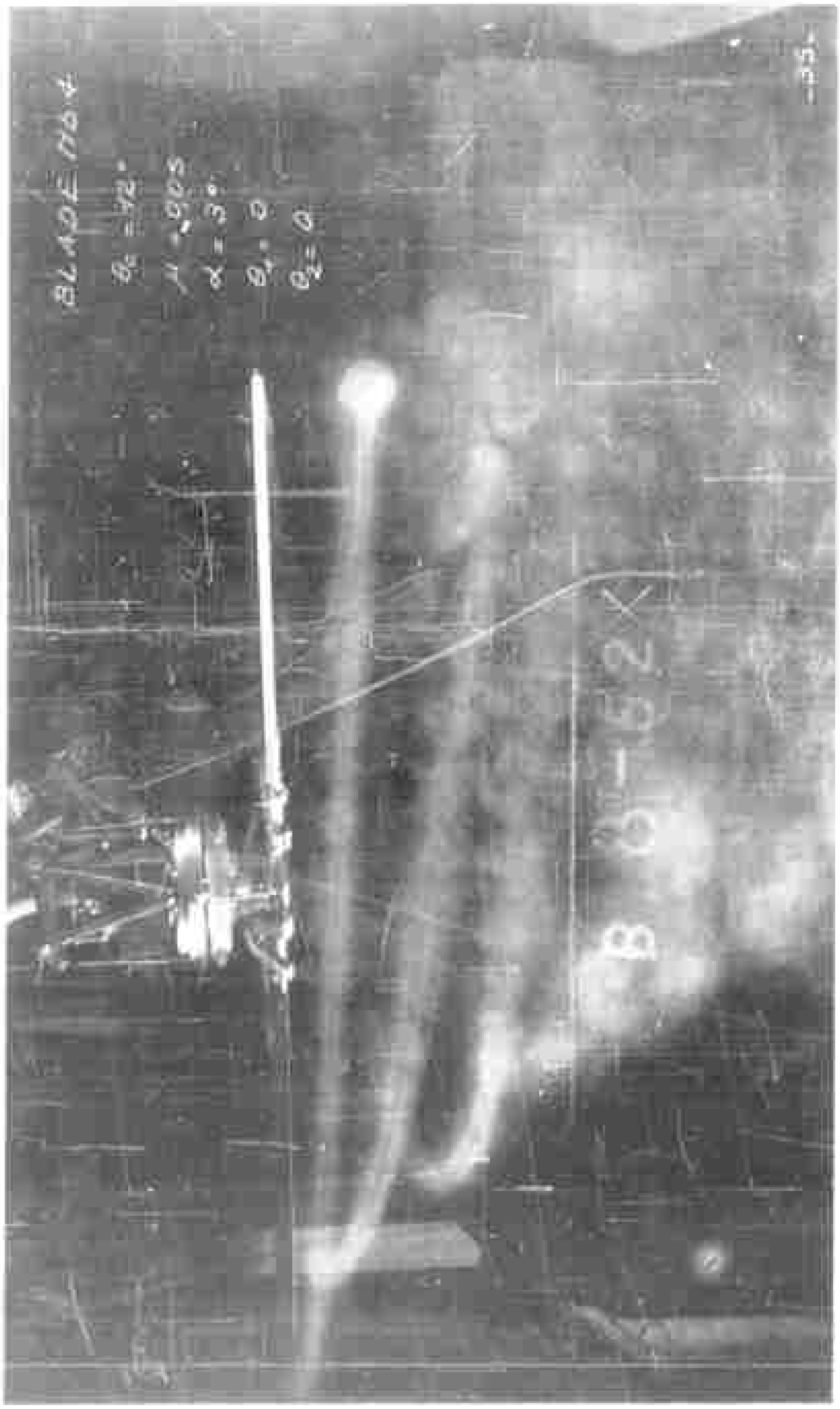

ESTABLISHED STATE. SMOKE EMISSION AT BLADE TIP

FIG. 37

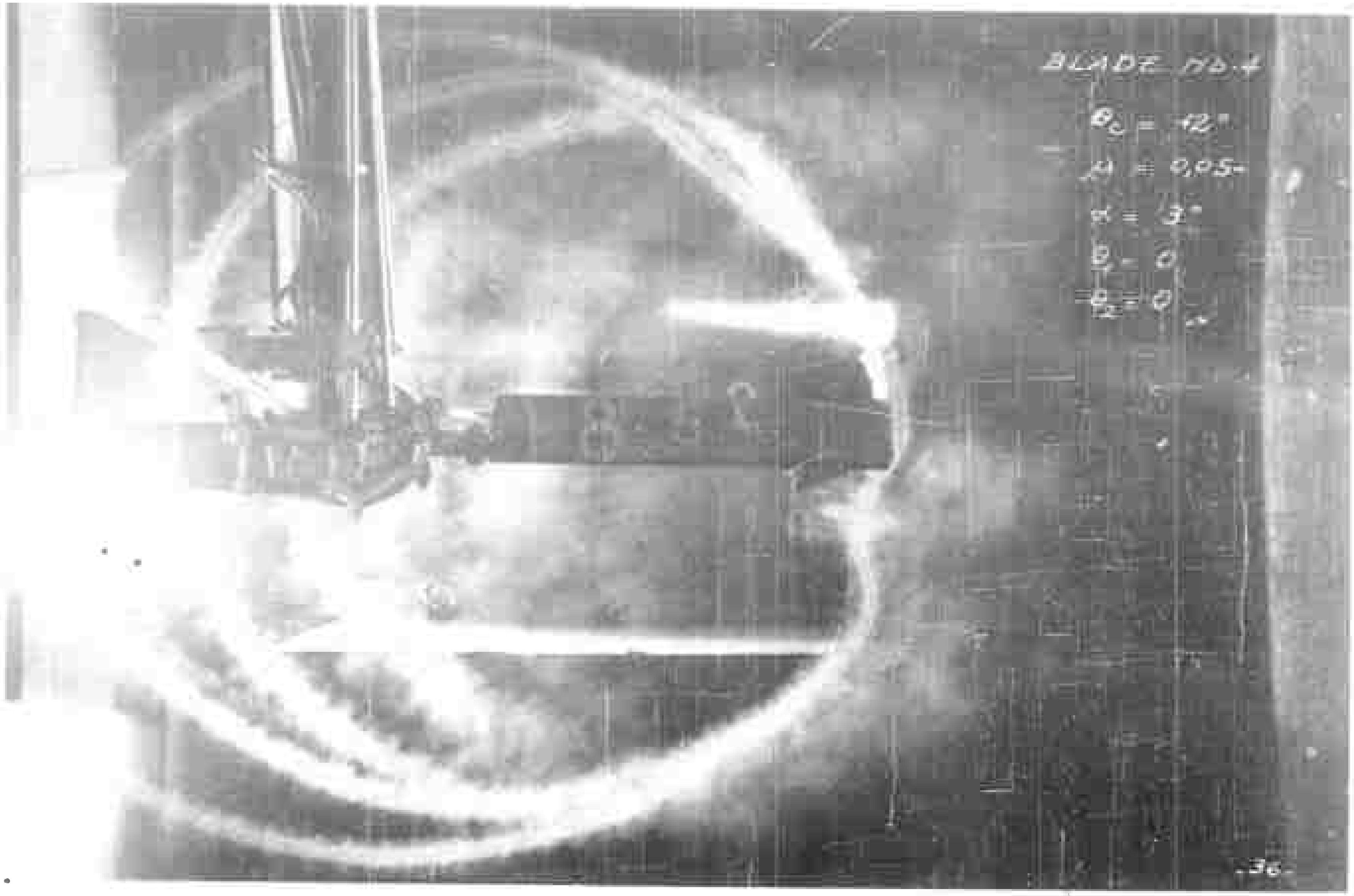

ESTABLISHED STATE. SMOKE EMISSION AT BLADE TIP

FIG. 38

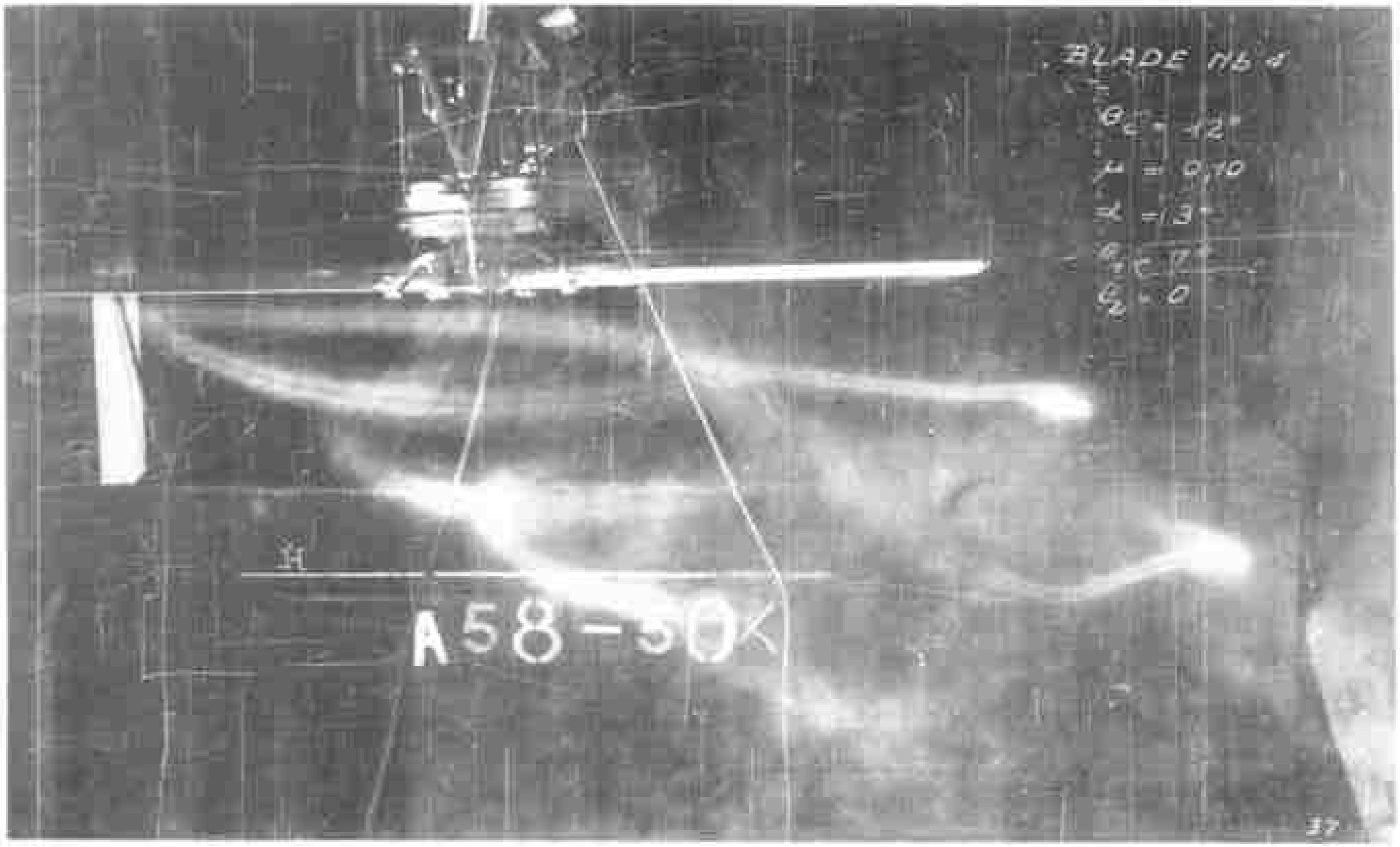

ESTABLISHED STATE. SMOKE EMISSION AT BLADE TIP

FIG. 39

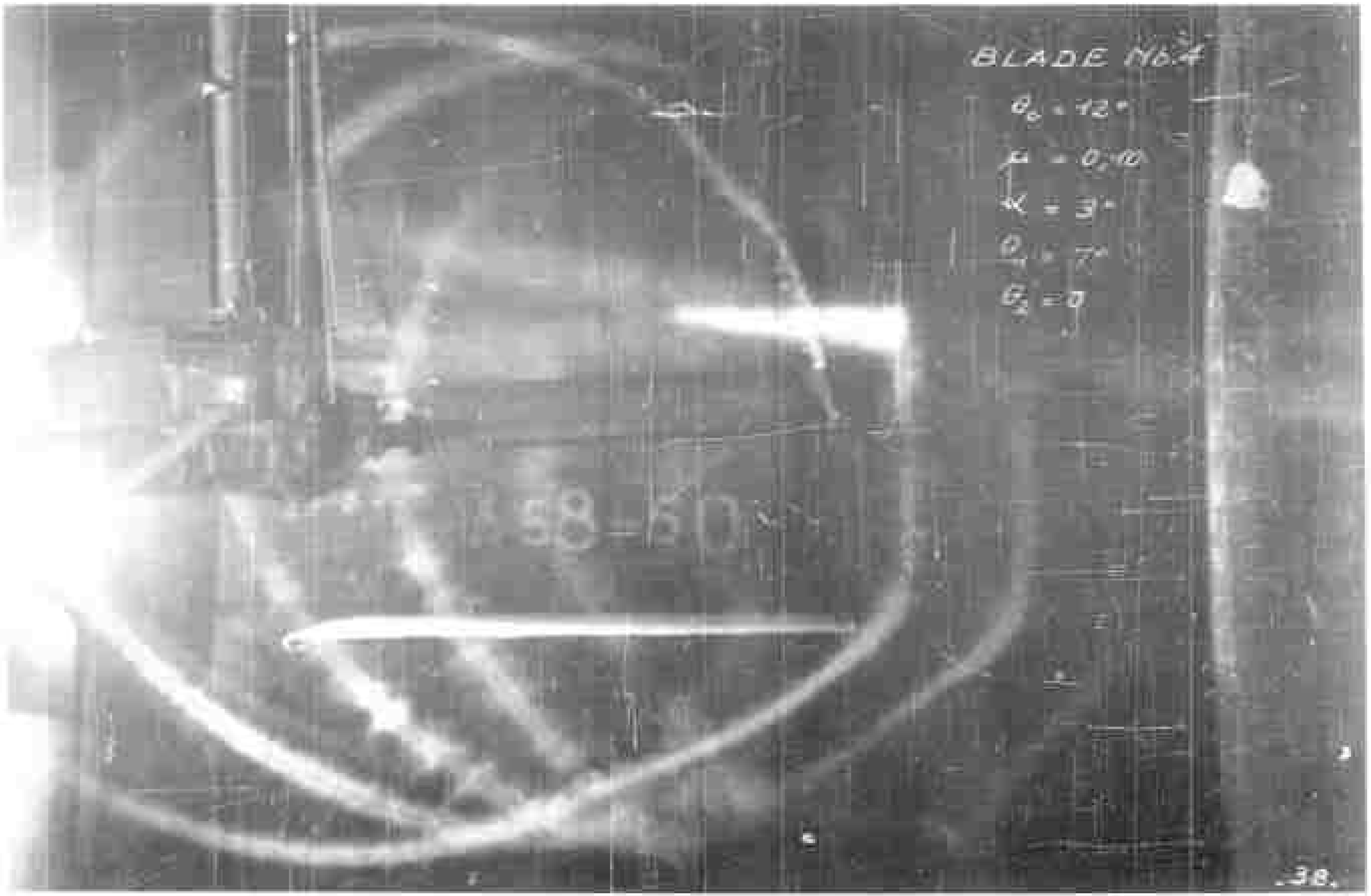

ESTABLISHED STATE. SMOKE EMISSION AT BLADE TIP

FIG. 40

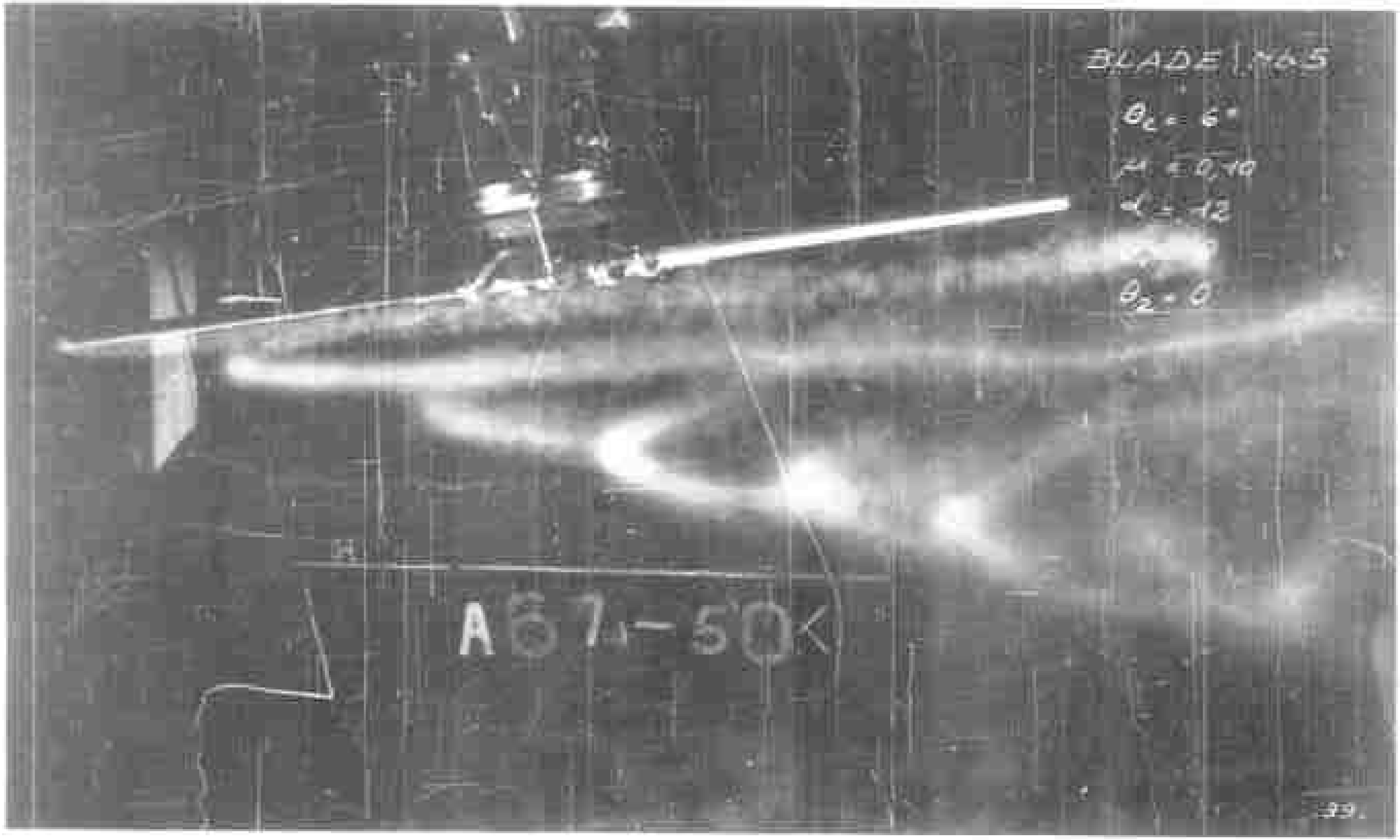

ESTABLISHED STATE. SMOKE EMISSION AT BLADE TIP FIG. 41

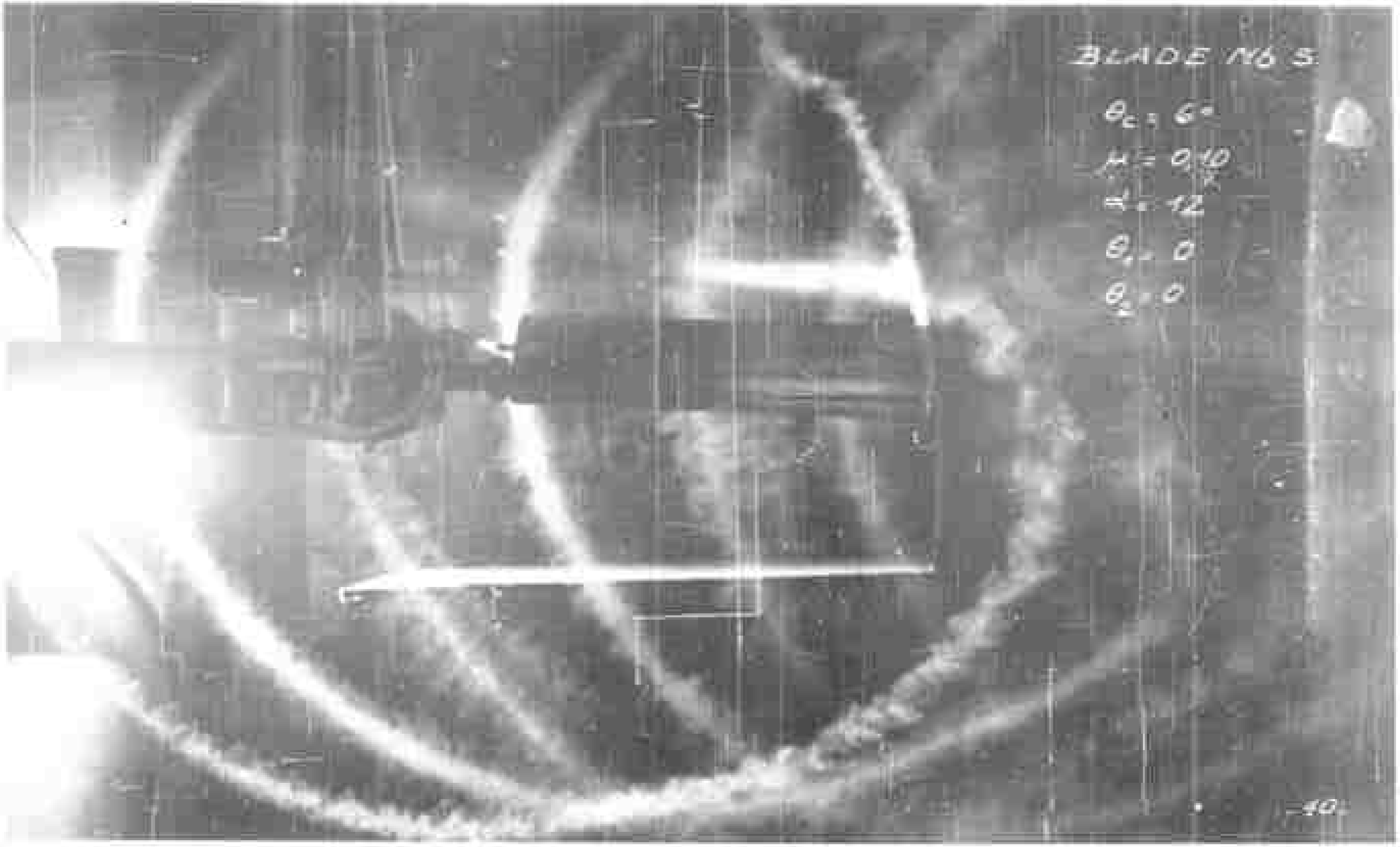

ESTABLISHED STATE. SMOKE EMISSION AT BLADE TIP

FIG. 42

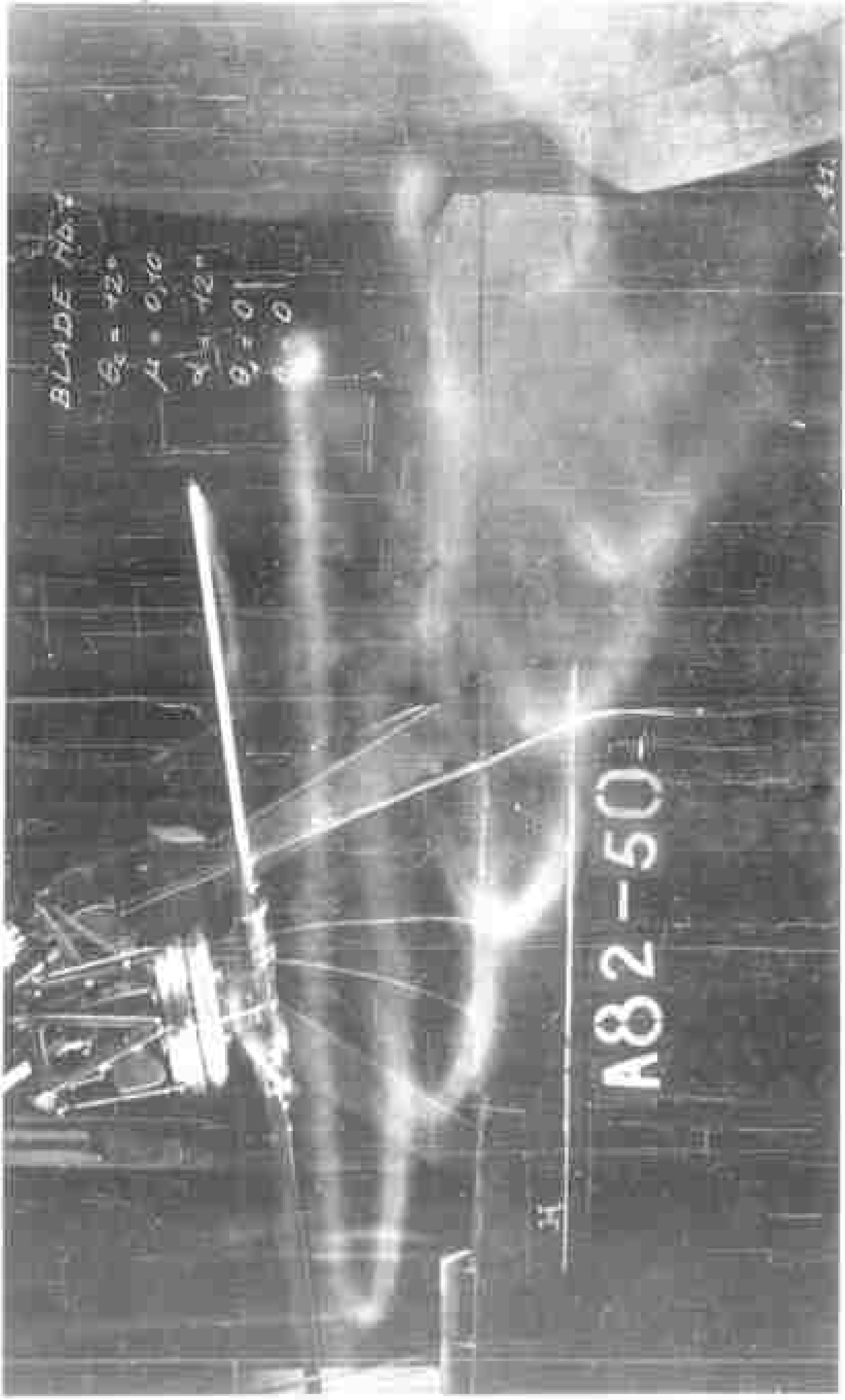

ESTABLISHED STATE. SMOKE EMISSION AT BLADE TIP

FIG. 43

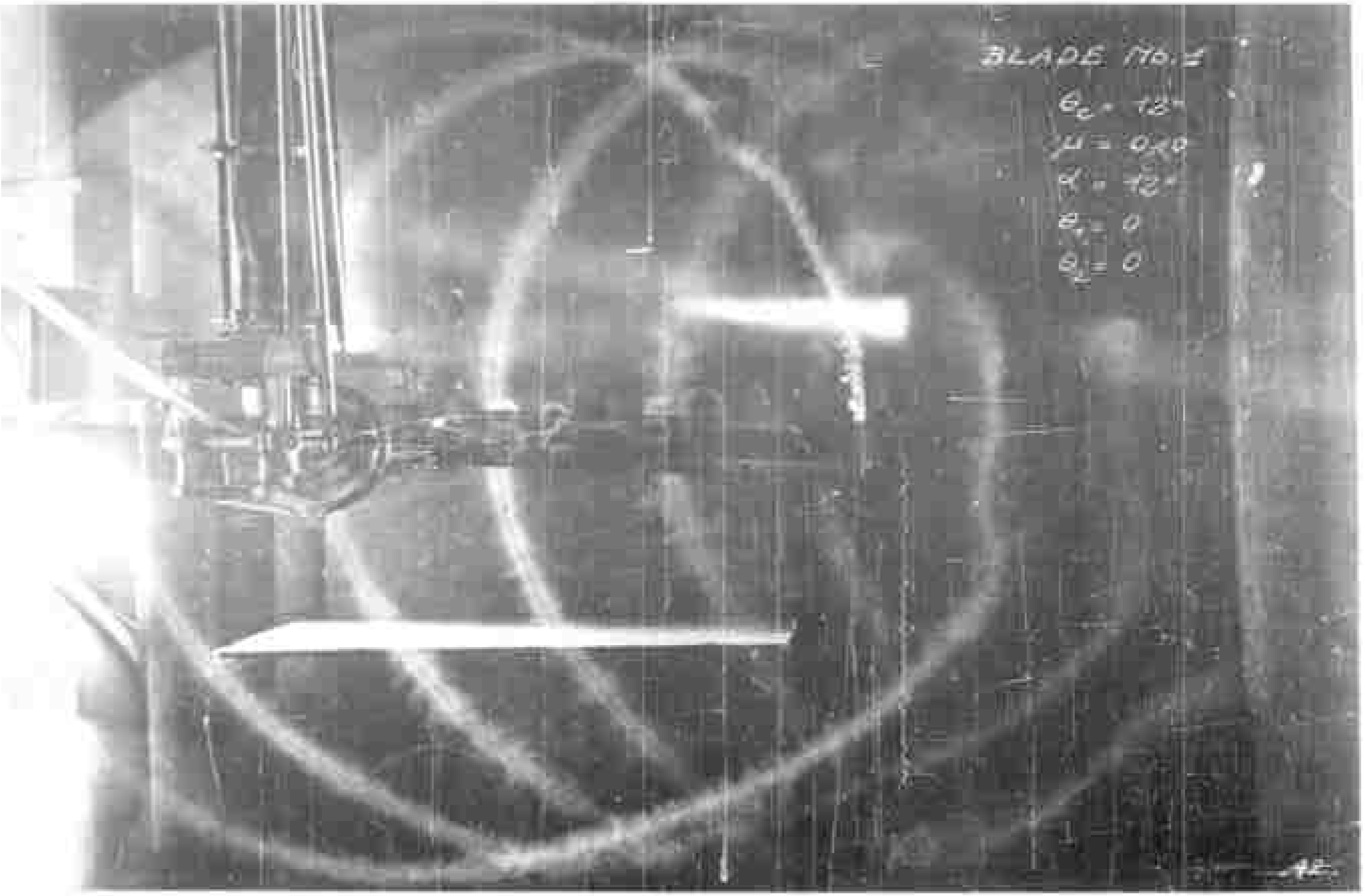

ESTABLISHED STATE. SMOKE EMISSION AT BLADE TIP

FIG. 44

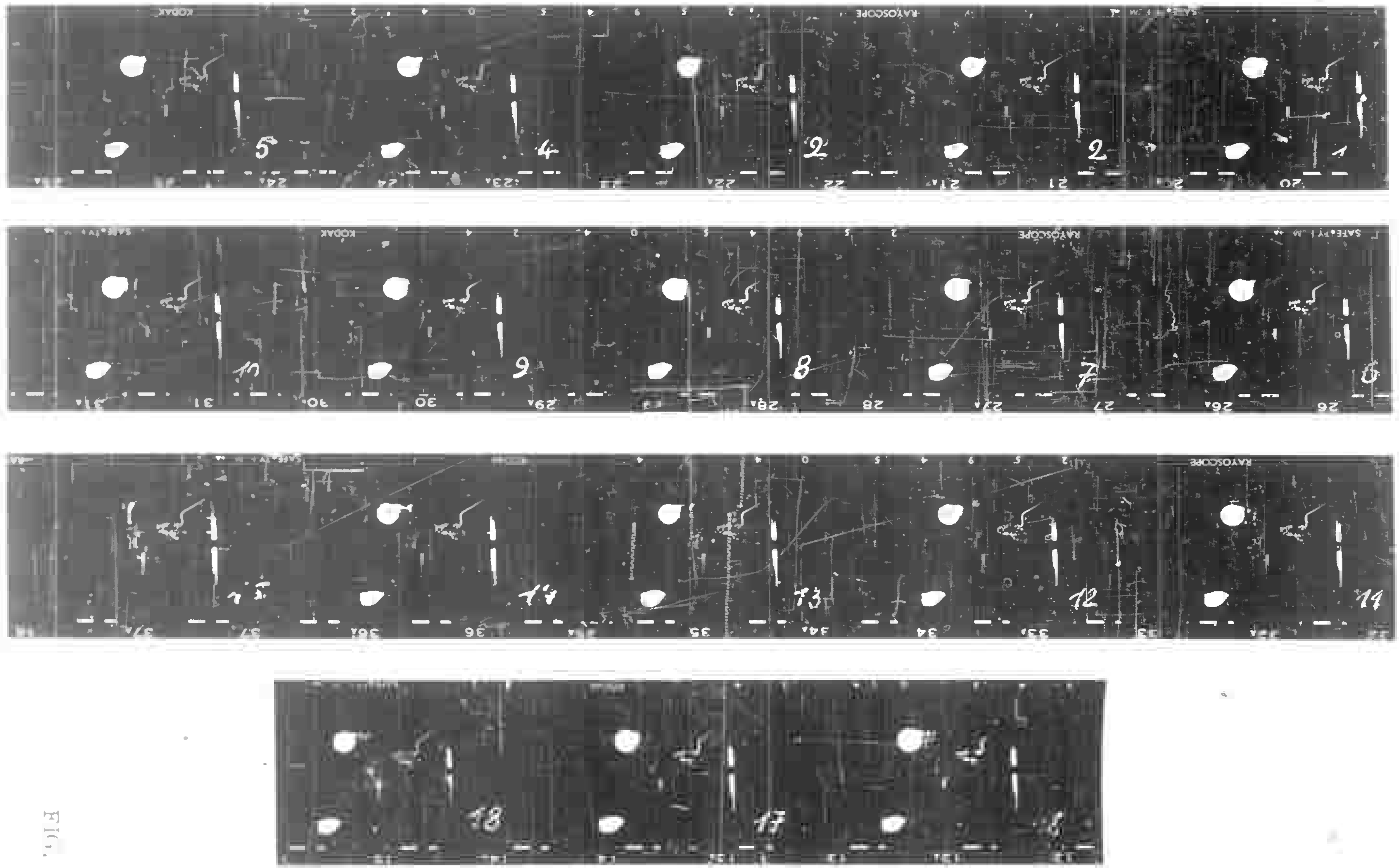

TRANSIENT STATE

INFLUENCE OF $\Delta\theta = 4°.15$. FREQUENCY 0.5 c.p.s.

INITIAL SETTING : $\theta_c = 10°$ $\mu = \alpha = \theta_1 = \theta_2 = 0$ Blade Nb. 2

FIG. 45

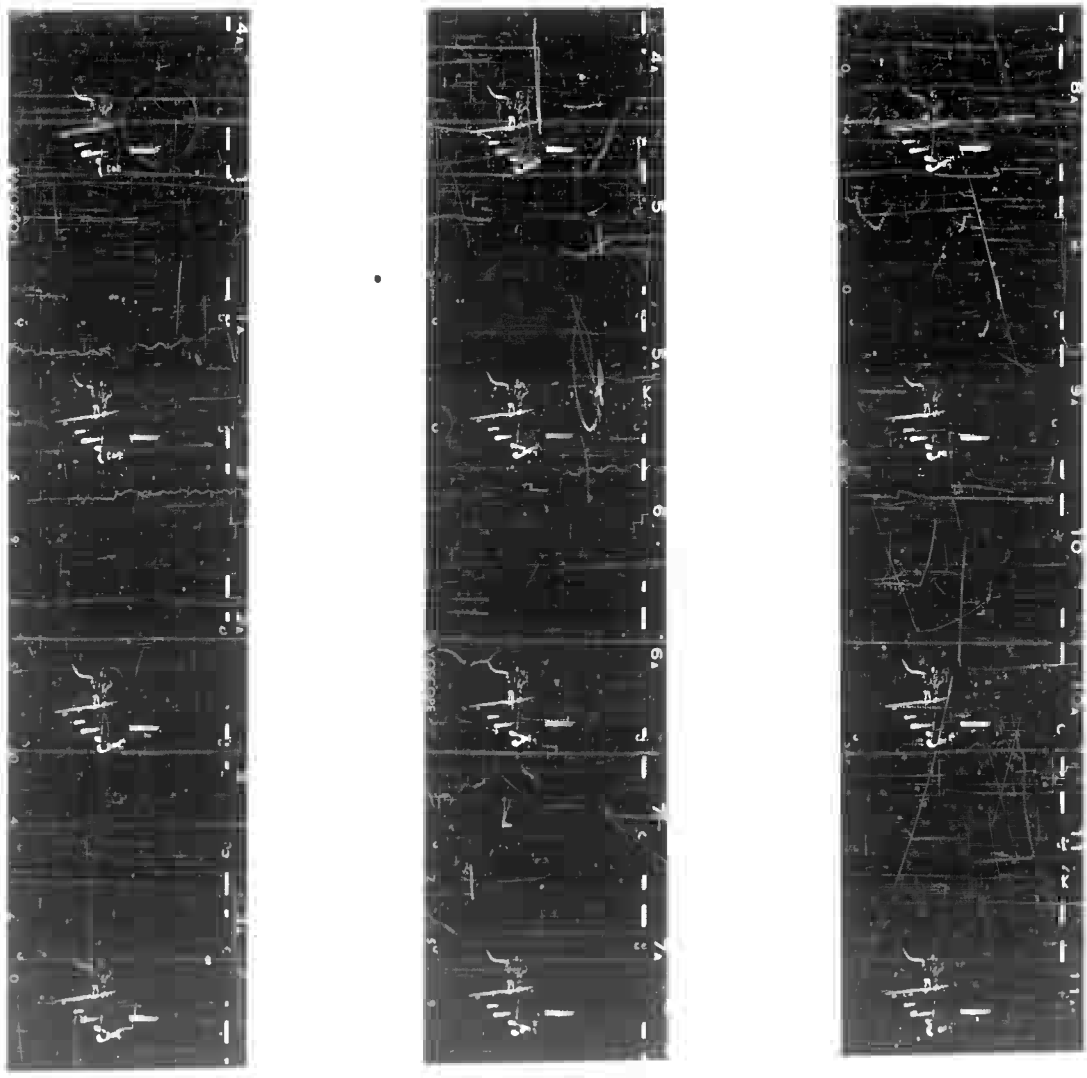

TRANSIENT STATE

FIG. 46

INFLUENCE OF $\Delta\alpha = 4°$ FREQUENCY 1.0 c.p.s.

INITIAL SETTING : $\alpha = 7°$ $\theta_c = 10°.15$ $\mu = 0.05$

$\theta_1 = \theta_2 = 0$ BLADE Nb. 2

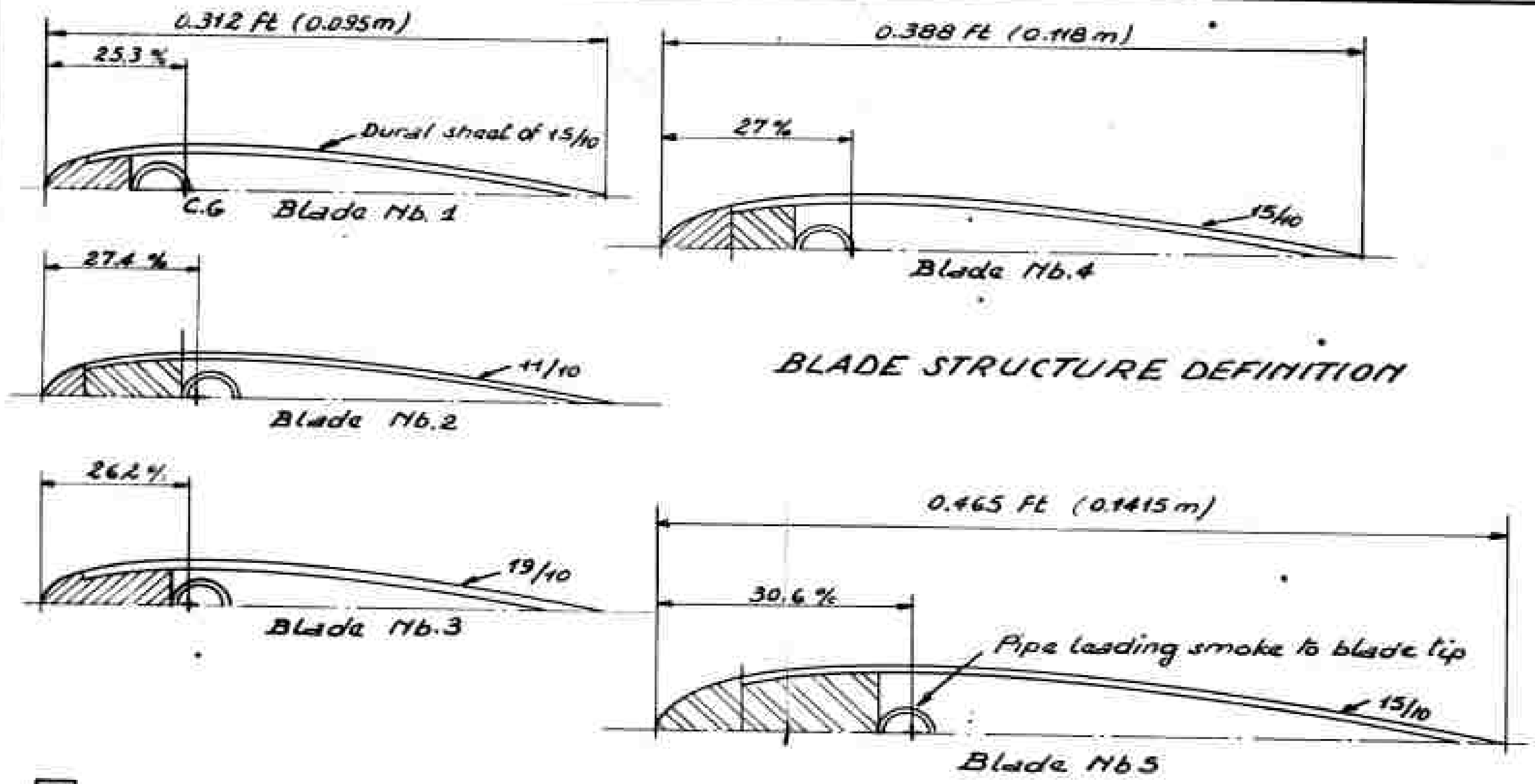

BLADE STRUCTURE DEFINITION

Dimensions are in ft. and in meters

NACA 0018 Airfoil Section

FIG.47

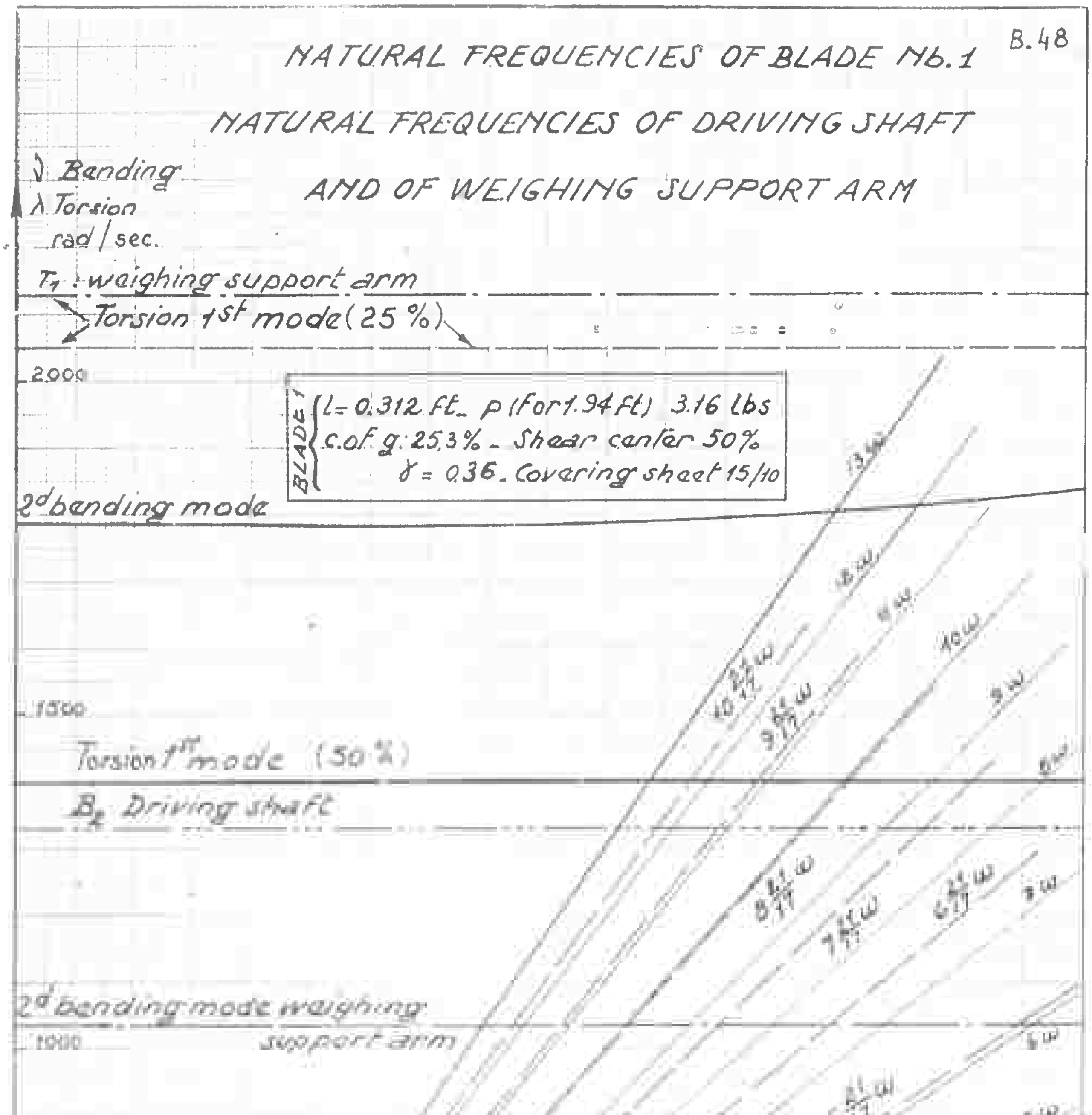
NATURAL FREQUENCIES OF BLADE Nb. 1
NATURAL FREQUENCIES OF DRIVING SHAFT
AND OF WEIGHING SUPPORT ARM
ν Bending
λ Torsion
rad / sec.
T1 : weighing support arm
Torsion 1st mode (25 %)
2000
BLADE 1
l = 0.312 ft. p (for 1.94 ft) 3.16 lbs
c. of g. 25.3 % - Shear center 50%
γ = 0.36 - Covering sheet 15/10
2d bending mode
1500
Torsion 1st mode (50 %)
B2 Driving shaft
2d bending mode weighing support arm
1000
1st bending mode
500
B1 weighing support arm
B1 driving shaft
0
50
100
150 ω rad/sec

FIG. 48

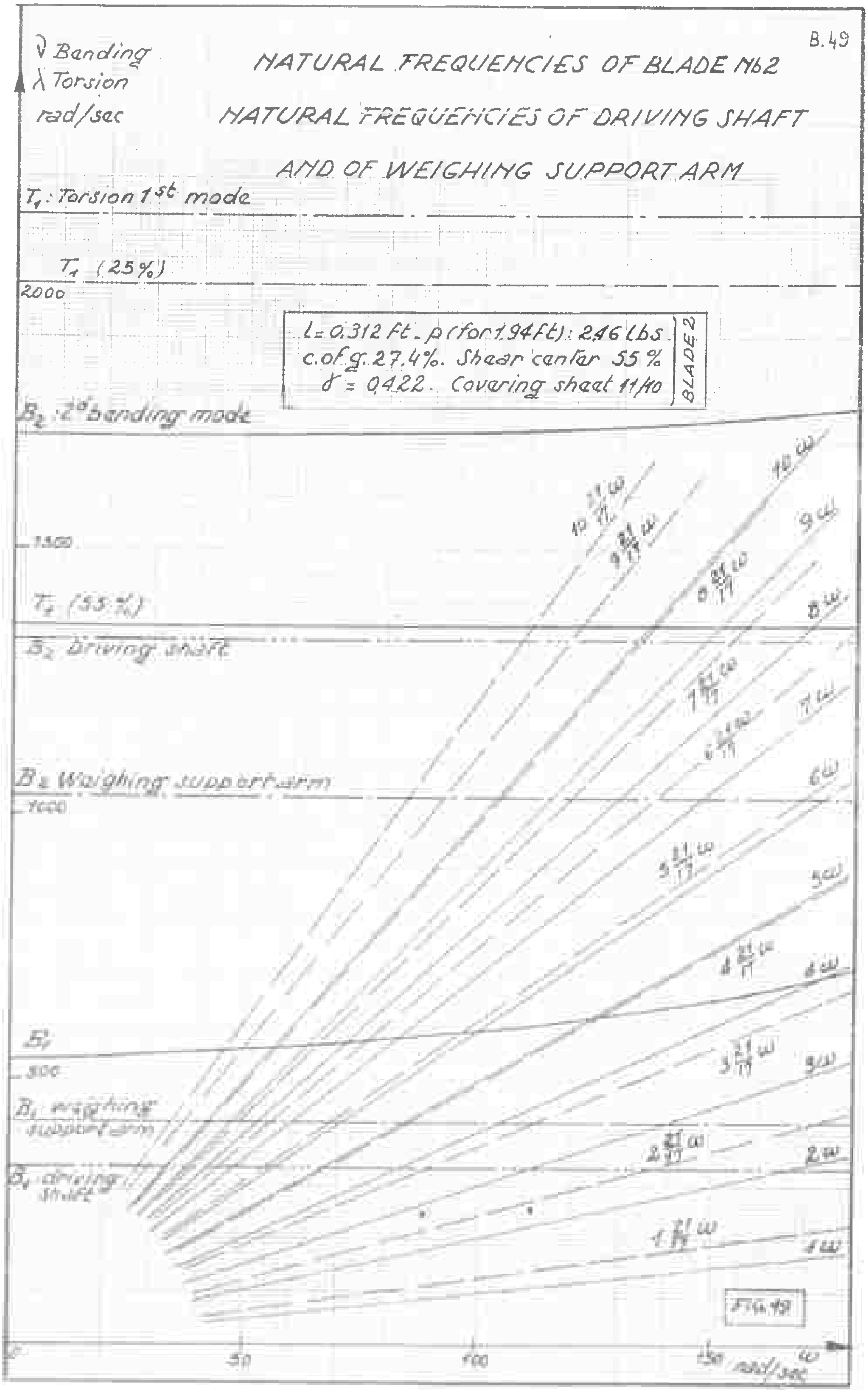
B.49
NATURAL FREQUENCIES OF BLADE Nb2
NATURAL FREQUENCIES OF DRIVING SHAFT
AND OF WEIGHING SUPPORT ARM
ϑ Bending
λ Torsion
rad/sec
T1 : Torsion 1st mode
T1 (25%)
2000
l=0.312 Ft _ p (for 1.94 Ft): 2.46 Lbs
c. of g. 27.4%. Shear center 55%
δ = 0.422. Covering sheet 11/10
BLADE 2
B2 2d bending mode
1500
T1 (55%)
B2 Driving shaft
B2 Weighing support arm
1000
B1
500
B1 weighing support arm
B1 driving shaft
10 ω
9 ω
8 ω
7 ω
6 ω
5 ω
4 ω
3 ω
2 ω
1 ω
50
100
150
ω rad/sec
FIG.49

NATURAL FREQUENCIES OF BLADE Nb 3
NATURAL FREQUENCIES OF DRIVING SHAFT AND OF WEIGHING SUPPORT ARM

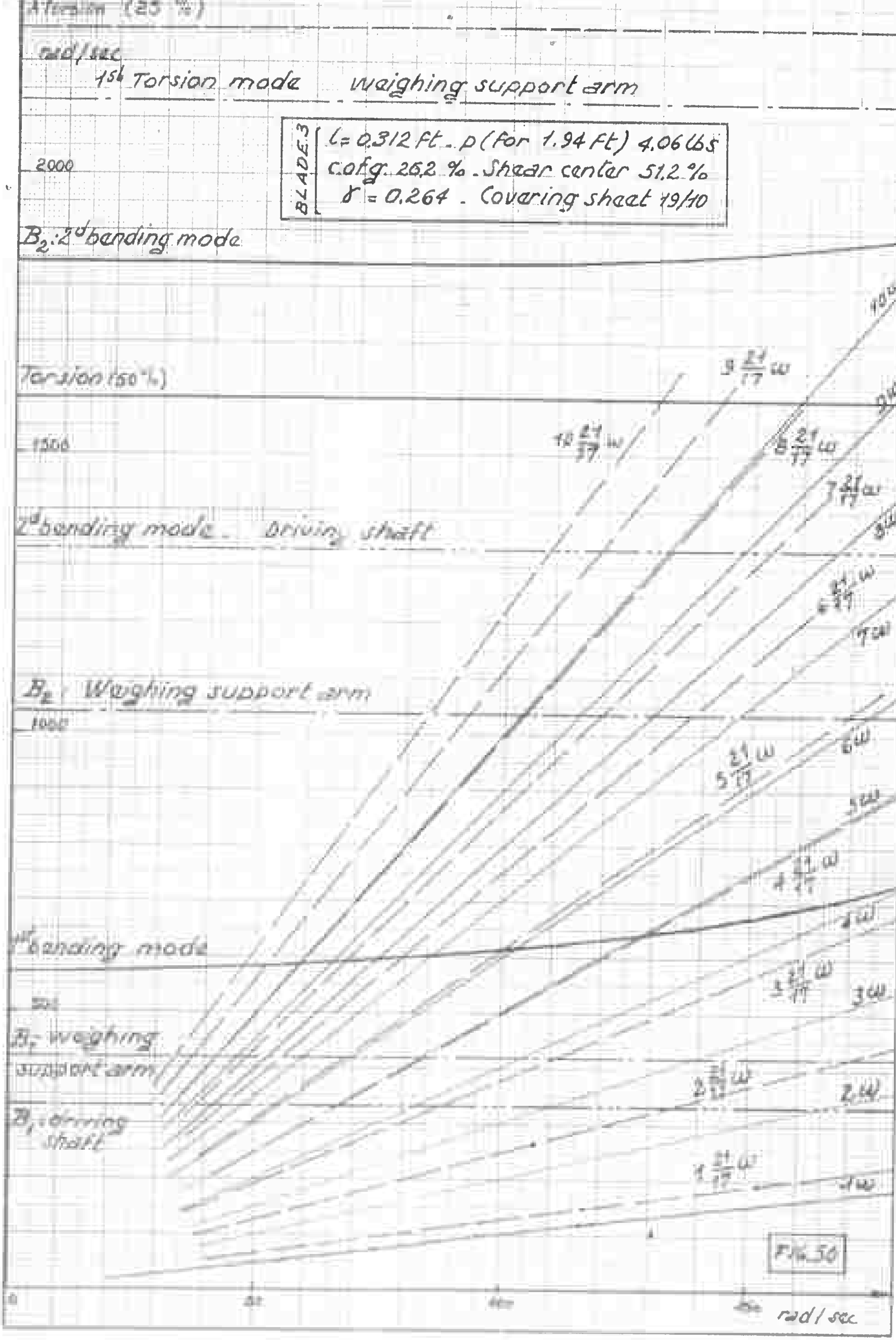

FIG. 50

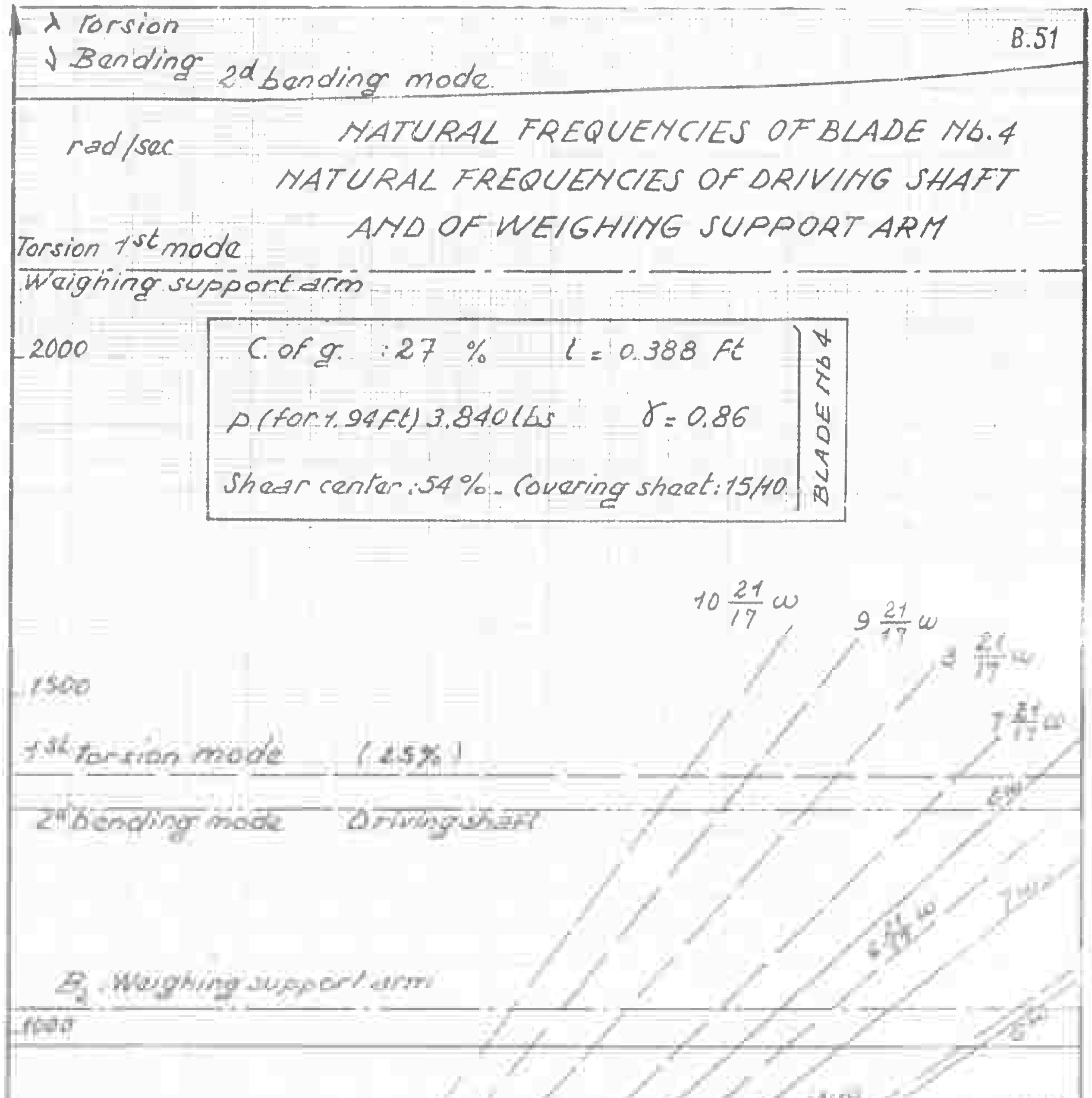
B.51
λ Torsion
ν Bending
2d bending mode
rad/sec
NATURAL FREQUENCIES OF BLADE No.4
NATURAL FREQUENCIES OF DRIVING SHAFT
AND OF WEIGHING SUPPORT ARM
Torsion 1st mode
Weighing support arm
2000
C. of g. : 27 %
l = 0.388 Ft
p (for 1.94 Ft) 3.840 lbs
γ = 0.86
Shear center : 54 % - Covering sheet : 15/10
BLADE No 4
1500
1st torsion mode (25%)
2d bending mode Driving shaft
B2 Weighing support arm
1000
1st bending mode
500
B1 weighing support arm
B1 driving shaft
10 21/17 ω
9 21/17 ω
8 21/17 ω
7 21/17 ω
6 21/17 ω
5 21/17 ω
4 21/17 ω
3 21/17 ω
2 21/17 ω
1 21/17 ω
8ω
7ω
6ω
5ω
4ω
3ω
2ω
1ω
50
100
150
ω rad/sec
FIG. 51

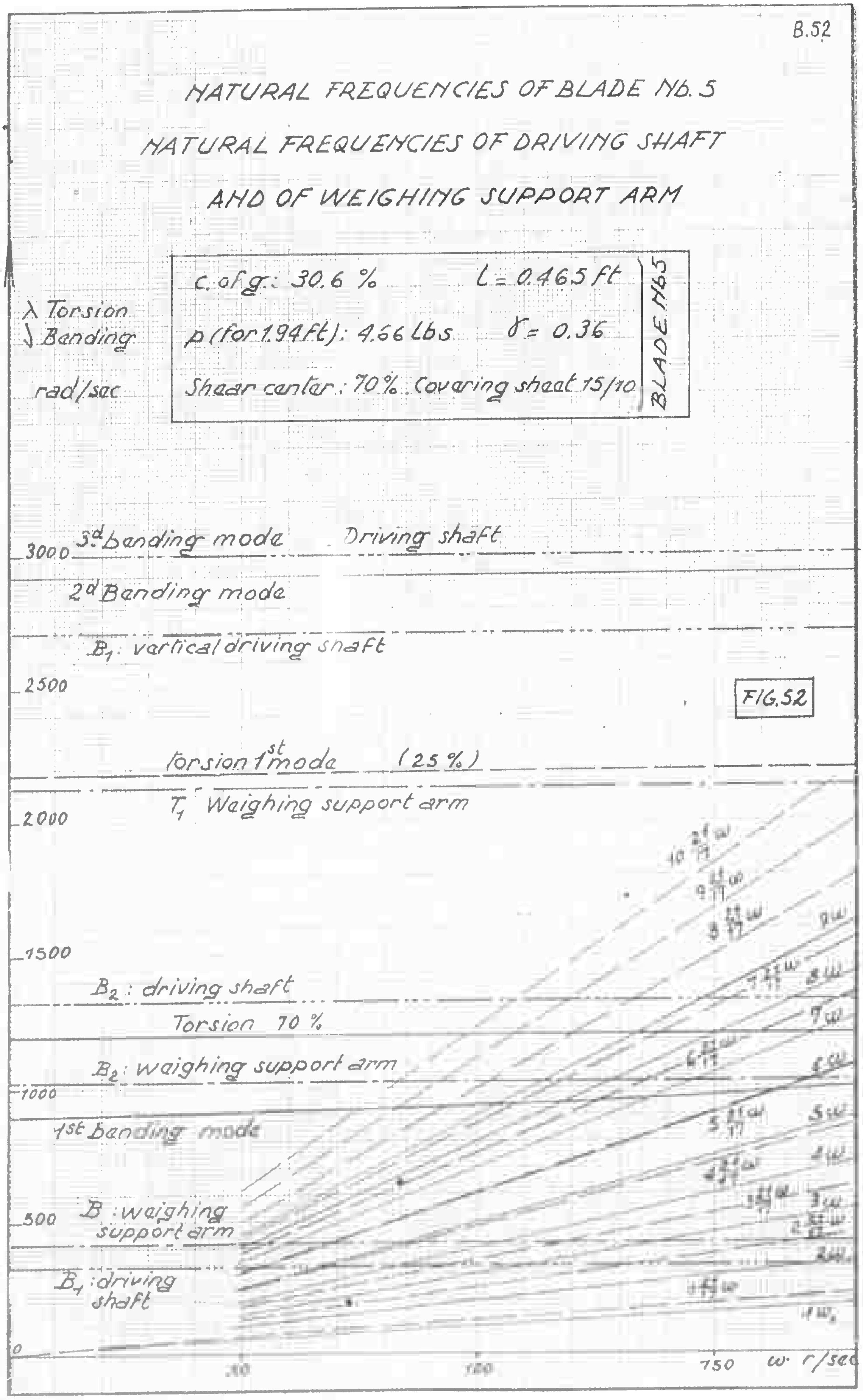
NATURAL FREQUENCIES OF BLADE No. 5
NATURAL FREQUENCIES OF DRIVING SHAFT
AND OF WEIGHING SUPPORT ARM
c. of g.: 30.6 %
l = 0.465 ft
p (for 1.94 ft): 4.66 lbs
δ = 0.36
Shear center: 70 %
Covering sheet 15/10
BLADE No. 5
λ Torsion
ϑ Bending
rad/sec
3rd bending mode
Driving shaft
2d Bending mode
B1: vertical driving shaft
torsion 1st mode (25 %)
T1 Weighing support arm
B2: driving shaft
Torsion 70 %
B2: weighing support arm
1st Bending mode
B: weighing support arm
B1: driving shaft
3000
2500
2000
1500
1000
500
0
250
500
750
ω r/sec
9ω
8ω
7ω
6ω
5ω
4ω
3ω
2ω
1ω
FIG. 52

COMPARISON OF NATURAL FREQUENCIES OF BLADE ROTATING PARTS AND CONTROLS

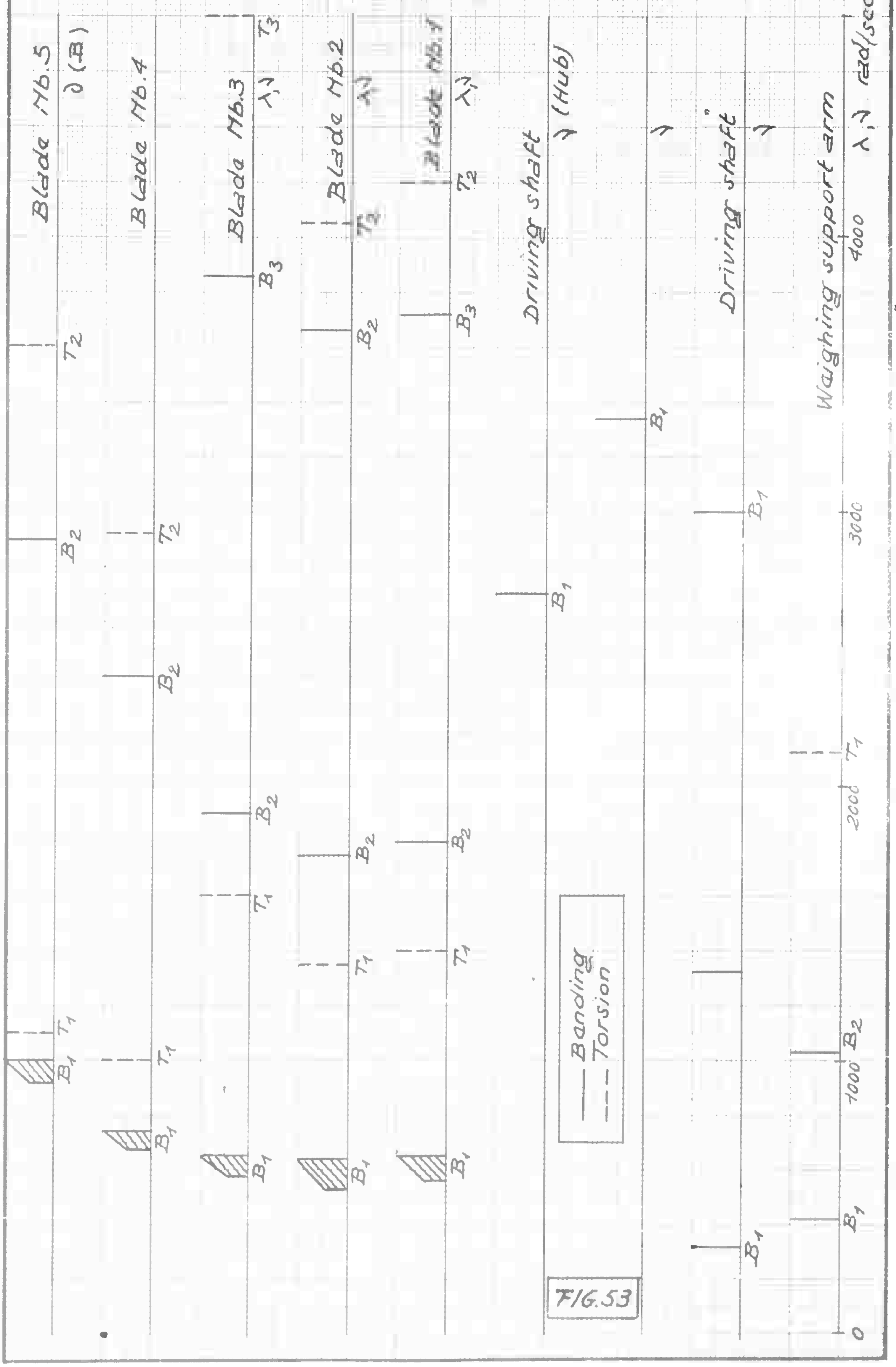

FIG.53

LOCATION OF CAMERAS WITH RESPECT TO ROTOR

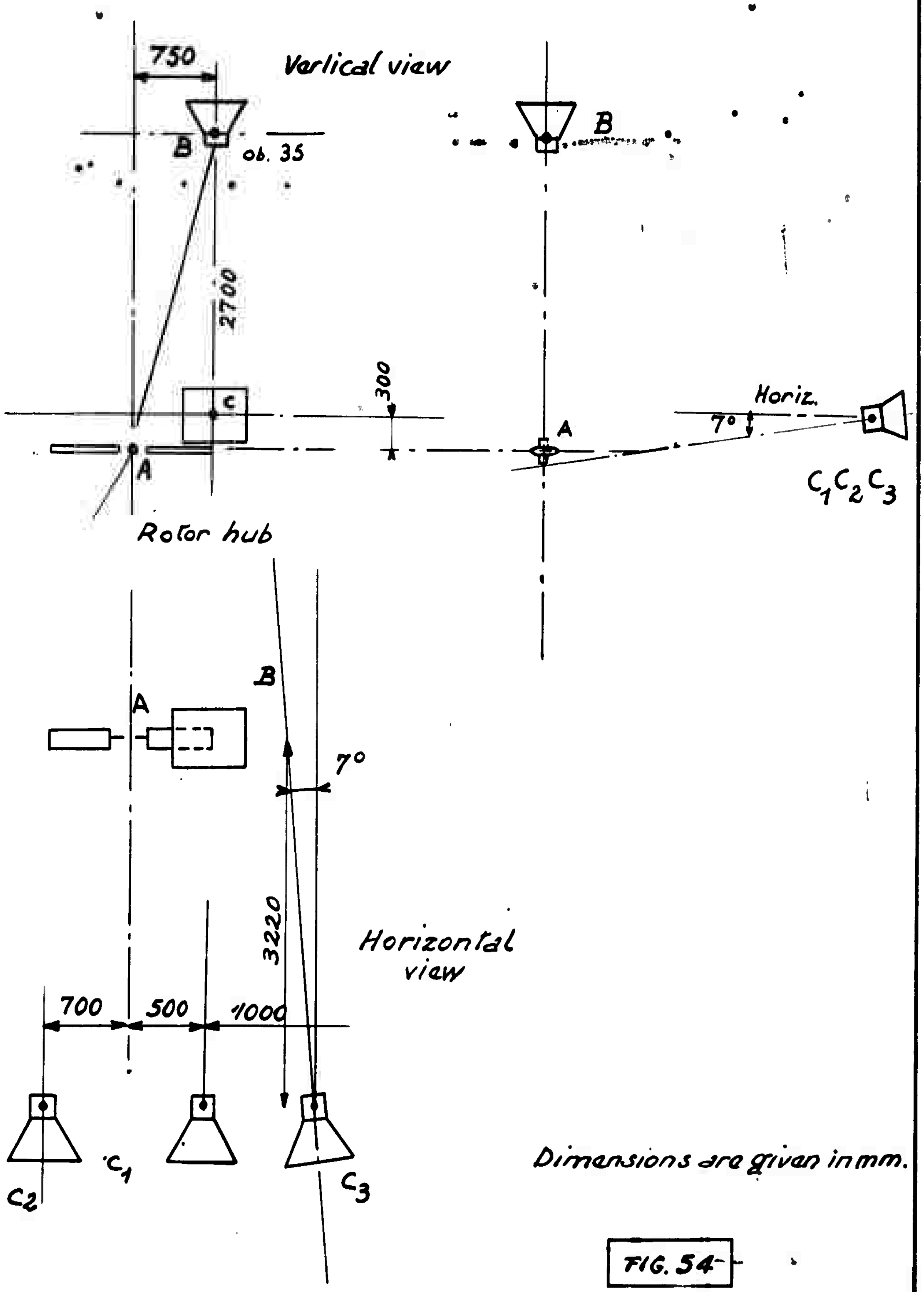

Dimensions are given in mm.

FIG. 54

PRINCIPLE OF SMOKE VISUALISATION ANALYSIS

EXTERNAL SMOKE EMISSION

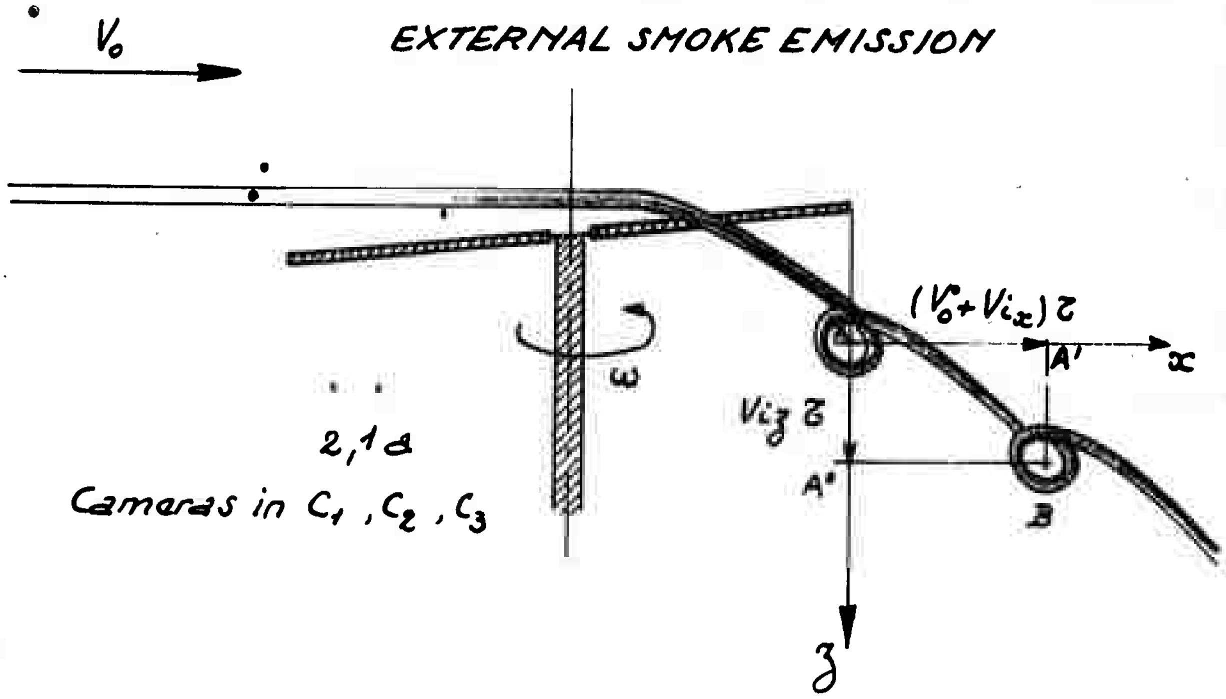

2,1 a

Cameras in C_1, C_2, C_3

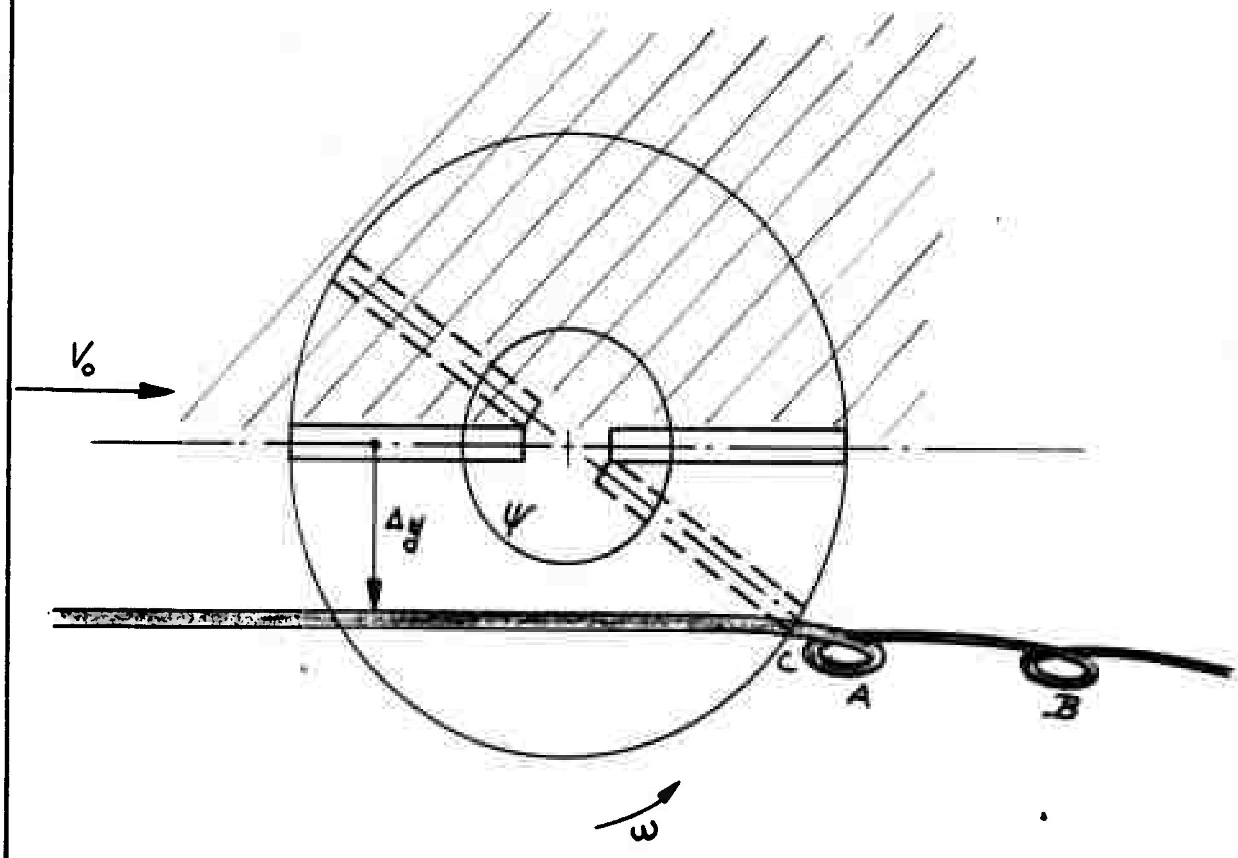

2,1 b

FIG. 55

Camera in B

PRINCIPLE OF SMOKE VISUALISATION ANALYSIS

SMOKE EMISSION FROM BLADE

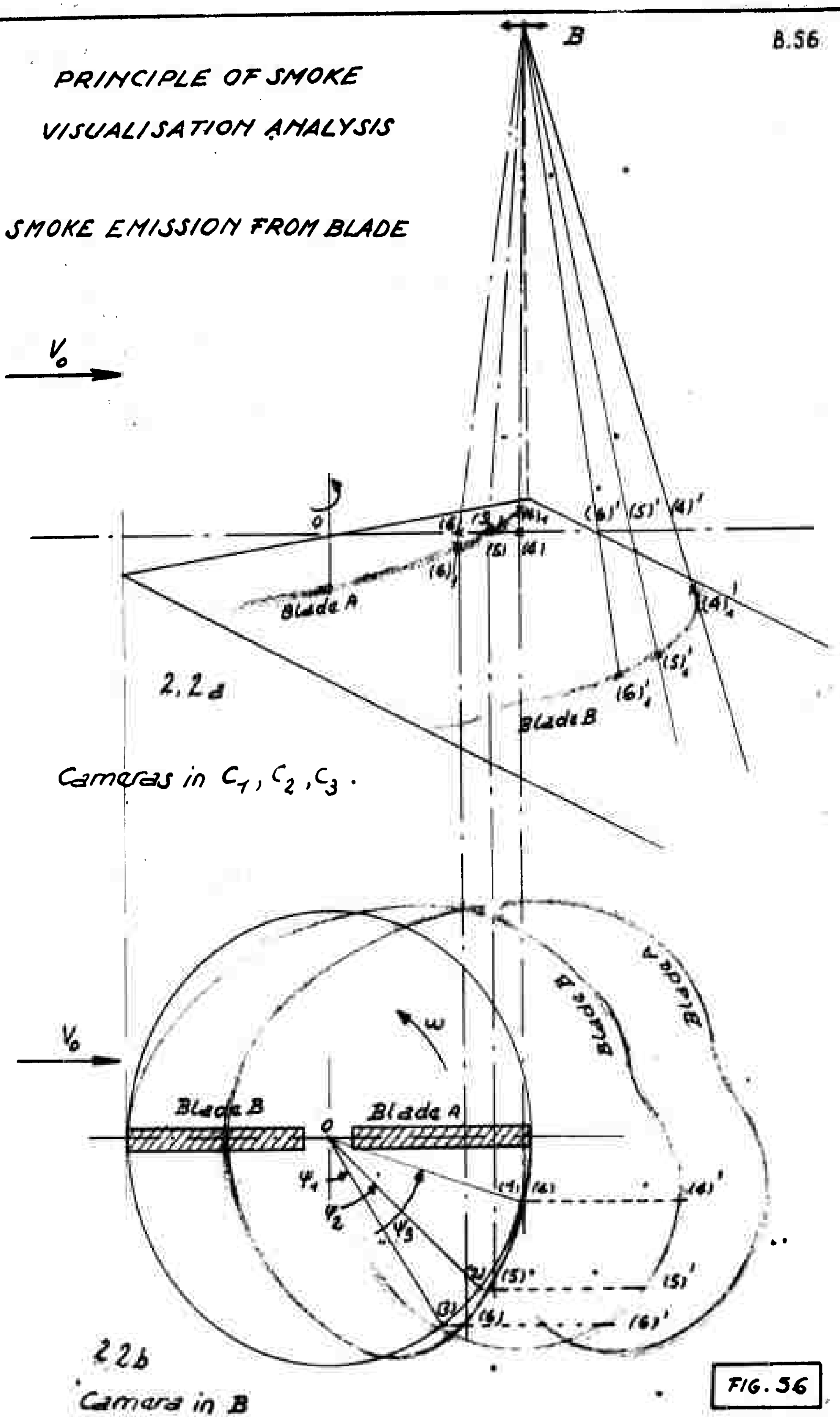

FIG. 56

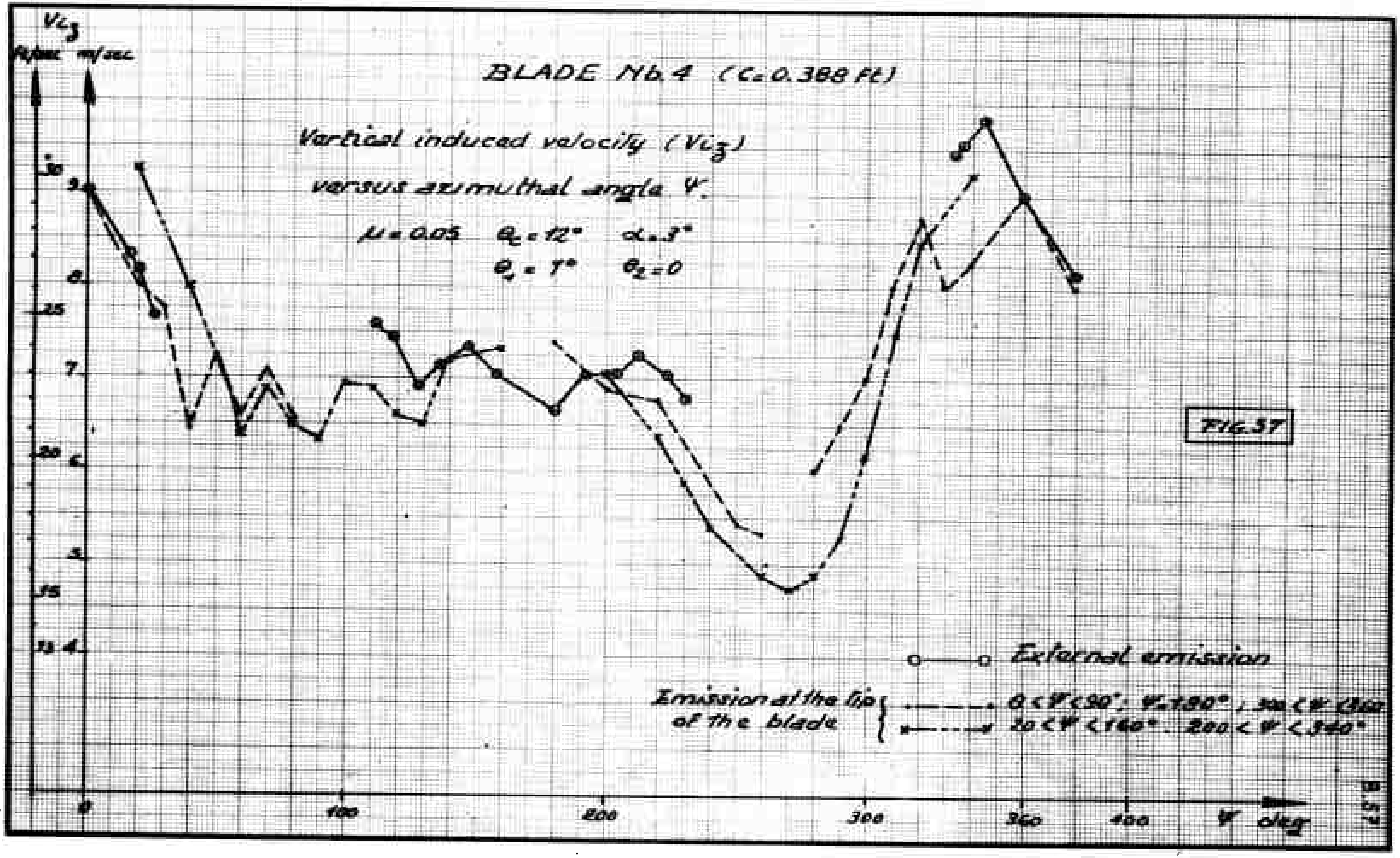

B.57
BLADE Nb 4 (C=0.388 Ft)
Vertical induced velocity (V_{iz})
versus azimuthal angle Ψ.
μ=0.05 θ0=12° α=3°
θ1=7° θ2=0
External emission
Emission at the tip of the blade
0<Ψ<90°; Ψ=180°; 300<Ψ<360
20<Ψ<160°; 200<Ψ<340°
Ψ deg
m/sec
ft/sec

FIG. 37

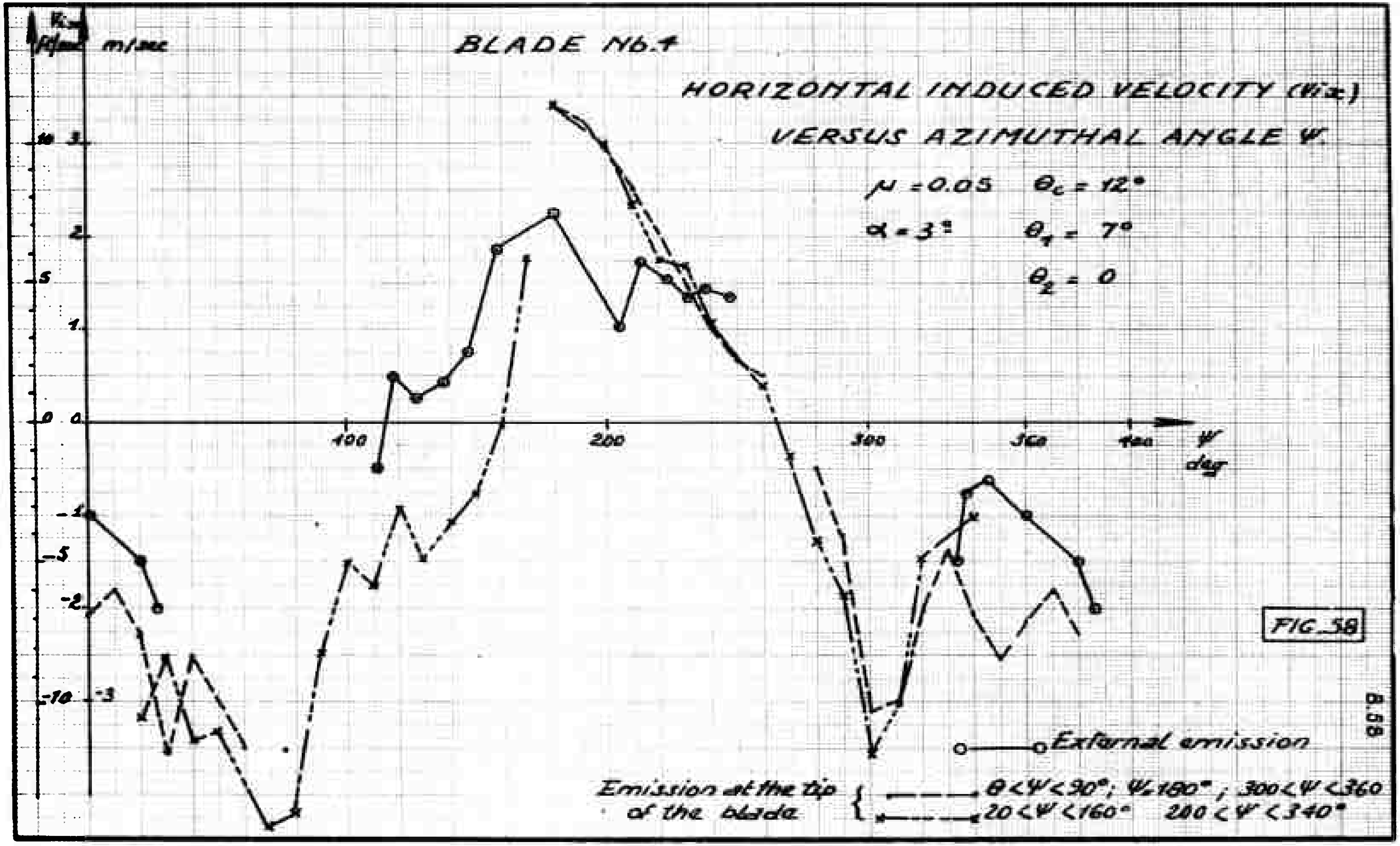

BLADE No.1
HORIZONTAL INDUCED VELOCITY (Viz)
VERSUS AZIMUTHAL ANGLE Ψ.
μ = 0.05 θc = 12°
α = 3° θ1 = 7°
θ2 = 0
m/sec
ft/sec
10 3
2
5
1
0 0
-1
-5
-2
-10 -3
100
200
300
360
400
Ψ deg
External emission
Emission at the tip of the blade
0 < Ψ < 90°; Ψ=180°; 300 < Ψ < 360
20 < Ψ < 160° 280 < Ψ < 340°

FIG. 58

8.58

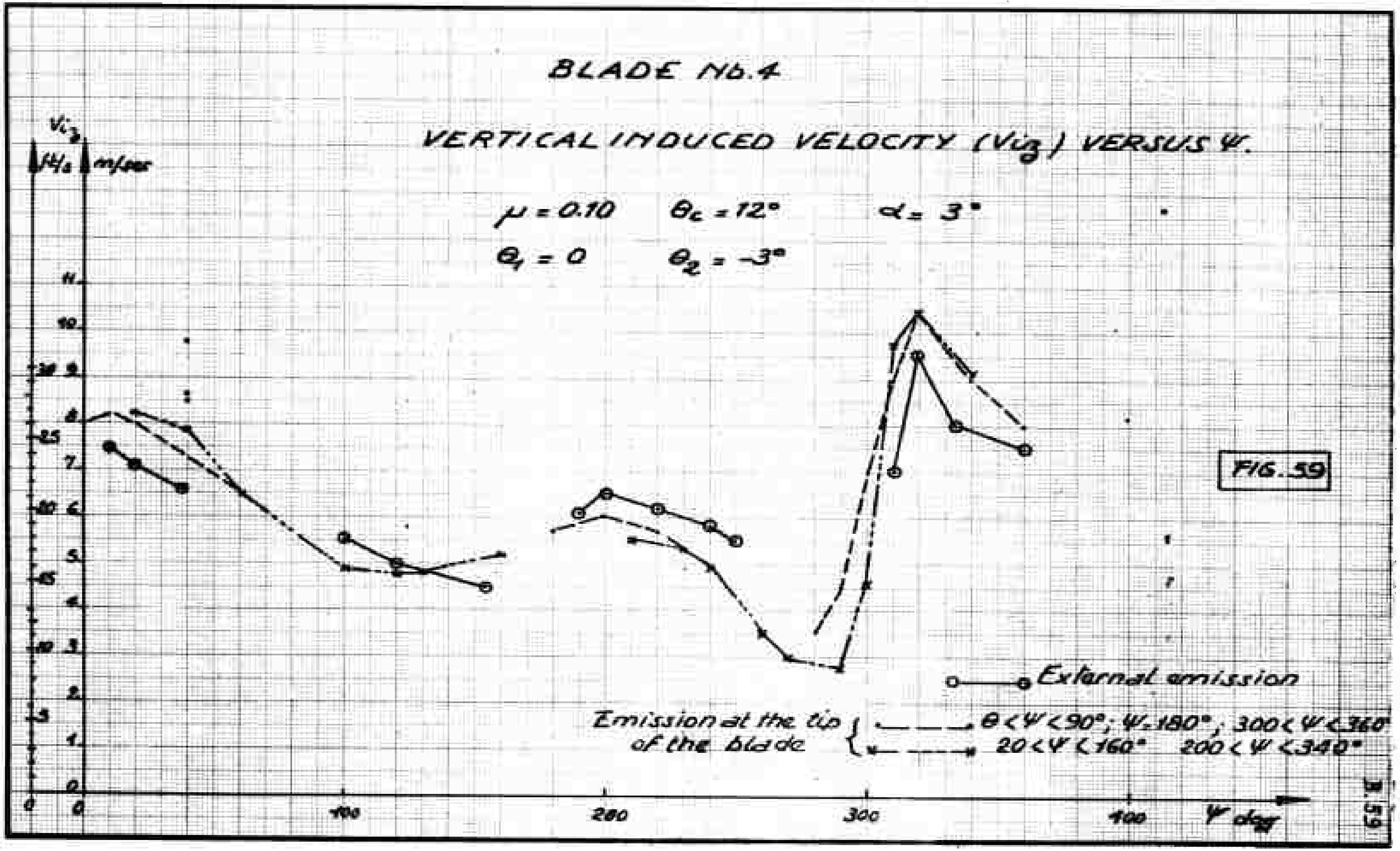
BLADE No.4
VERTICAL INDUCED VELOCITY (V_{iz}) VERSUS Ψ.
μ = 0.10
θc = 12°
α = 3°
θ1 = 0
θ2 = -3°
V_{iz}
ft/s
m/sec
External emission
Emission at the tip of the blade
0 < Ψ < 90°; Ψ = 180°; 300 < Ψ < 360°
20 < Ψ < 160°
200 < Ψ < 340°
Ψ deg
0
100
200
300
400
FIG. 59
B.59

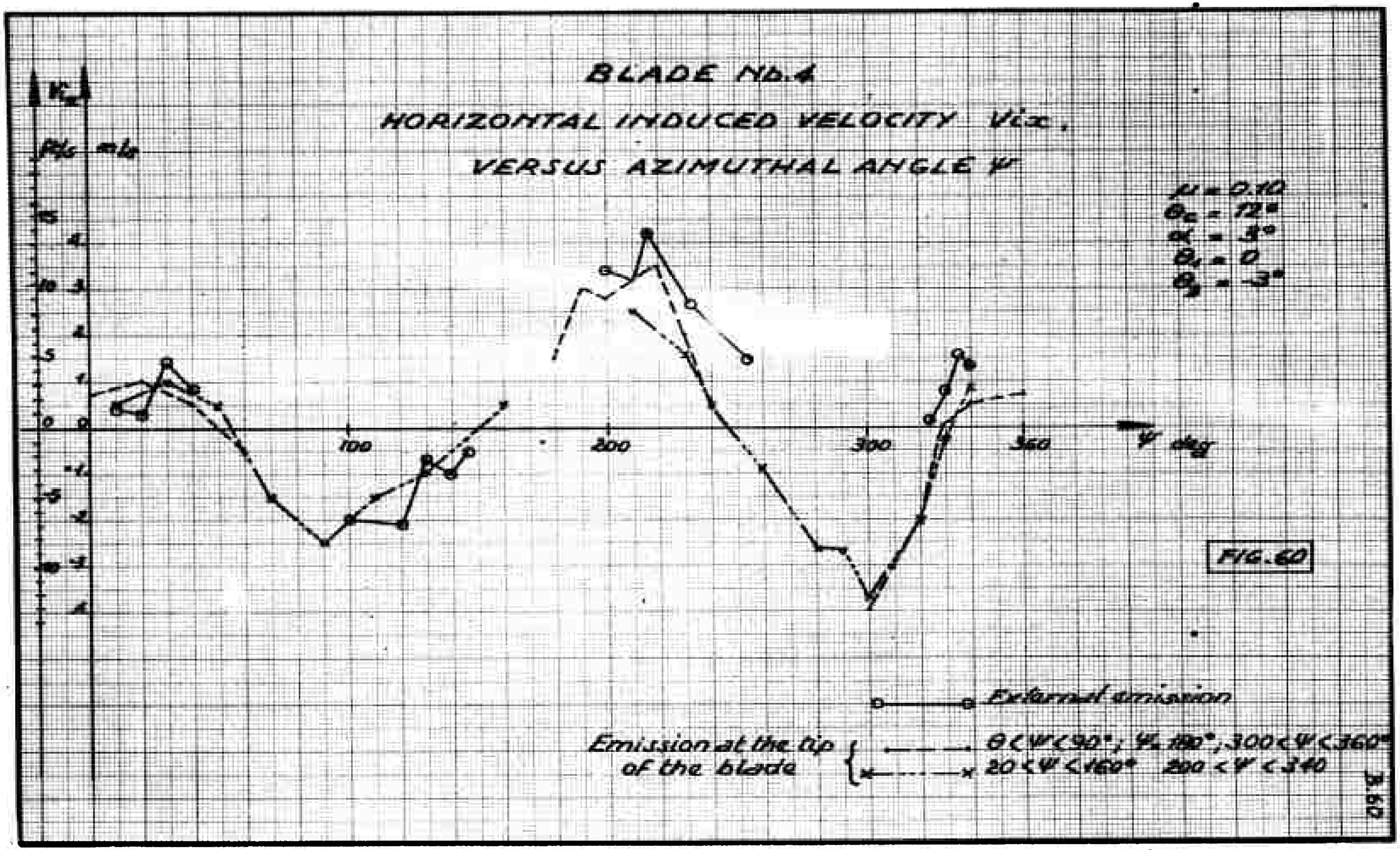
BLADE No. 4
HORIZONTAL INDUCED VELOCITY Vix,
VERSUS AZIMUTHAL ANGLE Ψ
$\mu = 0.10$
$\theta_c = 12°$
$\alpha = 3°$
$\theta_1 = 0$
$\theta_3 = -3°$
Ψ deg
100
200
300
350
ft/s
m/s
External emission
Emission at the tip of the blade
$0 < \Psi < 90°$; $\Psi = 180°$; $300 < \Psi < 360°$
$20 < \Psi < 160°$ $200 < \Psi < 340$
3.60

FIG. 60

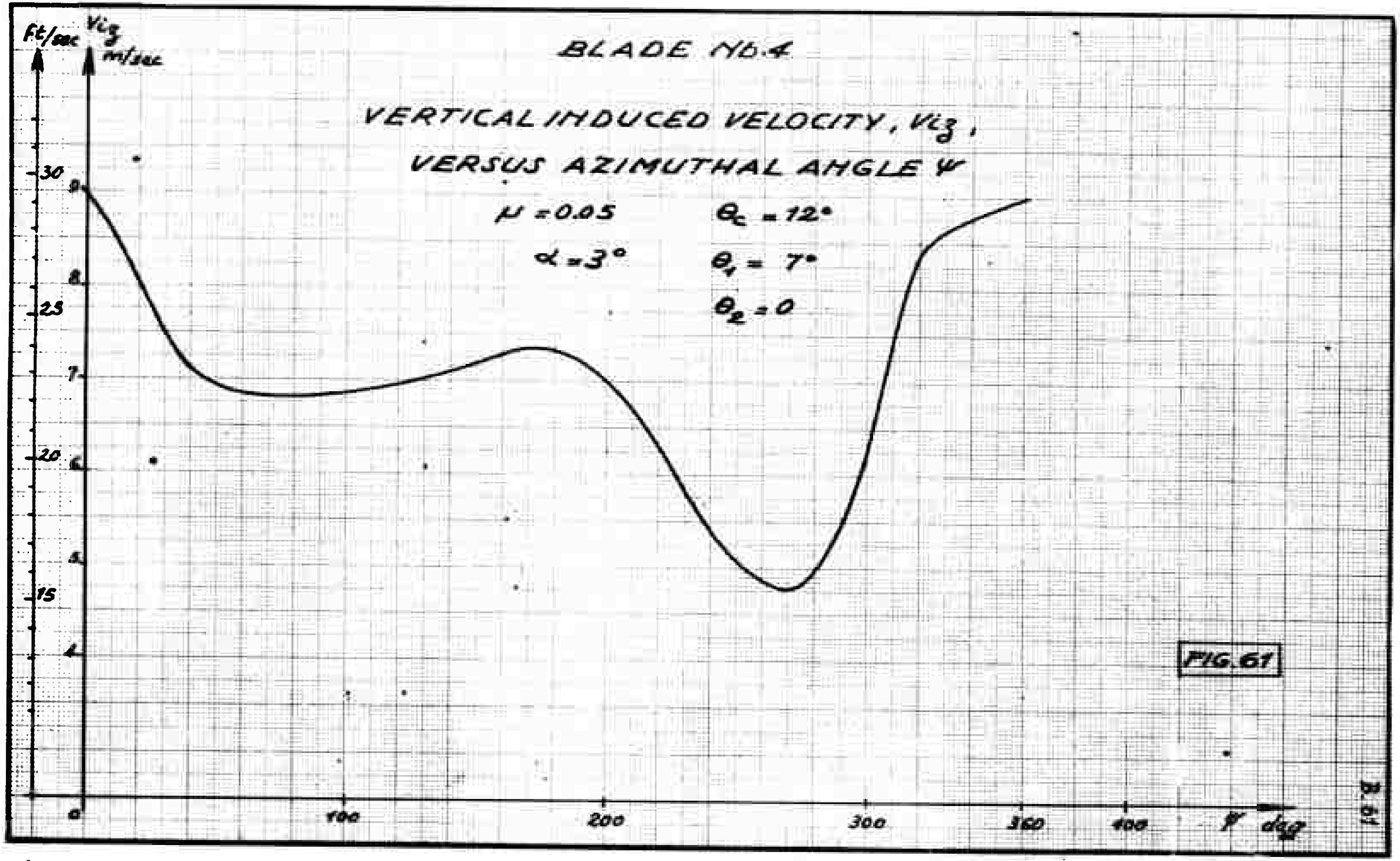

BLADE No.4
VERTICAL INDUCED VELOCITY, V_{iz},
VERSUS AZIMUTHAL ANGLE Ψ
$\mu = 0.05$
$\alpha = 3°$
$\theta_c = 12°$
$\theta_1 = 7°$
$\theta_2 = 0$
ft/sec
V_{iz} m/sec
30
25
20
15
9
8
7
6
5
4
0
100
200
300
360
400
Ψ deg

FIG. 61

B. 61

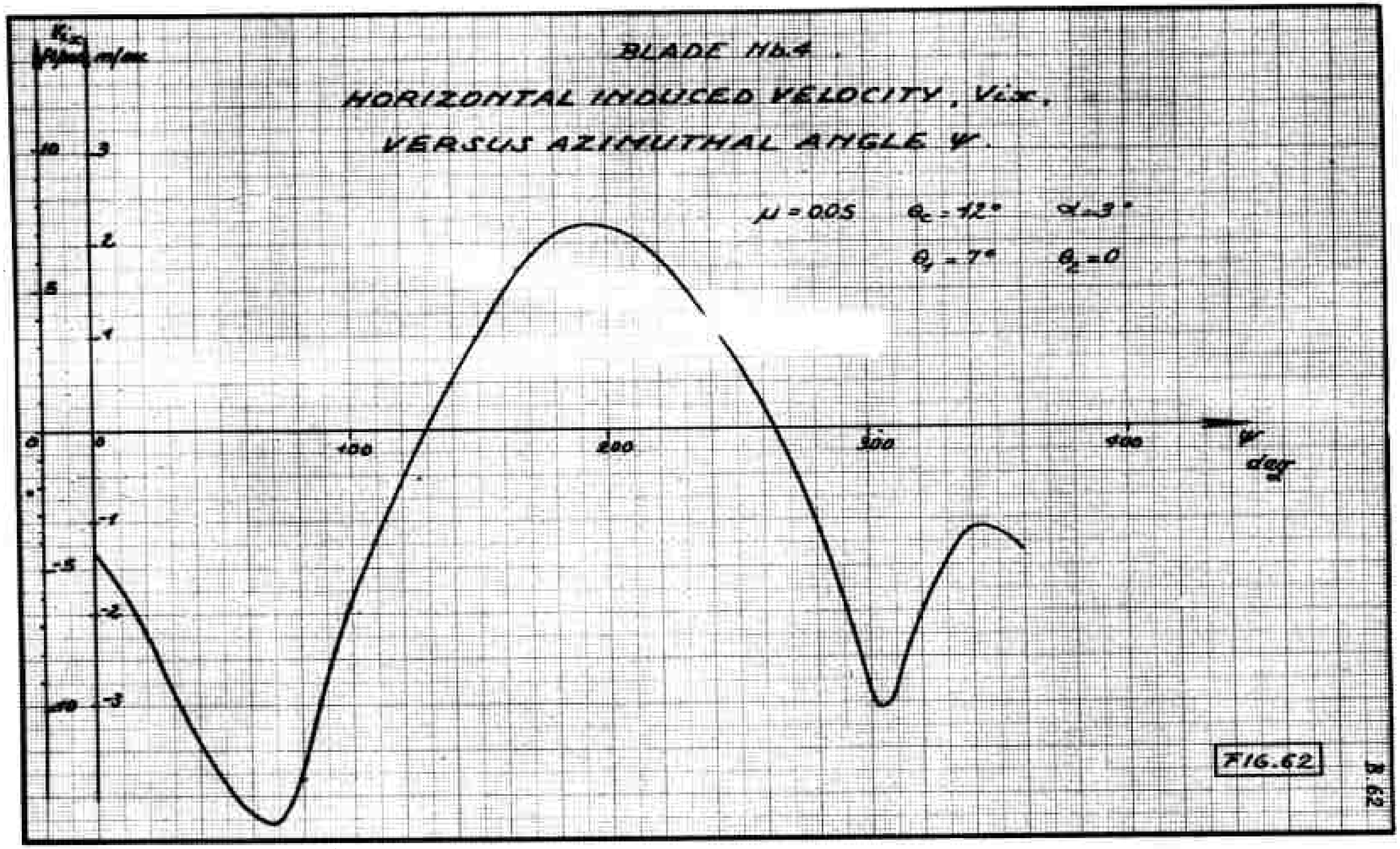
BLADE No.4.
HORIZONTAL INDUCED VELOCITY, Vix,
VERSUS AZIMUTHAL ANGLE Ψ.
μ = 0.05
θc = 12°
α = 3°
θ1 = 7°
θ2 = 0
Ψ deg
m/sec
0
100
200
300
400
10
5
-5
-10
3
2
1
-1
-2
-3

FIG.62

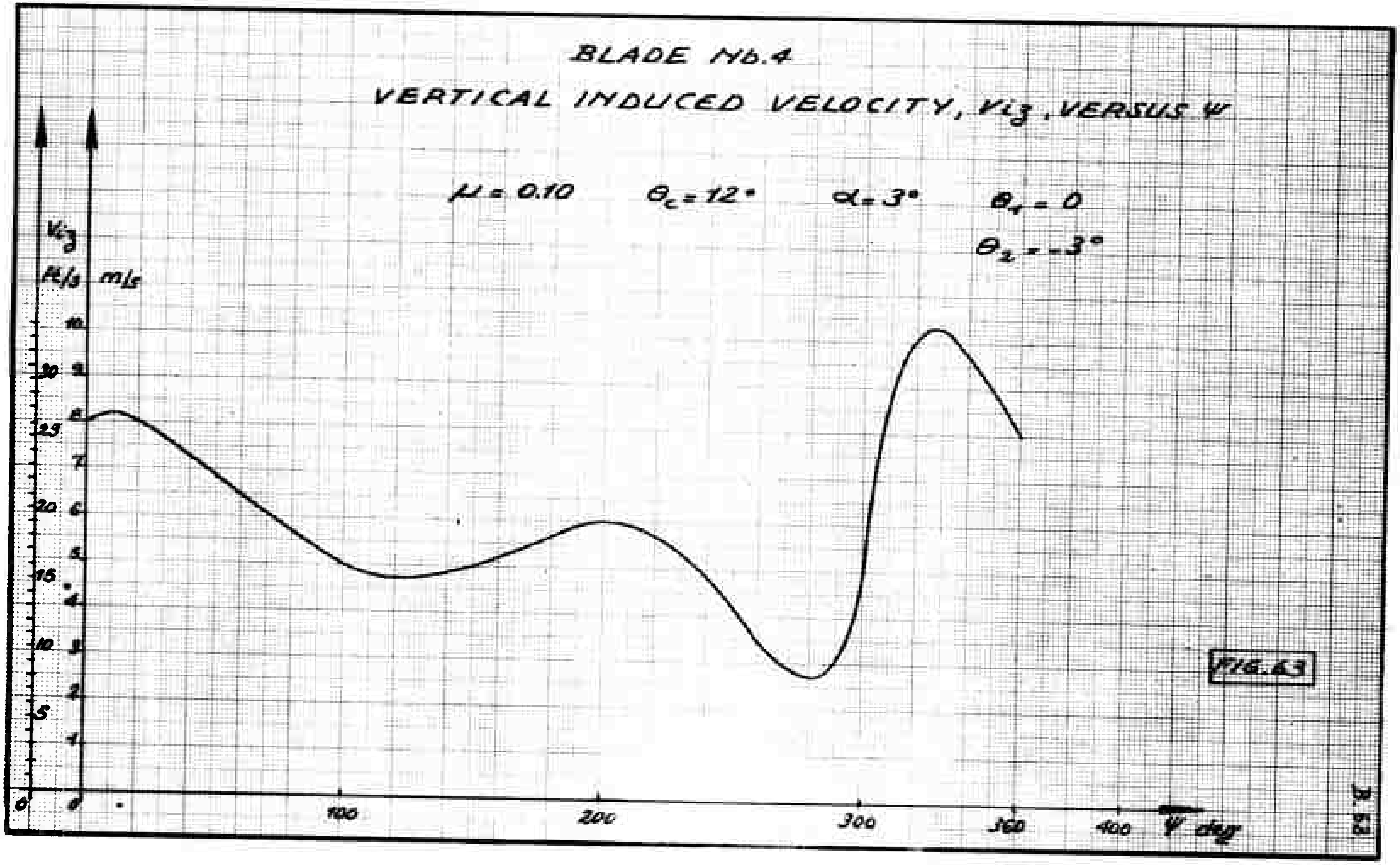

BLADE No.4
VERTICAL INDUCED VELOCITY, V_{iz}, VERSUS ψ
$\mu = 0.10$
$\theta_c = 12°$
$\alpha = 3°$
$\theta_1 = 0$
$\theta_2 = -3°$
V_{iz}
ft/s
m/s
0
5
10
15
20
25
30
1
2
3
4
5
6
7
8
9
10
100
200
300
360
400
ψ deg
B.58

FIG. 63

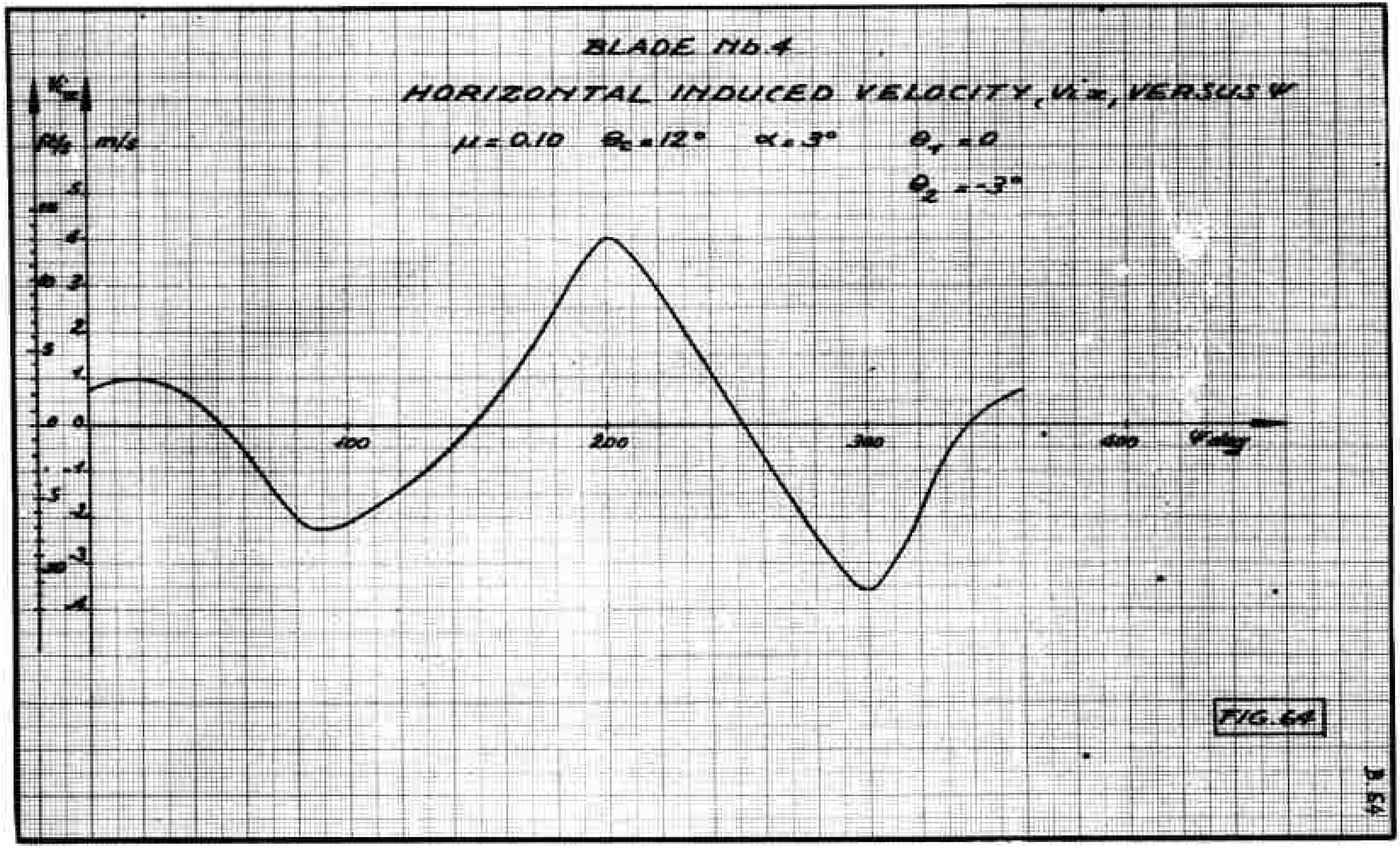
BLADE No. 4
HORIZONTAL INDUCED VELOCITY, V_{ix}, VERSUS Ψ
$\mu = 0.10$ $\theta_c = 12°$ $\alpha = 3°$ $\theta_1 = 0$
$\theta_2 = -3°$
ft/s
m/s
100
200
300
400
Ψ deg

FIG. 64

B.64

BLADE No.4 EFFECT OF θ_c IN HOVERING (V_{iz} versus ψ)

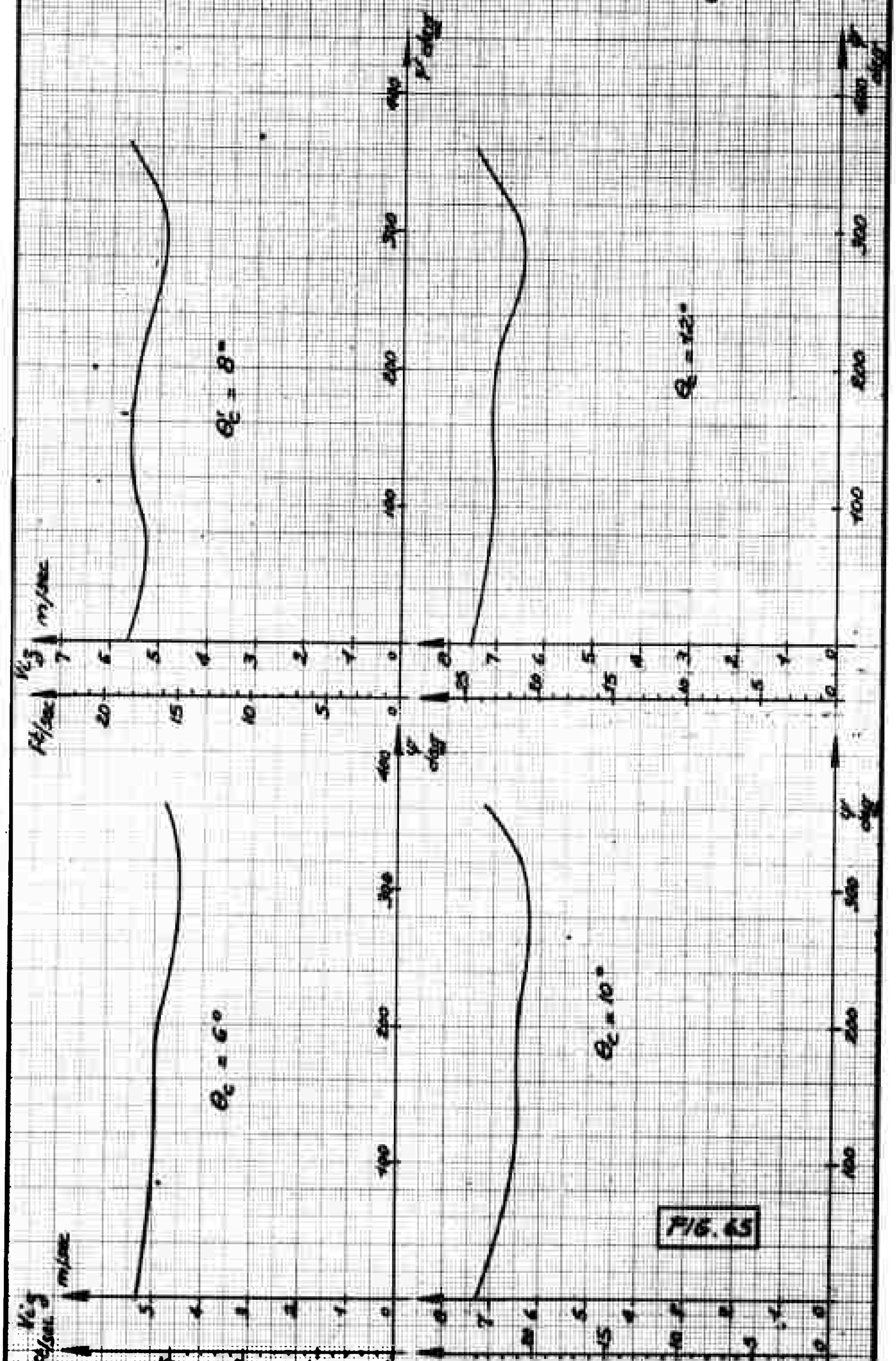

FIG. 65

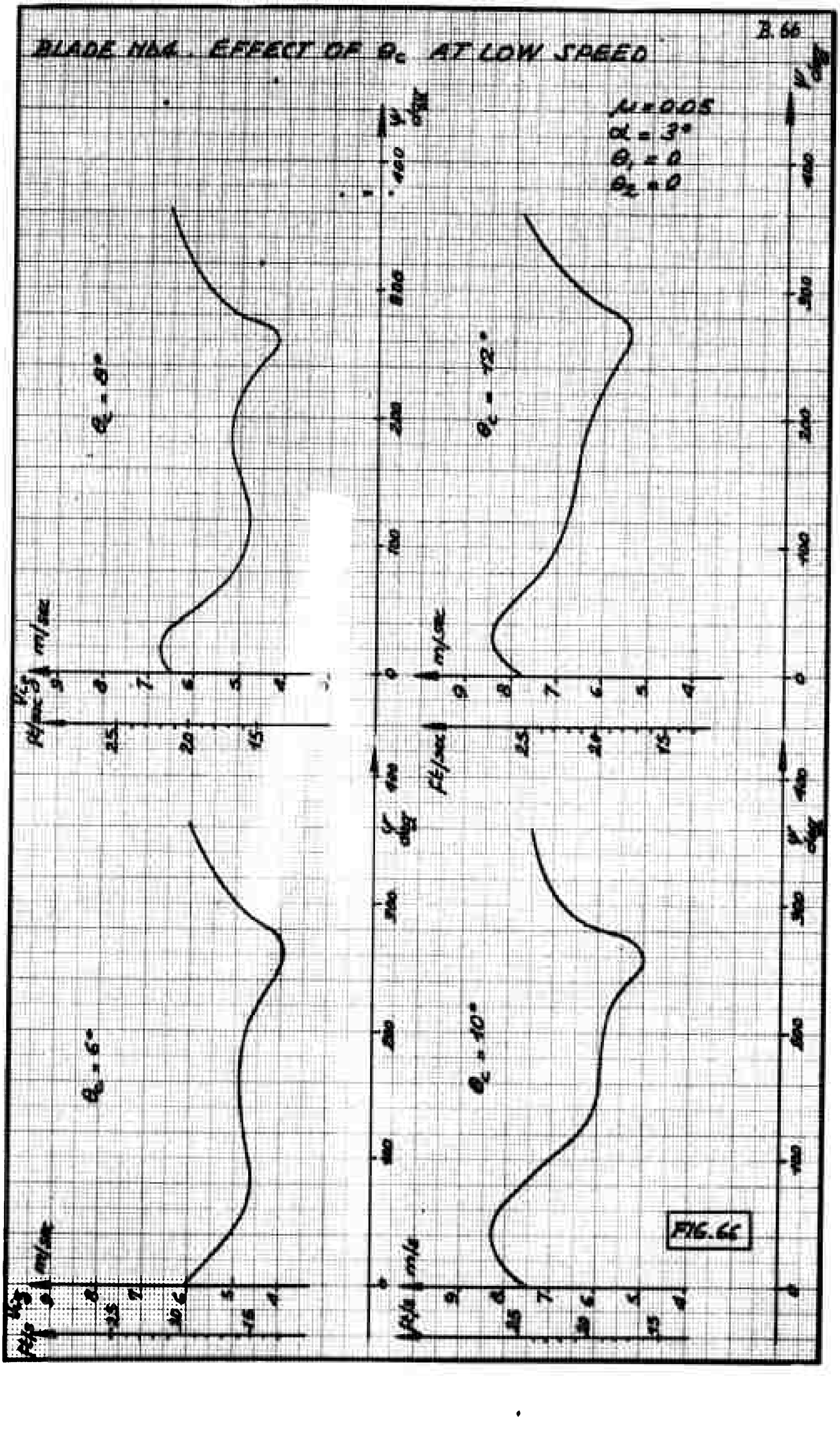
B.66
BLADE NO4. EFFECT OF θc AT LOW SPEED
μ = 0.05
α = 3°
θ1 = 0
θ2 = 0
θc = 8°
θc = 12°
θc = 6°
θc = 10°
ψ deg
Vi,s
ft/sec
m/sec
FIG. 6C

BLADE No 4

EFFECT OF θ_c

$\mu = 0.10$ $\alpha = 3°$ $\theta_1 = 0$ $\theta_2 = 0$

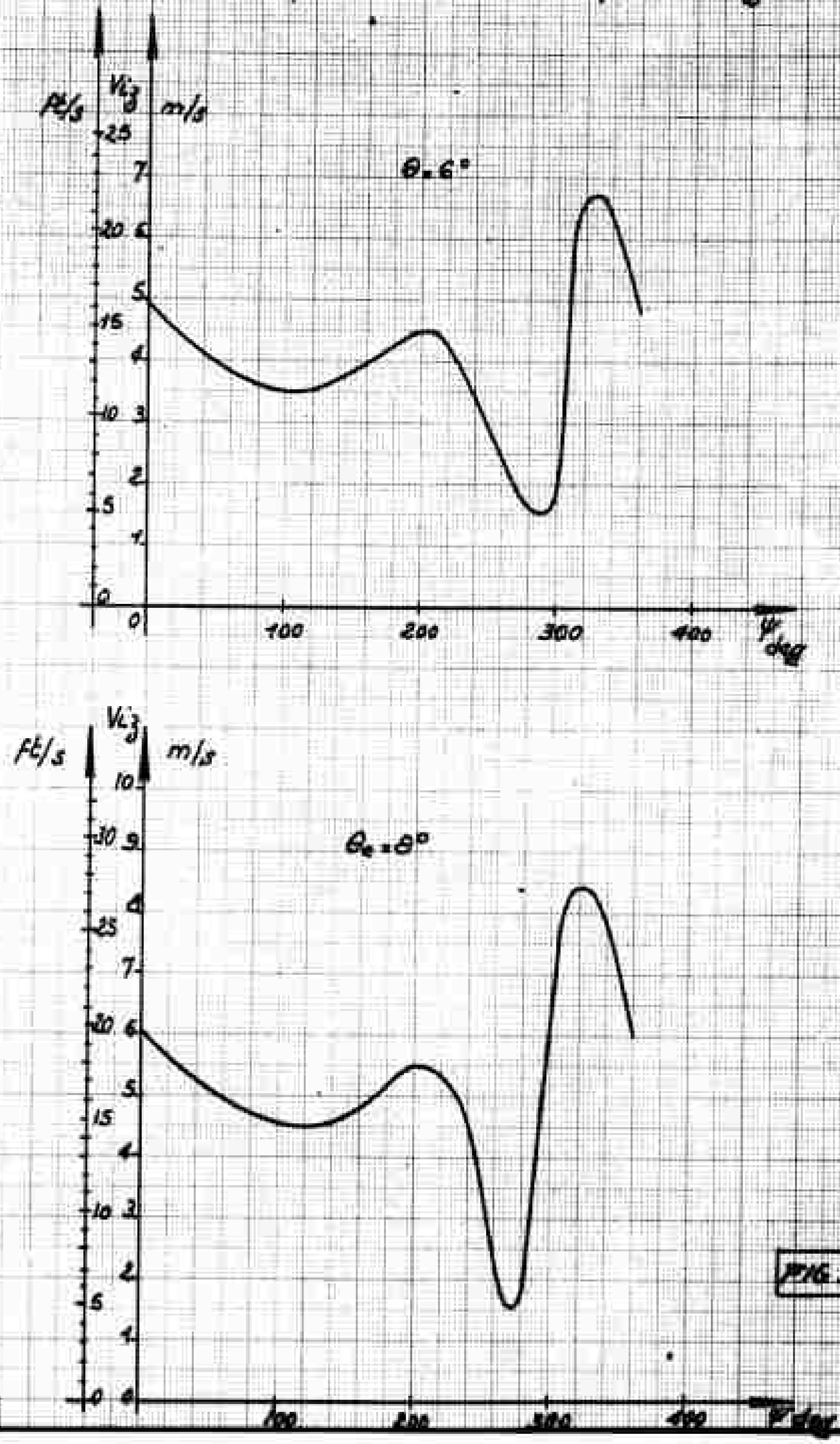

FIG. 67

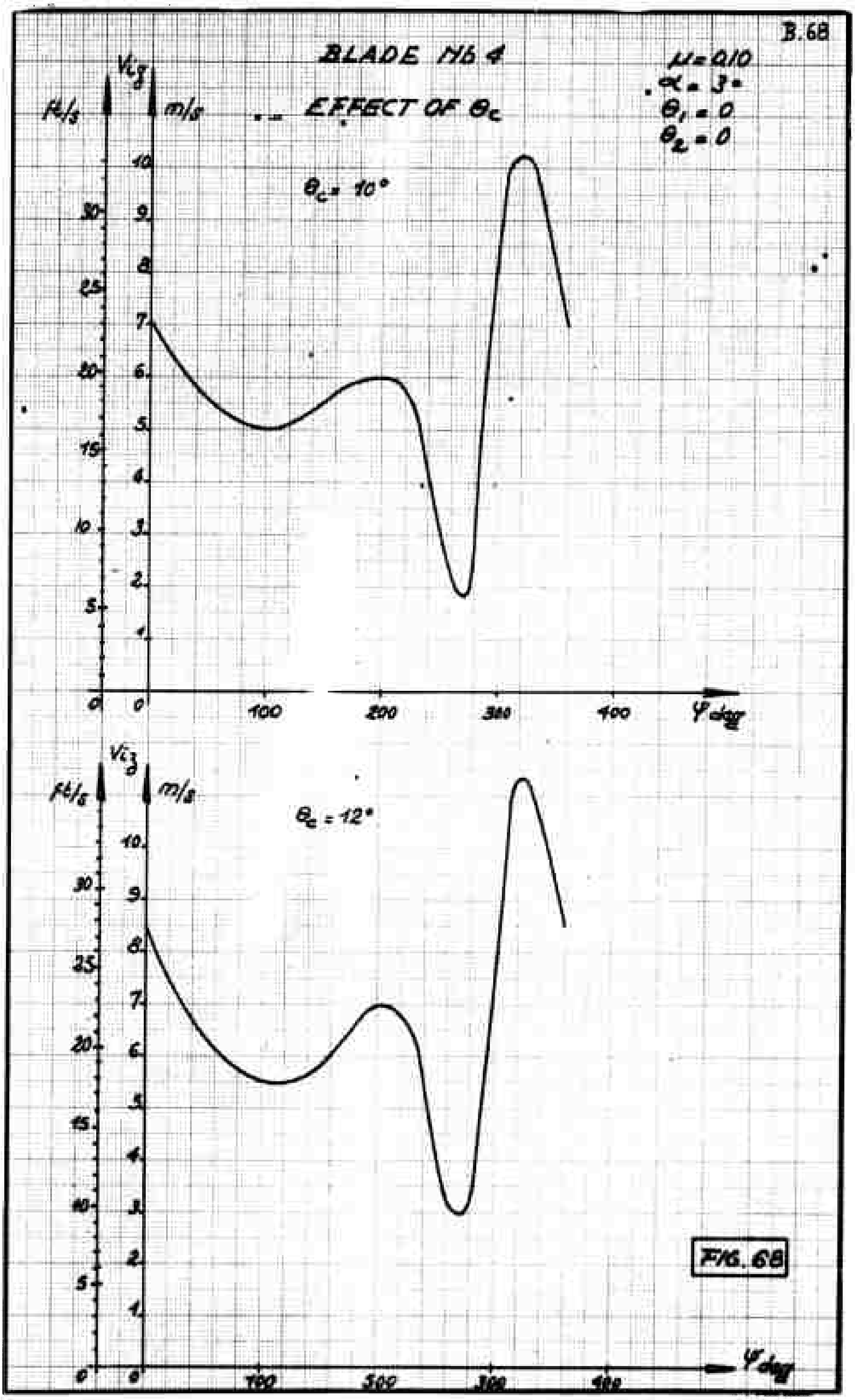
BLADE Nb 4
EFFECT OF θ_c
$\mu = 0.10$
$\alpha = 3°$
$\theta_1 = 0$
$\theta_2 = 0$
V_{i_3}
ft/s
m/s
$\theta_c = 10°$
$\theta_c = 12°$
ψ deg
0
100
200
300
400

FIG. 68

BLADE No4 EFFECT OF θ_c

$\mu = 0.15$ $\alpha_s = 3°$

$\theta_1 = 0$ $\theta_2 = 0$

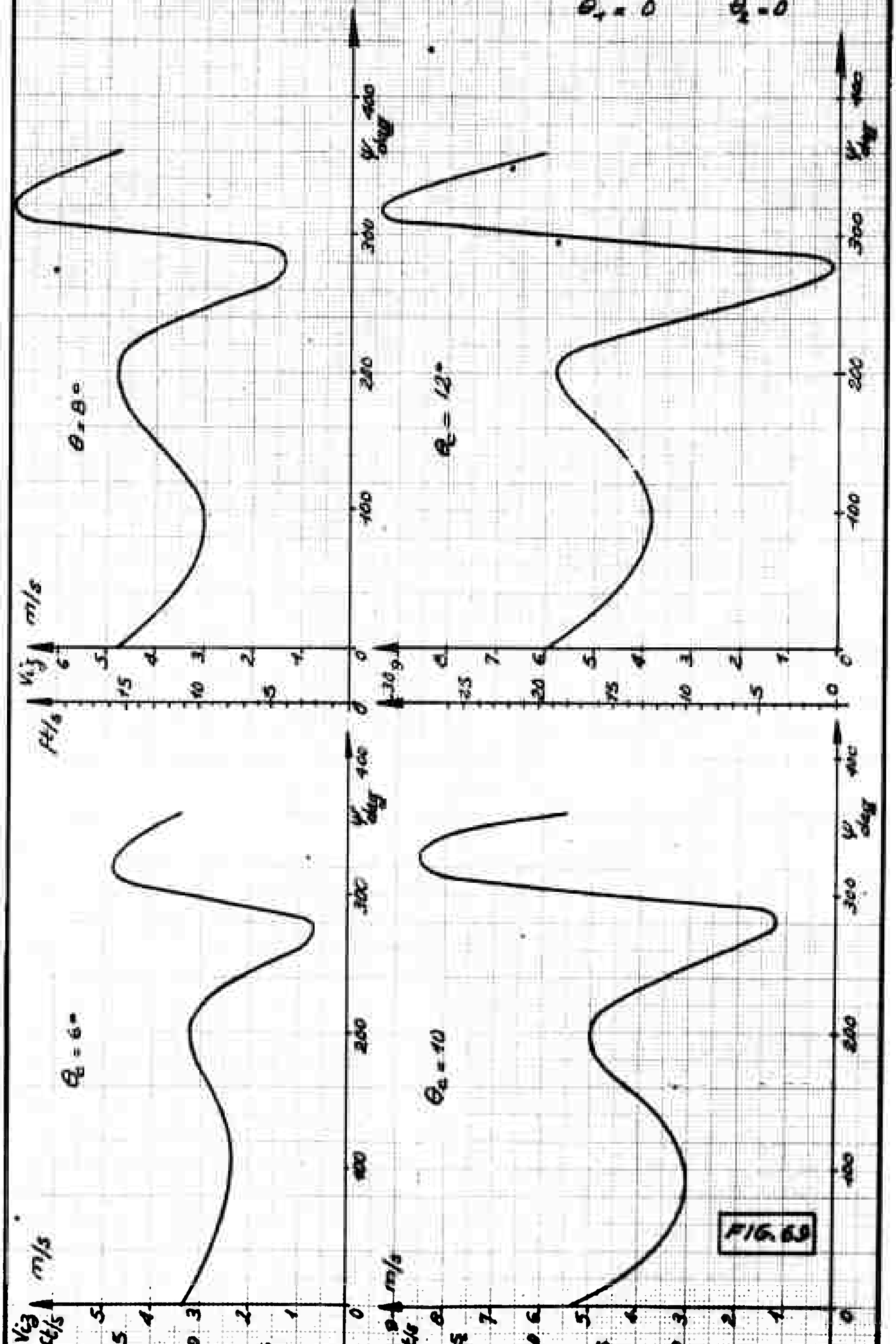

FIG. 69

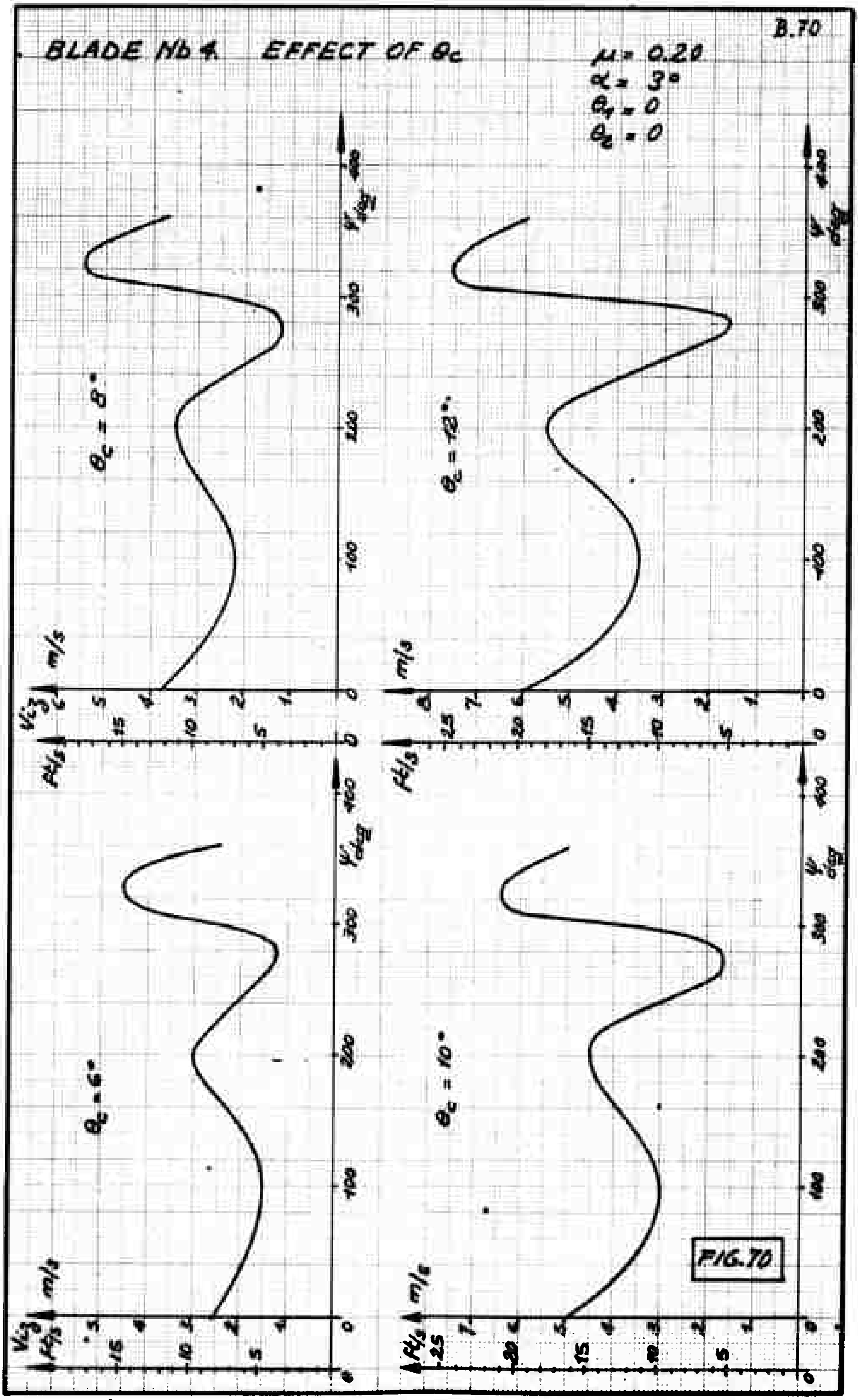
BLADE No 4. EFFECT OF θc
μ = 0.20
α = 3°
θ1 = 0
θ2 = 0
θc = 6°
θc = 8°
θc = 10°
θc = 12°
Vi3 m/s
ft/s
ψ deg
0
100
200
300
400

FIG. 70

BLADE No 4. EFFECT OF α AT LOW SPEED

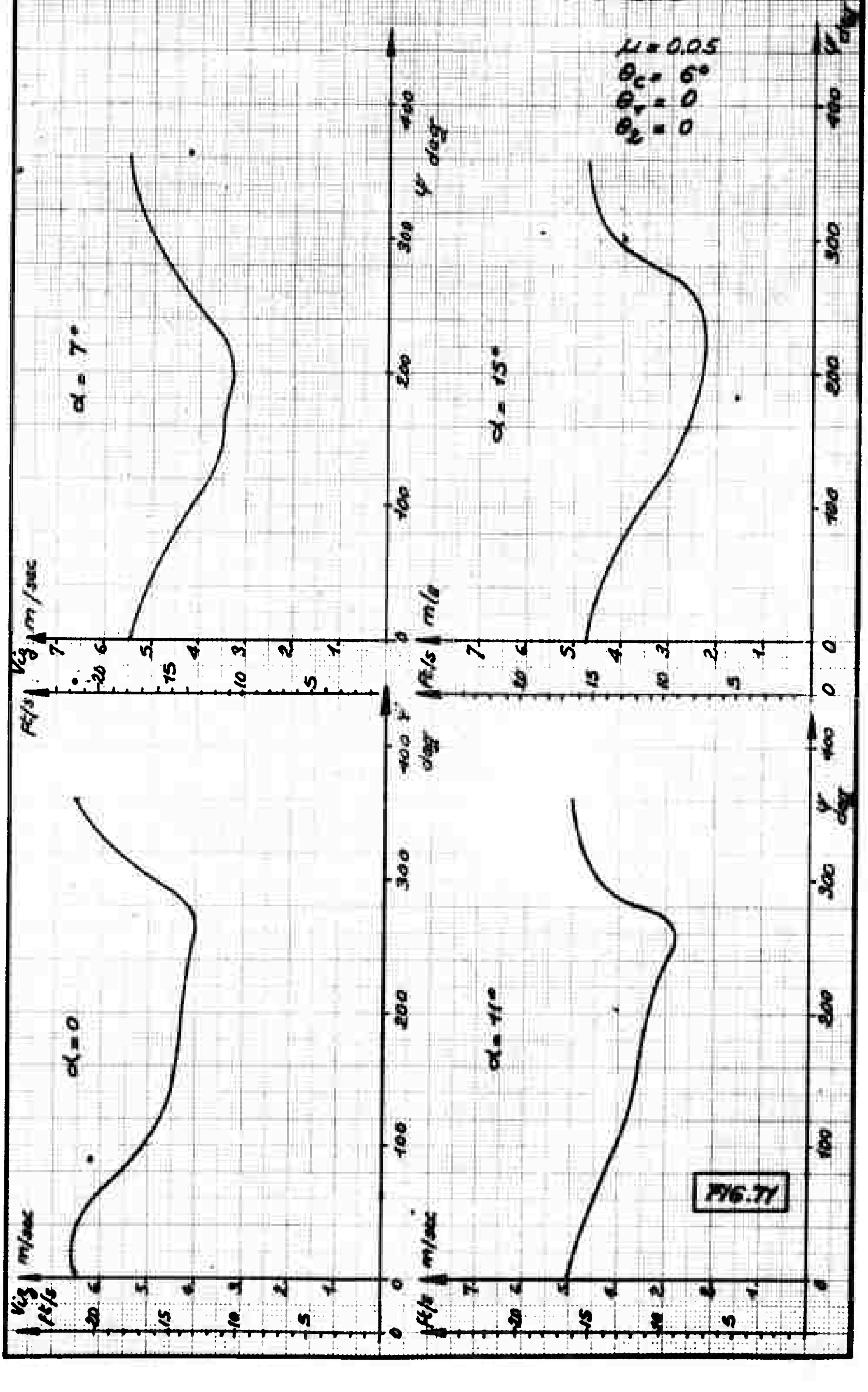

FIG. 71

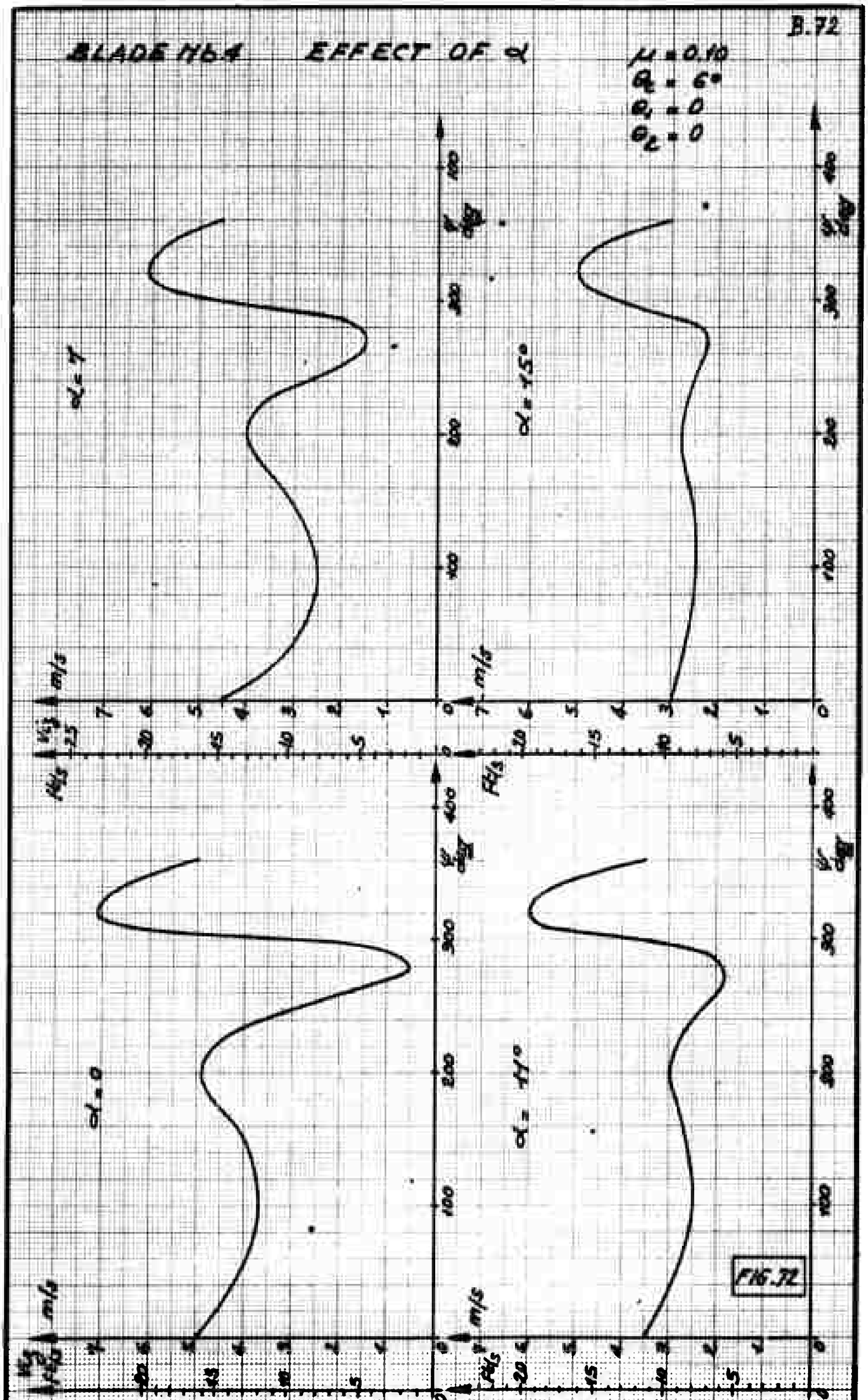

B.72
BLADE H64
EFFECT OF α
μ = 0.10
θ₀ = 6°
θ₁ = 0
θ₂ = 0
α = 0
α = 7°
α = 11°
α = 15°
m/s
ft/s
ψ deg
100
200
300
400
FIG. 72

BLADE No 4. EFFECT OF α

$\mu = 0.15$
$\theta_c = 6°$
$\theta_1 = 0$
$\theta_2 = 0$

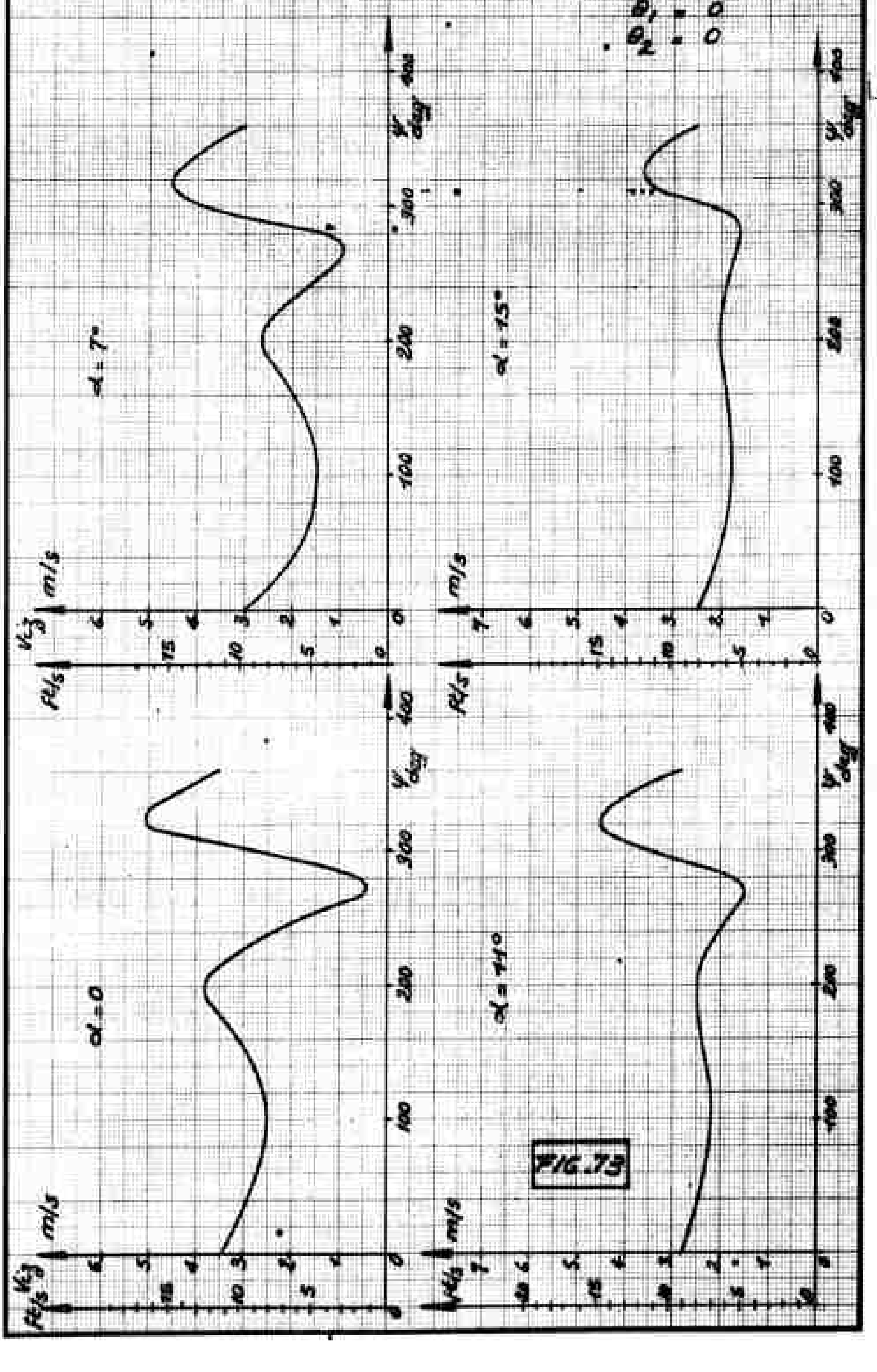

FIG. 73

BLADE No 4 EFFECT OF α

$\mu = 0.20$
$\theta_c = 6°$
$\theta_1 = 0$
$\theta_2 = 0$

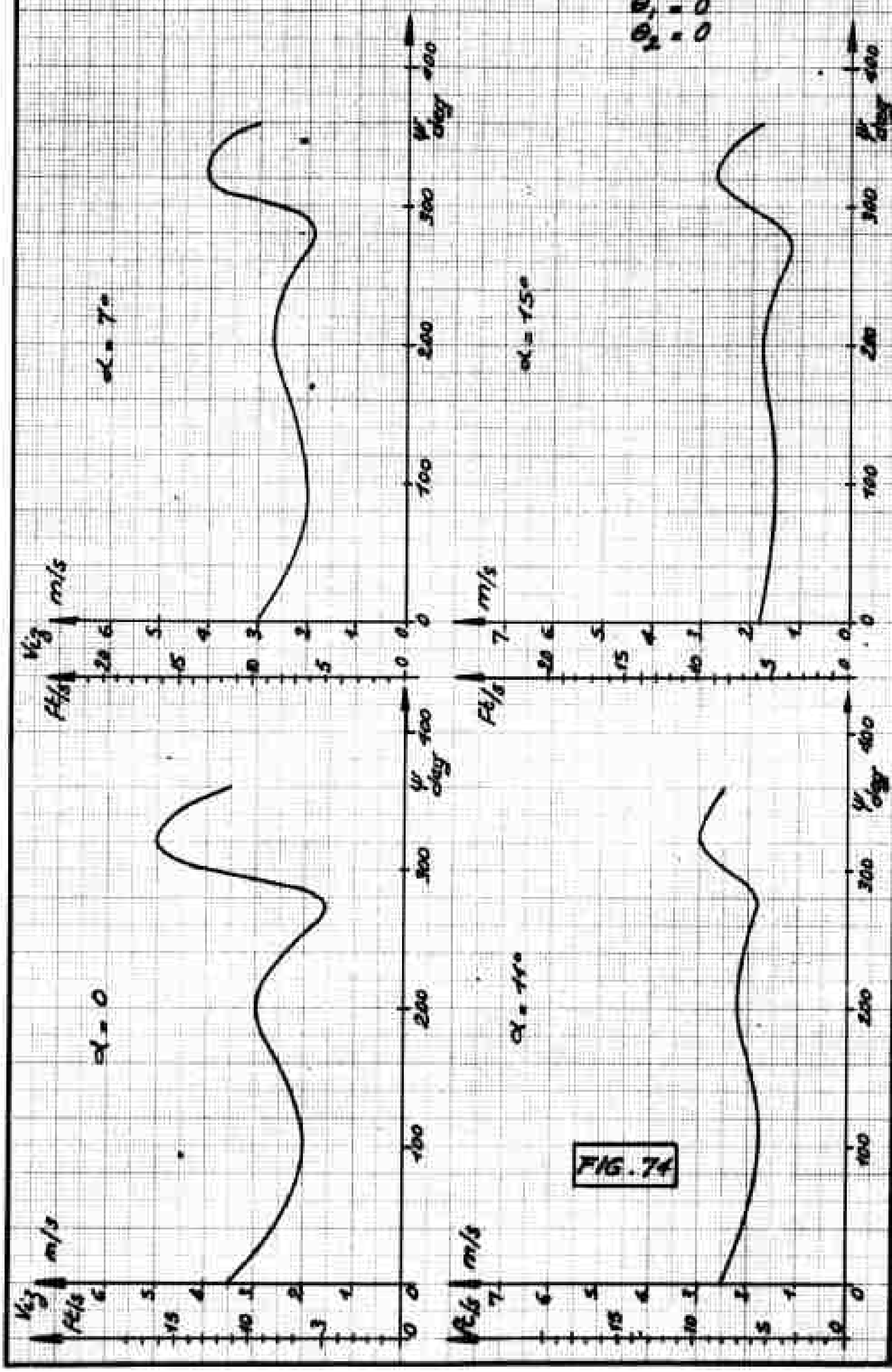

FIG. 74

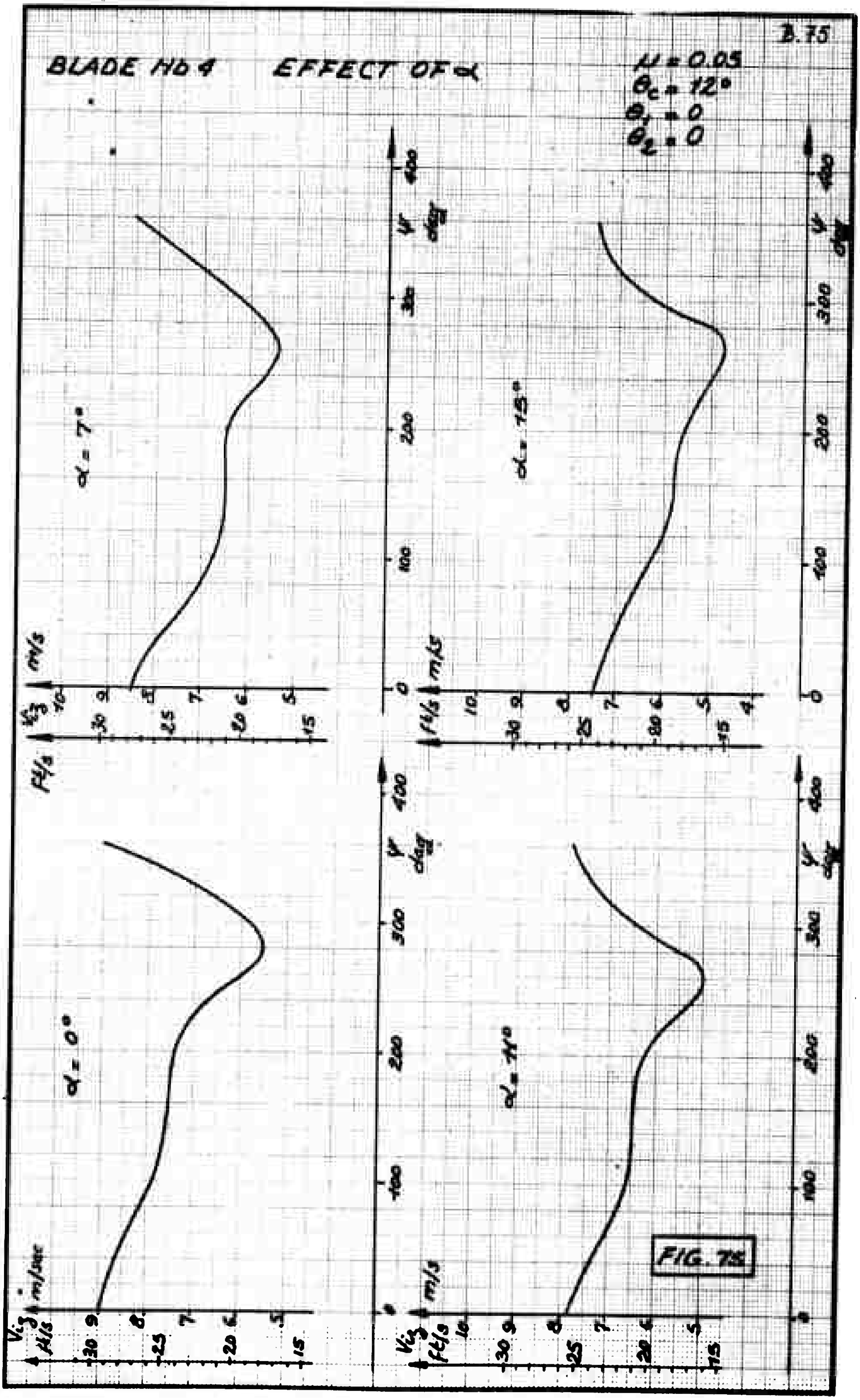
BLADE No 4 EFFECT OF α
μ = 0.05
θ_c = 12°
θ_1 = 0
θ_2 = 0
α = 0°
α = 7°
α = 11°
α = 15°
ψ deg
V_{i_3} m/sec
ft/s
m/s

FIG. 75

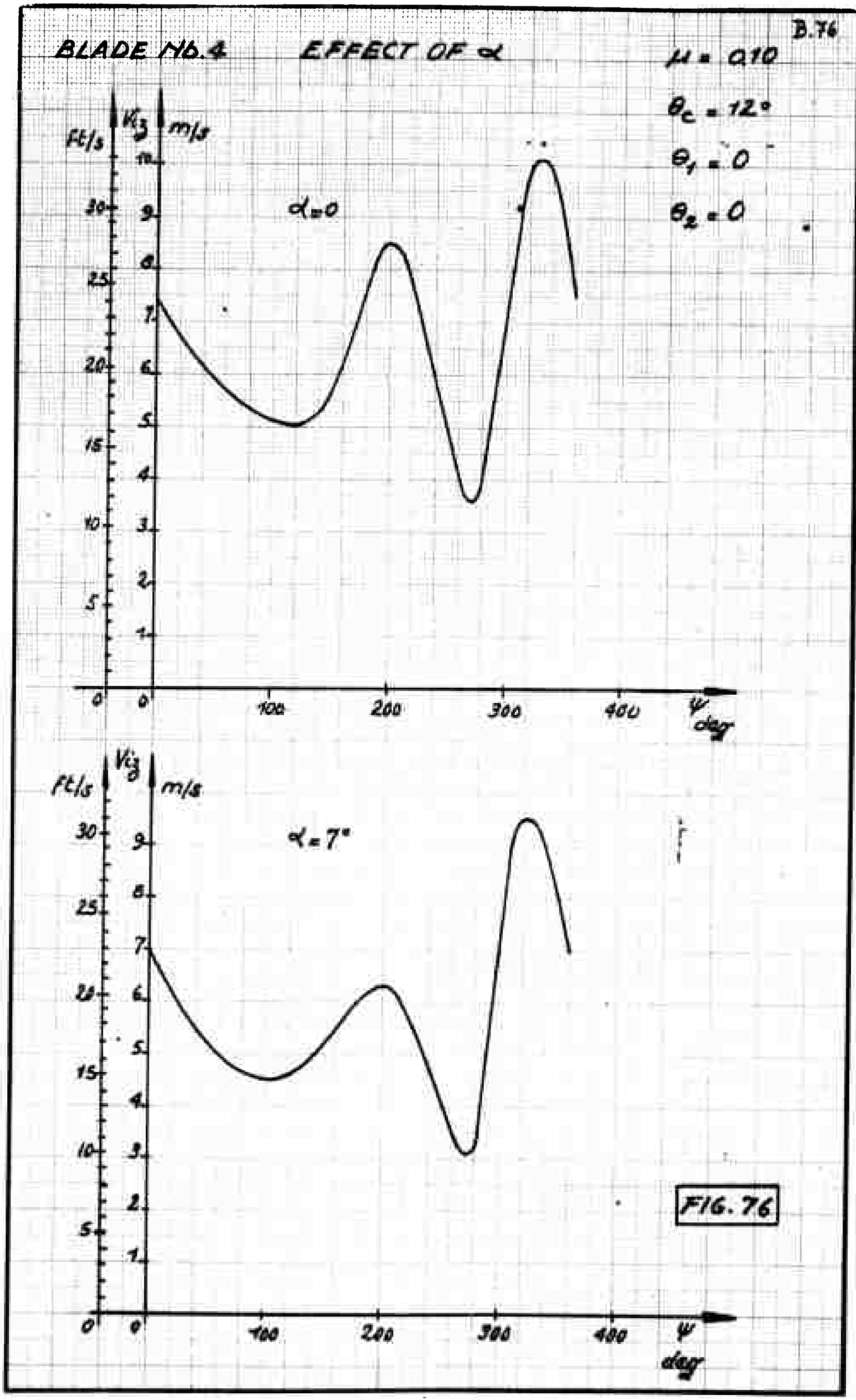
B.76
BLADE No. 4
EFFECT OF α
μ = 0.10
θc = 12°
θ1 = 0
θ2 = 0
ft/s
Viz
m/s
α = 0
α = 7°
ψ
deg
0
100
200
300
400
5
10
15
20
25
30
1
2
3
4
5
6
7
8
9
10

FIG. 76

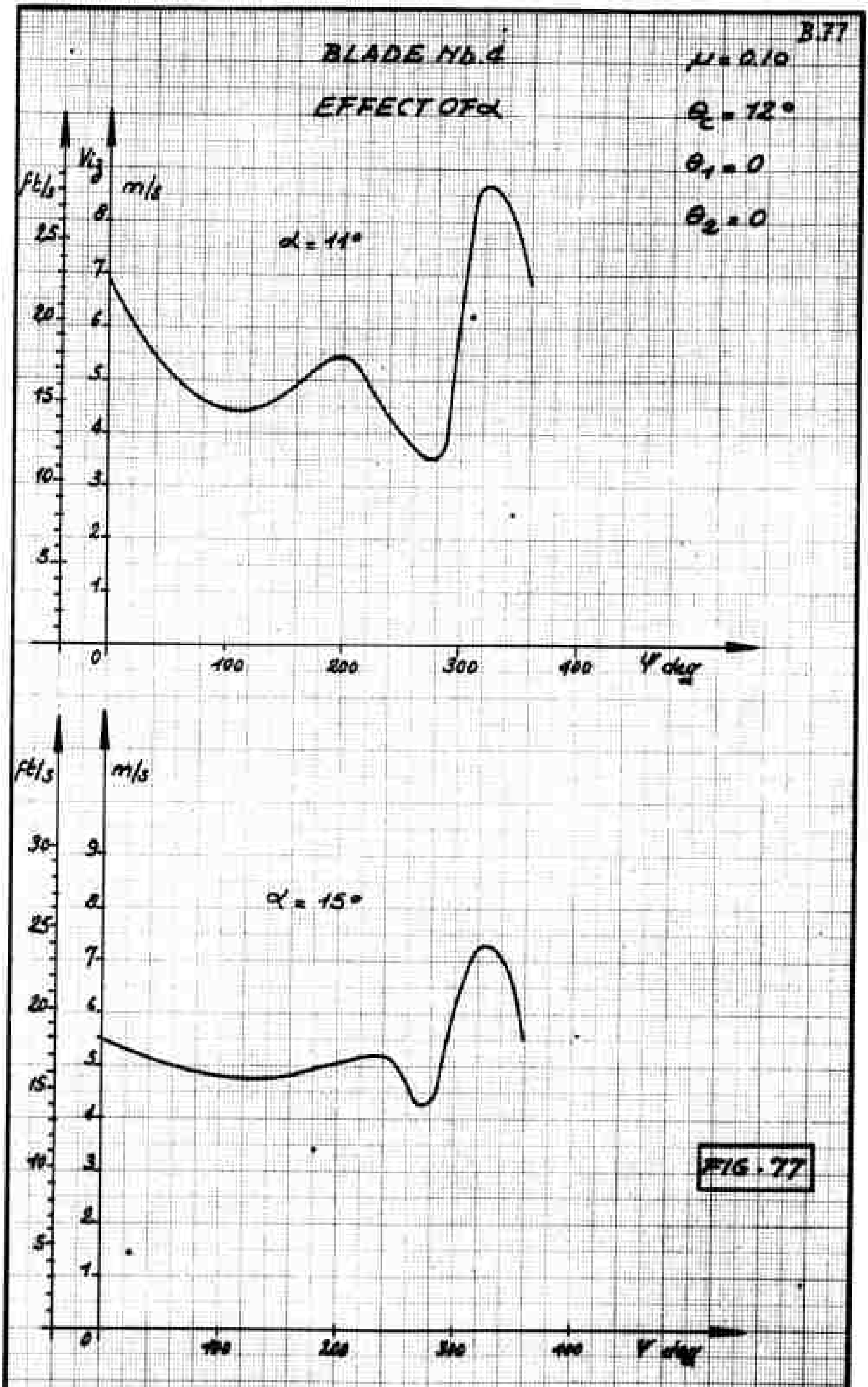
BLADE Nb.4
EFFECT OF α
μ = 0.10
θc = 12°
θ1 = 0
θ2 = 0
ft/s
m/s
α = 11°
α = 15°
0
100
200
300
400
Ψ deg

FIG. 77

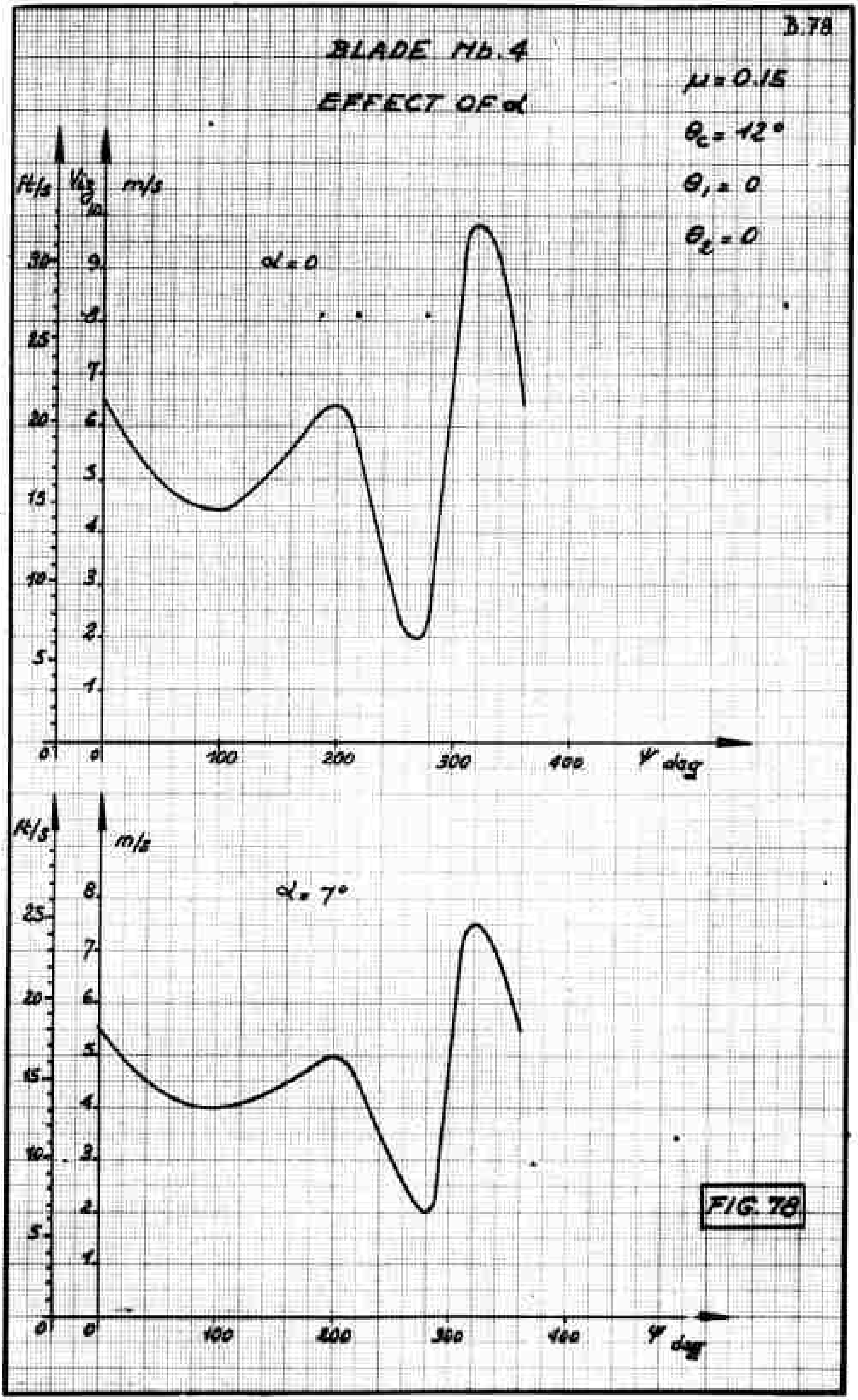
BLADE Nb.4
EFFECT OF α
μ = 0.15
θ_c = 12°
θ_1 = 0
θ_2 = 0
ft/s
m/s
α = 0
ψ deg
α = 7°

FIG. 78

BLADE Nb4

EFFECT OF α

$\mu = 0.15$

$\theta_c = 12°$

$\theta_1 = 0$

$\theta_2 = 0$

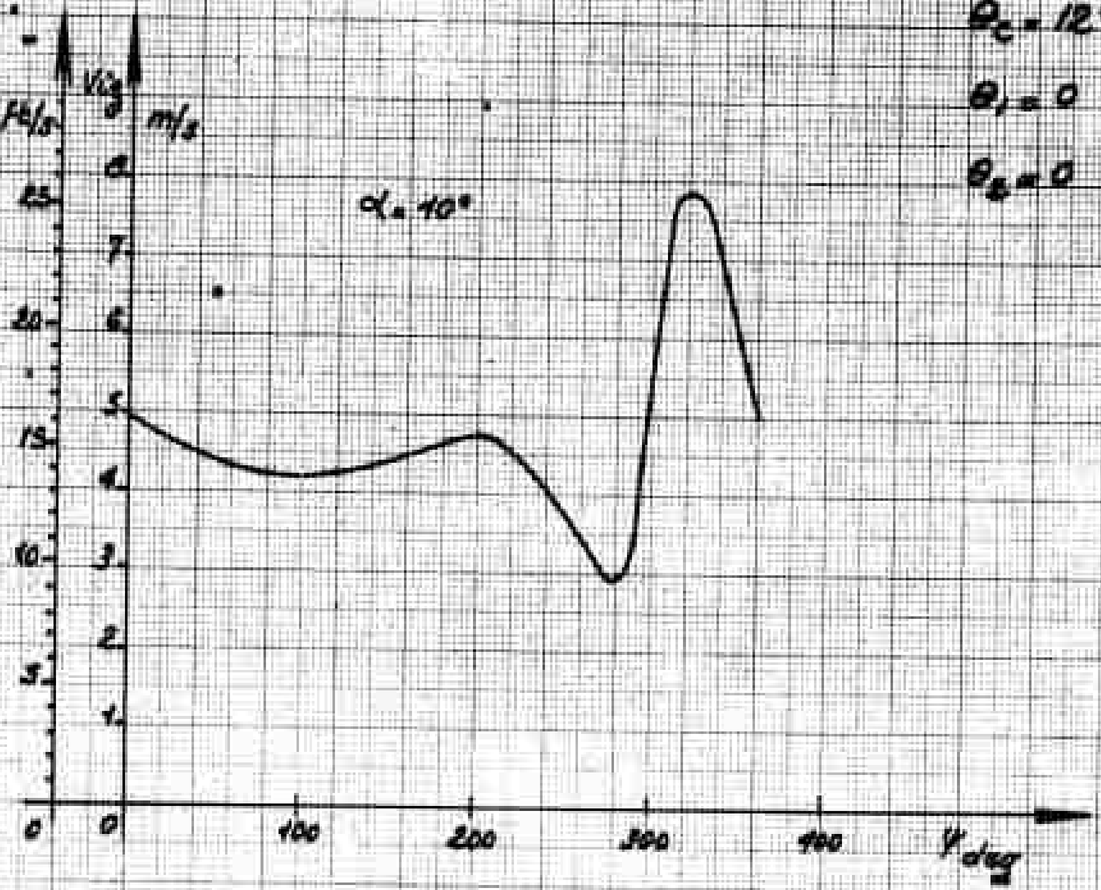

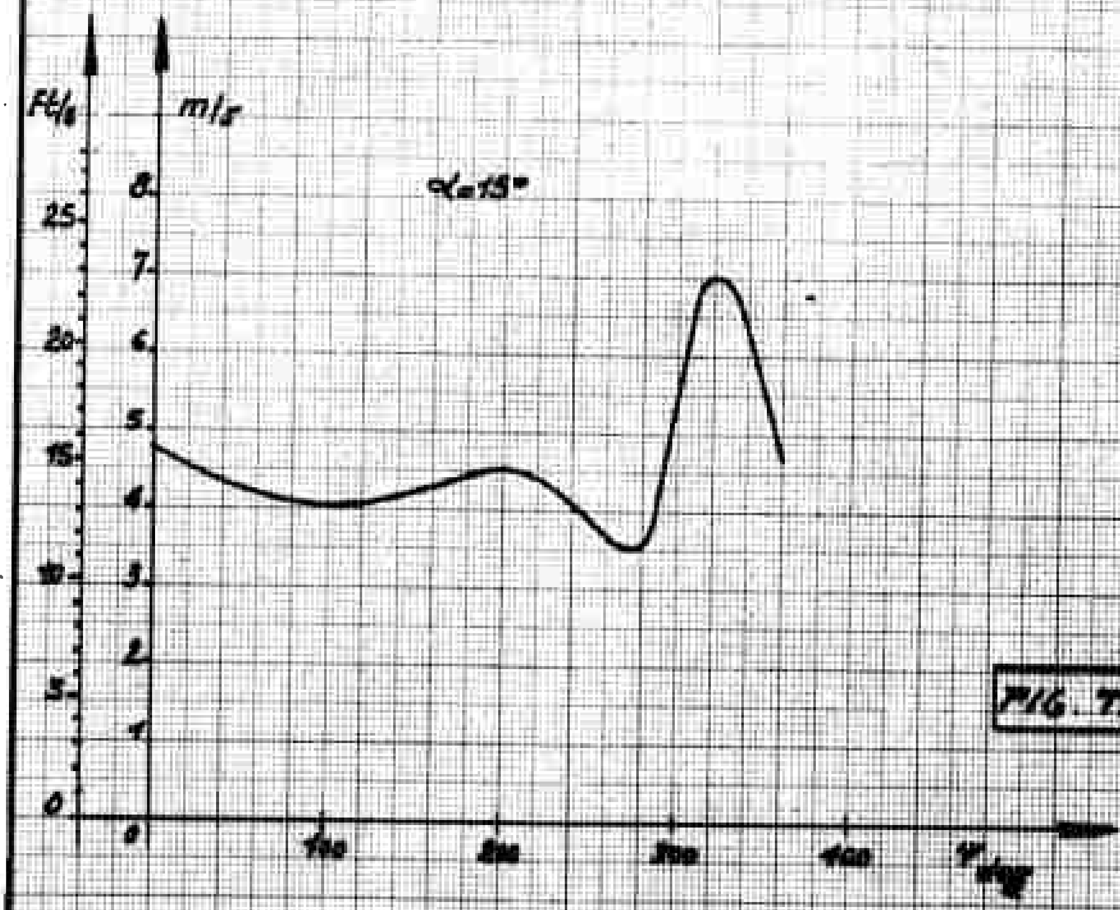

FIG. 79

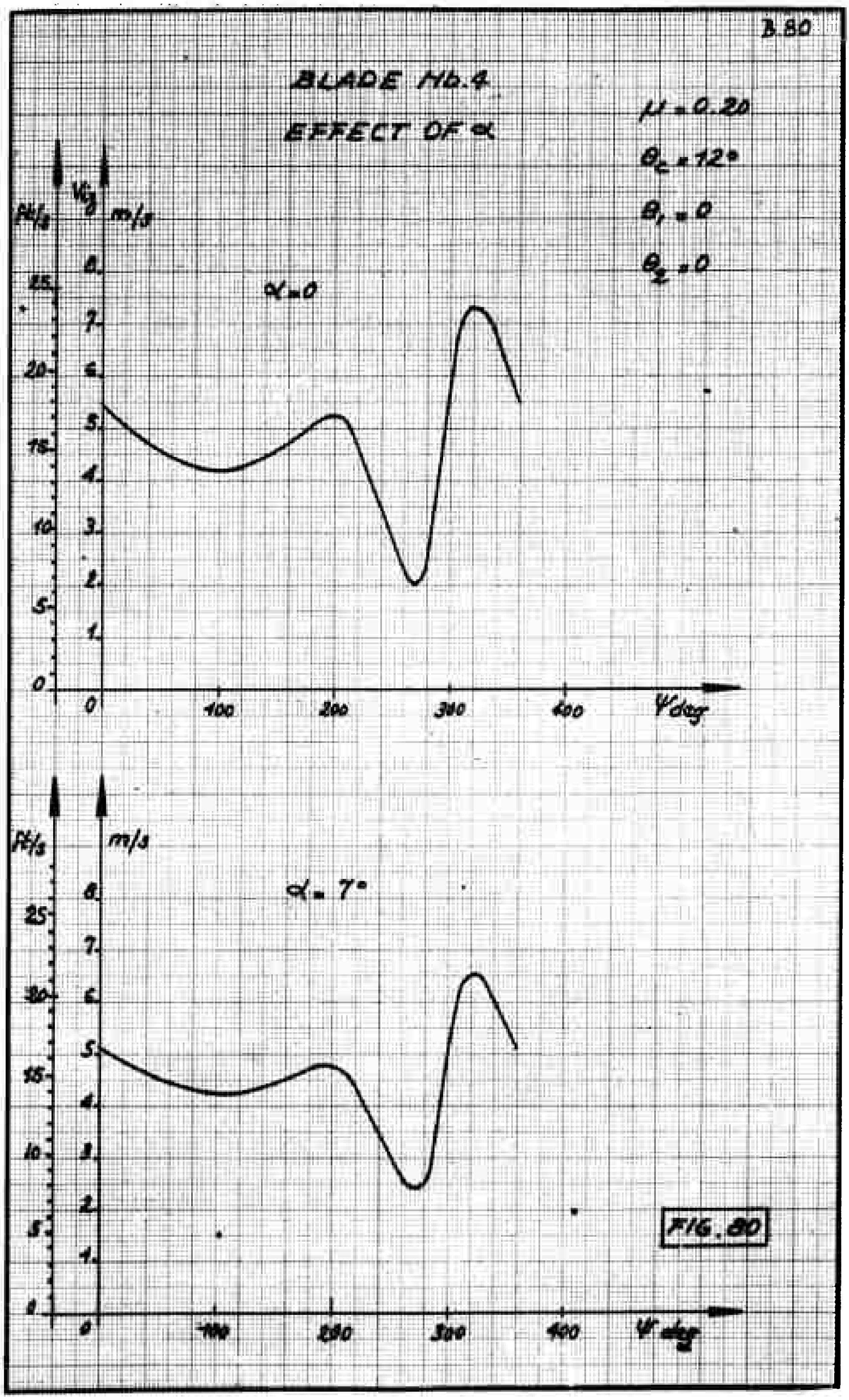

BLADE No.4
EFFECT OF α
μ = 0.20
θc = 12°
θ1 = 0
θ2 = 0
α = 0
ft/s
m/s
0
100
200
300
400
ψ deg
α = 7°

FIG. 80

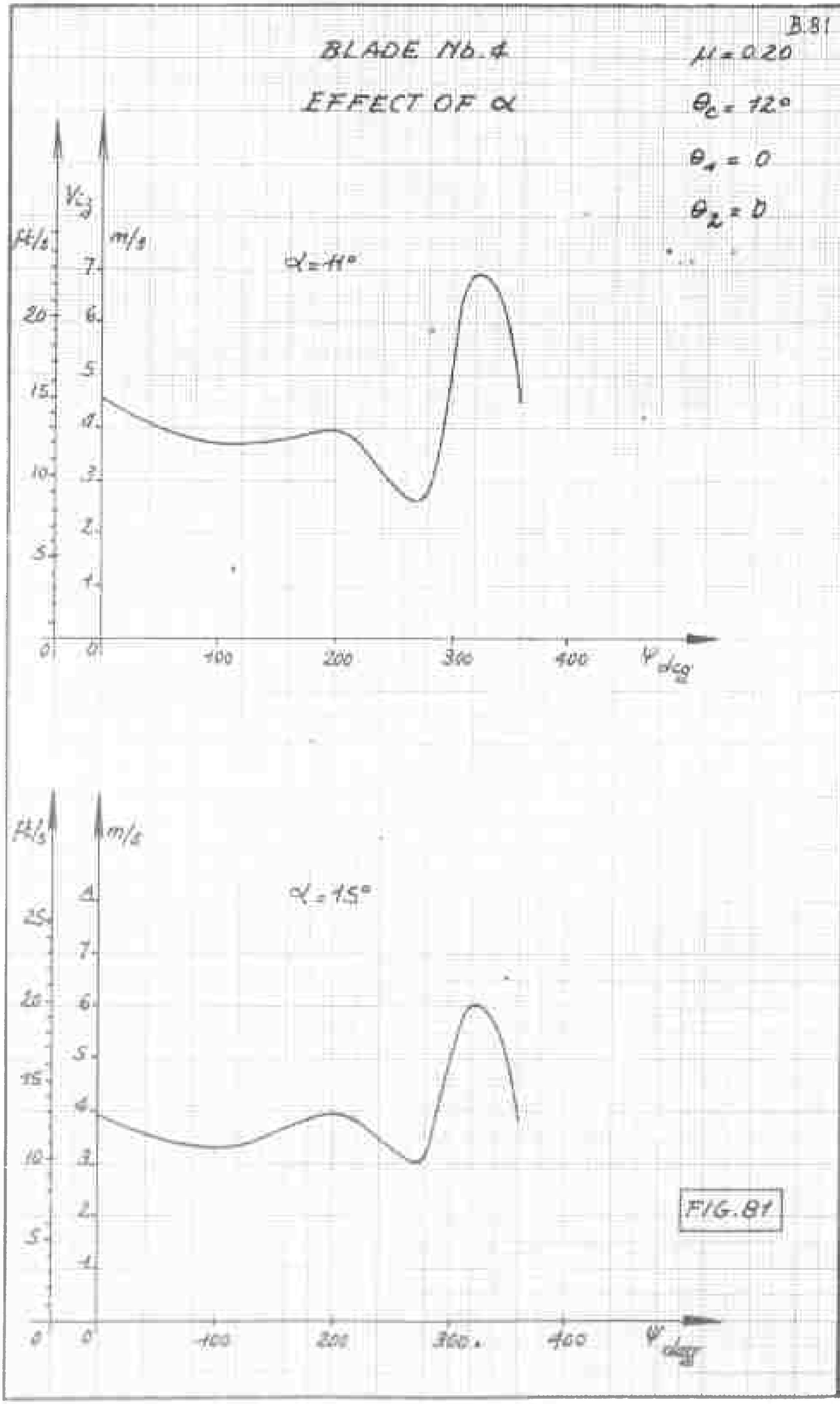
B.81
BLADE No. 4
EFFECT OF α
μ = 0.20
θc = 12°
θ1 = 0
θ2 = 0
ft/s
m/s
α = 11°
α = 15°
0 100 200 300 400
ψ deg

FIG. 81

BLADE No. 4

EFFECT OF θ_2

$\mu = 0.05$

$\theta_c = 6°$

$\alpha = 3°$

$\theta_1 = 0$

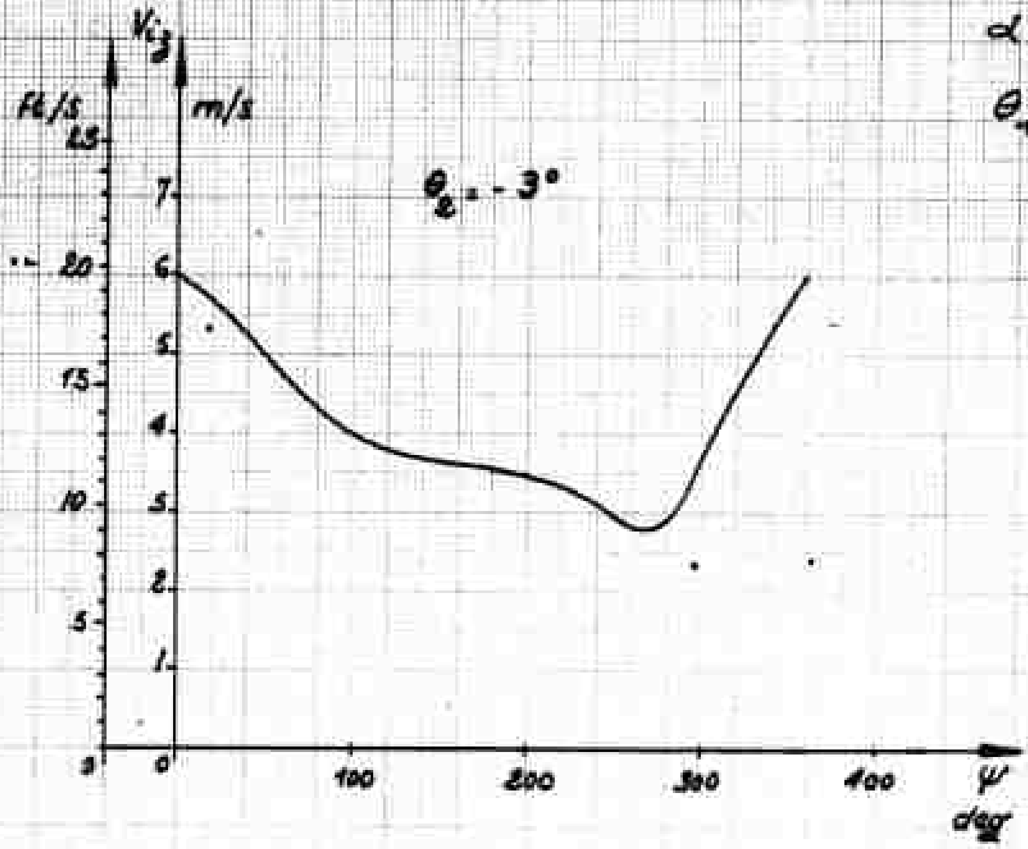

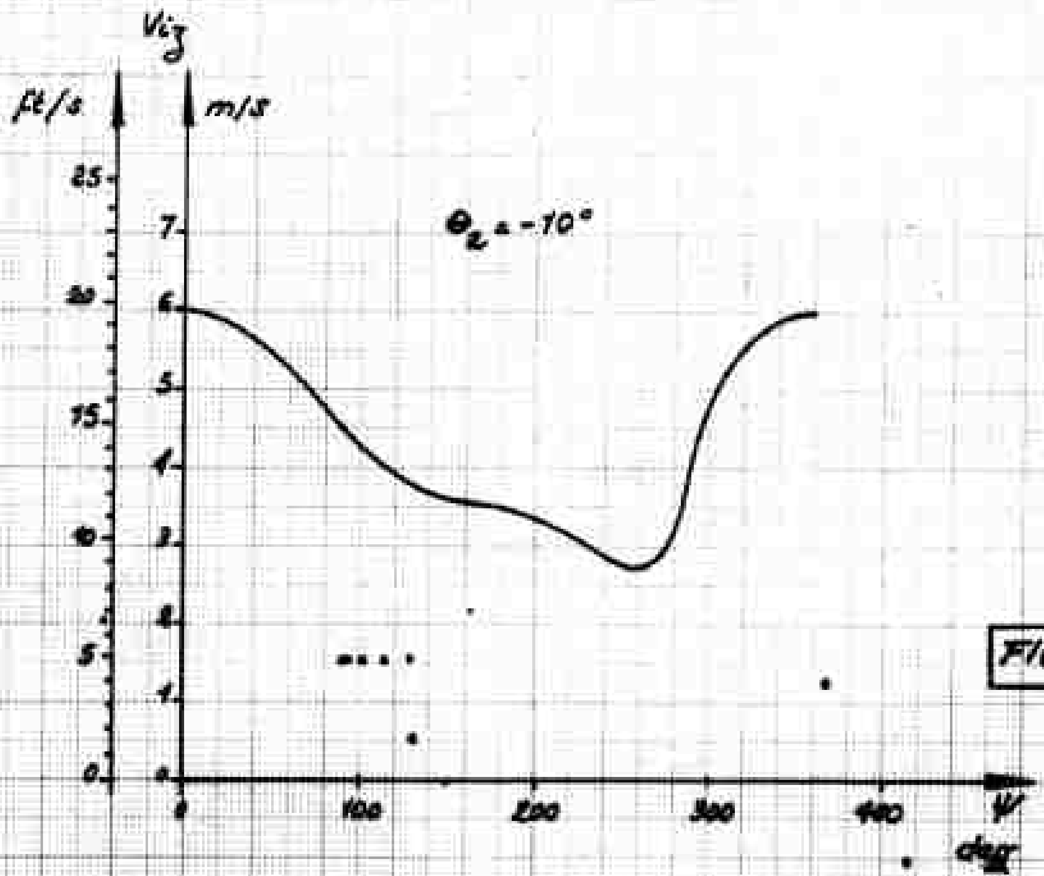

FIG. 82

BLADE No 4   EFFECT OF θ_2

$\mu = 0.10$

$\theta_c = 6°$

$\alpha = 3°$

$\theta_1 = 0$

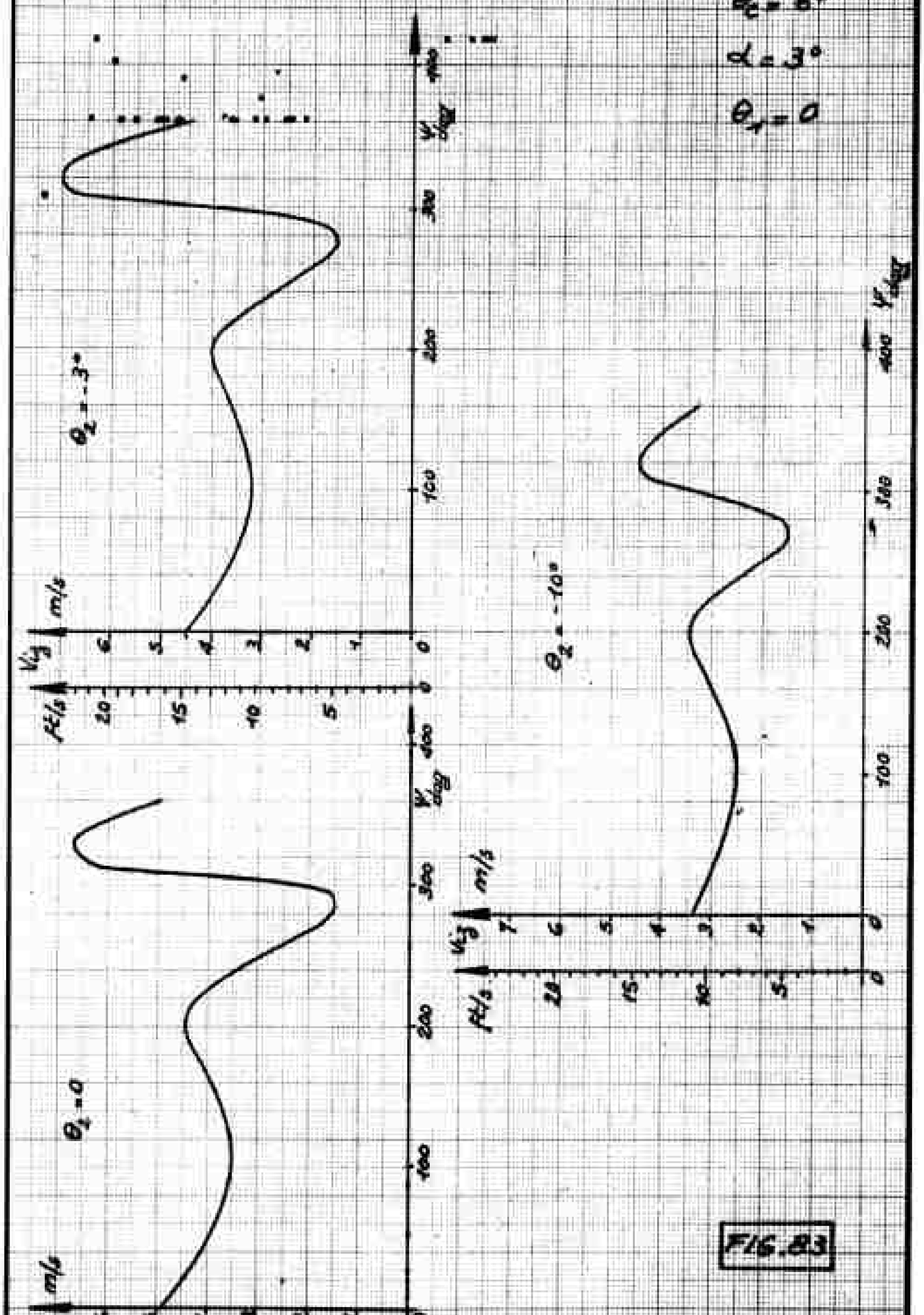

FIG. 83

BLADE No 4 EFFECT OF θ_2

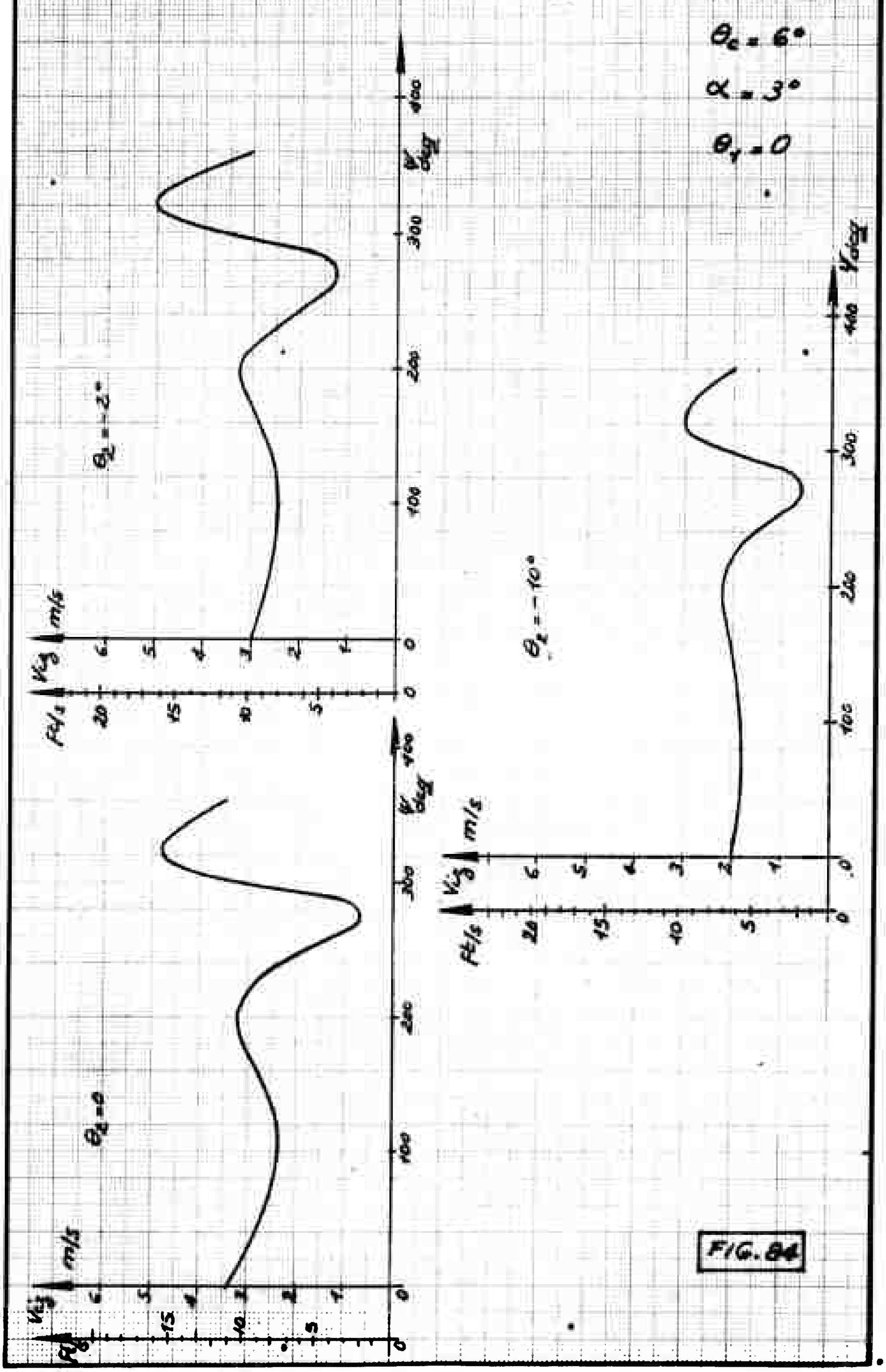

FIG. 84

BLADE No.4 EFFECT OF θ_2

$\mu = 0.20$

$\theta_c = 6°$

$\alpha = 3°$

$\theta_1 = 0$

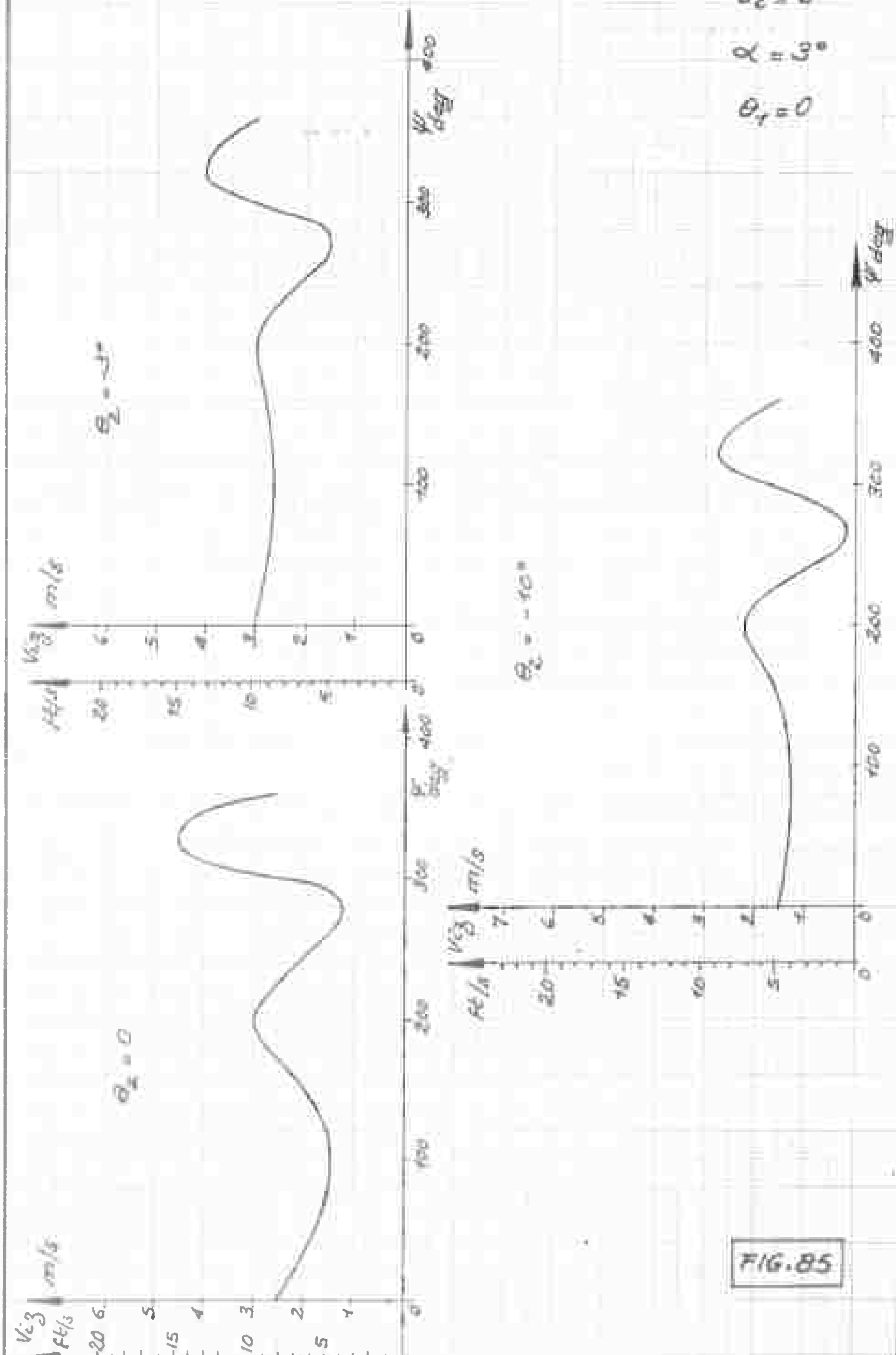

FIG. 85

BLADE Nb 4   EFFECT OF θ_1 AT LOW SPEED

$\mu = 0.05$ $\alpha = 3°$

$\theta_c = 6°$ $\theta_2 = 0$

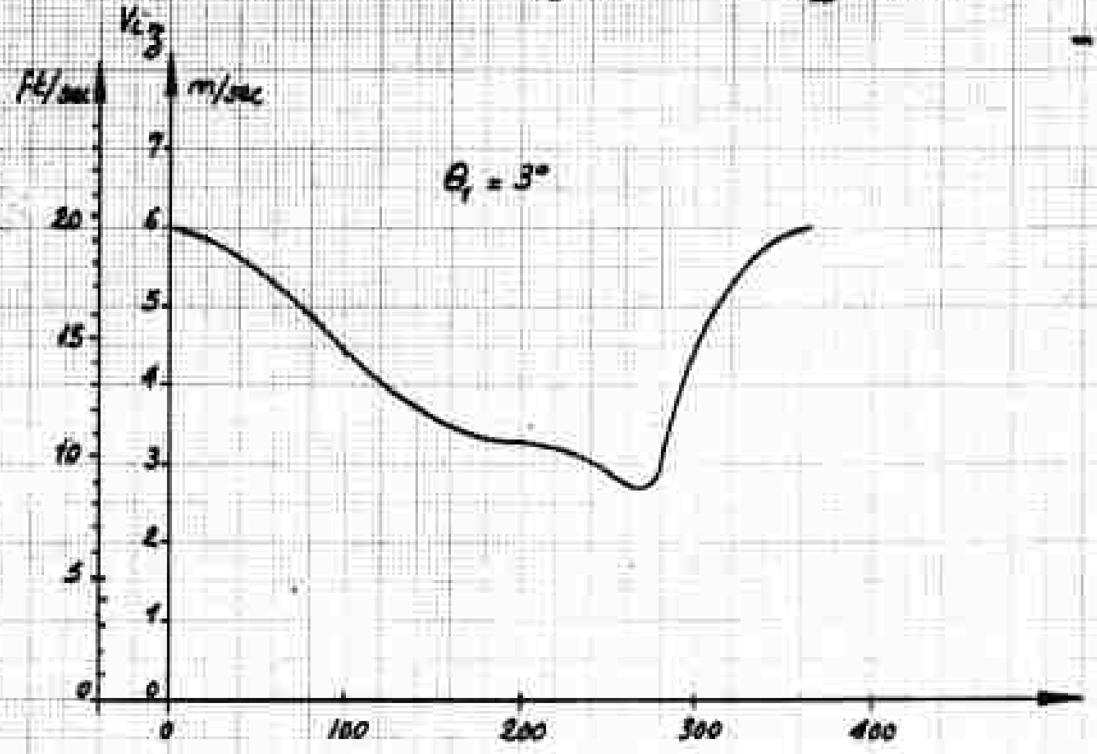

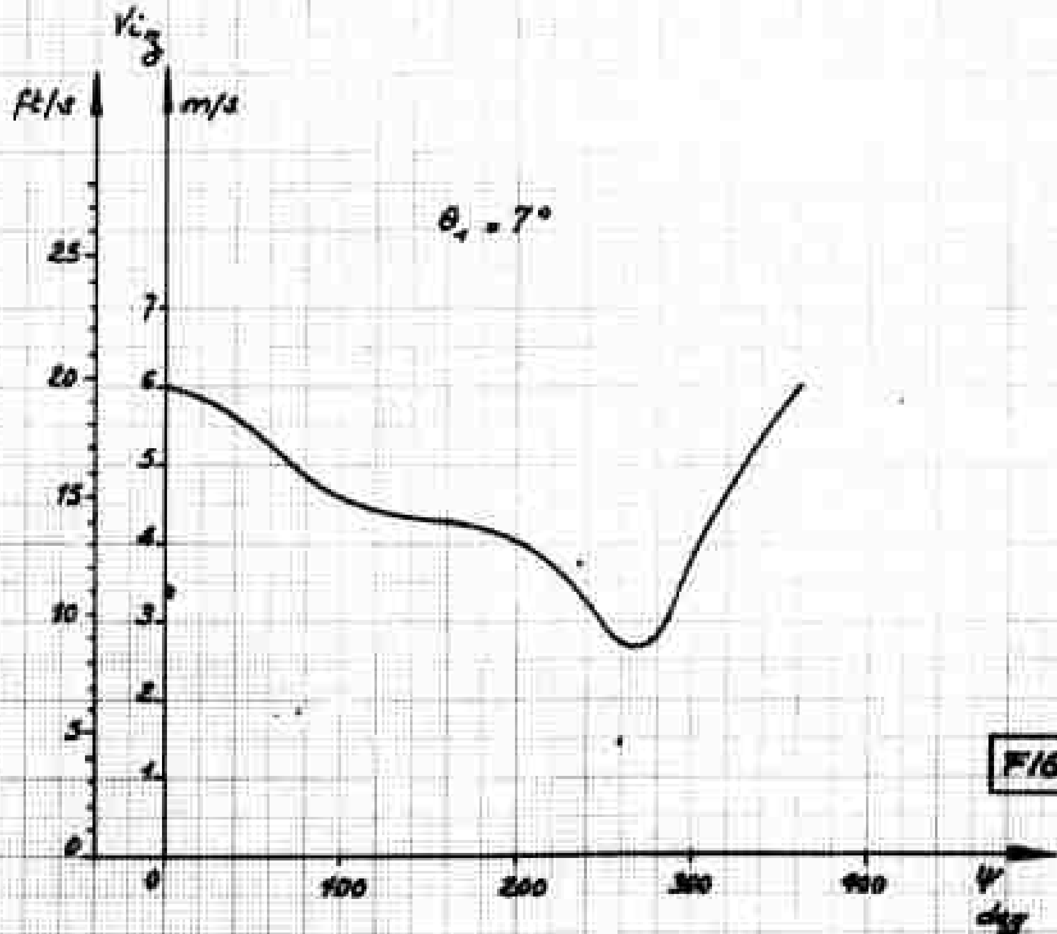

FIG. 86

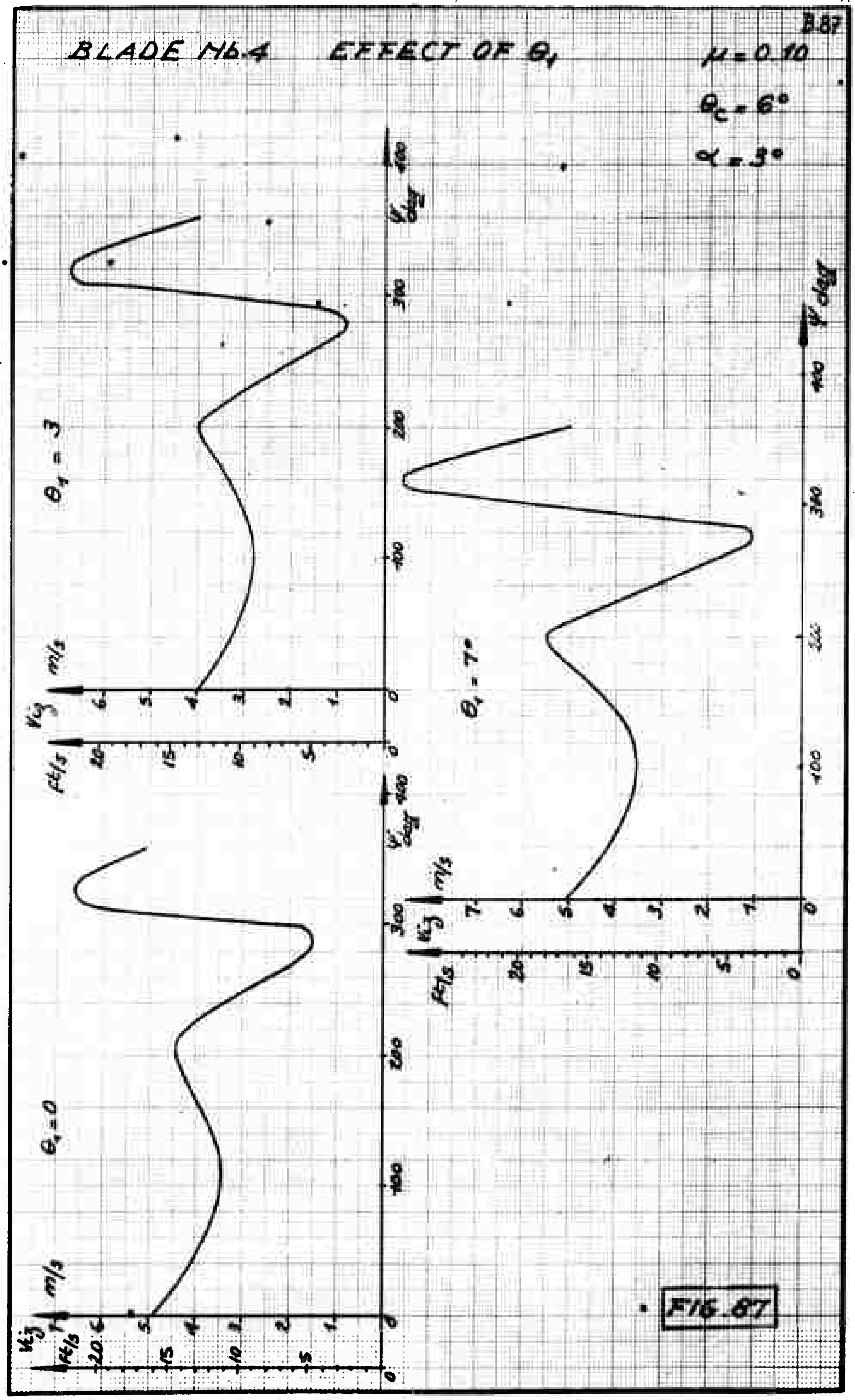
B.87
BLADE No.4 EFFECT OF θ_1
$\mu = 0.10$
$\theta_c = 6°$
$\alpha = 3°$
$\theta_1 = 0$
$\theta_1 = 3$
$\theta_1 = 7°$
V_{ij}
m/s
ft/s
ψ deg
FIG. 87

BLADE No.4 EFFECT OF θ_1 $\mu = 0.15$

$\theta_c = 6°$

$\alpha = 3°$

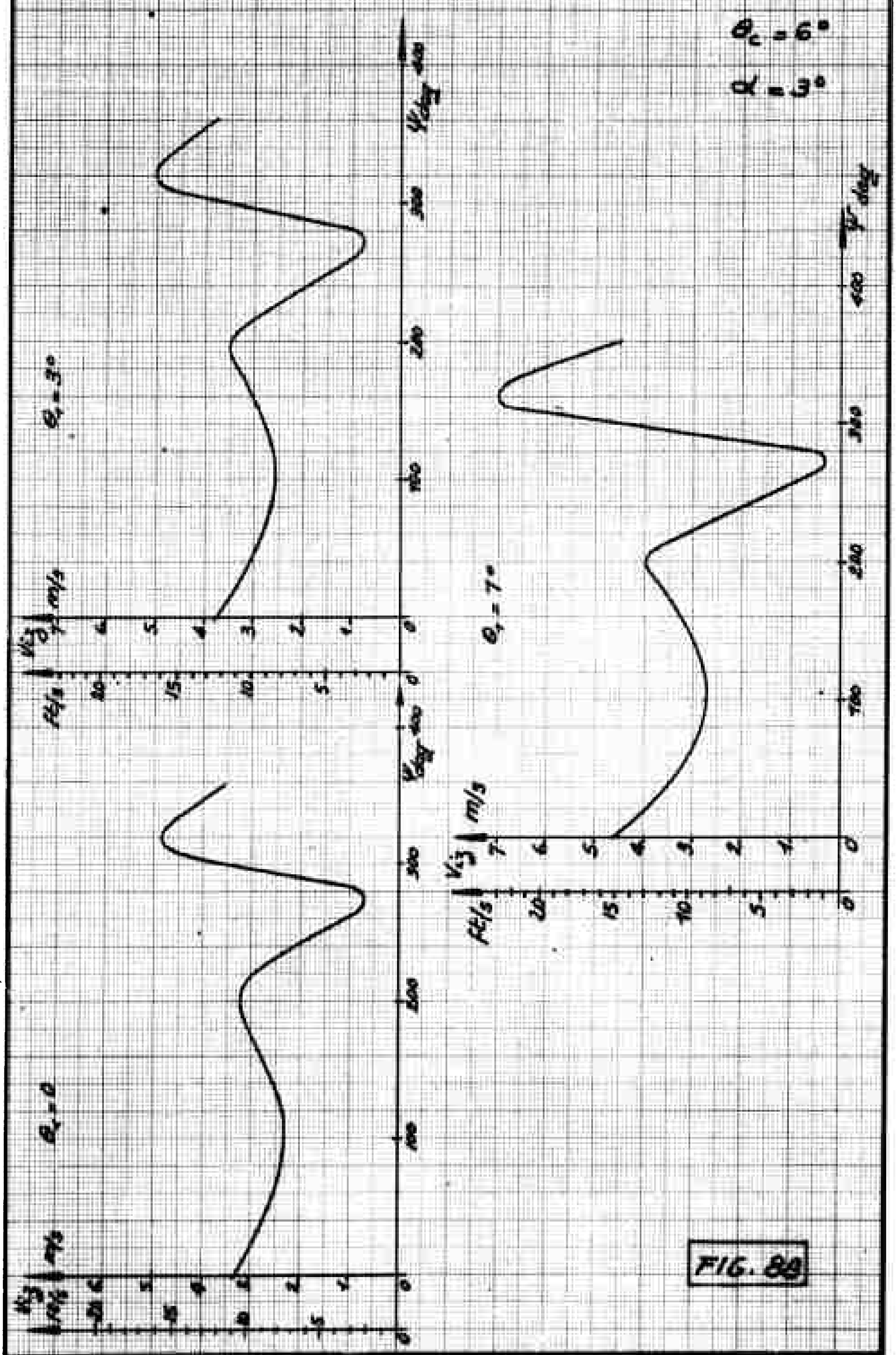

FIG. 88

BLADE No. 4 EFFECT OF θ_1 $\mu = 0.20$

$\alpha = 3°$

$\theta_2 = 0$

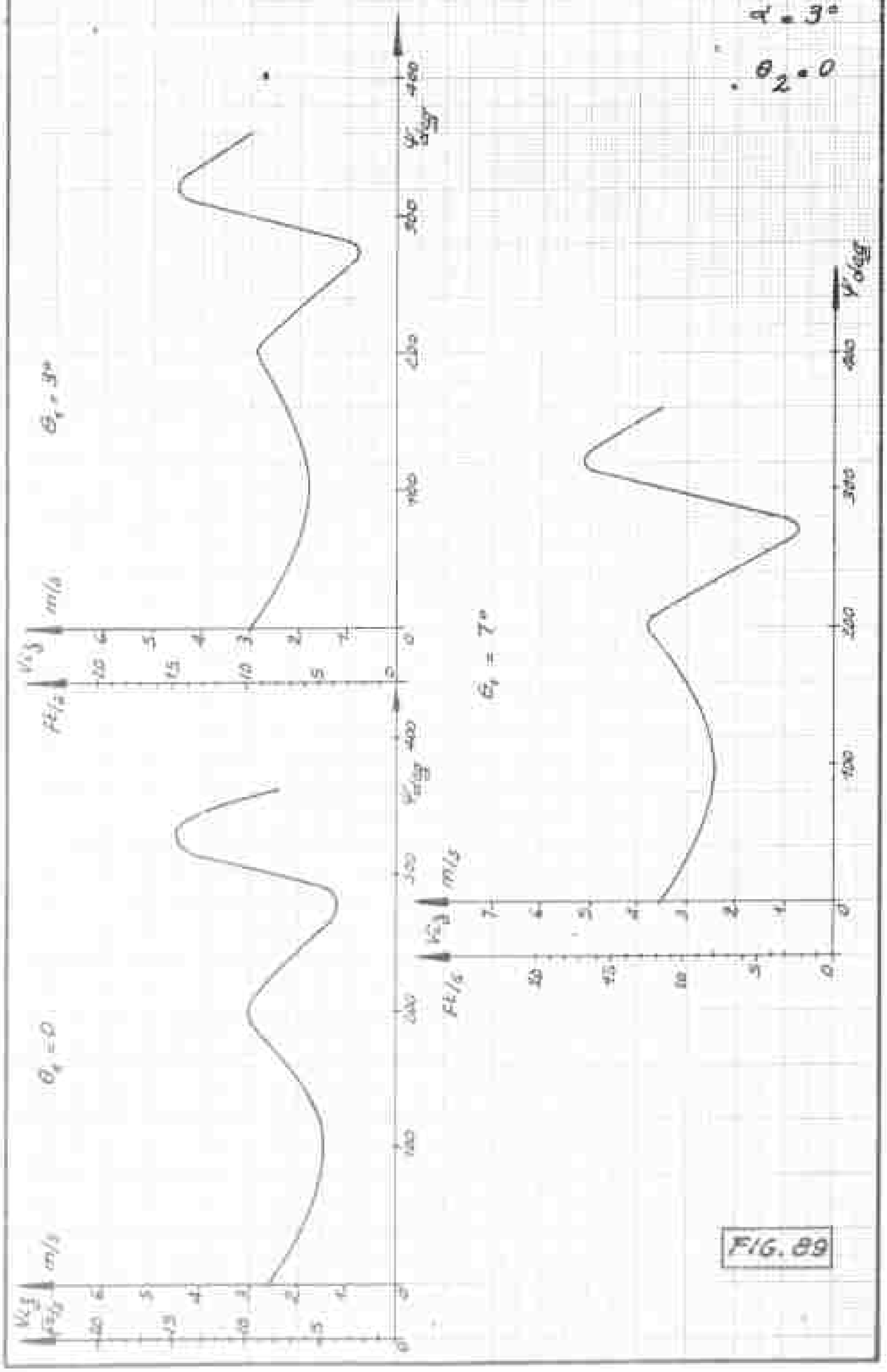

FIG. 89

EFFECT OF SOLIDITY σ AT LOW SPEED

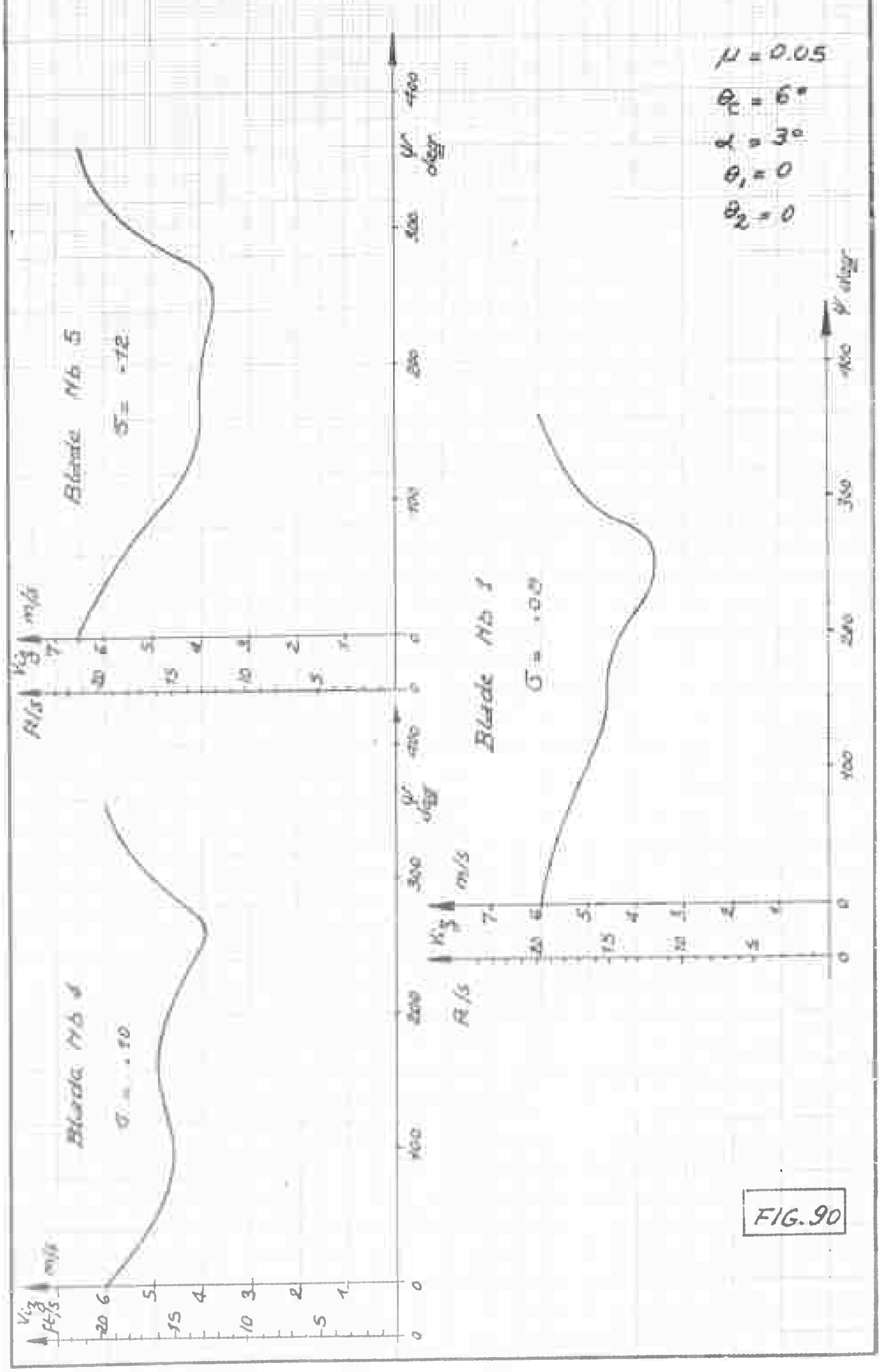

FIG. 90

EFFECT OF SOLIDITY σ

$\mu = 0.10$

$\theta_c = 6°$

$\alpha = 3°$

$\theta_1 = 0$

$\theta_2 = 0$

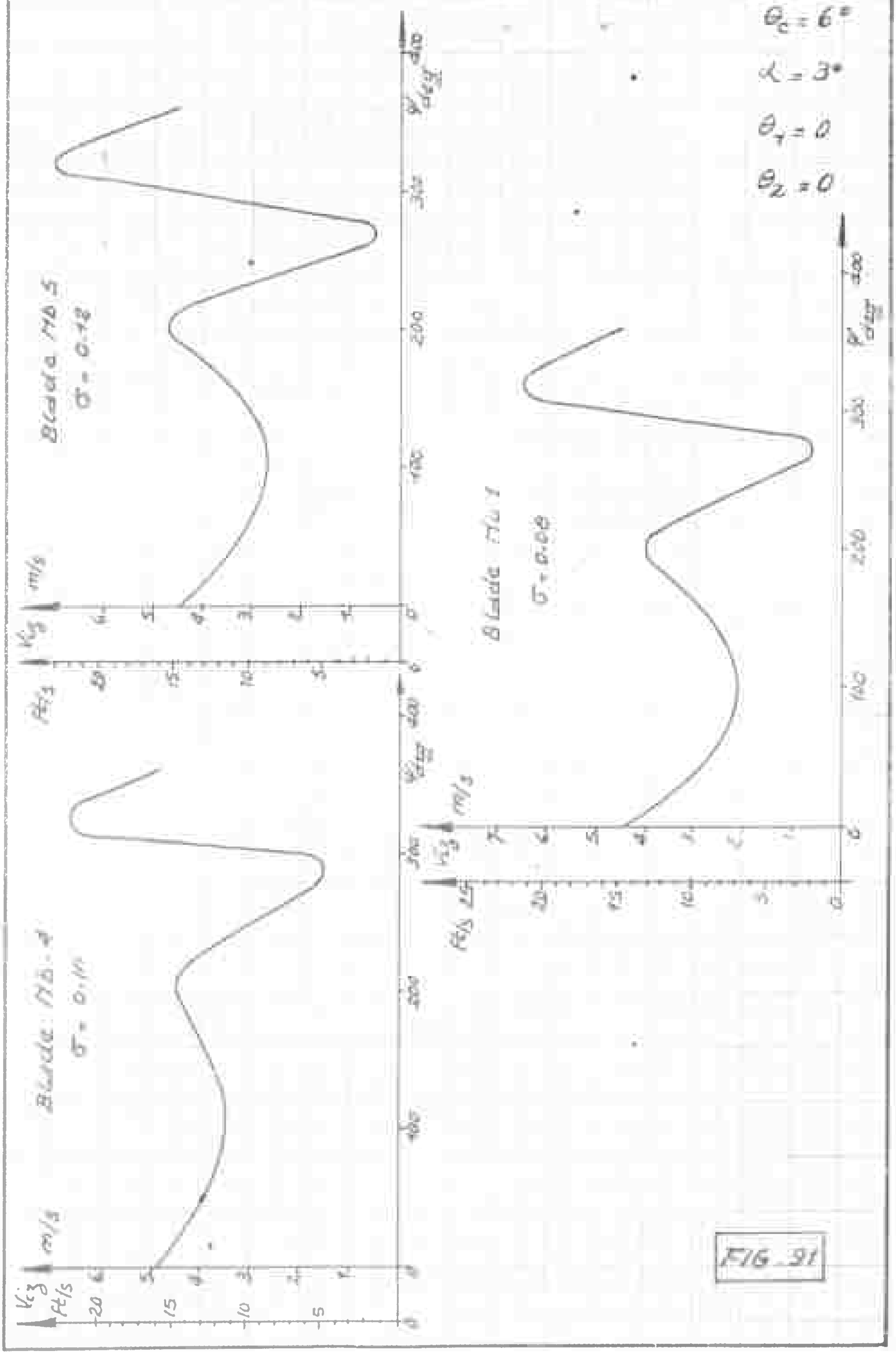

FIG. 91

EFFECT OF SOLIDITY σ

$\mu = 0.15$

$\alpha = 3°$

$\theta_1 = 0$

$\theta_2 = 0$

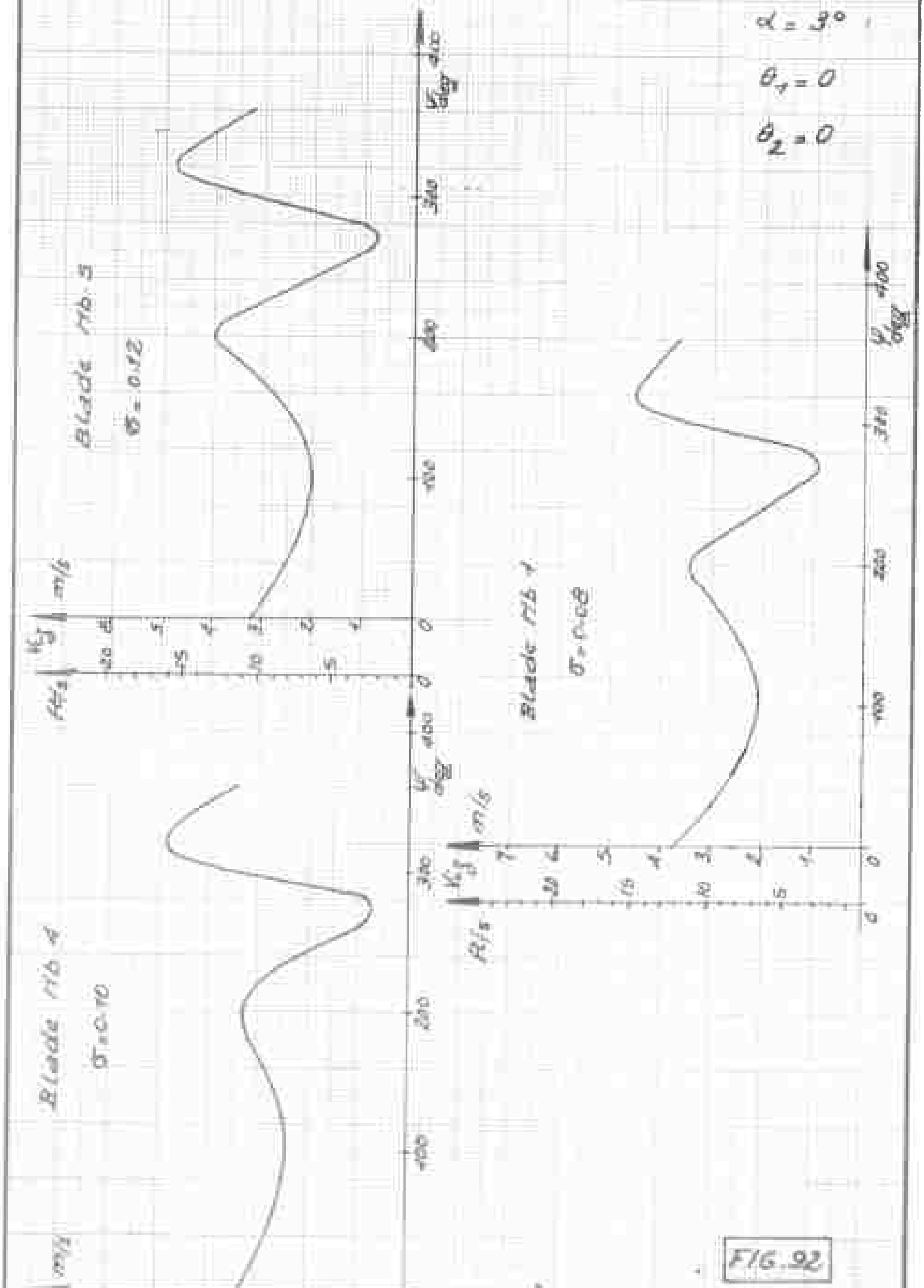

FIG. 92

EFFECT OF SOLIDITY σ

$\mu = 0.20$

$\alpha = 3°$

$\theta_0 = 6°$

$\theta_1 = 0$

$\theta_2 = 0$

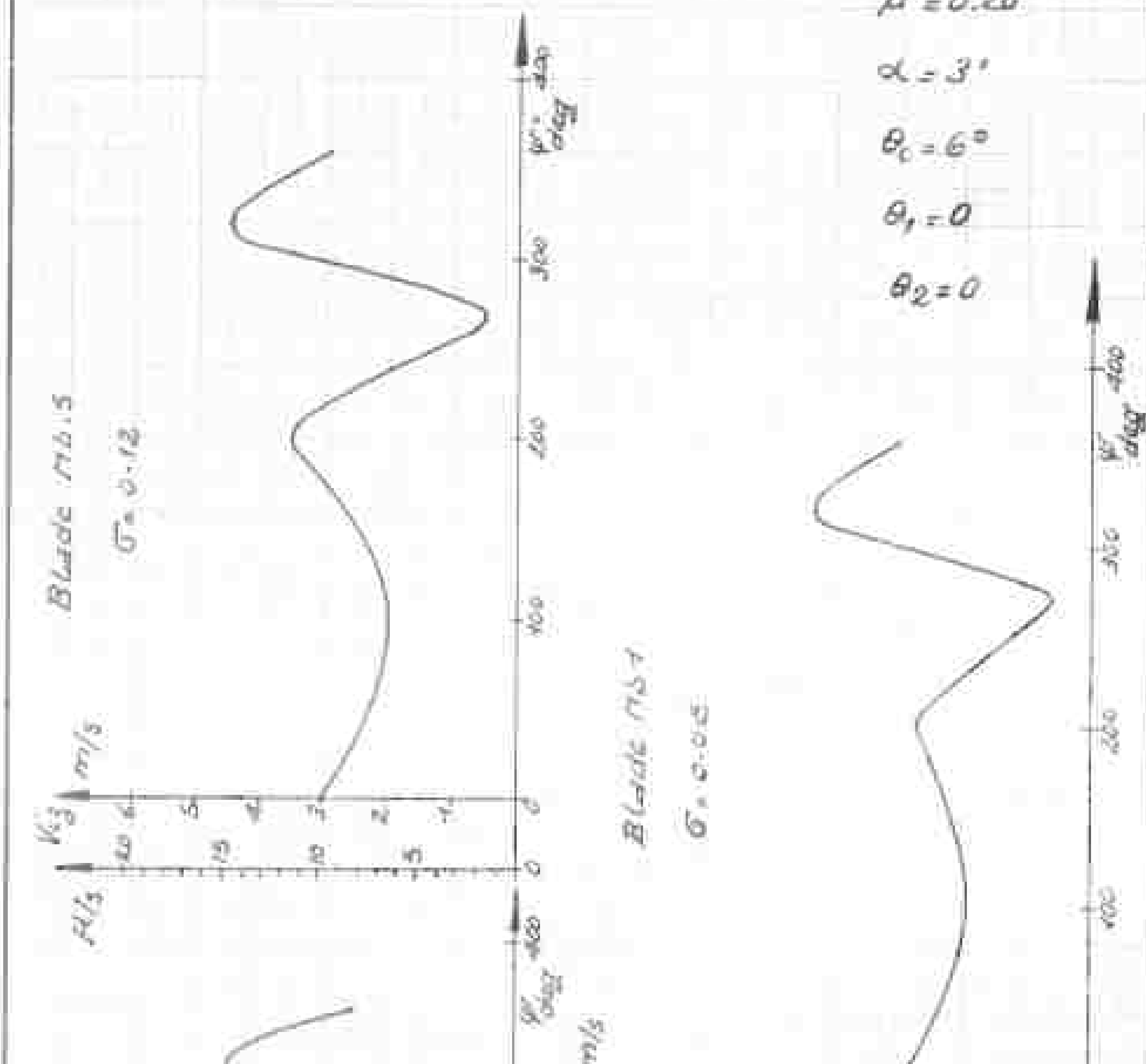

FIG. 93

EFFECT OF THE LOCK NUMBER γ

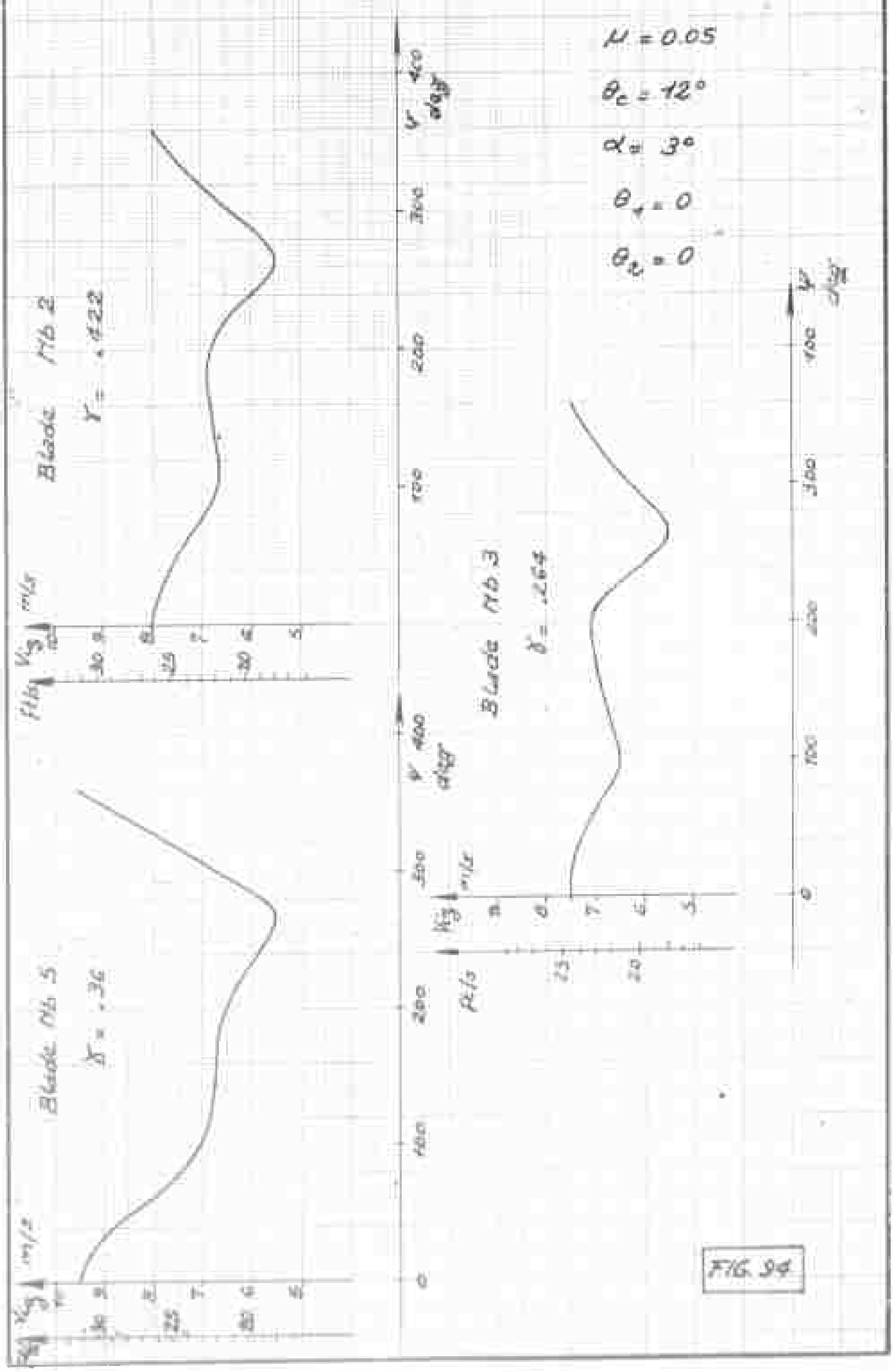

FIG. 94

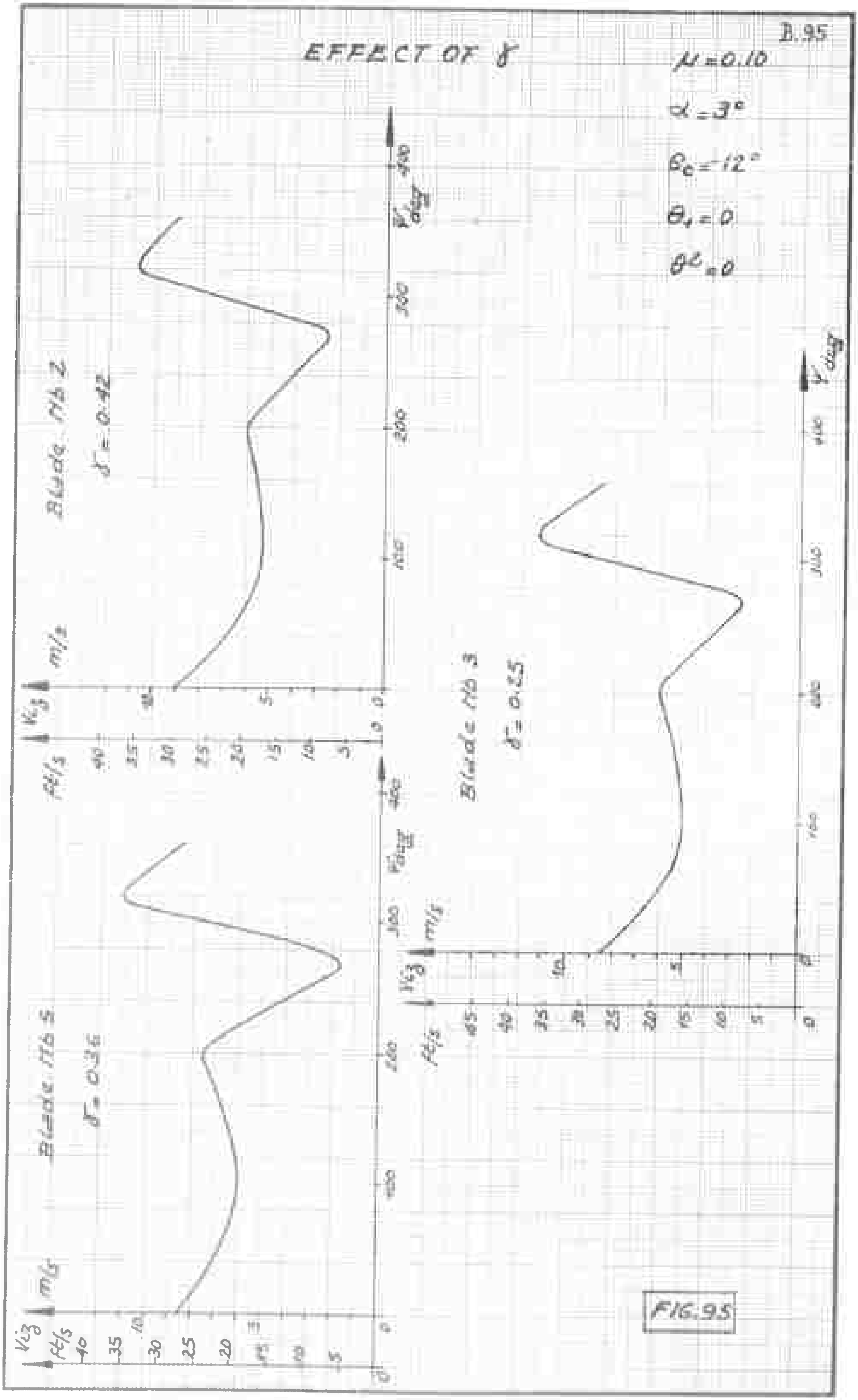
EFFECT OF γ
μ = 0.10
α = 3°
θ0 = 12°
θ1 = 0
θ2 = 0
Blade No 2
γ = 0.42
Blade No 3
γ = 0.55
Blade No 5
γ = 0.36
Vz3
ft/s
m/s
ψ deg

FIG. 95

EFFECT OF γ

$\mu = 0.15$

$\theta_c = 12^\circ$

$\alpha = 3^\circ$

$\theta_1 = 0$

$\theta_2 = 0$

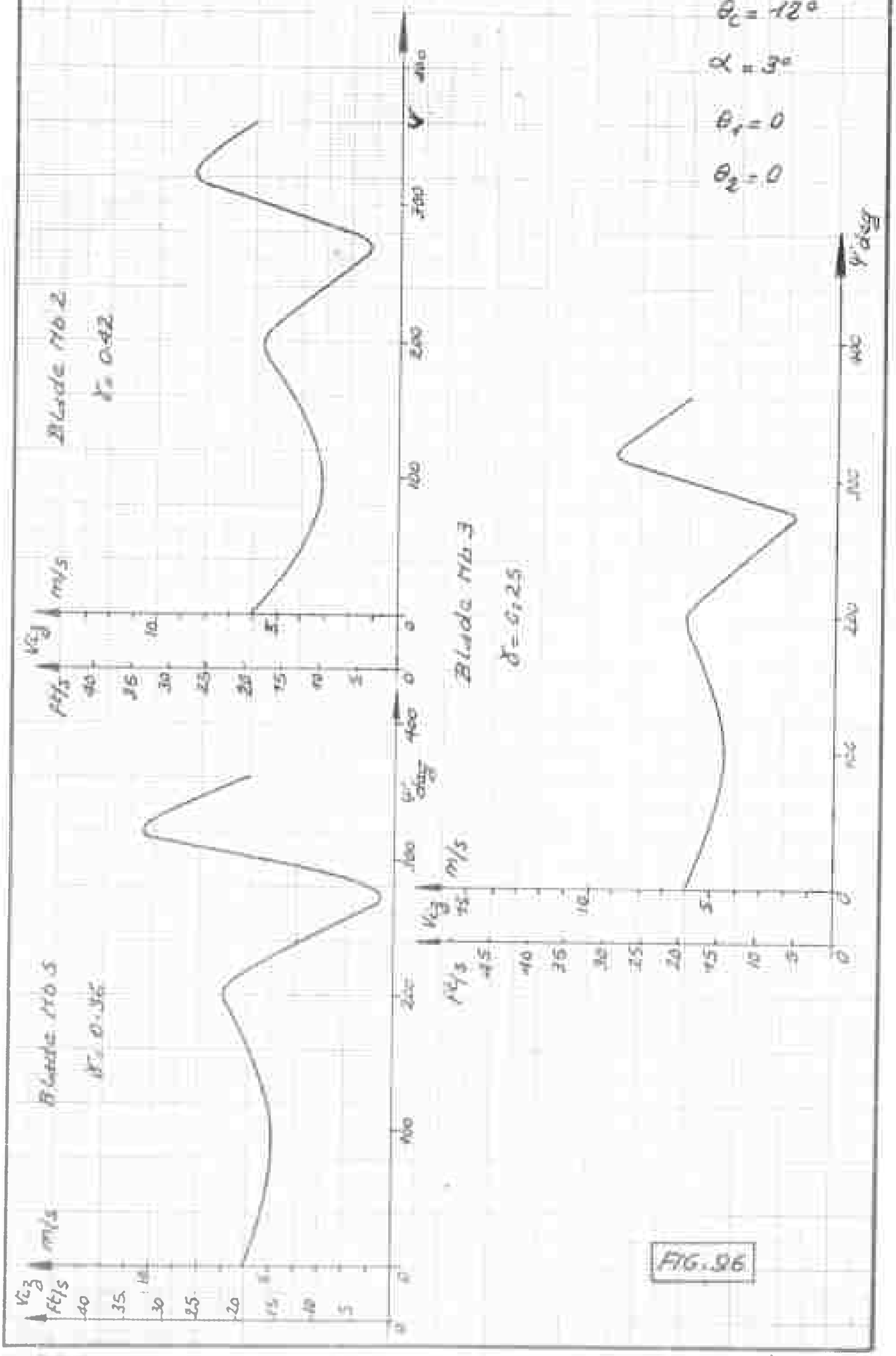

FIG. 96

EFFECT OF γ

$\mu = 0.20$

$\theta_c = 12^\circ$

$\alpha = 3^\circ$

$\theta_1 = 0$

$\theta_2 = 0$

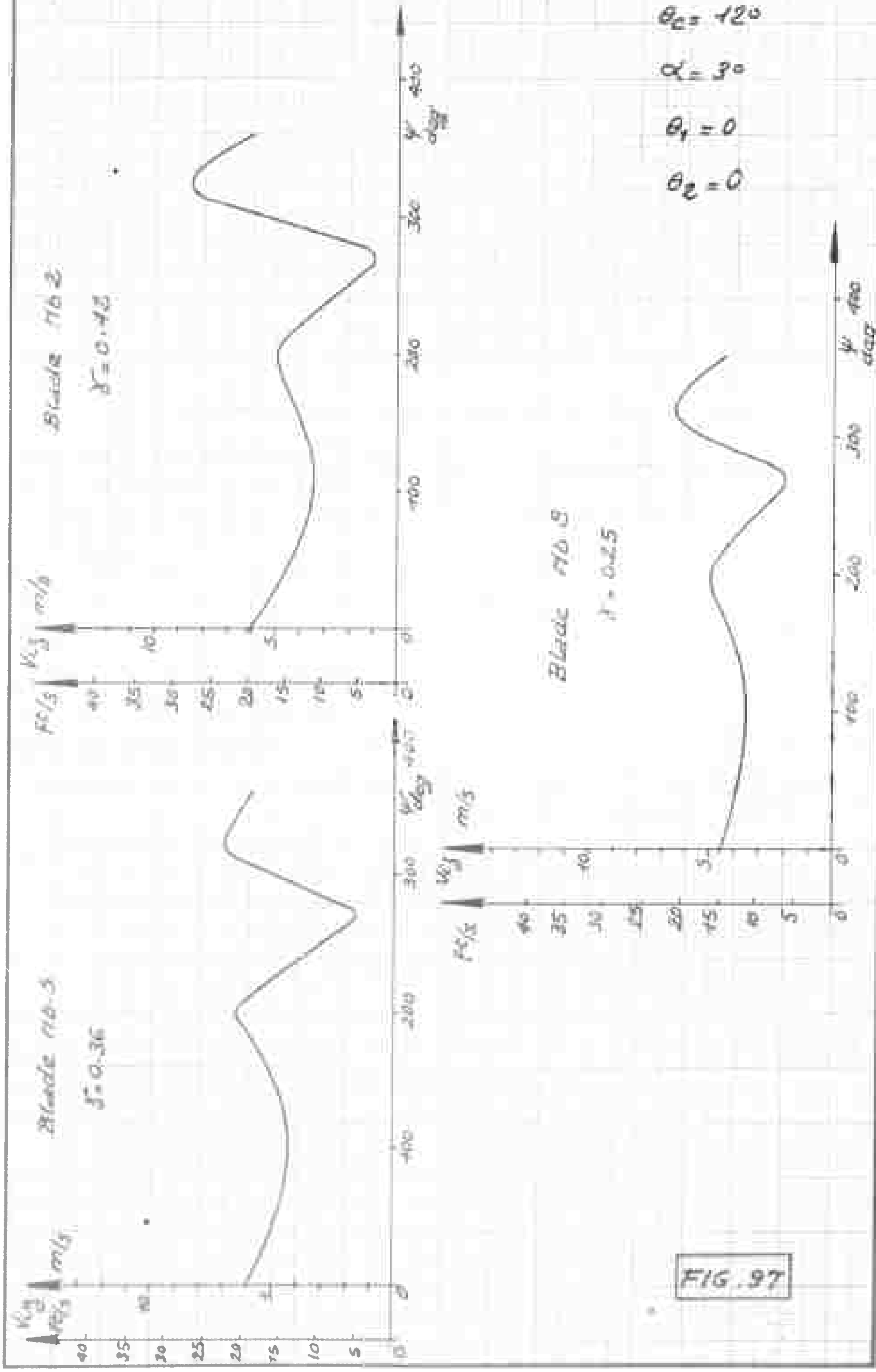

FIG. 97

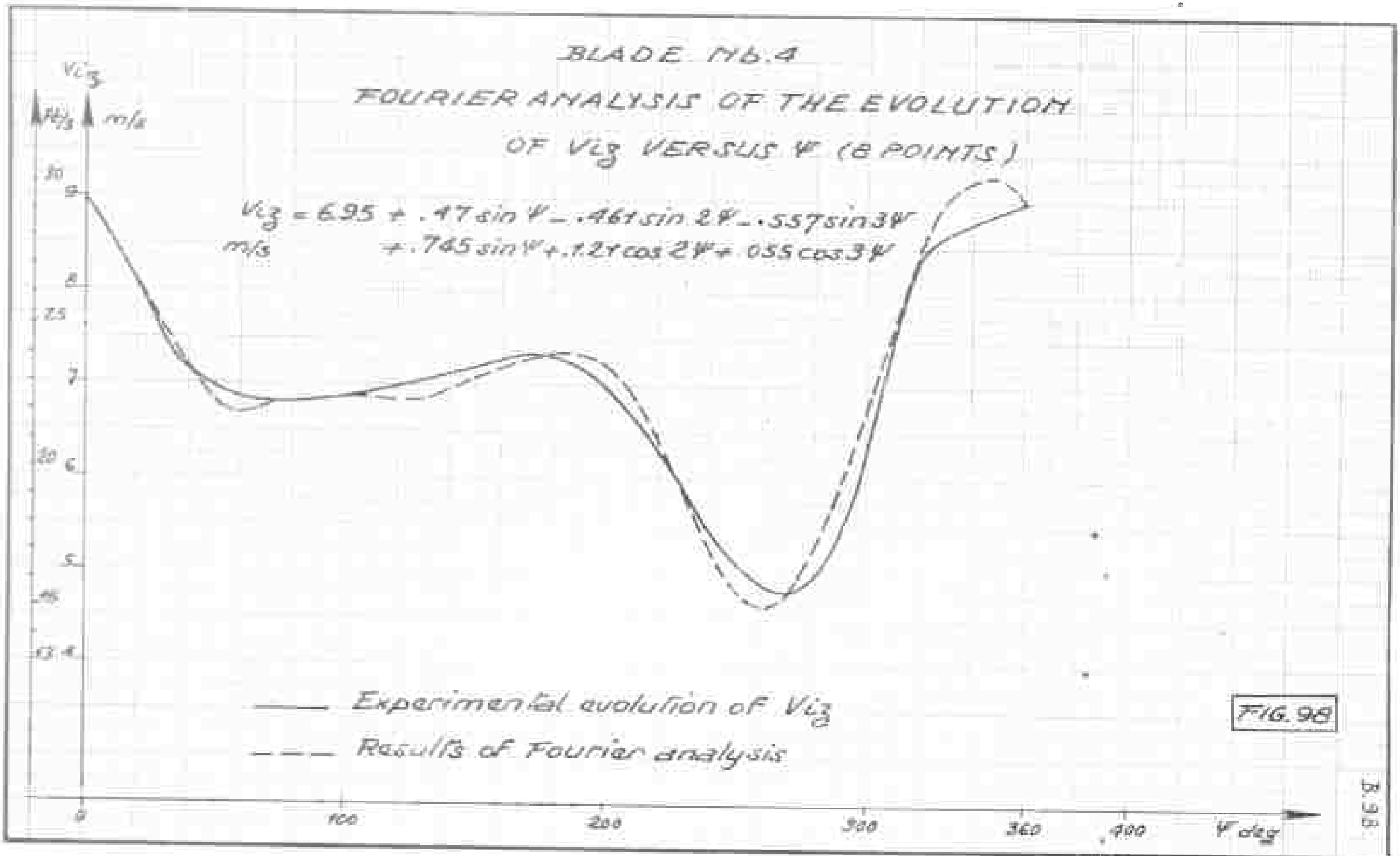
BLADE Nb.4
FOURIER ANALYSIS OF THE EVOLUTION
OF V_{iz} VERSUS Ψ (8 POINTS)
$V_{iz} = 6.95 + .47 \sin\Psi - .461 \sin 2\Psi - .557 \sin 3\Psi$
m/s $+ .745 \sin\Psi + .121 \cos 2\Psi + .055 \cos 3\Psi$
V_{iz}
m/s
9
8
7
6
5
4
30
25
20
15
13
0
100
200
300
360
400
Ψ deg
Experimental evolution of V_{iz}
Results of Fourier analysis

FIG. 98

B.98

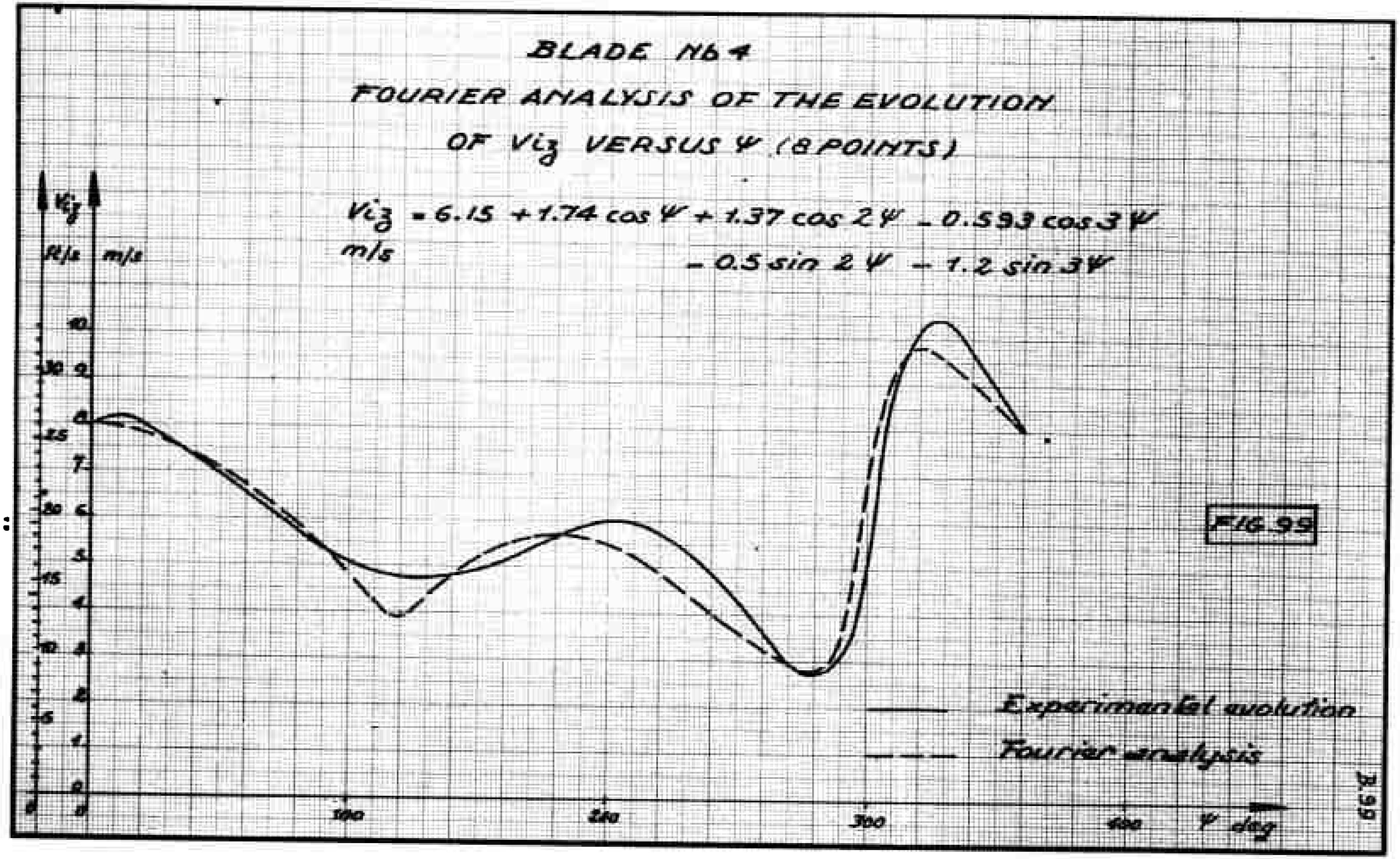
BLADE Nb 4
FOURIER ANALYSIS OF THE EVOLUTION
OF Viz VERSUS Ψ (8 POINTS)
Viz = 6.15 + 1.74 cos Ψ + 1.37 cos 2Ψ − 0.593 cos 3Ψ − 0.5 sin 2Ψ − 1.2 sin 3Ψ
m/s
Viz
ft/s
m/s
Experimental evolution
Fourier analysis
Ψ deg
100
200
300
400

FIG. 99

BLADE Nb. 4

VERTICAL MEAN INDUCED VELOCITY VERSUS μ

EFFECT OF θ_c

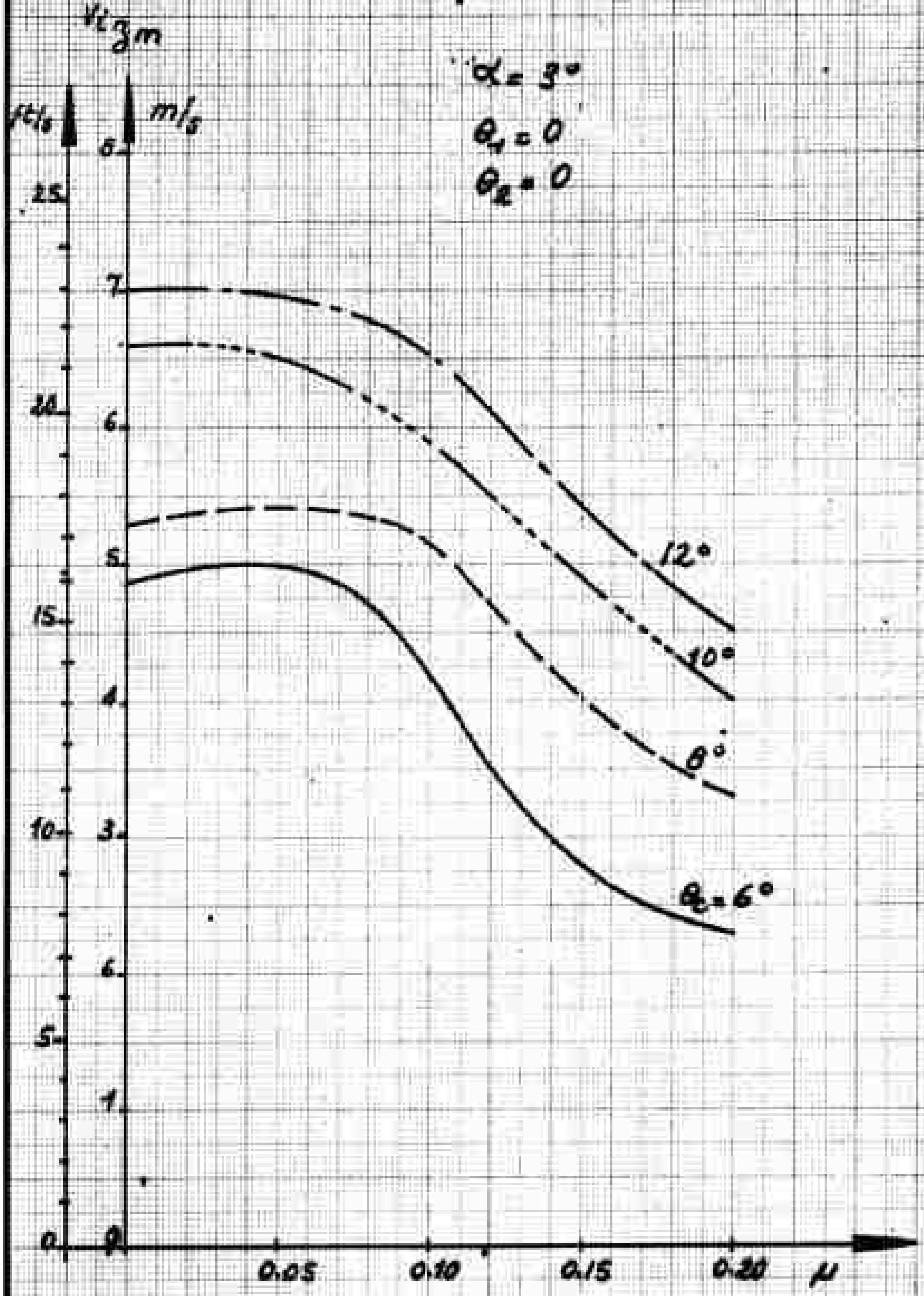

FIG. 100

BLADE Nb 4

VERTICAL MEAN INDUCED VELOCITY

VERSUS μ

EFFECT OF α

$\theta_c = 6°$

$\theta_1 = 0$

$\theta_2 = 0$

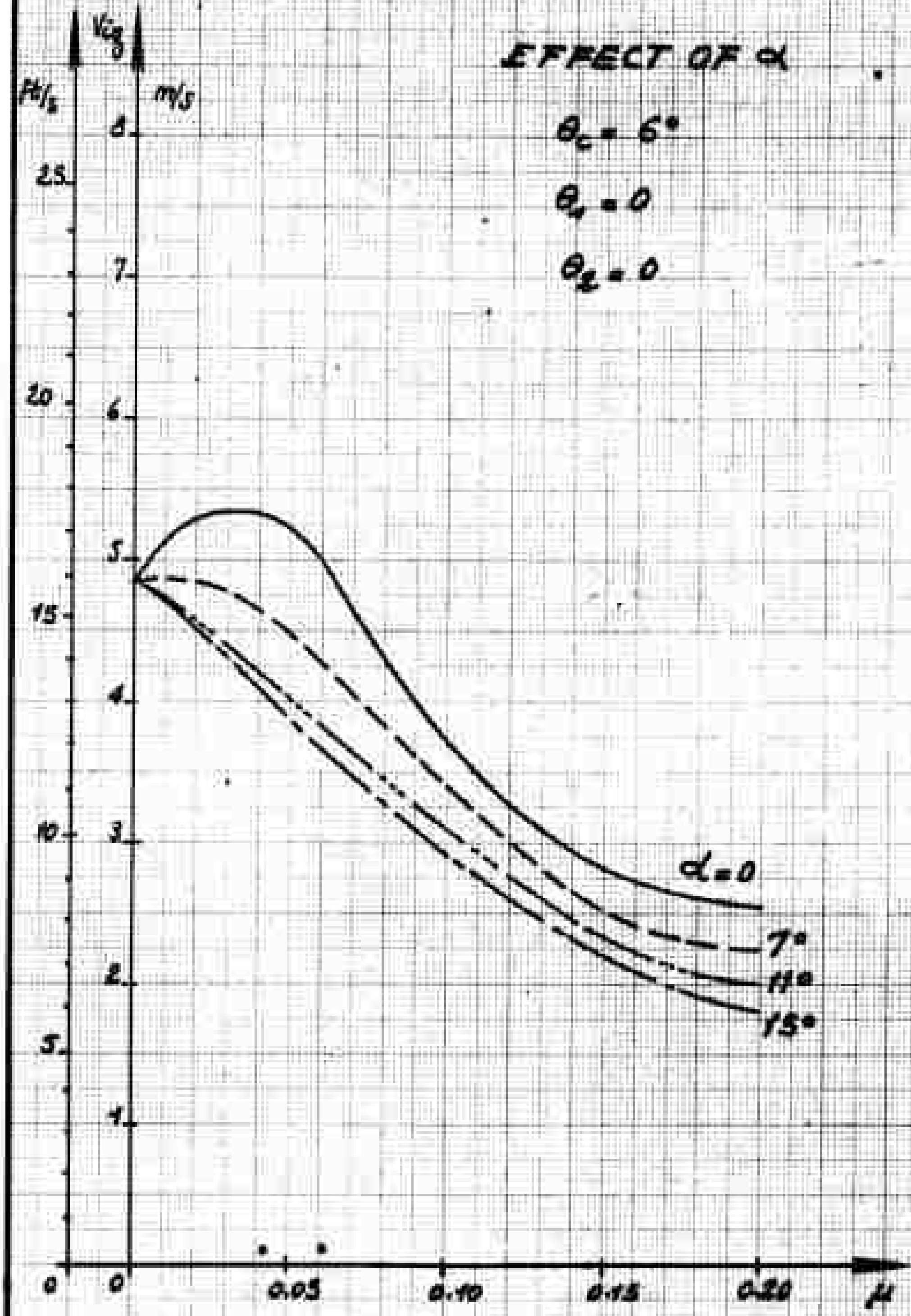

FIG. 101

BLADE Nb. 4

VERTICAL MEAN INDUCED VELOCITY VERSUS μ

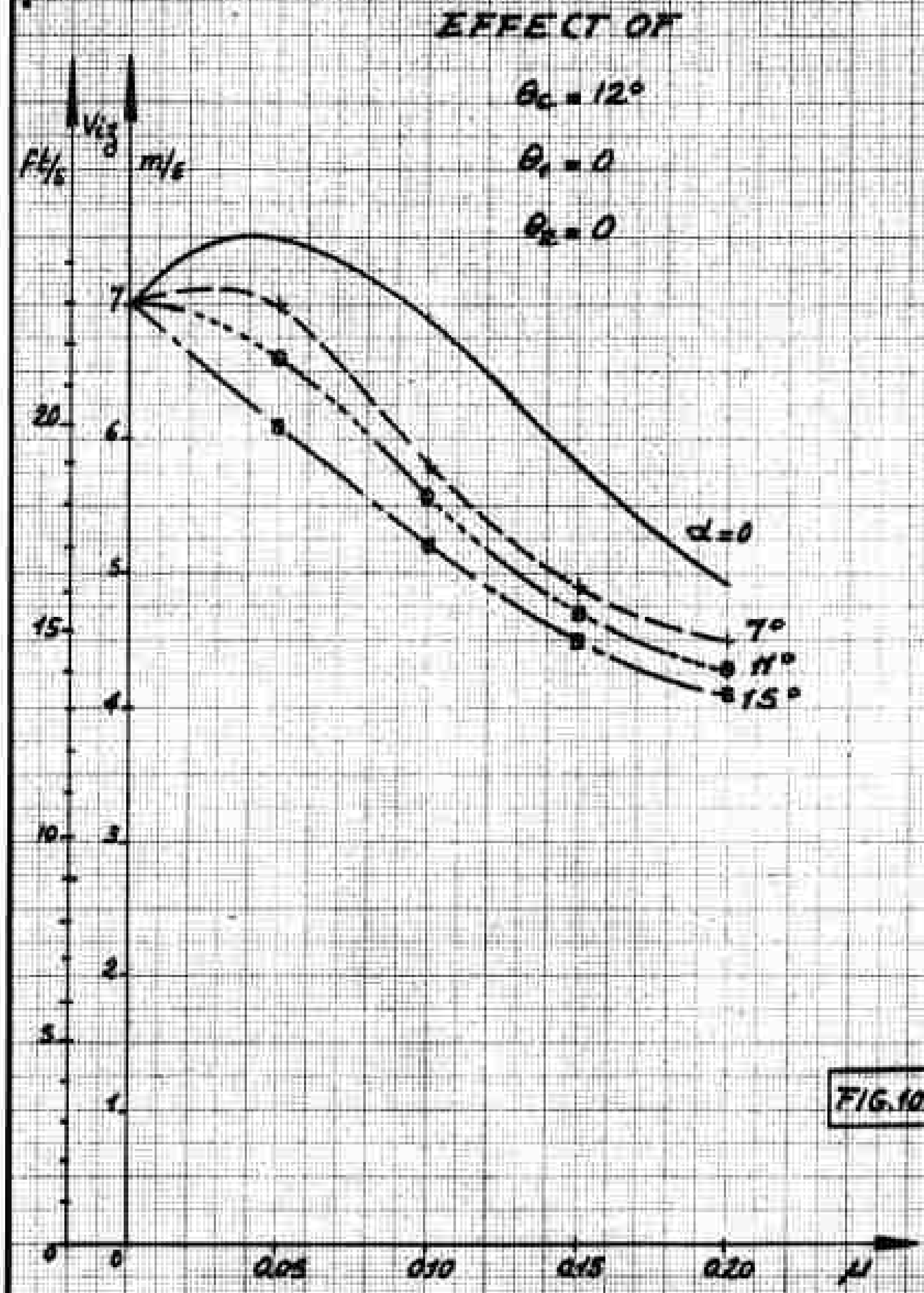

FIG.102

BLADE No 4

VERTICAL MEAN INDUCED VELOCITY VERSUS μ

EFFECT OF θ_2

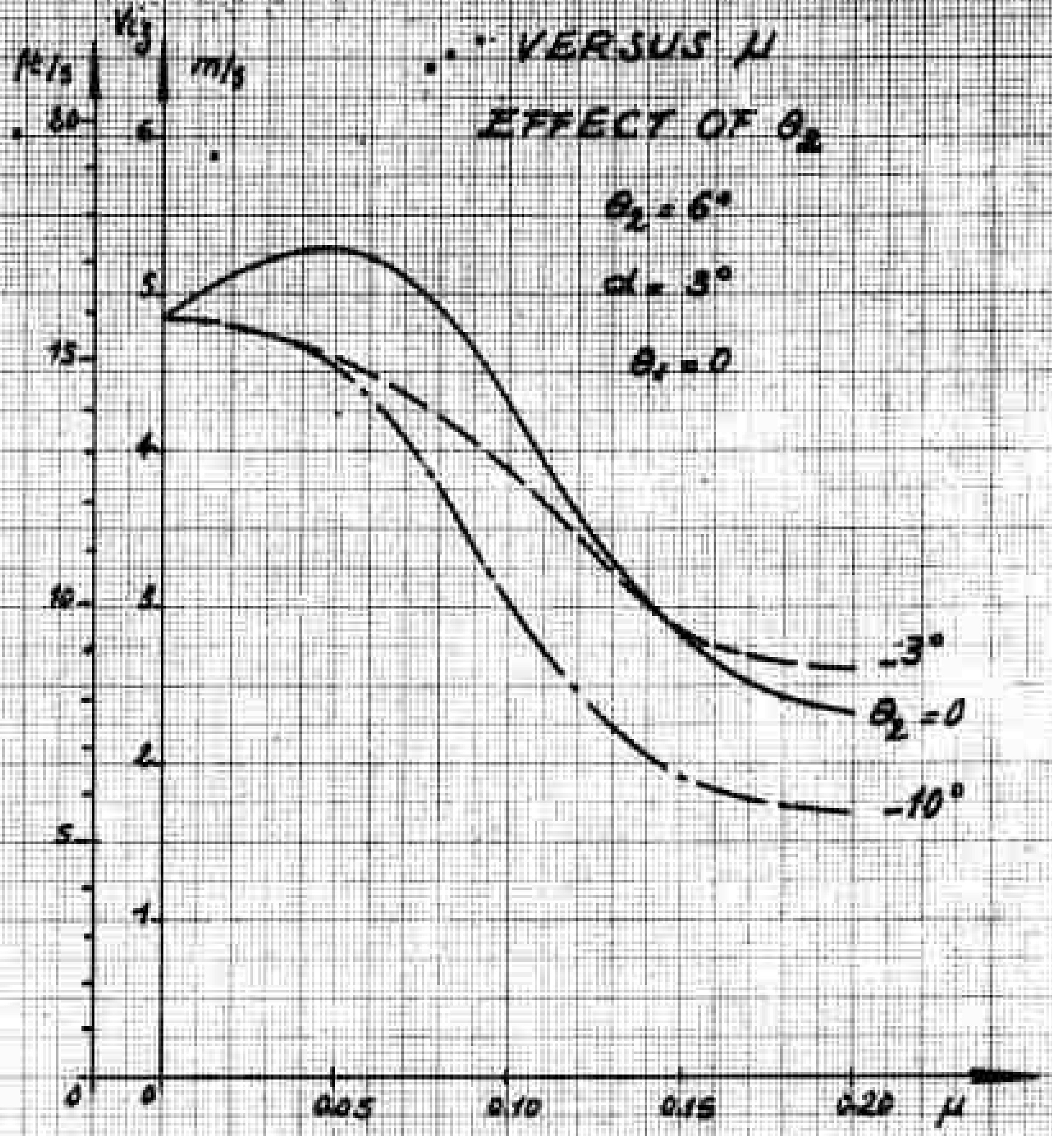

FIG. 103

BLADE No.4

VERTICAL MEAN INDUCED VELOCITY

VERSUS μ

EFFECT OF θ_1

$\theta_c = 6°$

$\alpha = 3°$

$\theta_2 = 0°$

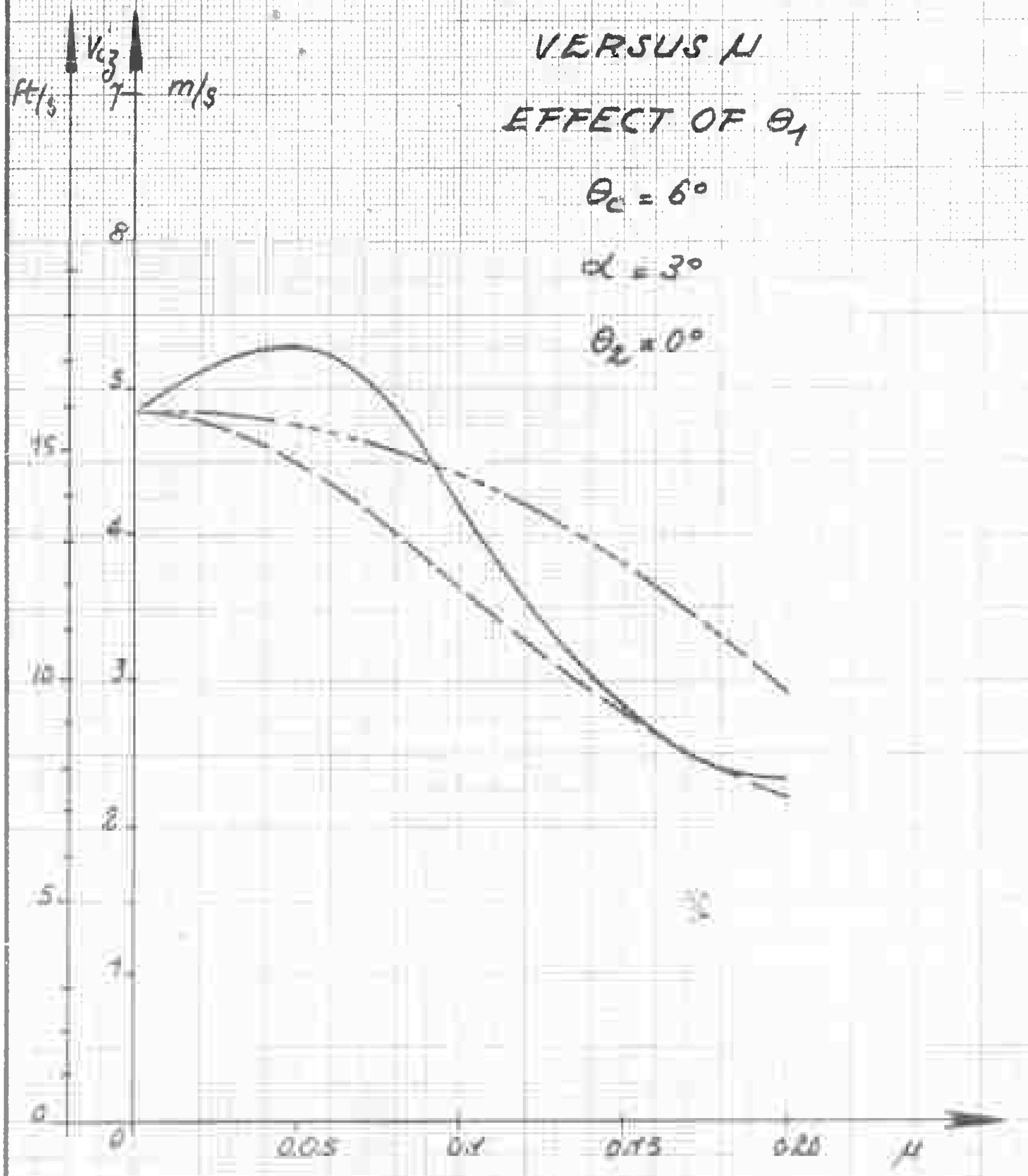

FIG.104

VERTICAL MEAN INDUCED VELOCITY VERSUS μ

EFFECT OF SOLIDITY σ

$\theta_c = 6°$ $\alpha = 3°$ $\theta_1 = 0$ $\theta_2 = 0$

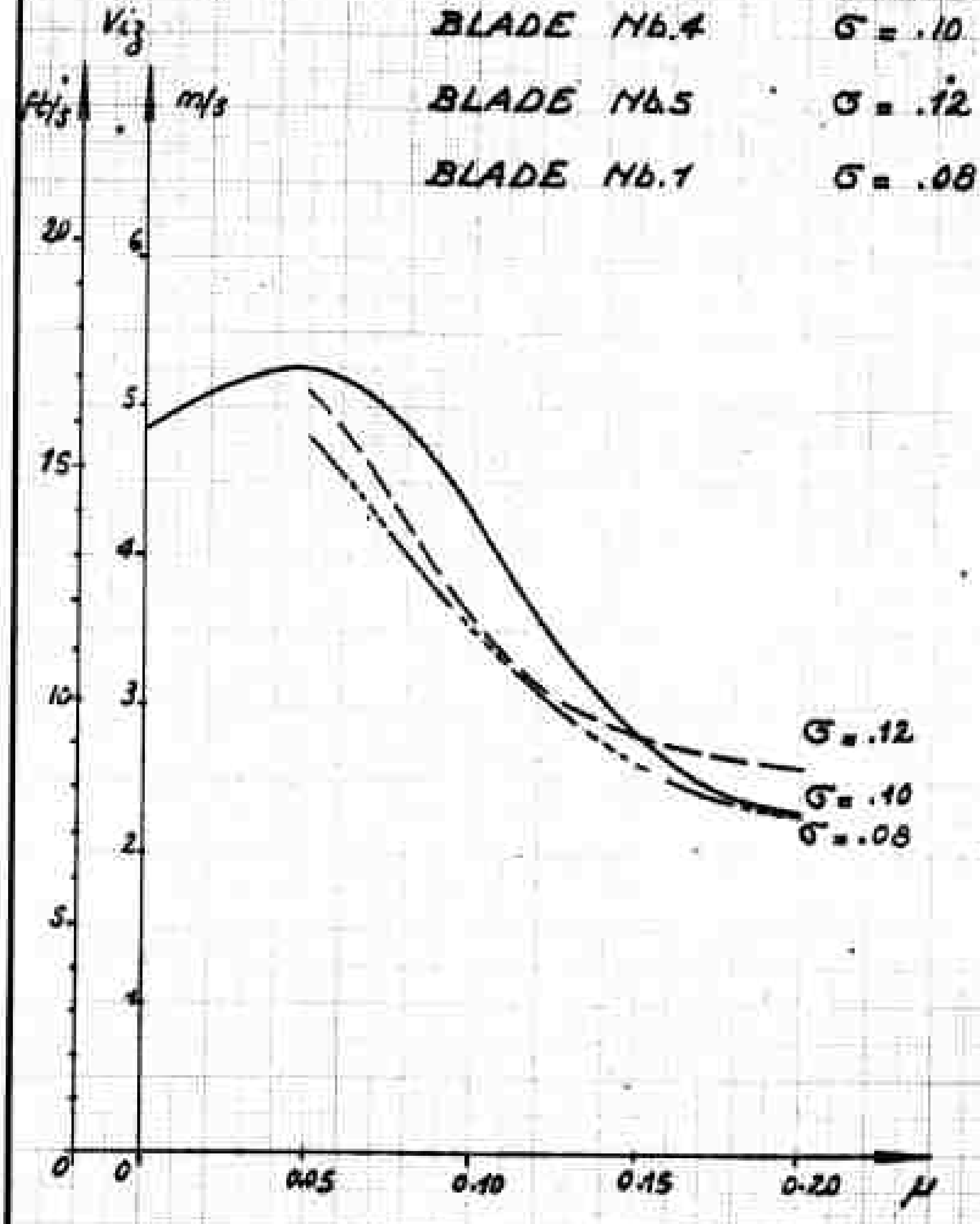

FIG.105

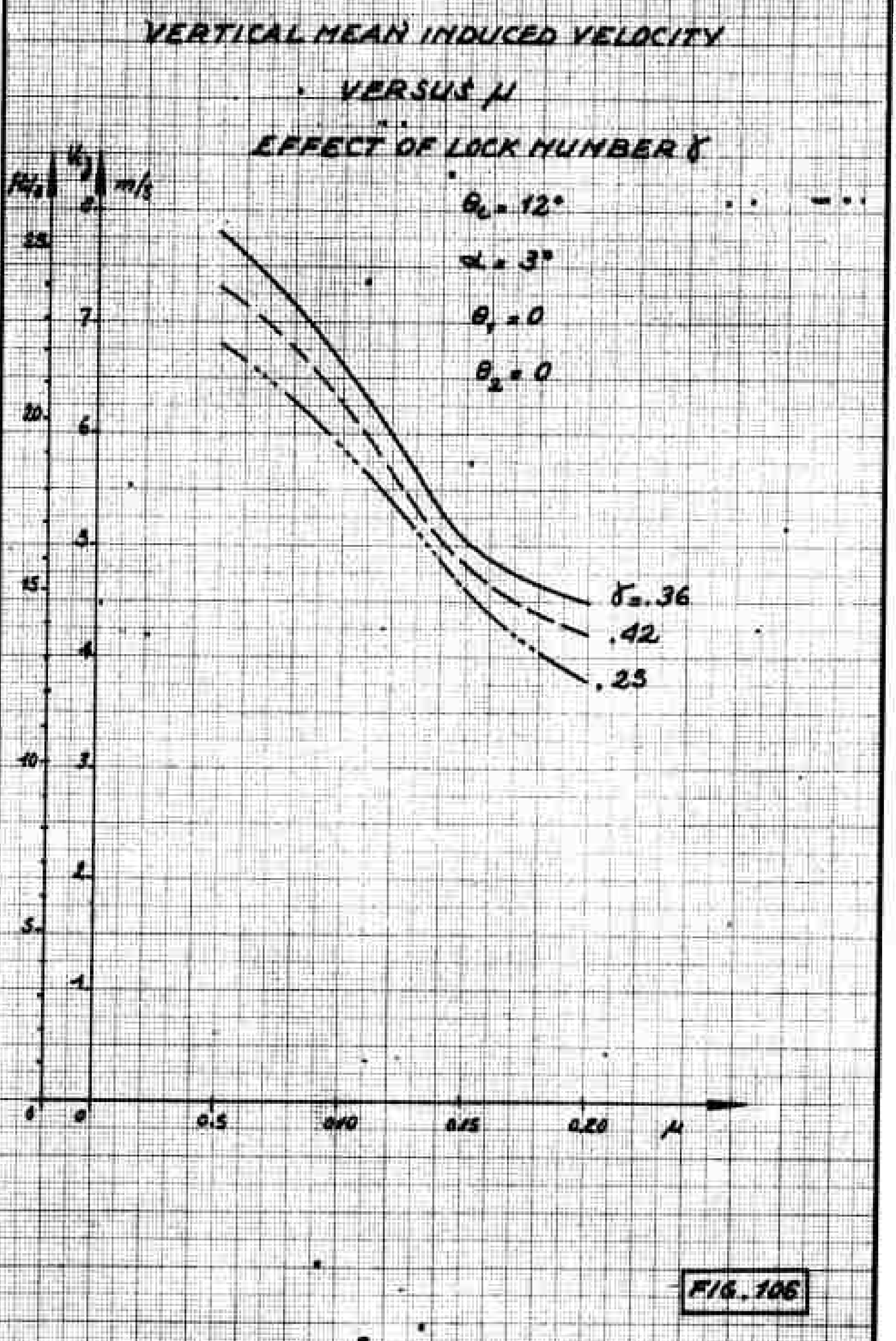
VERTICAL MEAN INDUCED VELOCITY
VERSUS μ
EFFECT OF LOCK NUMBER γ
θ = 12°
α = 3°
θ1 = 0
θ2 = 0
γ = .36
.42
.23
m/s
μ
0.5
0.10
0.15
0.20

FIG. 106

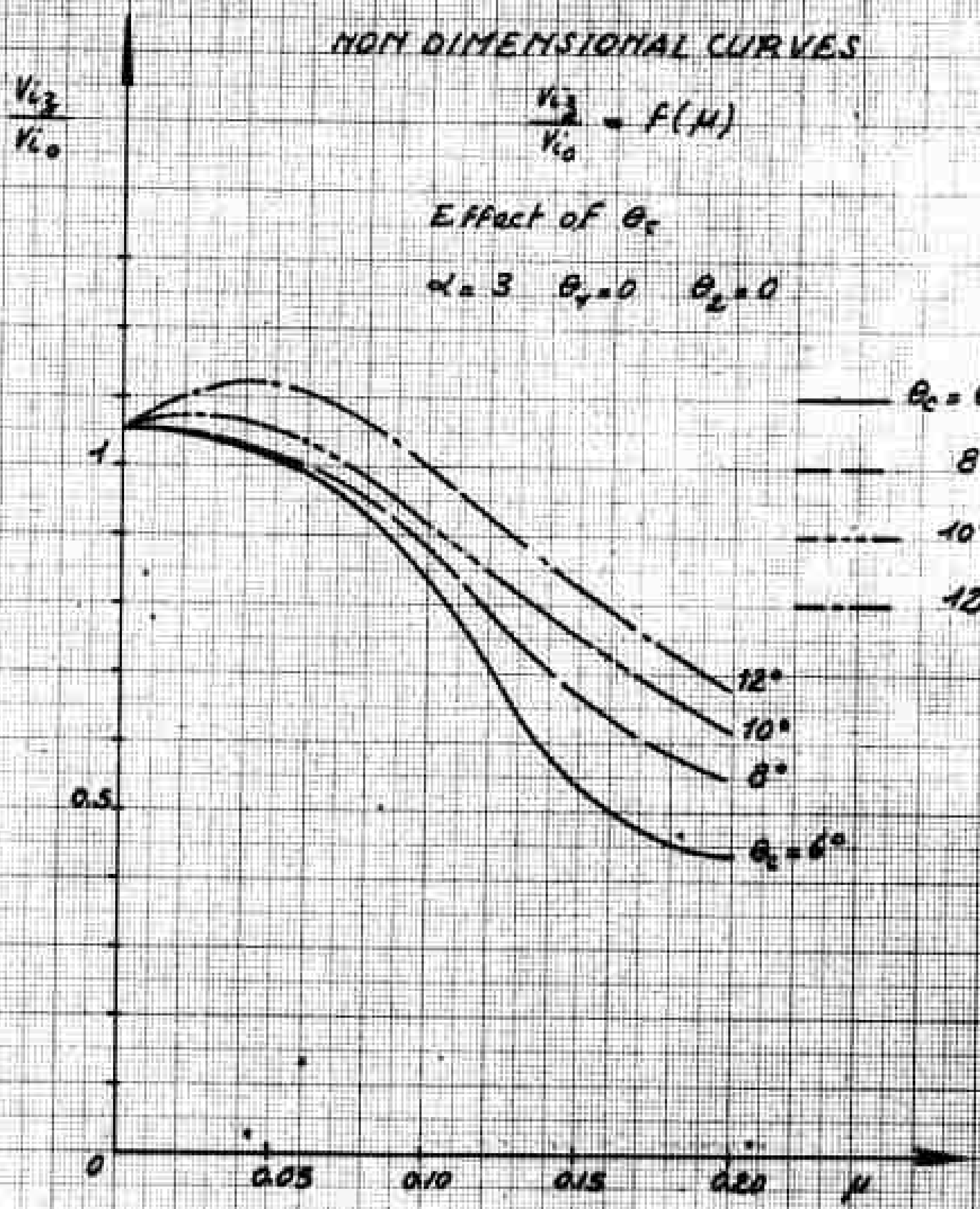
NON DIMENSIONAL CURVES
$\frac{V_{i_z}}{V_{i_0}} = f(\mu)$
Effect of θ_c
$\alpha = 3 \quad \theta_v = 0 \quad \theta_L = 0$
$\frac{V_{i_z}}{V_{i_0}}$
1
0.5
0
0.05
0.10
0.15
0.20
μ
$\theta_c = 6°$
8°
10°
12°
12°
10°
8°
$\theta_c = 6°$

FIG. 107

NON DIMENSIONAL CURVES

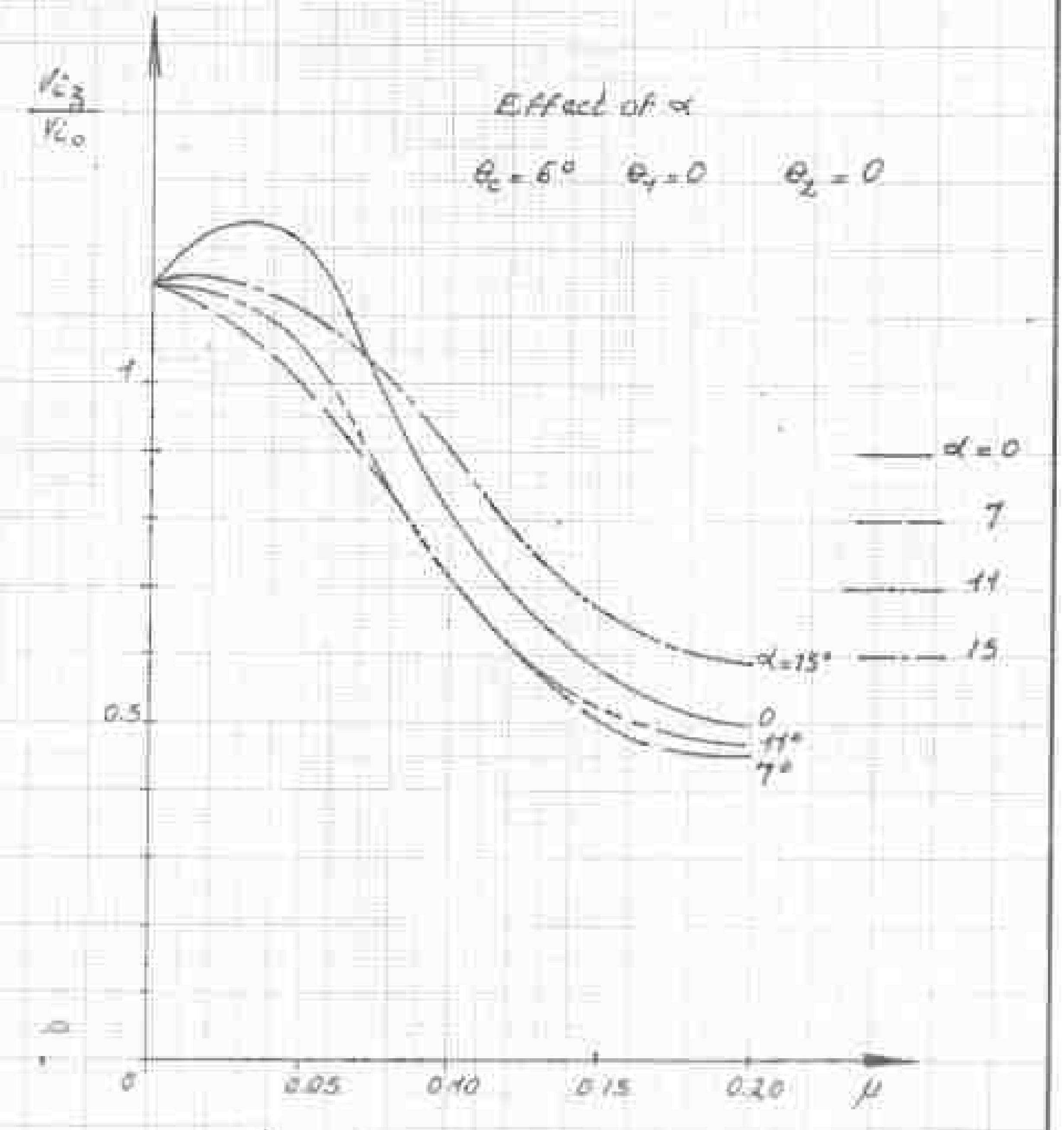

FIG. 108

NON DIMENSIONAL CURVES

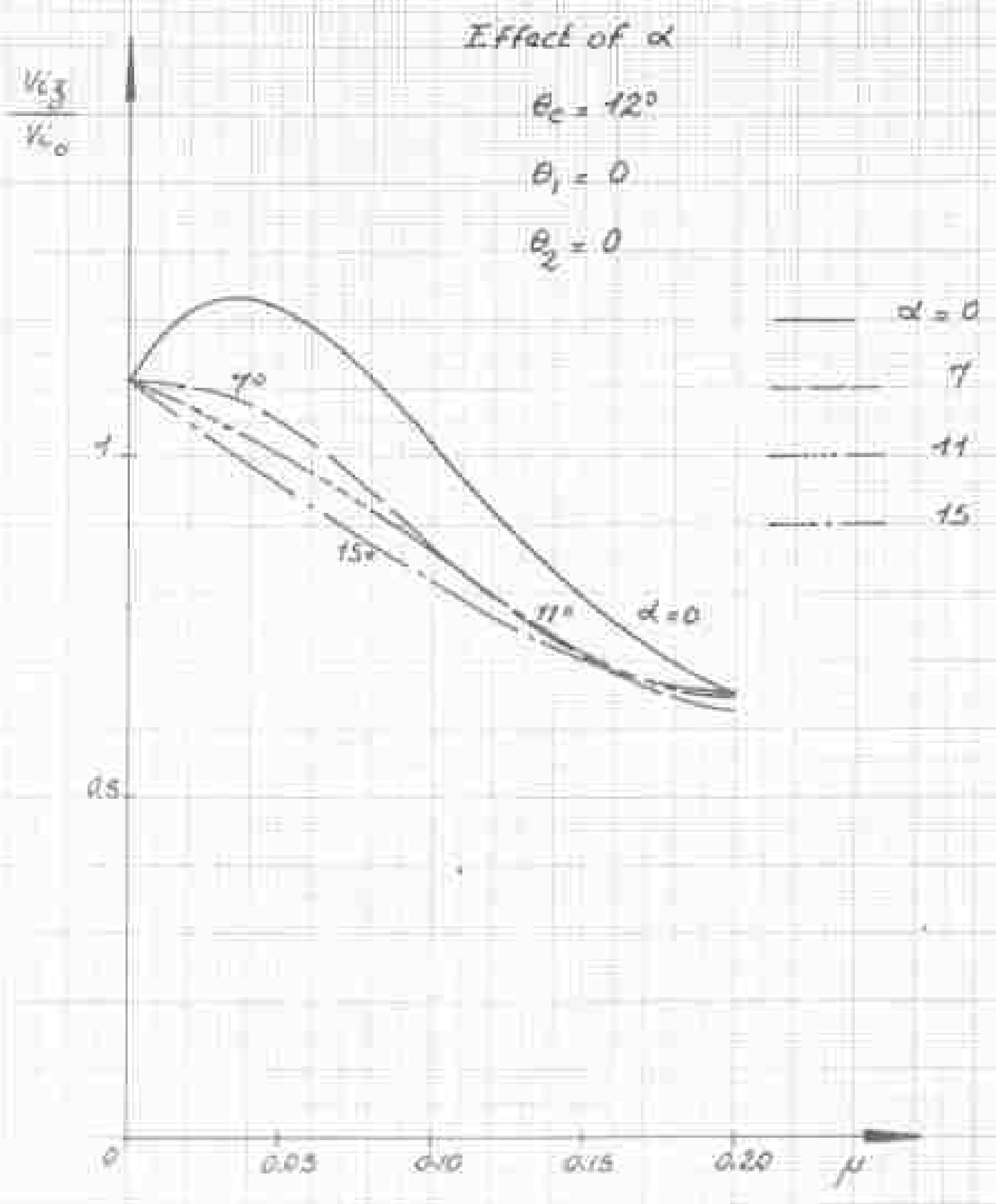

FIG. 109

NON DIMENSIONAL CURVES

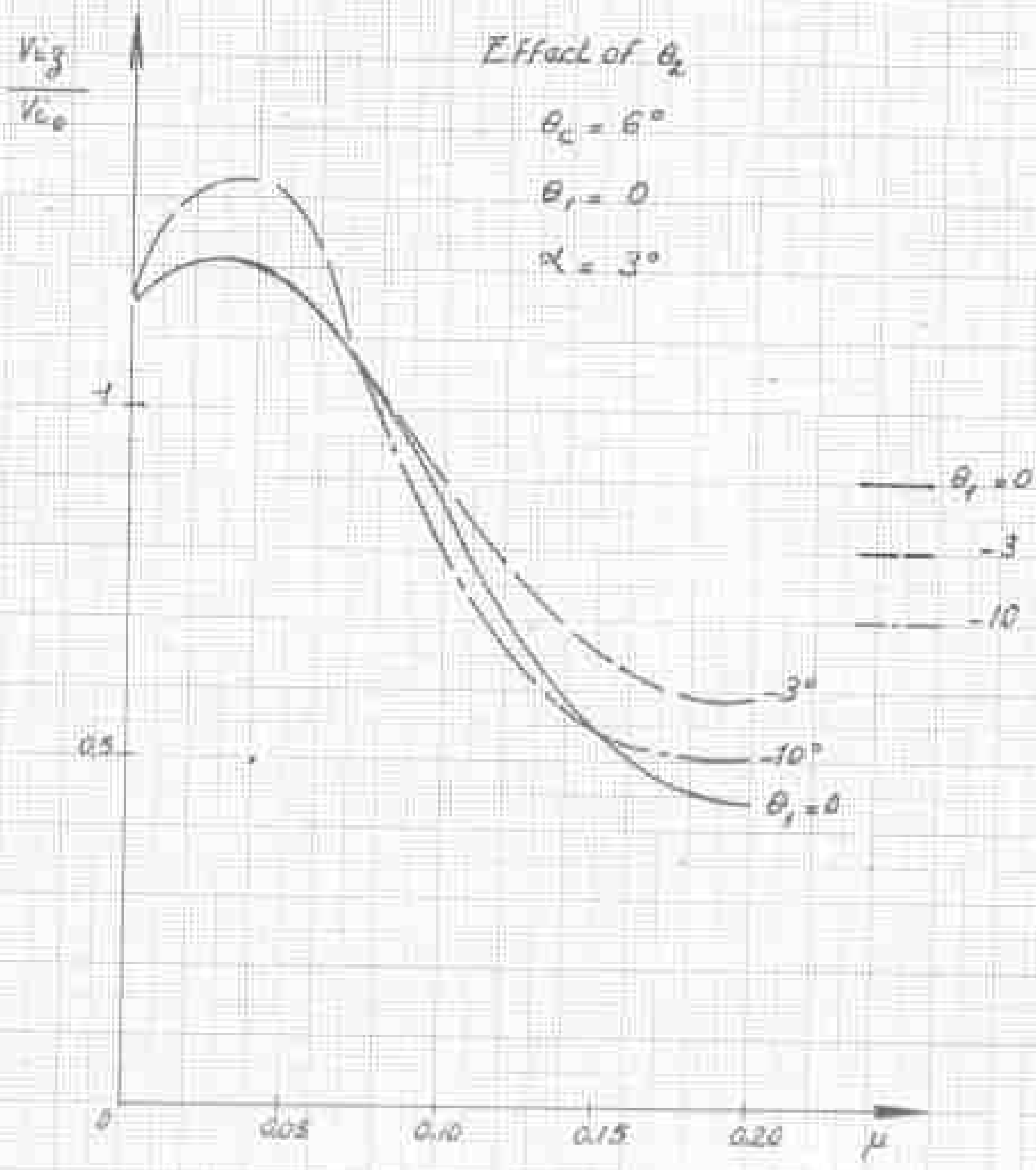

FIG. 110

NON DIMENSIONAL CURVES

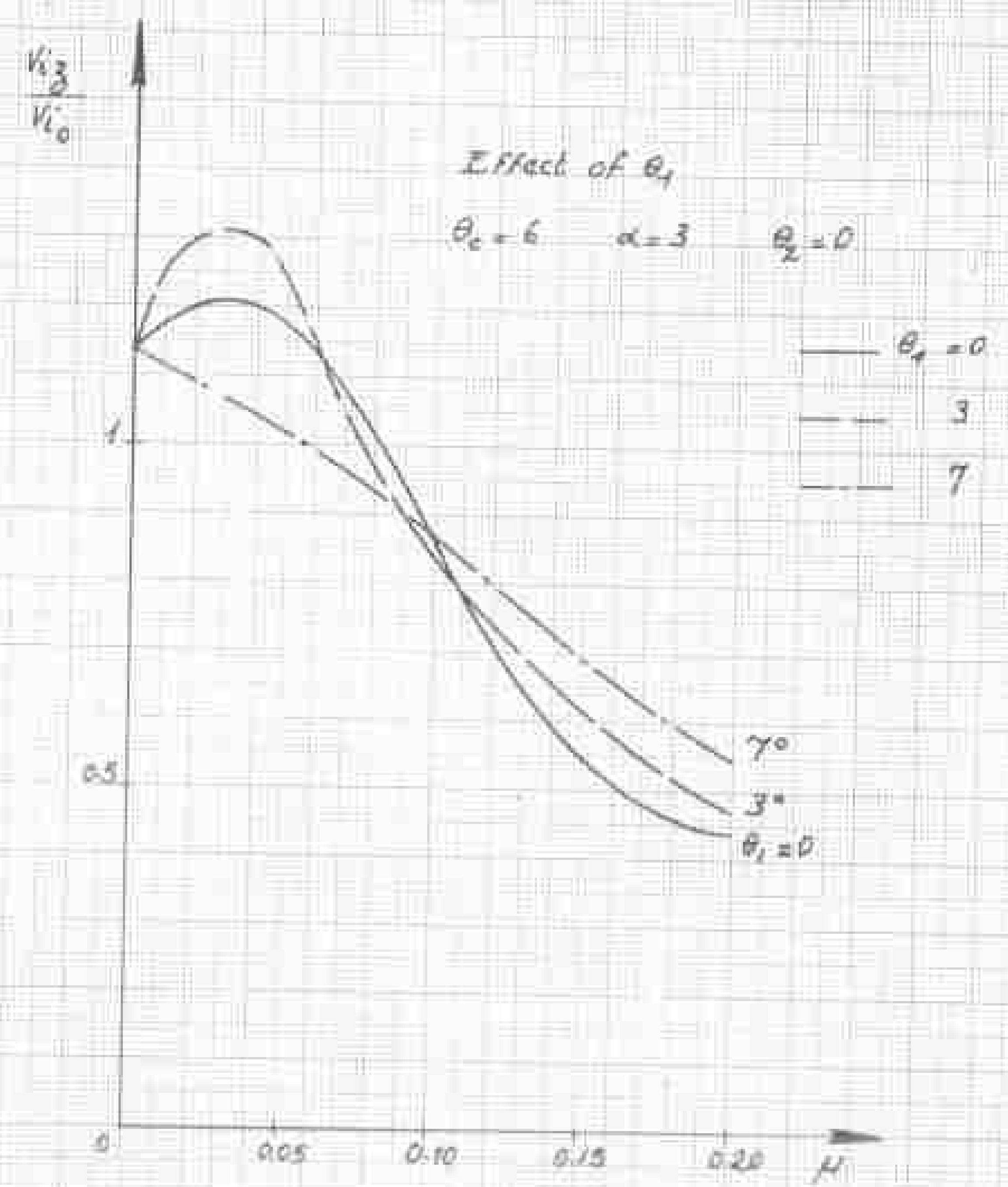

FIG. 111

NON DIMENSIONAL CURVES

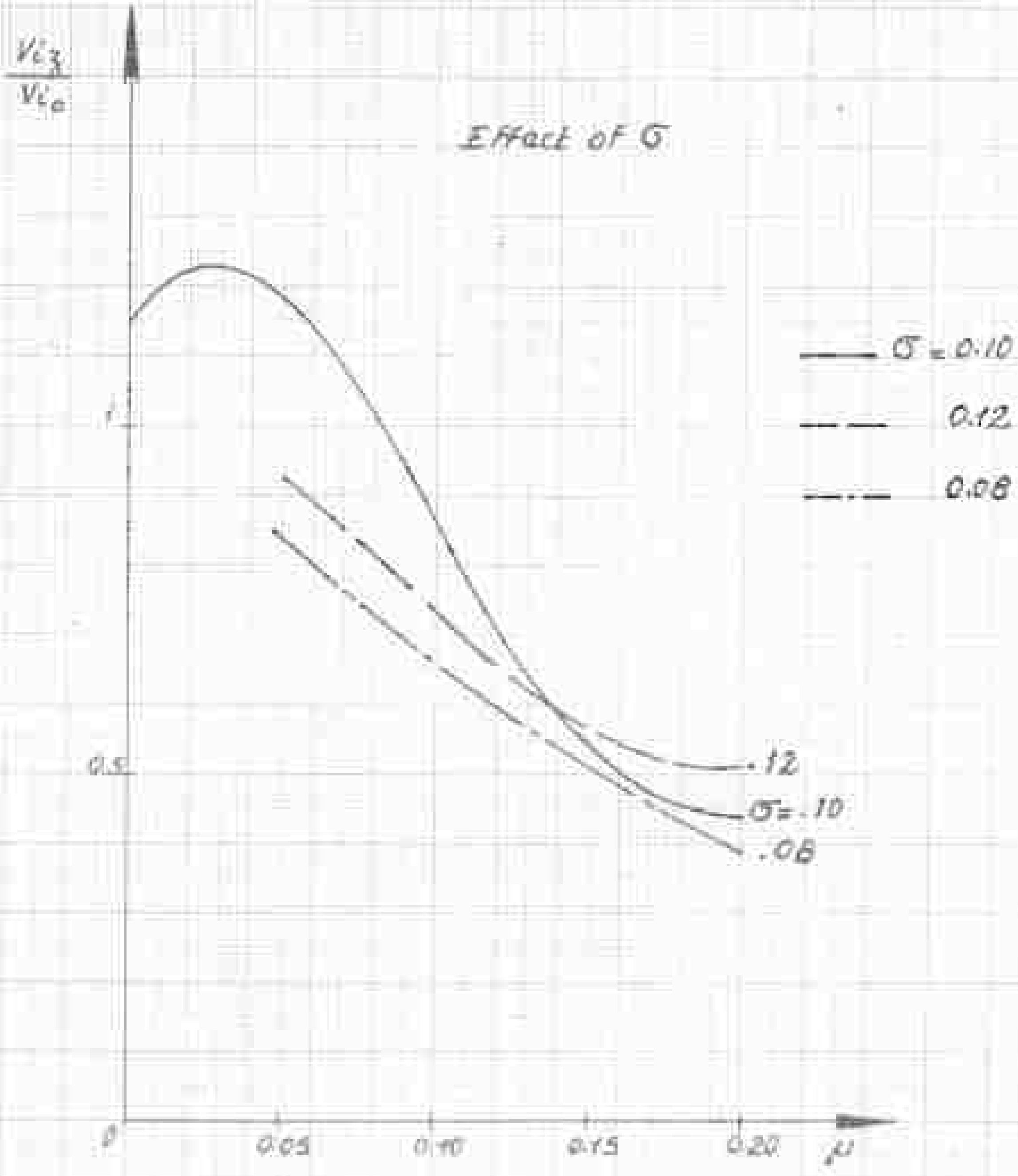

FIG.112

NON DIMENSIONAL CURVES

Effect of γ

$\theta_c = 12°$

$\alpha = 3°$

$\theta_1 = 0$

$\theta_2 = 0$

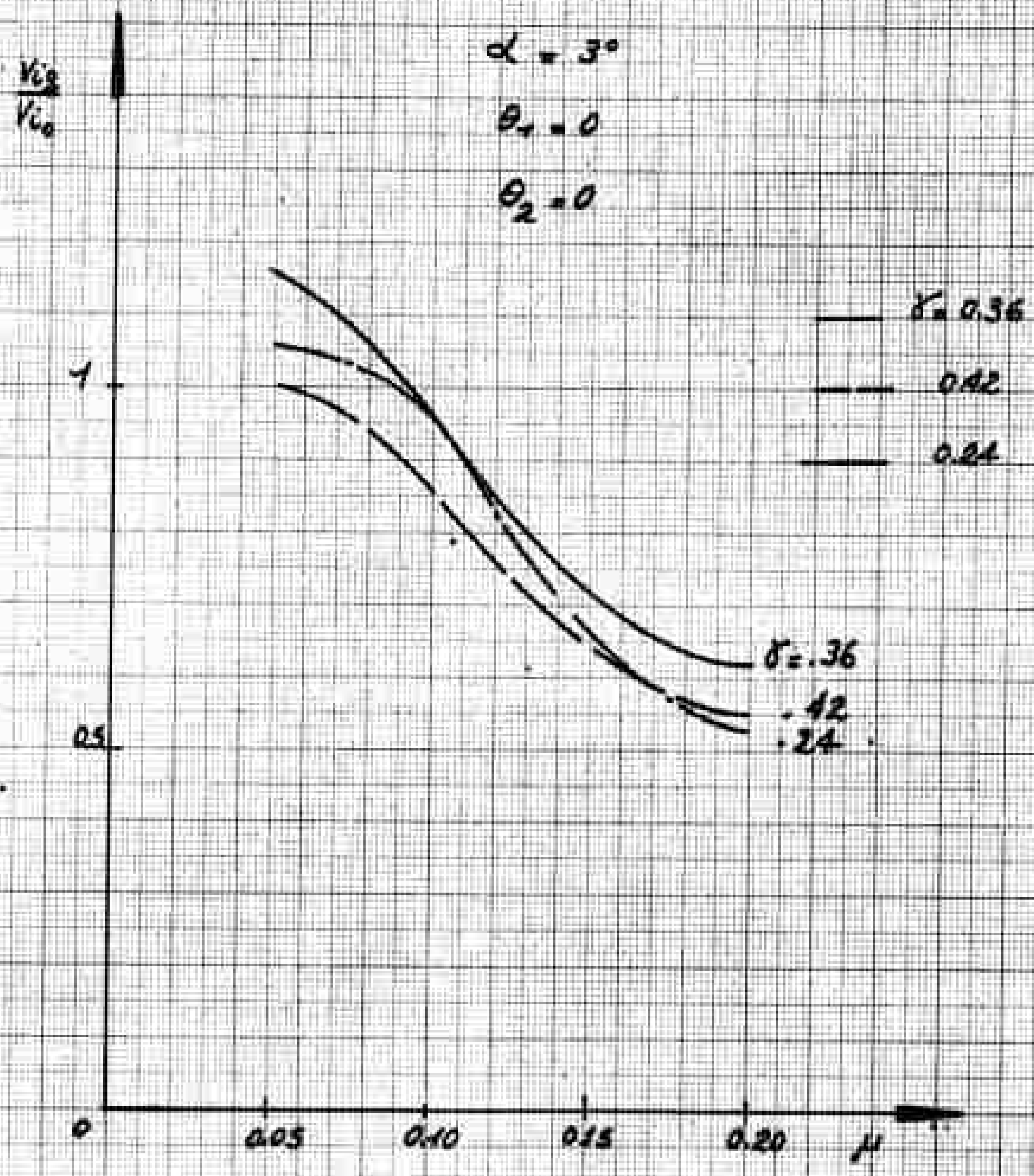

FIG. 113

LOCATION OF THE CIRCLES WHICH MAY BE SUBSTITUTED TO THE SPIRAL VORTICES...

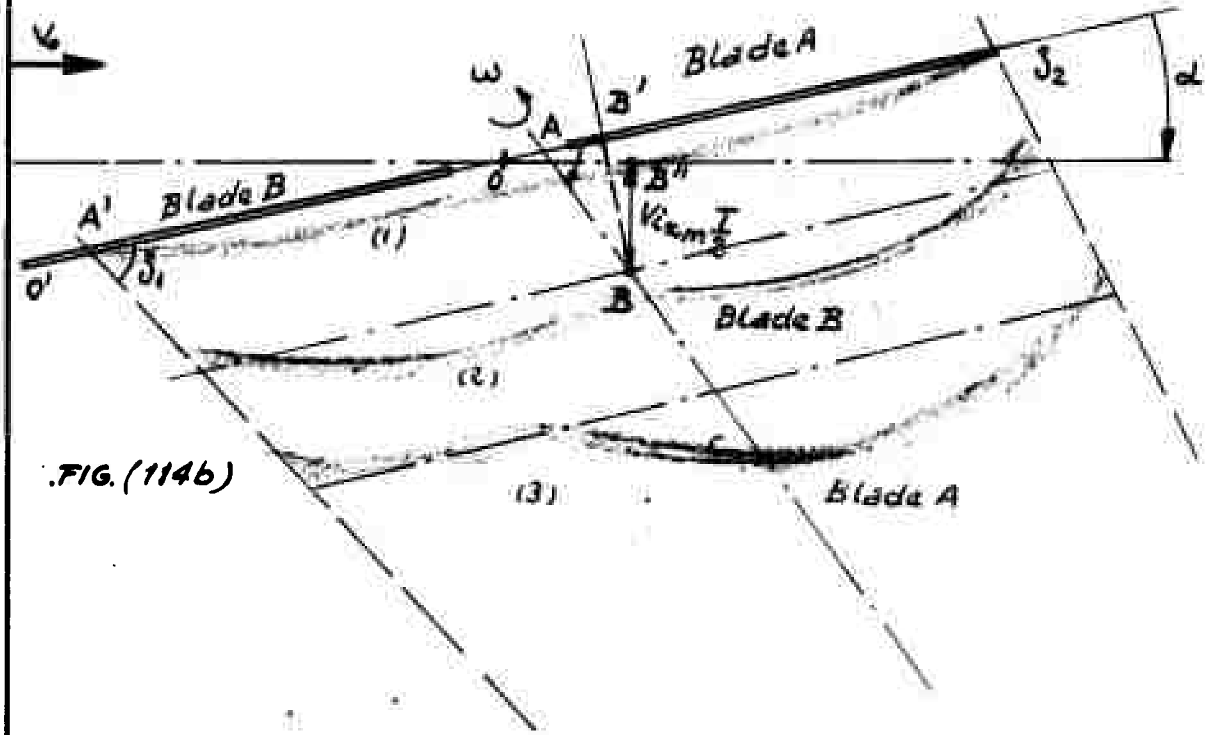

.FIG. (114b)

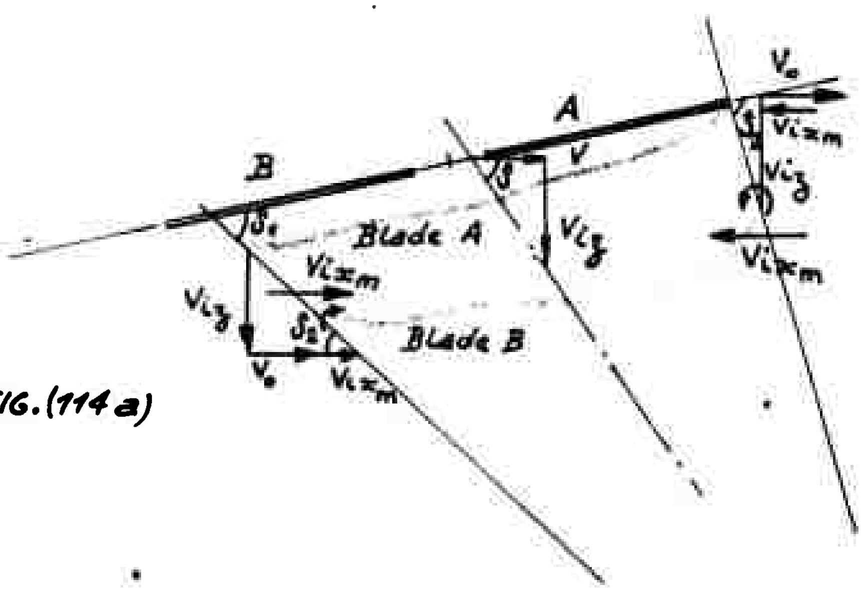

FIG. (114 a)

$$\tan \delta = \frac{V_{iz} + V_0 \sin\alpha}{V_0}$$

$$\tan \delta_1 = \frac{V_{iz} + V_0 \sin\alpha}{V_0 + V_{ixm}}$$

$$\tan \delta_2 = \frac{V_{iz} + V_0 \sin\alpha}{V_0 + V_{ixm}}$$

FIG. 114

B.115

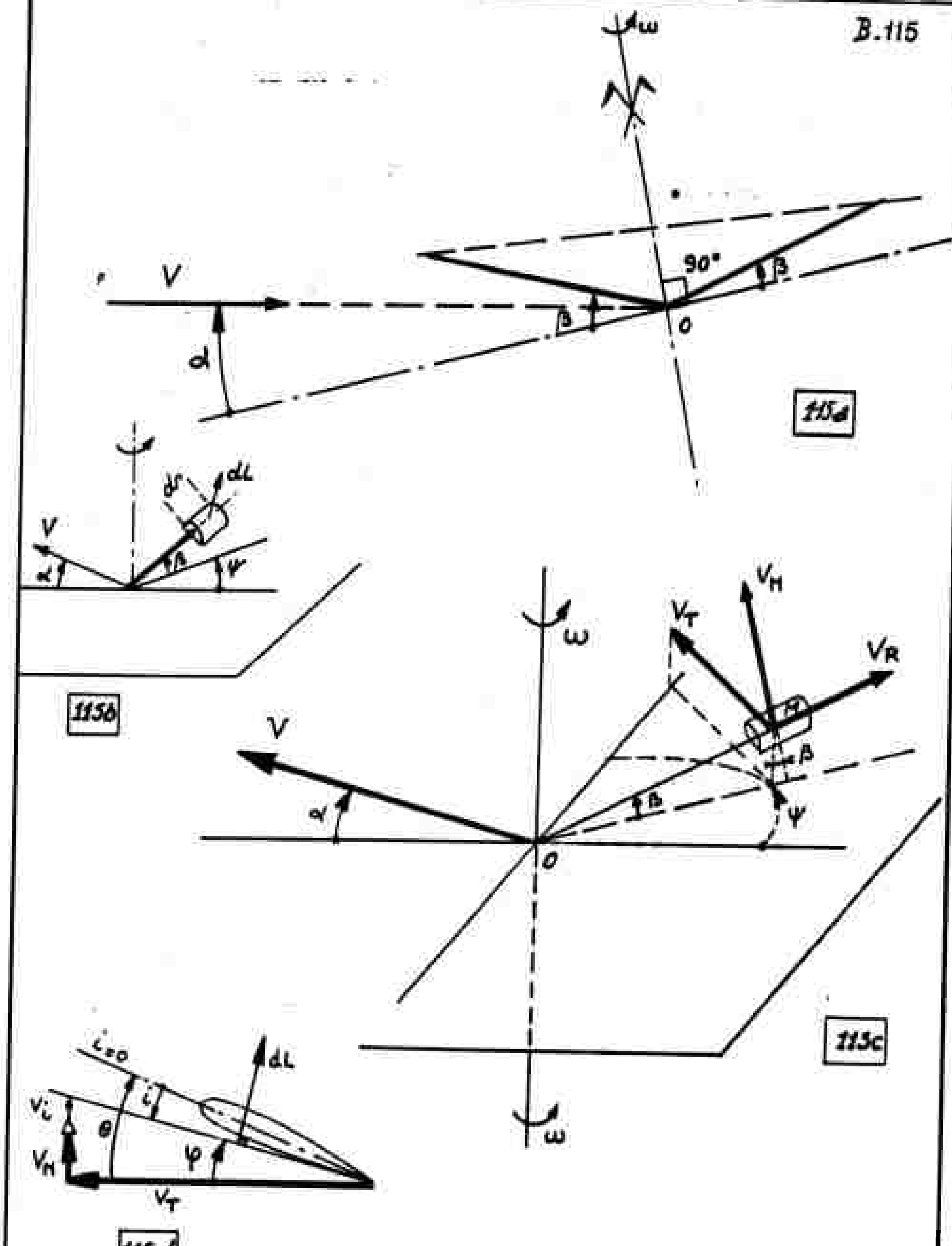

$$
\begin{cases}
V_T = \omega r \cos\beta + V \cos\alpha \sin\Psi \\
V_H' = r \dfrac{d\beta}{dt} + V \sin\alpha \cos\beta + V \cos\alpha \cos\Psi \sin\beta \\
V_R = V \sin\alpha \sin\beta - V \cos\alpha \sin\Psi \cos\beta
\end{cases}
$$

$$\operatorname{tg}\varphi = \frac{V_i + V_H}{V_T}$$

FIG.115

COMPARISON BETWEEN RIGID AND FLEXIBLE BLADES.

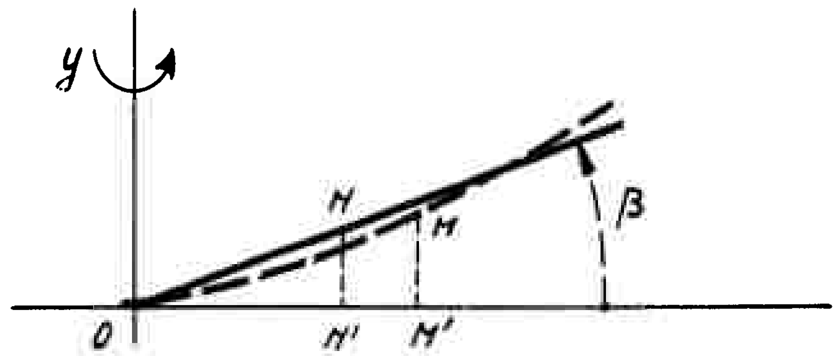

	RIGID BLADE	FLEXIBLE BLADE
Ordonate	βr	$y(r)$
Slope	$\frac{d\beta r}{dr} = \beta$	$\frac{\partial y}{\partial r}(r,t)$
Velocity	$r\,\frac{d\beta}{dt}$	$\frac{\partial y}{\partial t}$
Acceleration	$r\,\frac{d^2\beta}{dt^2}$	$\frac{\partial^2}{\partial t^2}\,y(r,t)$

FIG. 116

HELIX FREE VORTICES

Hélicoptar blade

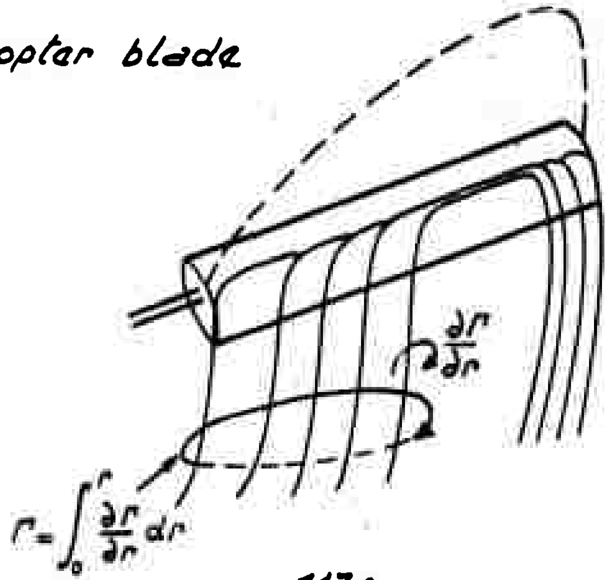

117a

Fixed wing

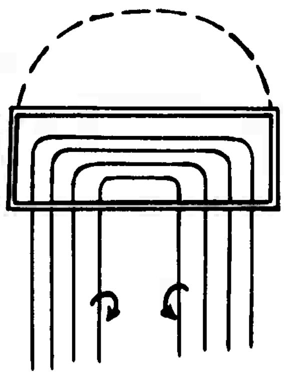

117b

FIG.117

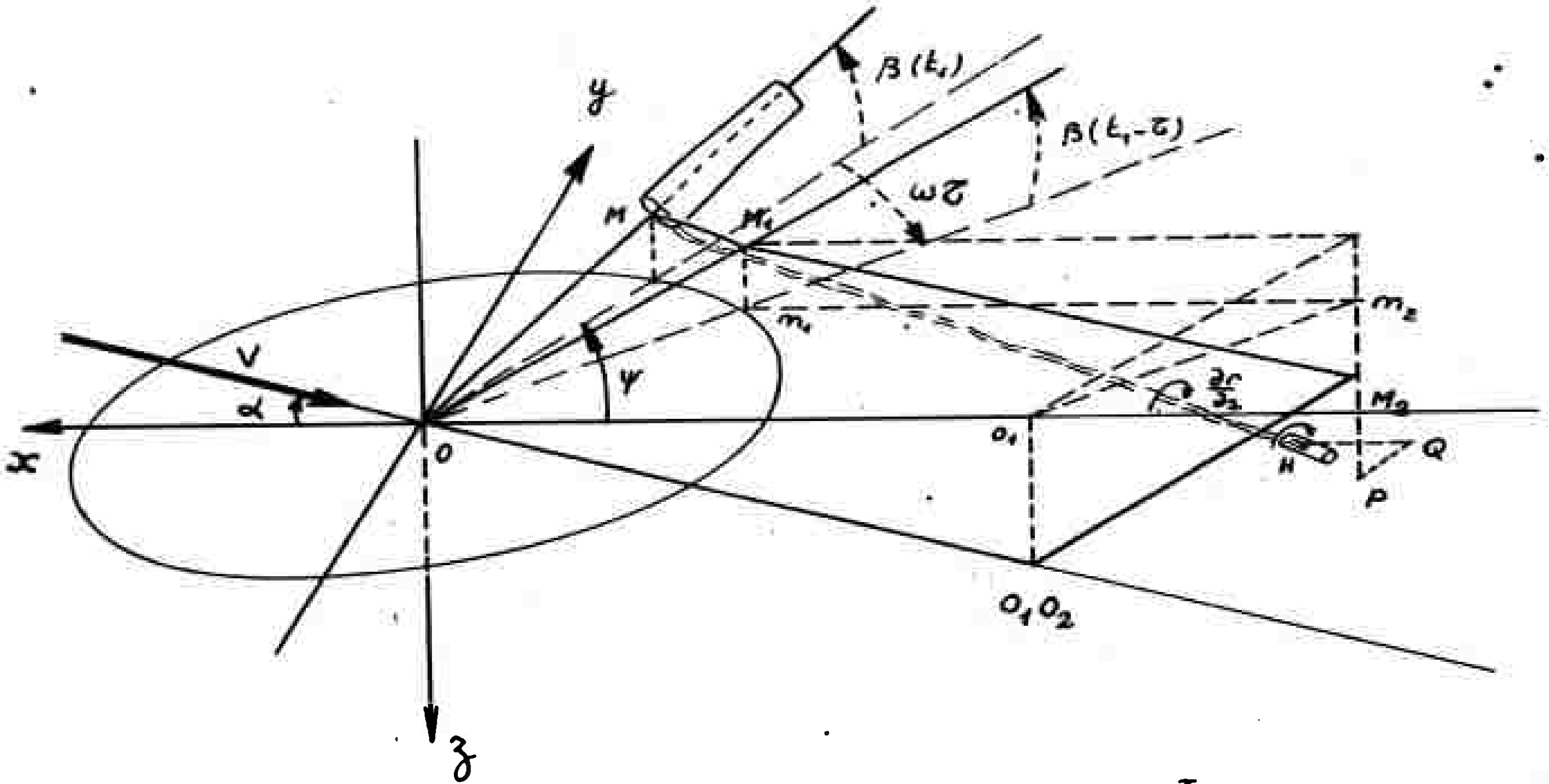

$$
\left\{
\begin{aligned}
QH &= \int_0^\tau V_{ix}\, d\tau \\
PQ &= \int_0^\tau V_{iy}\, d\tau \\
M_2P &= \int_0^\tau V_{iz}\, d\tau
\end{aligned}
\right.
$$

FIG. 118

B.118

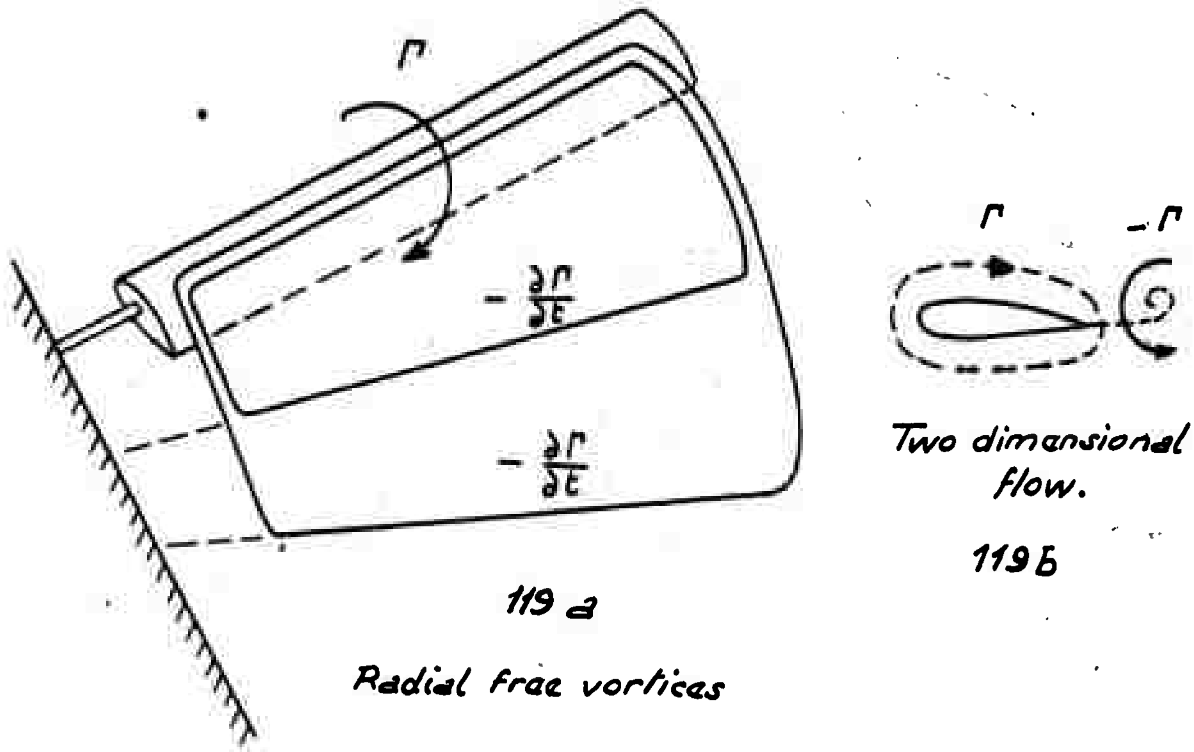

FIG. 119

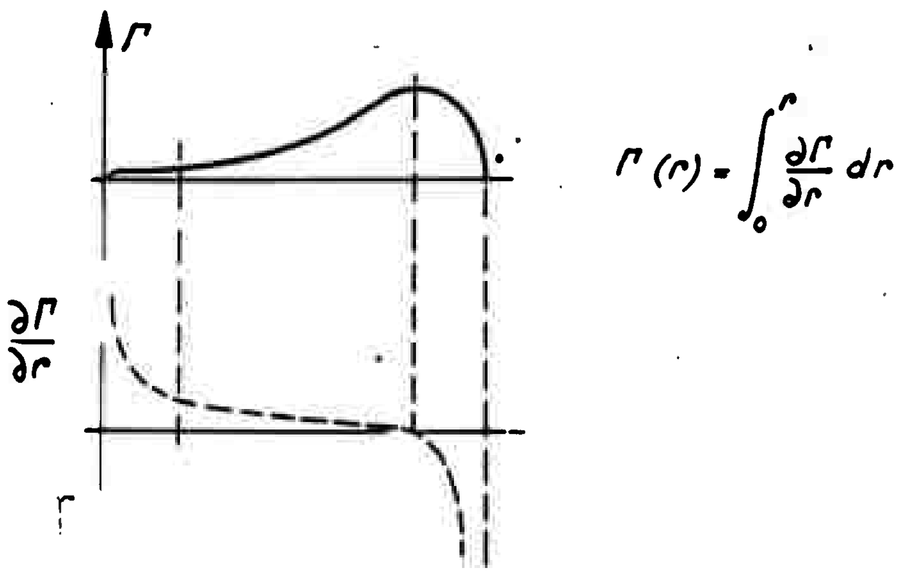

FIG. 120

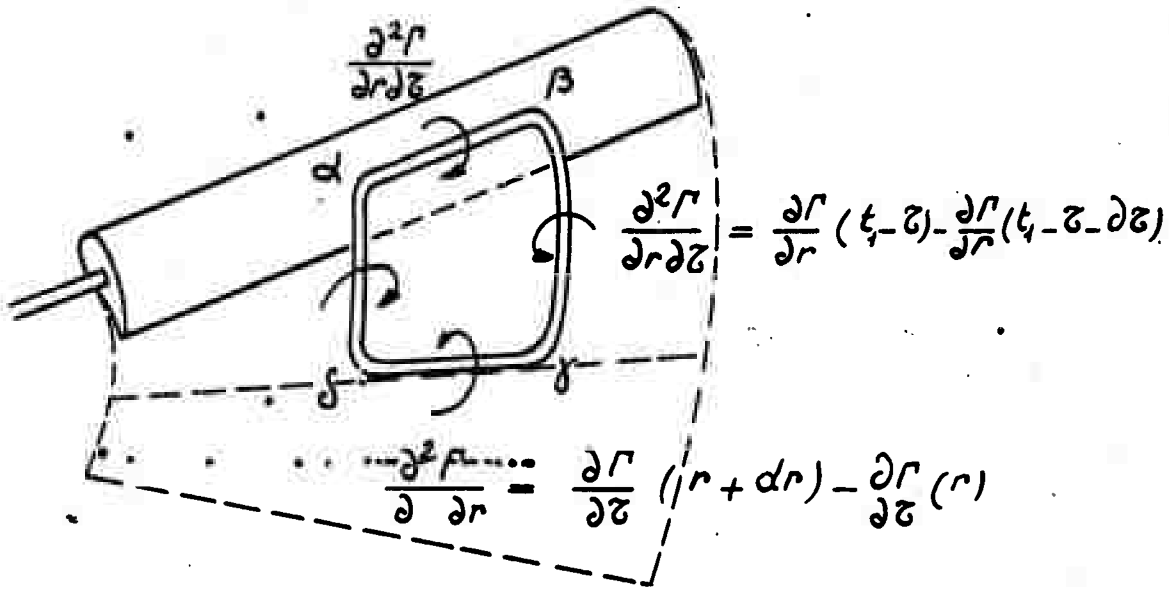

121 a

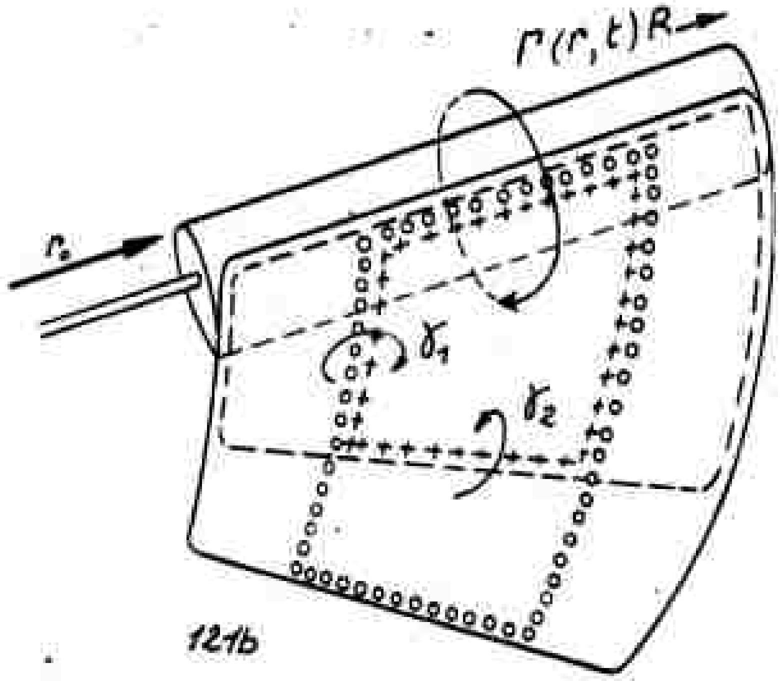

121b

FIG.121

$$
\left\{
\begin{aligned}
\Gamma\,(r,t) &= \int_{r=0}^{r} \int_{\tau=0}^{\tau=\infty} \frac{\partial^2 \Gamma}{\partial r\,\partial \tau}\; r_1(t-\tau)\; dr\,d\tau \\
\gamma_1 &= \frac{\partial \Gamma}{\partial r}\,(r, t-\tau_1) = \int_{\tau=\infty}^{\tau=\tau_1} \frac{\partial^2 \Gamma}{\partial r\,\partial \tau}\, d\tau \\
\gamma_2 &= \frac{\partial \Gamma}{\partial \tau}\,(r, t-\tau_1) = \int_{r=r_0}^{r} \frac{\partial^2 \Gamma}{\partial r\,\partial \tau}\, dr
\end{aligned}
\right.
$$

VARIATION OF THE CIRCULATION Γ^* VERSUS Ψ AND $\bar{r}$

$$\Gamma^* = \frac{1}{\bar{r}+\mu \sin\Psi} \; \frac{d_L}{dr}$$

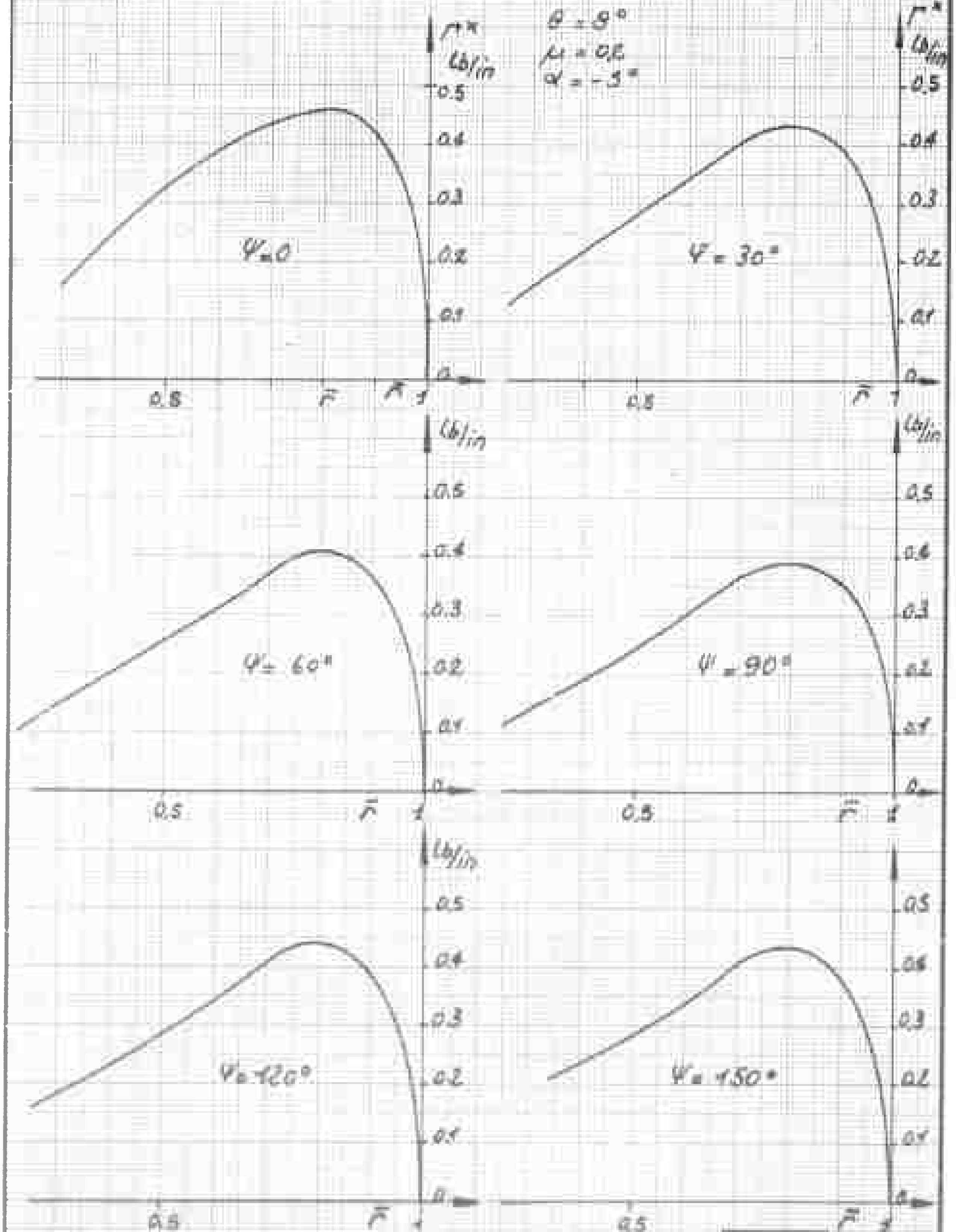

FIG 122

VARIATION OF THE CIRCULATION Γ^* VERSUS Ψ AND $\bar{r}$

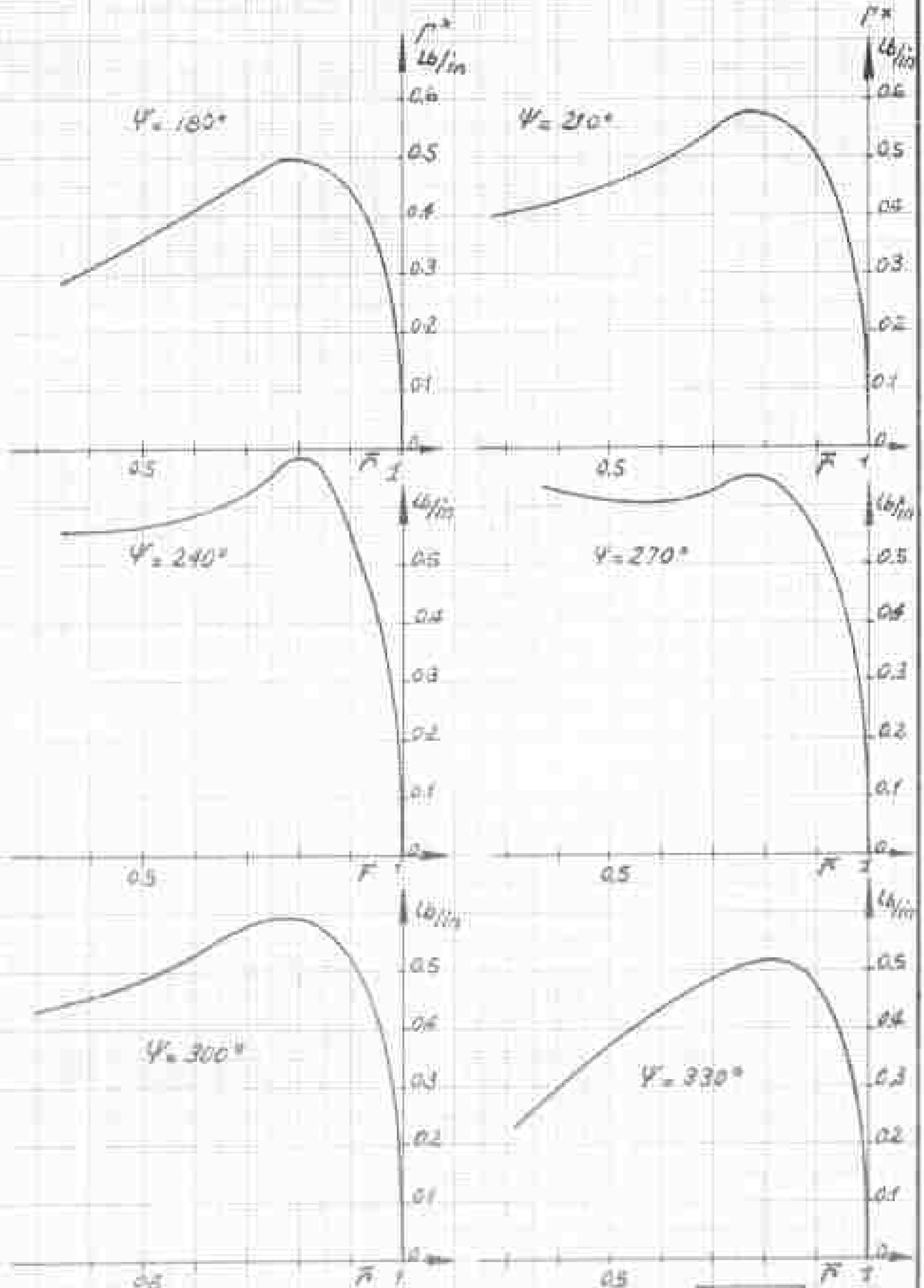

FIG. 123

VARIATION OF THE CIRCULATION
AND OF THE INDUCED VELOCITY
VERSUS $\bar{r}$ IN HOVERING

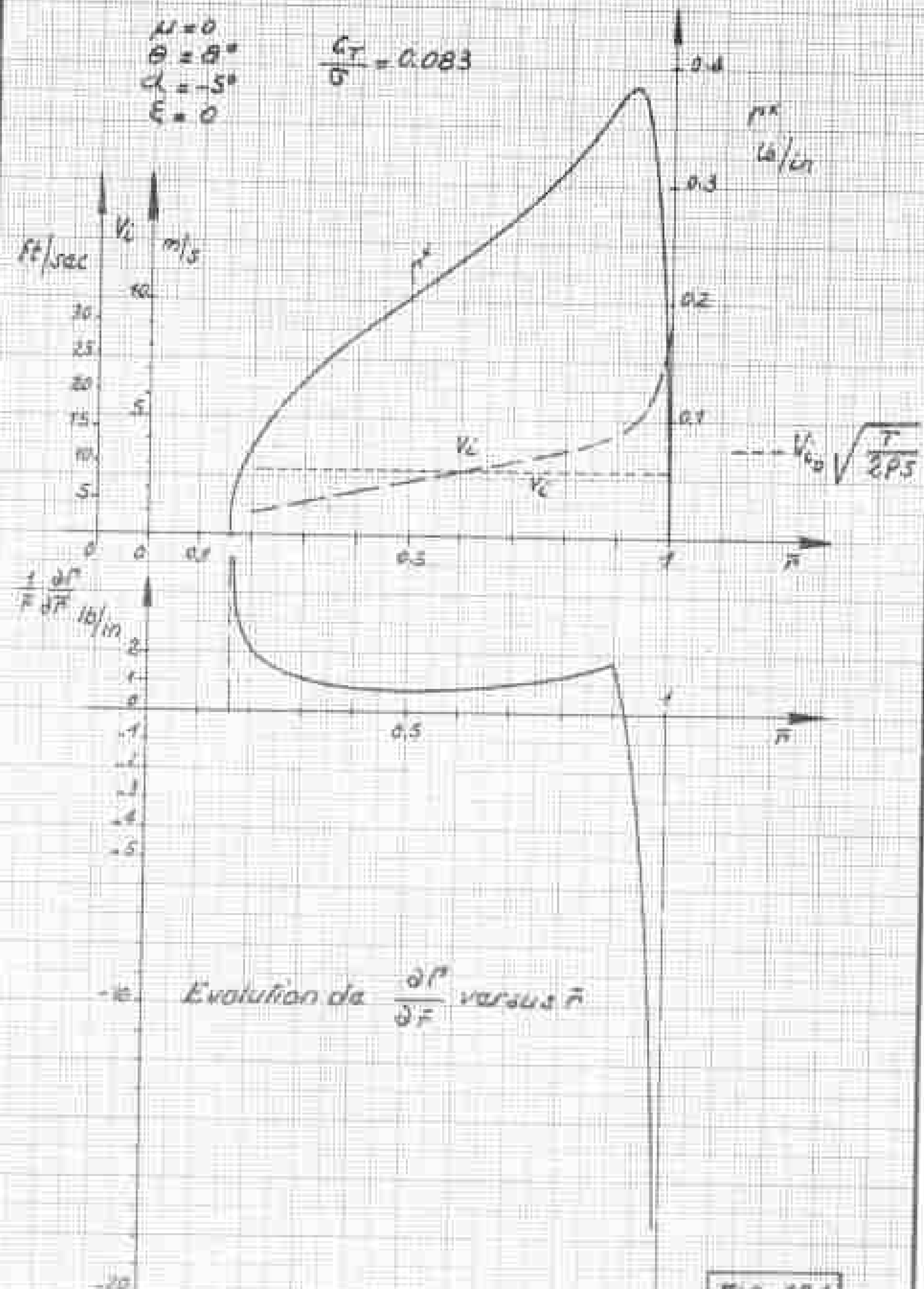

FIG. 124

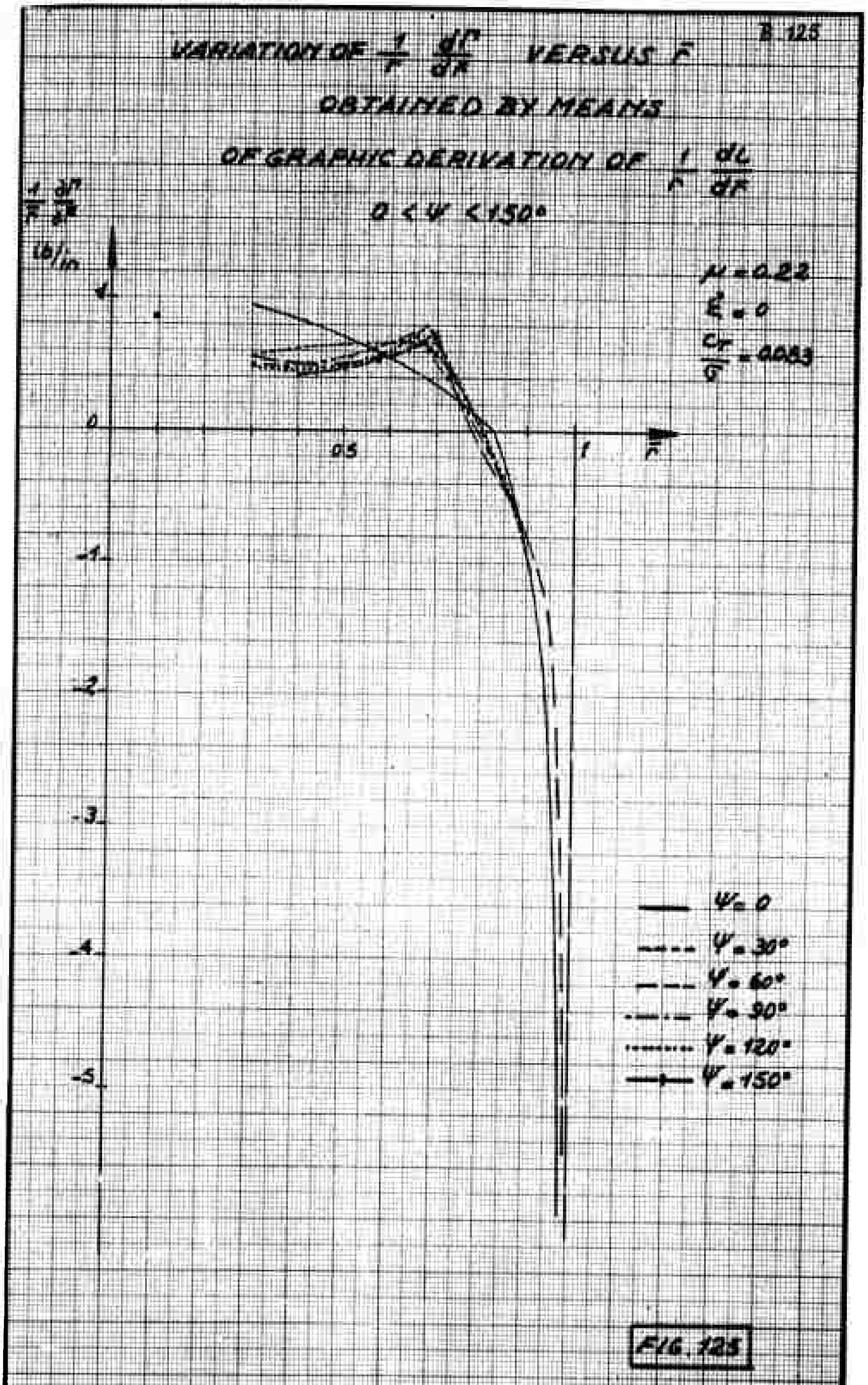
VARIATION OF $\frac{1}{\bar{r}}\frac{d\Gamma}{d\bar{r}}$ VERSUS $\bar{r}$
OBTAINED BY MEANS
OF GRAPHIC DERIVATION OF $\frac{1}{\bar{r}}\frac{dL}{d\bar{r}}$
$0 < \psi < 150°$
$\frac{1}{\bar{r}}\frac{d\Gamma}{d\bar{r}}$
lb/in
$\mu = 0.22$
$\xi = 0$
$\frac{C_T}{\sigma} = 0.083$
1
0
-1
-2
-3
-4
-5
0.5
1
$\bar{r}$
$\psi = 0$
$\psi = 30°$
$\psi = 60°$
$\psi = 90°$
$\psi = 120°$
$\psi = 150°$

FIG. 125

VARIATION OF $\frac{1}{\bar{r}}\frac{d\Gamma}{d\bar{r}}$ VERSUS $\bar{r}$

OBTAINED BY MEANS

OF GRAPHIC DERIVATION OF $\frac{1}{\bar{r}}\frac{dL}{d\bar{r}}$

$180 < \Psi < 330°$

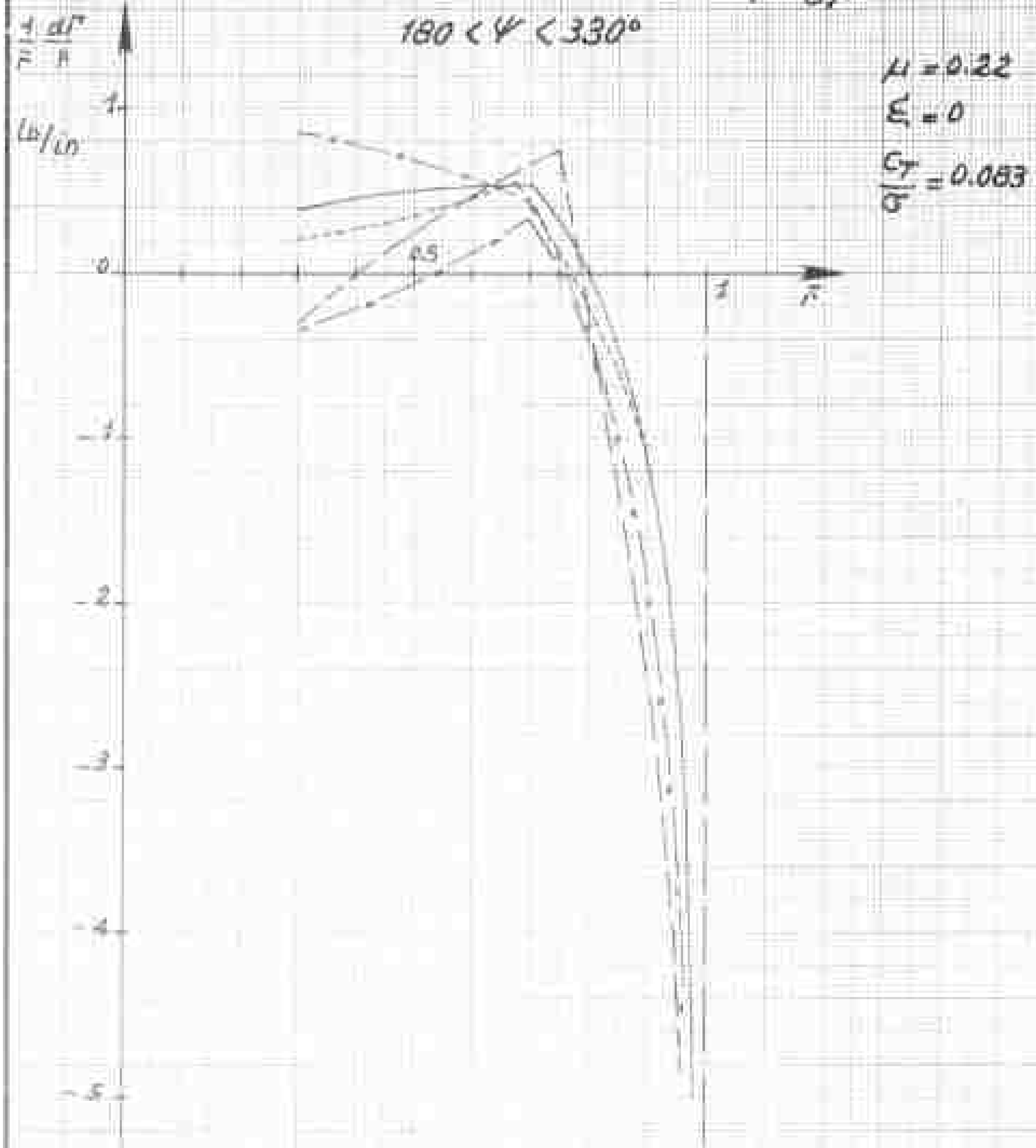

FIG.126

VARIATION OF THE INDUCED VELOCITY V_i VERSUS Ψ AND $\bar{r}$

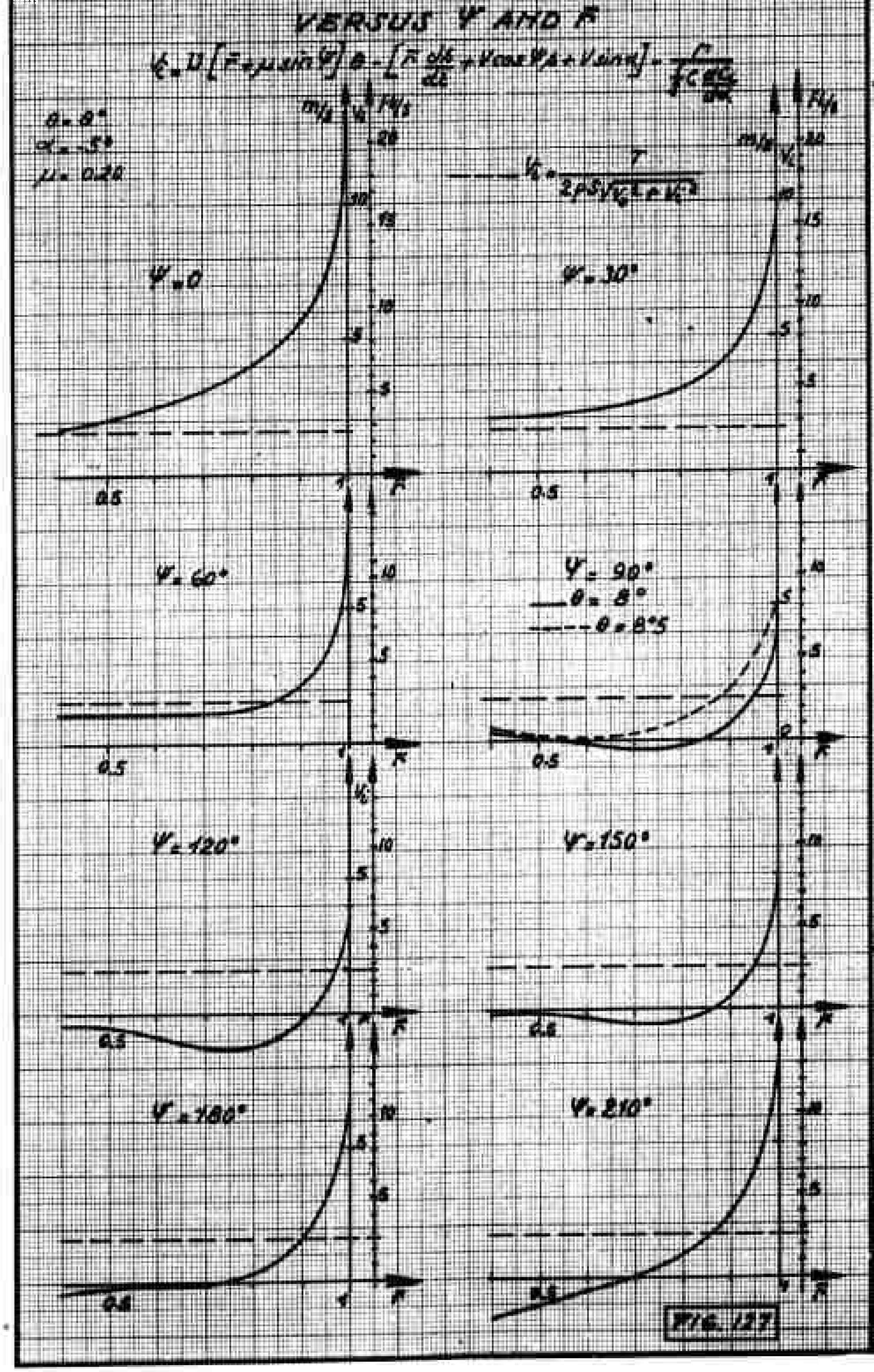

FIG. 127

VARIATION OF THE INDUCED VELOCITY V_i

VERSUS Ψ AND $\bar{r}$

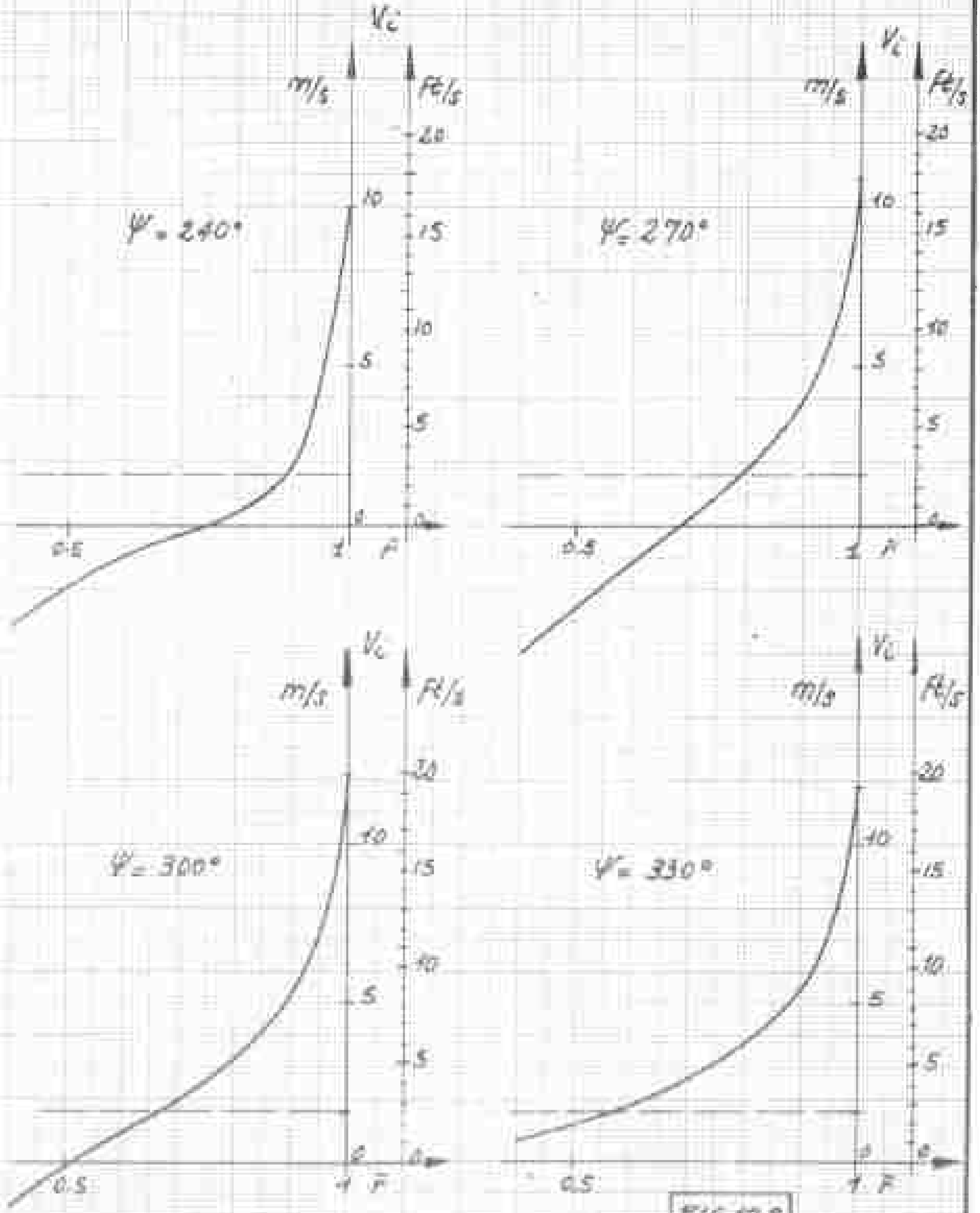

FIG. 128

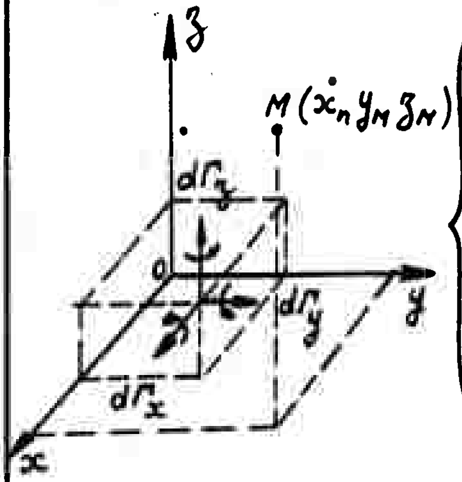

$$\begin{cases} dV_{iz} = \dfrac{1}{4\pi}\,\dfrac{d\Gamma_x(y_M - y_H) - d\Gamma_y(x_M - x_H)}{\left[(x_M - x_H)^2 + (y_M - y_H)^2 + (z_M - z_H)^2\right]^{3/2}} \\[2ex] dV_{iy} = \dfrac{1}{4\pi}\,\dfrac{d\Gamma_z(x_M - x_H) - d\Gamma_x(z_M - z_H)}{\left[(x_M - x_H)^2 + (y_M - y_H)^2 + (y_M - z_H)^2\right]^{3/2}} \\[2ex] dV_{ix} = \dfrac{1}{4\pi}\,\dfrac{d\Gamma_y(z_M - z_H) - d\Gamma_z(y_M - y}{\left[(x_M - x_H)^2 + (y_M - y_H)^2 + (z_M - z_H)^2\right]} \end{cases}$$

129 a

129 b

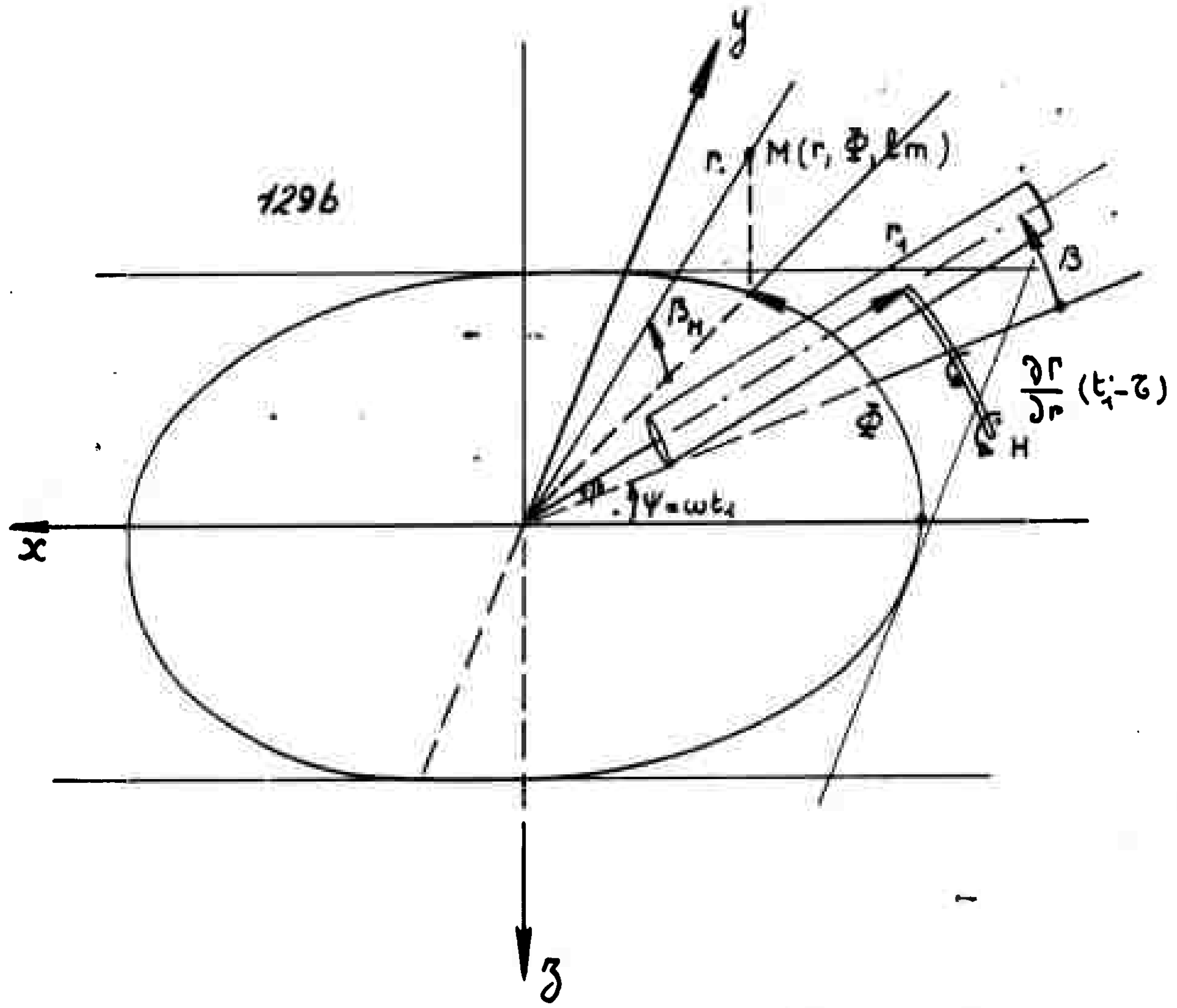

FIG. 129

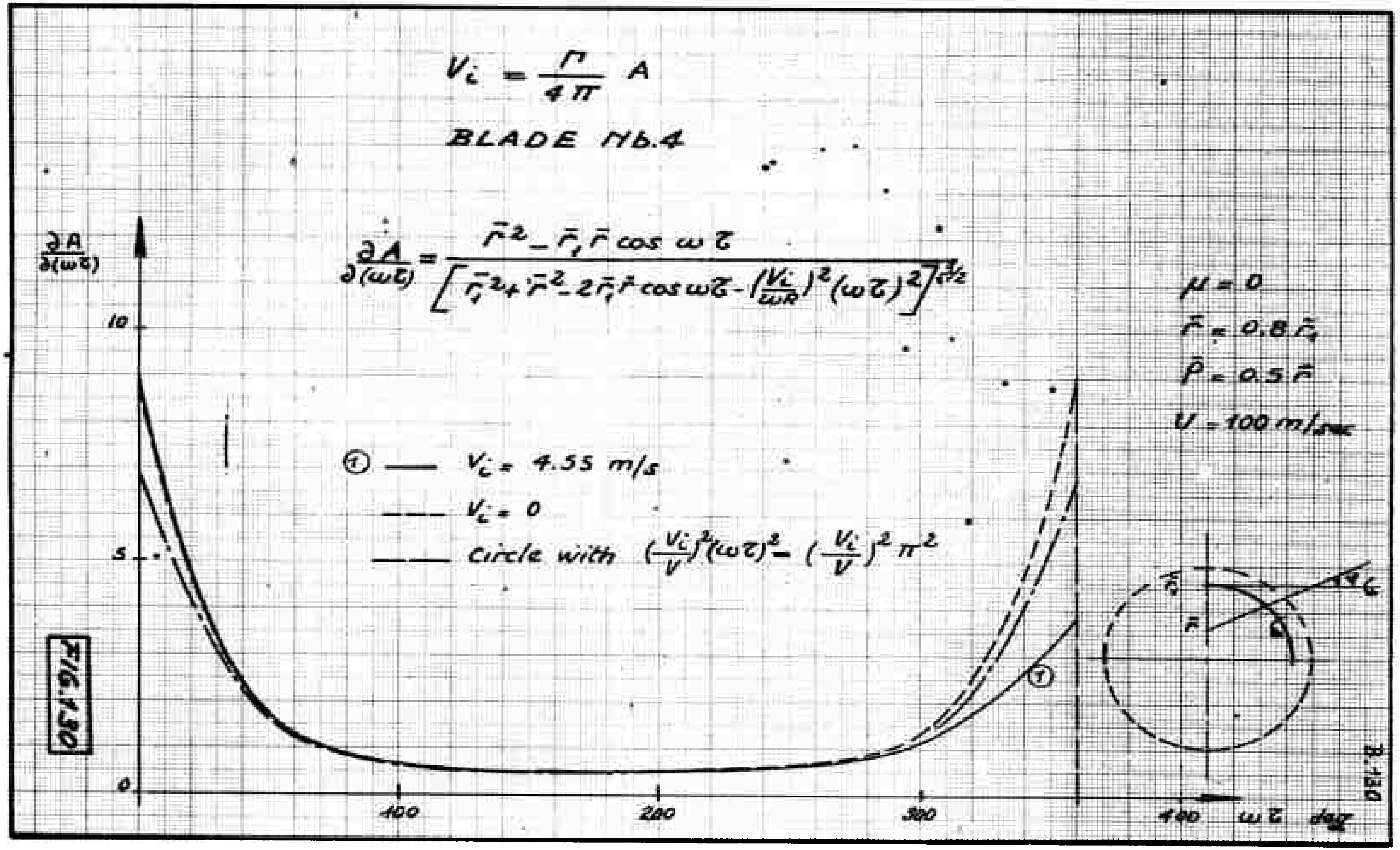

$V_i = \frac{\Gamma}{4\pi} A$
BLADE Nb.4
$\frac{\partial A}{\partial(\omega\tau)} = \frac{\bar{r}^2 - \bar{r}_i \bar{r} \cos \omega\tau}{\left[\bar{r}_i^2 + \bar{r}^2 - 2\bar{r}_i \bar{r} \cos \omega\tau - \left(\frac{V_i}{\omega R}\right)^2 (\omega\tau)^2\right]^{3/2}}$
$\mu = 0$
$\bar{r} = 0.8\,\bar{r}_i$
$\bar{\rho} = 0.5\,\bar{r}$
$U = 100$ m/sec
① $V_i = 4.55$ m/s
$V_i = 0$
circle with $\left(\frac{V_i}{V}\right)^2 (\omega\tau)^2 = \left(\frac{V_i}{V}\right)^2 \pi^2$
$\frac{\partial A}{\partial(\omega\tau)}$
10
5
0
100
200
300
400
$\omega\tau$ deg
B.130

FIG.130

B.131

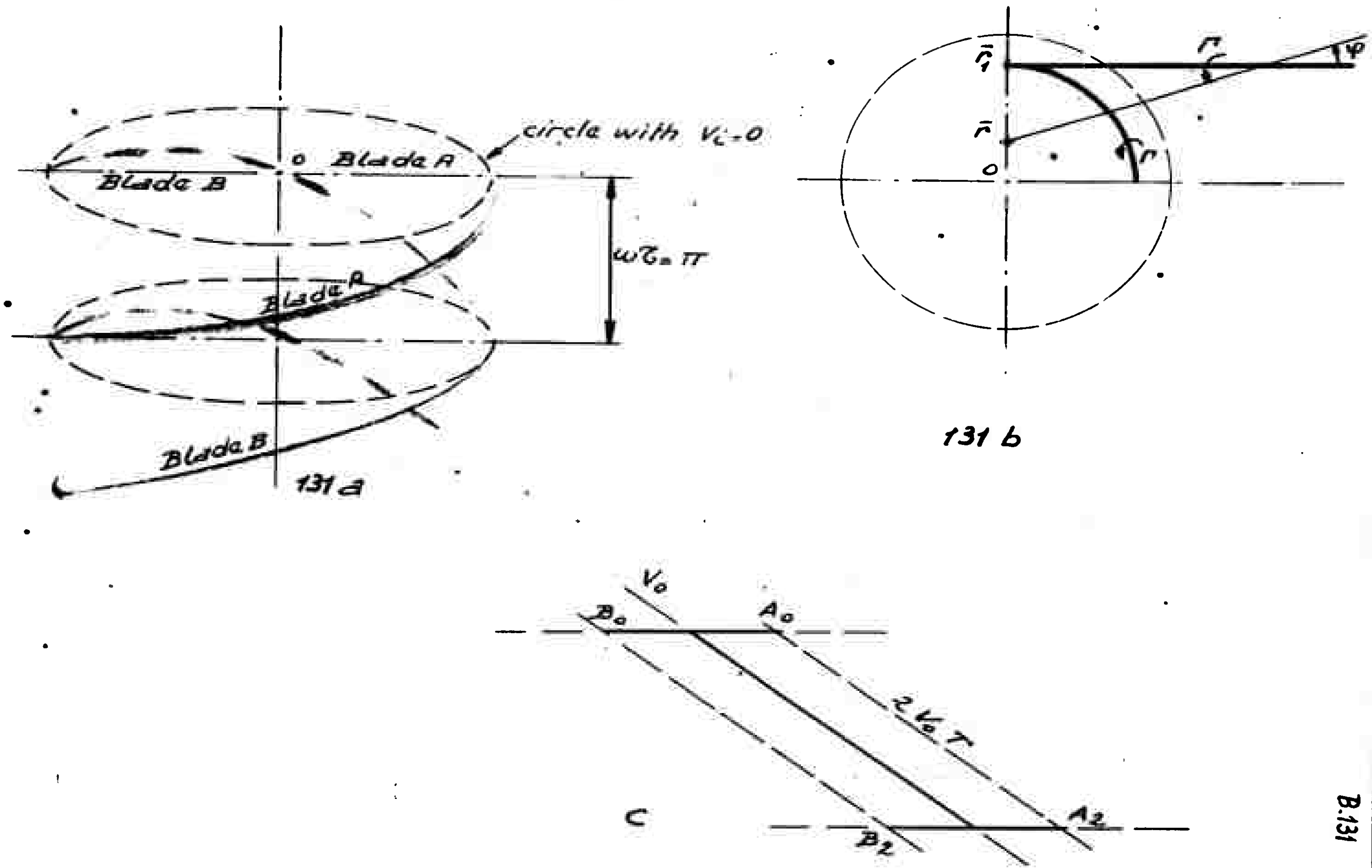
circle with $V_i = 0$
Blade A
Blade B
o
$\omega\tau = \pi$
Blade A
Blade B
131 a
$\bar{r}_1$
$\bar{r}$
0
Γ
Γ
φ
131 b
V_0
B_0
A_0
$2 V_0 T$
A_2
B_2
C

FIG. 131

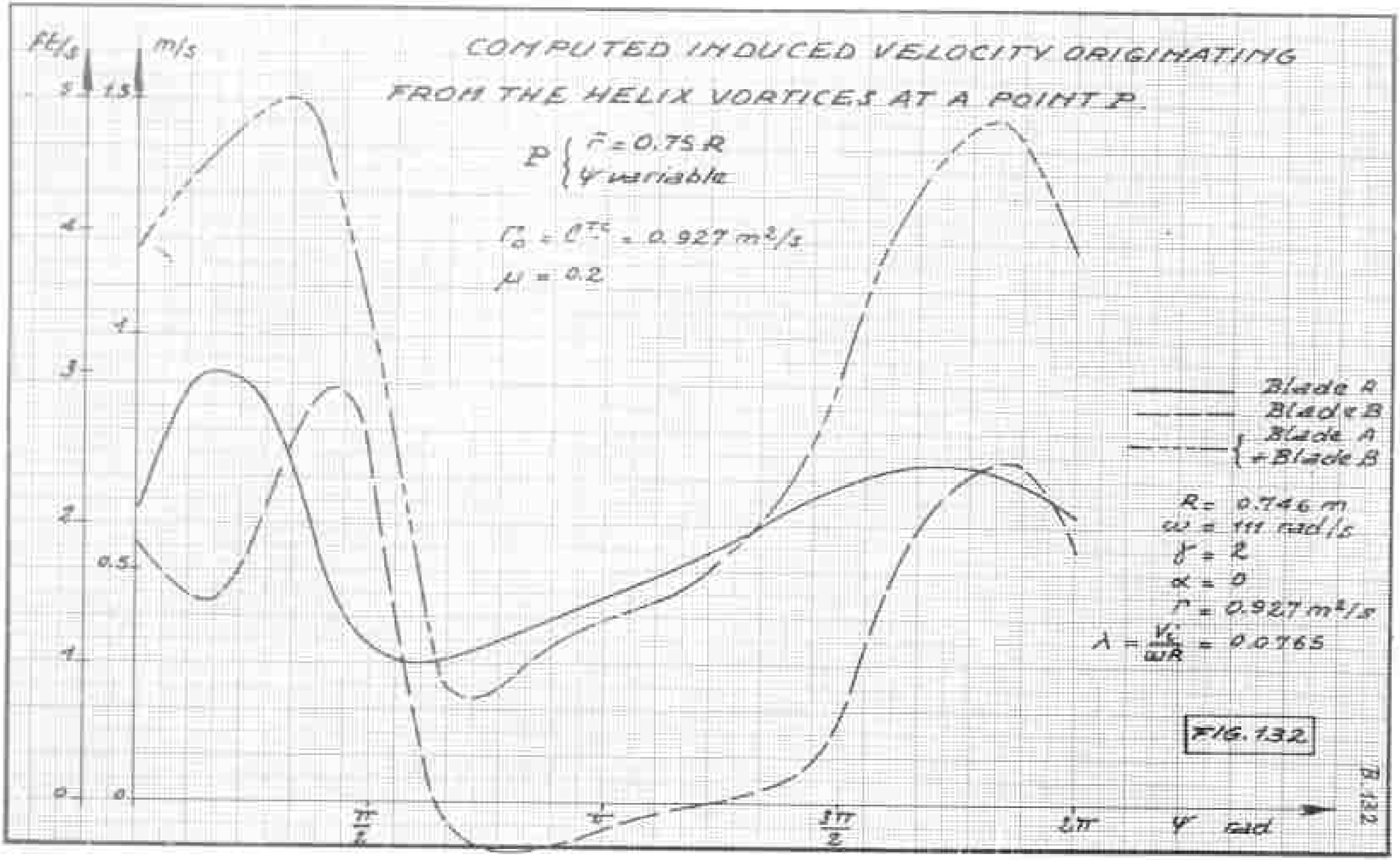

COMPUTED INDUCED VELOCITY ORIGINATING FROM THE HELIX VORTICES AT A POINT P.
P { r = 0.75 R ; ψ variable
$\Gamma_0 = C^{te} = 0.927\ m^2/s$
$\mu = 0.2$
ft/s
m/s
Blade A
Blade B
Blade A + Blade B
R = 0.746 m
ω = 111 rad/s
γ = 2
α = 0
Γ = 0.927 m²/s
$\lambda = \frac{V_i}{\omega R} = 0.0765$
ψ rad
B.132

FIG. 132

VELOCITY INDUCED BY THE HALF OF A LINE VORTEX AT POINT M :

$$V_i = \frac{\Gamma}{4\pi D}\left[1-\cos\varphi\right] = \frac{\Gamma}{4\pi D}\left[1+\frac{\xi}{\sqrt{D^2+\xi^2}}\right]$$

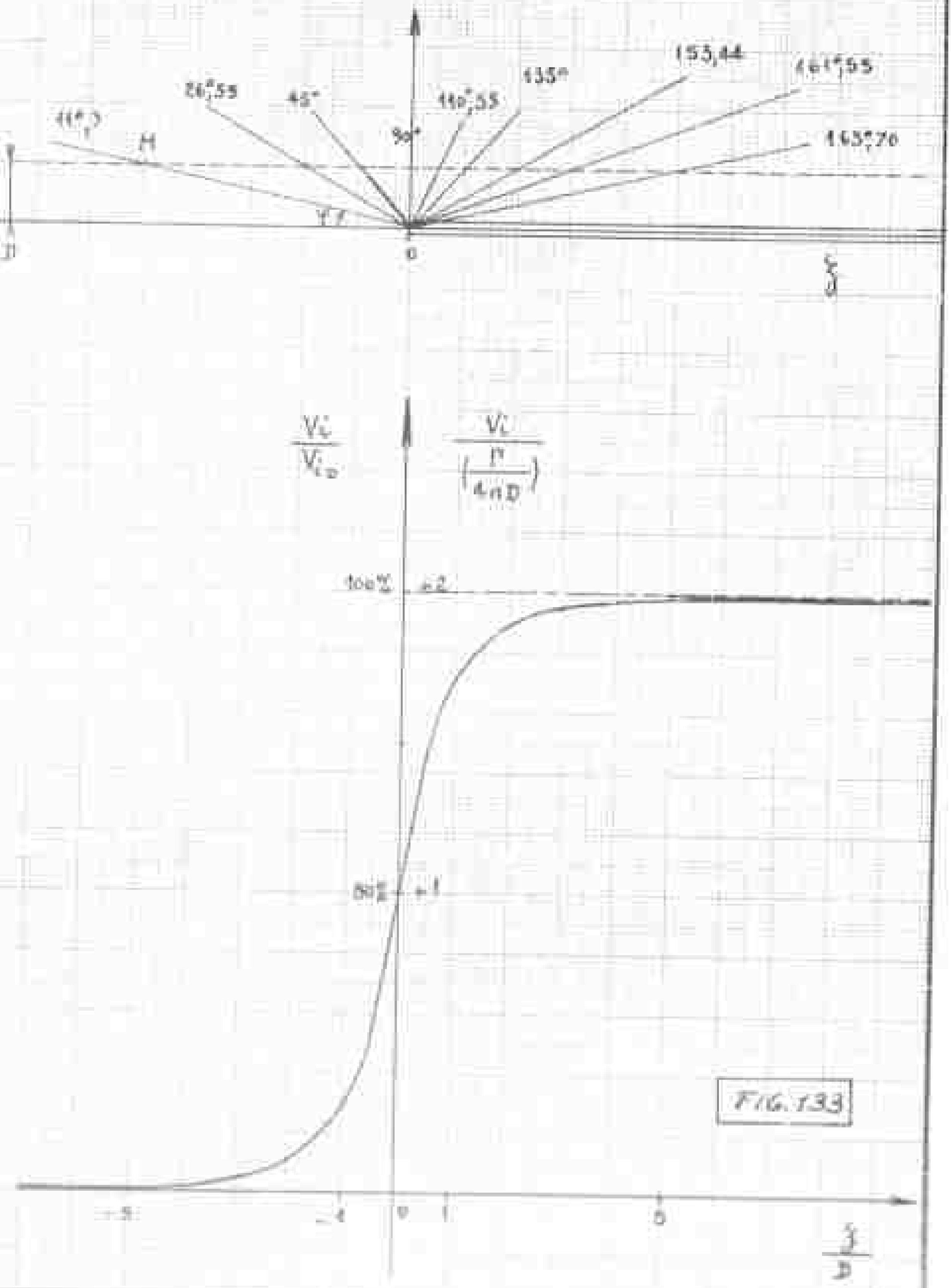

FIG. 133

FIG. 1.34

HELICOPTER ROTOR IN HOVERING CONDITIONS

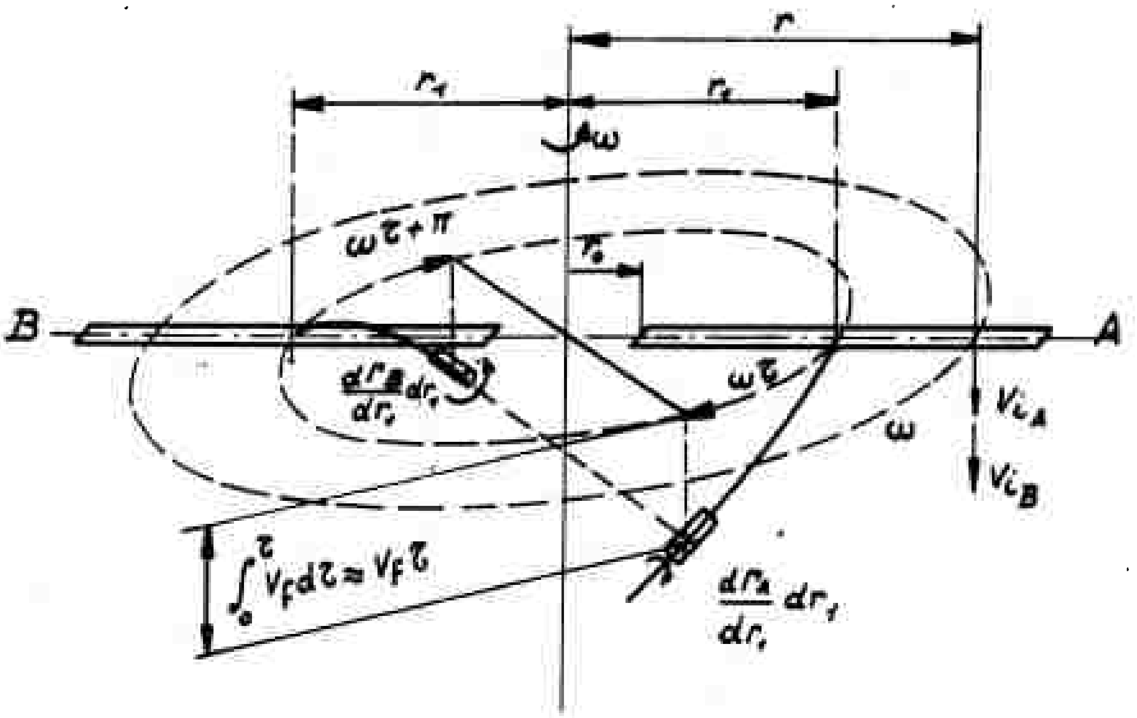

Normal induced velocities at a point r of blade A.

III 1.18

$$\begin{cases} V_{i_A}(r) = \dfrac{1}{4\pi}\displaystyle\int_{r_1=r_0}^{r=R}\int_{\omega\tau=0}^{\omega\tau\to\infty} \dfrac{\partial\Gamma_{A(r_1)}}{\partial r_1}dr_1 \; \dfrac{(r\cos\omega\tau - r_1)r_1\, d\omega\tau}{\left[r_1^2+r^2-2rr_1\cos\omega\tau+(V_f\tau)^2\right]^{3/2}} \\[2ex] V_{i_B}(r) = \dfrac{(-1)}{4\pi}\displaystyle\int_{r_1=r_0}^{r=R}\int_{\omega\tau=0}^{\omega\tau\to\infty} \dfrac{\partial\Gamma_{B(r_1)}}{\partial r_1}dr_1 \; \dfrac{(r\cos\omega\tau + r_1)r_1\, d\omega\tau}{\left[r_1^2+r^2+2rr_1+\cos\omega\tau+(V_f\tau)^2\right]^{3/2}} \end{cases}$$

<u>NUCLEUS</u>

III 1.19

$$\begin{cases} N_A(r,r_1) = \dfrac{1}{4\pi}\displaystyle\int_{\omega\tau=0}^{\omega\tau\to\infty} \dfrac{(r\cos\omega\tau - r_1)\, r_1\, d\omega\tau}{\left[r_1^2+r^2-2rr_1\cos\omega\tau+(V_f\tau)^2\right]^{3/2}} \\[2ex] N_B(r,r_1 = \dfrac{1}{4\pi}\displaystyle\int_{\omega\tau=0}^{\omega\tau\to\infty} \dfrac{(-1)(r\cos\omega\tau+r_1)r_1\, d\omega\tau}{\left[r_1^2+r^2+2rr_1\cos\omega\tau+(V_f\tau)^2\right]^{3/2}} \end{cases}$$

FIG. 134

VARIATION VERSUS φ

OF J. RABBOTT'S CIRCULATION Γ

ωR = 496 ft/sec = 151 m/sec

$C_T = 0.00518$

$\theta = 9°2$

c = 14 inches = 0.35 m

$$\Gamma = \bar{\Gamma}_0 + \frac{1 - \bar{\Gamma}_0}{2}\,(1 - \cos\varphi)$$

$\bar{\Gamma}_0 = 0.18$

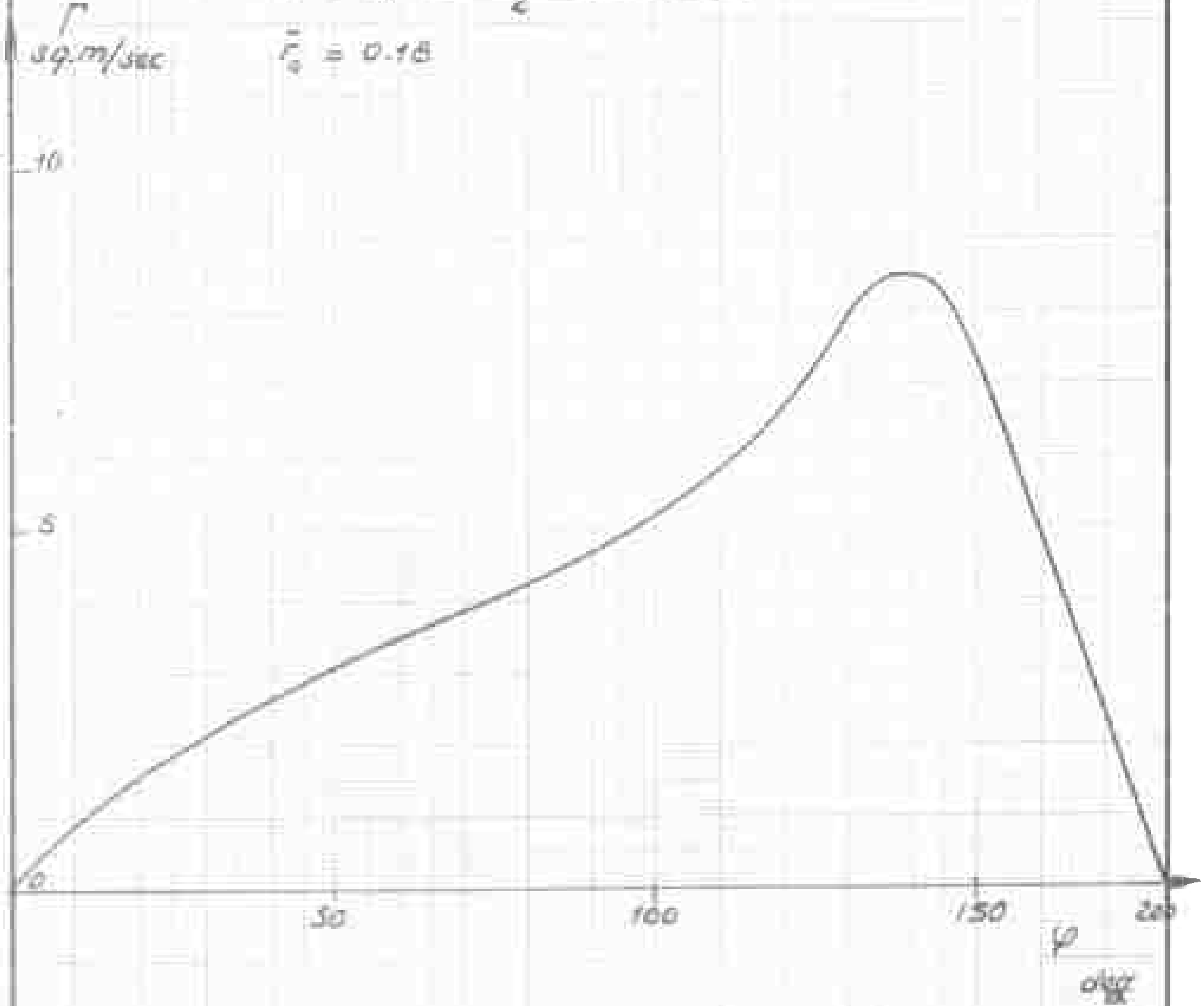

FIG. 135

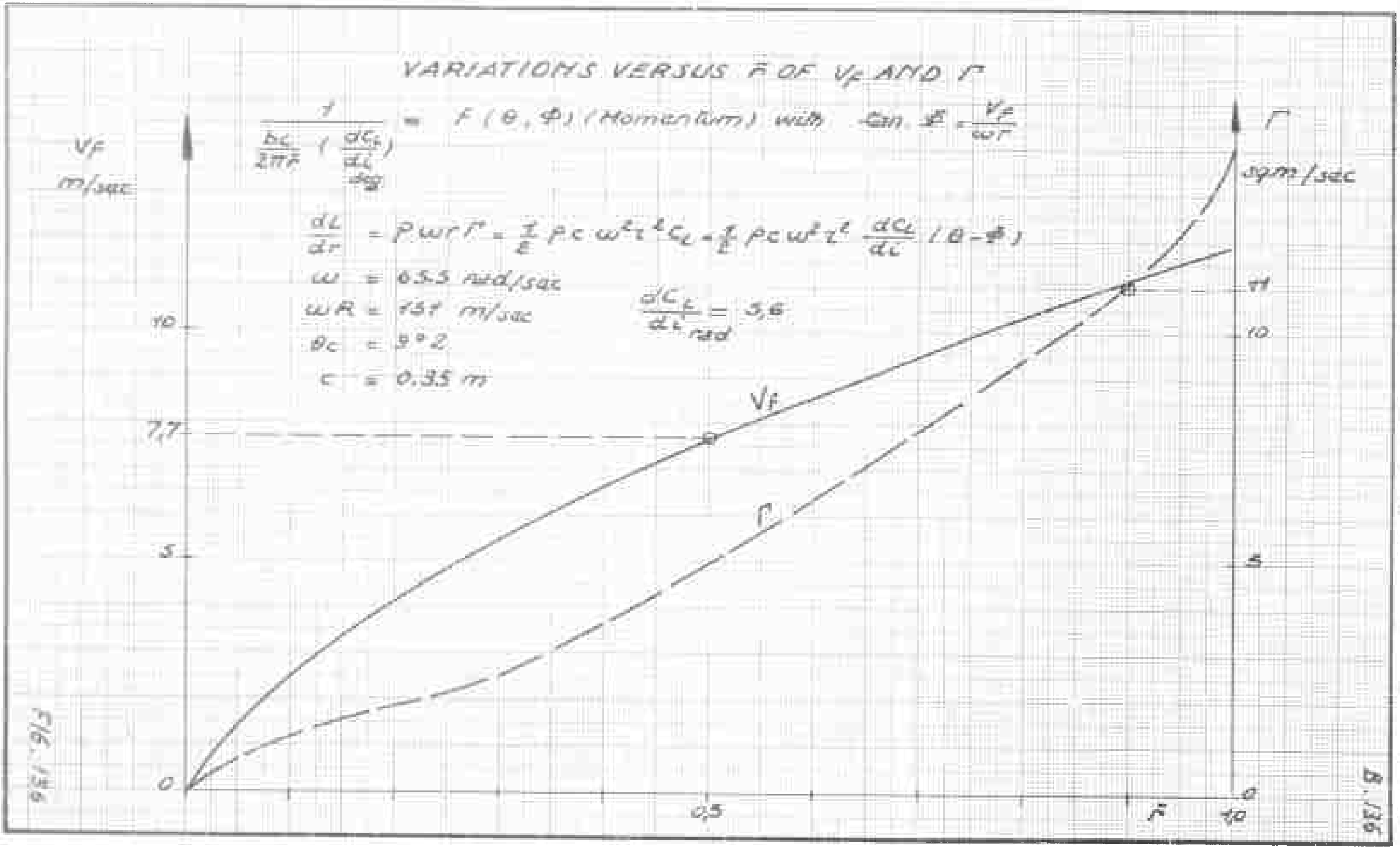

B. 136
VARIATIONS VERSUS $\bar{r}$ OF V_f AND Γ
$\frac{1}{\frac{bc}{2\pi r}\left(\frac{dC_L}{d\iota}\right)_{deg}} = F(\theta, \Phi)$ (Momentum) with $\tan\Phi = \frac{V_f}{\omega r}$
$\frac{dL}{dr} = \rho \omega r \Gamma = \frac{1}{2}\rho c \omega^2 r^2 C_L = \frac{1}{2}\rho c \omega^2 r^2 \frac{dC_L}{d\iota}(\theta - \Phi)$
$\omega = 65.5$ rad/sec
$\omega R = 151$ m/sec
$\theta_c = 9°2$
$c = 0.35$ m
$\left(\frac{dC_L}{d\iota}\right)_{rad} = 5{,}6$
V_f
m/sec
Γ
sqm/sec
0
5
7,7
10
11
0,5
1,0
$\bar{r}$
V_f
Γ

FIG. 136

RECENT VORTICES

VARIATIONS VERSUS ψ OF $\frac{V_{CA}}{\Gamma_H}$ AND $\frac{V_{CB}}{\Gamma_H}$

- Distance of V_{CB} to disc plane : $V_F \frac{T}{3}$
- Distance of V_{CA} to disc plane : $V_F\, T$

$V_F = 7.7$ m/sec — Outside circle $r = R = 2.30$ m

$T = 0.096$ sec — Inside circle $r = 0.36R = 0.827$ m

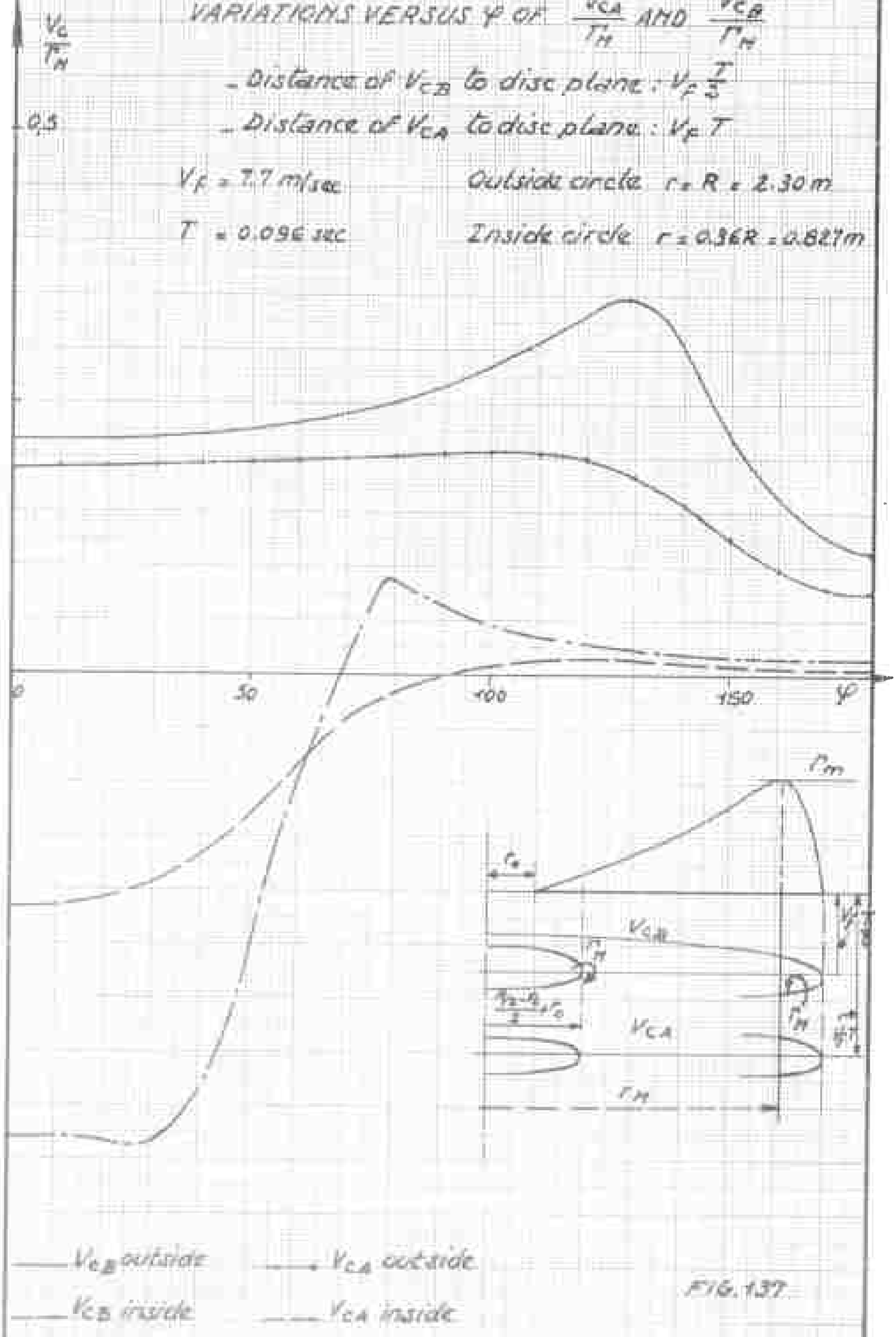

FIG. 137

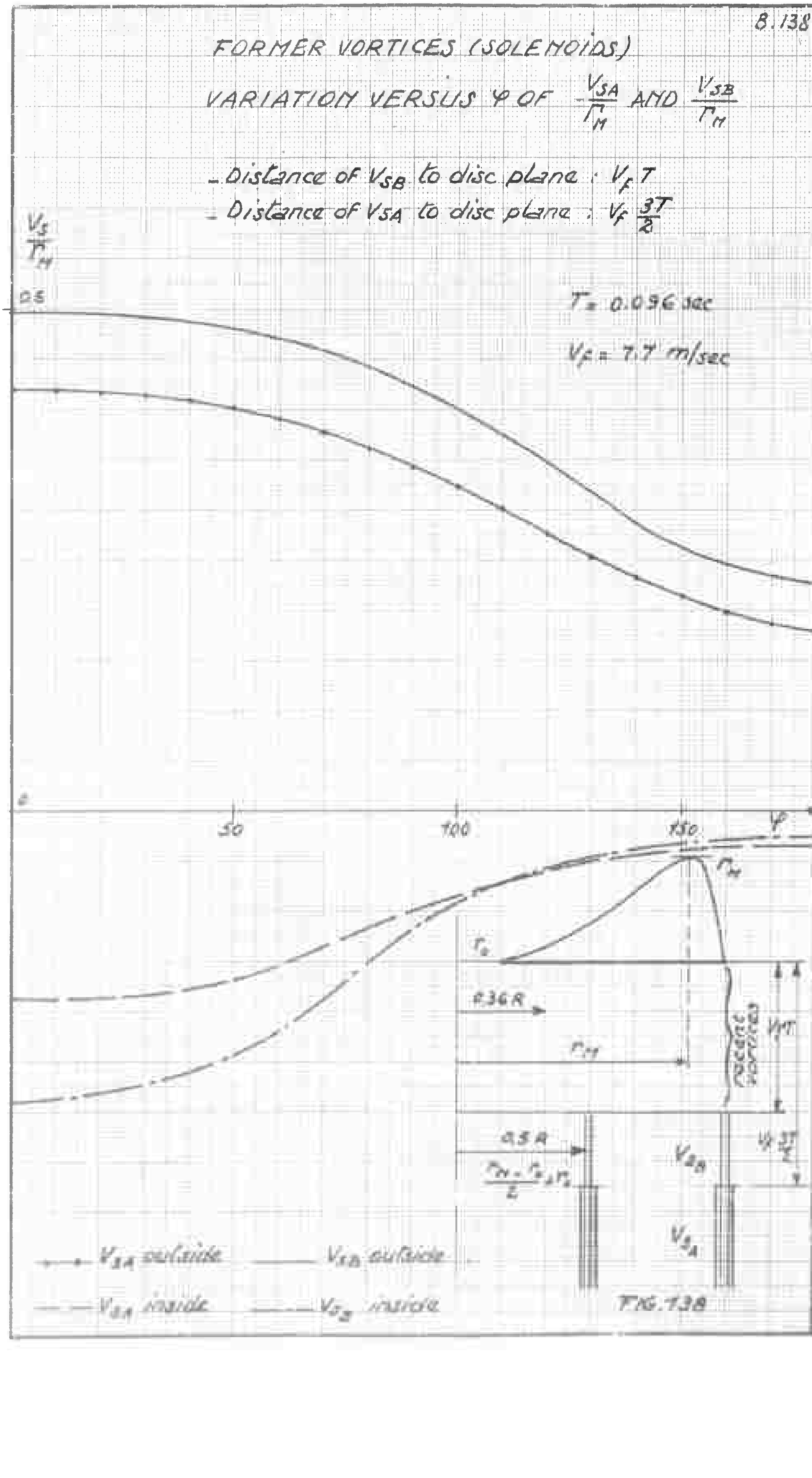
FORMER VORTICES (SOLENOIDS)
VARIATION VERSUS φ OF $\frac{V_{SA}}{\Gamma_M}$ AND $\frac{V_{SB}}{\Gamma_M}$
- Distance of V_{SB} to disc plane : $V_f T$
- Distance of V_{SA} to disc plane : $V_f \frac{3T}{2}$
$\frac{V_S}{\Gamma_M}$
0.5
$T = 0.096$ sec
$V_f = 7.7$ m/sec
0
50
100
150
φ
Γ_M
r_o
0.36 R
r_M
recent vortices
$V_f T$
0.5 R
$V_f \frac{3T}{2}$
V_{S_B}
V_{S_A}
V_{SA} outside
V_{SB} outside
V_{SA} inside
V_{SB} inside

FIG. 138

DETERMINING $\Gamma = F(\varphi)$ FUNCTION

BY SUCCESSIVE APPROXIMATIONS OF Γ_M

Initial Γ_M = 11 sq.m/sec

(momentum equation for $\bar{r}$ = 0.5)

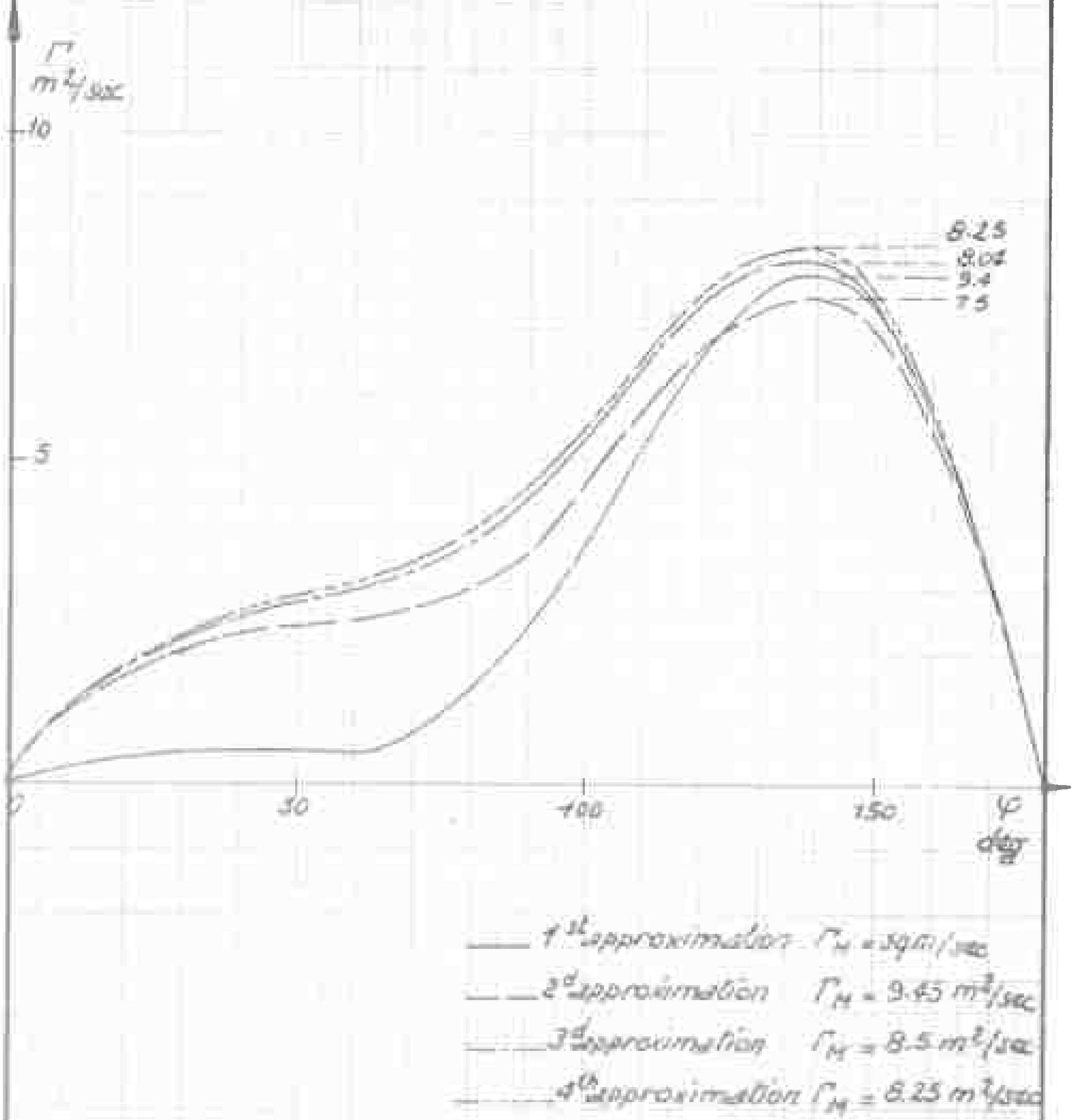

FIG. 139

COMPARISON BETWEEN J. RABBOTT'S EXPERIMENTAL CURVE, AND THEORETICAL CURVE DERIVED FROM EQUATION

$$\Gamma(\varphi) = \frac{1}{2} c \frac{dC_L}{d\alpha} \omega r \theta_c - \frac{1}{2} c \frac{dC_L}{d\alpha} \frac{2}{R-r_0} \frac{\pi}{na} \sum_{n=1}^{n=8} n \gamma_n \frac{\sin n\varphi}{\sin \varphi}$$

$$- \frac{1}{2} c \frac{dC_L}{d\alpha} \left(V_{C_A} + V_{C_B} + V_{S_A} + V_{S_B} \right)$$

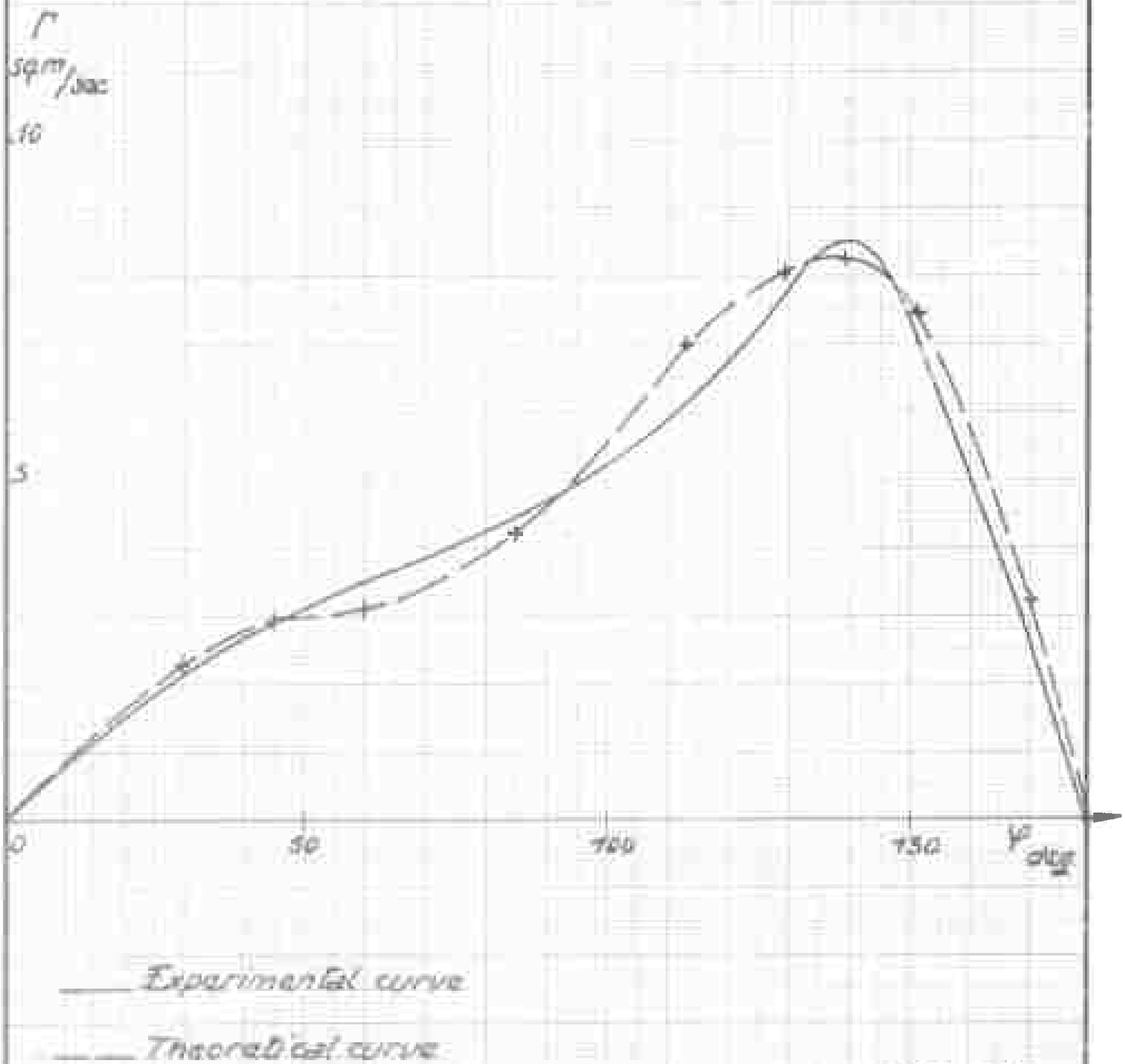

FIG. 140

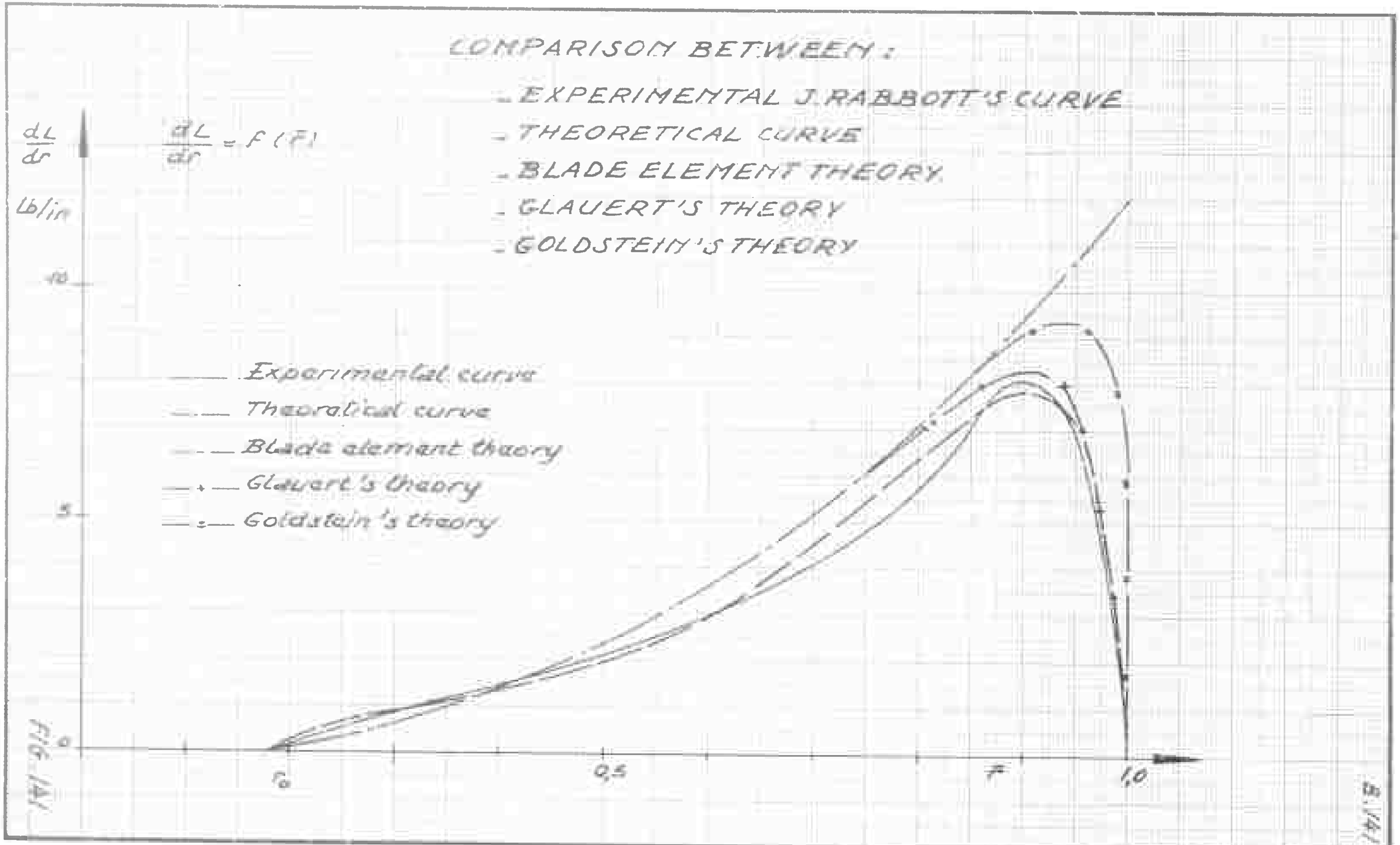
COMPARISON BETWEEN :
- EXPERIMENTAL J. RABBOTT'S CURVE
- THEORETICAL CURVE
- BLADE ELEMENT THEORY
- GLAUERT'S THEORY
- GOLDSTEIN'S THEORY
dL/dr = F (r)
dL/dr
lb/in
10
5
0
Experimental curve
Theoretical curve
Blade element theory
Glauert's theory
Goldstein's theory
r₀
0,5
r
1,0
B.141

FIG. 141

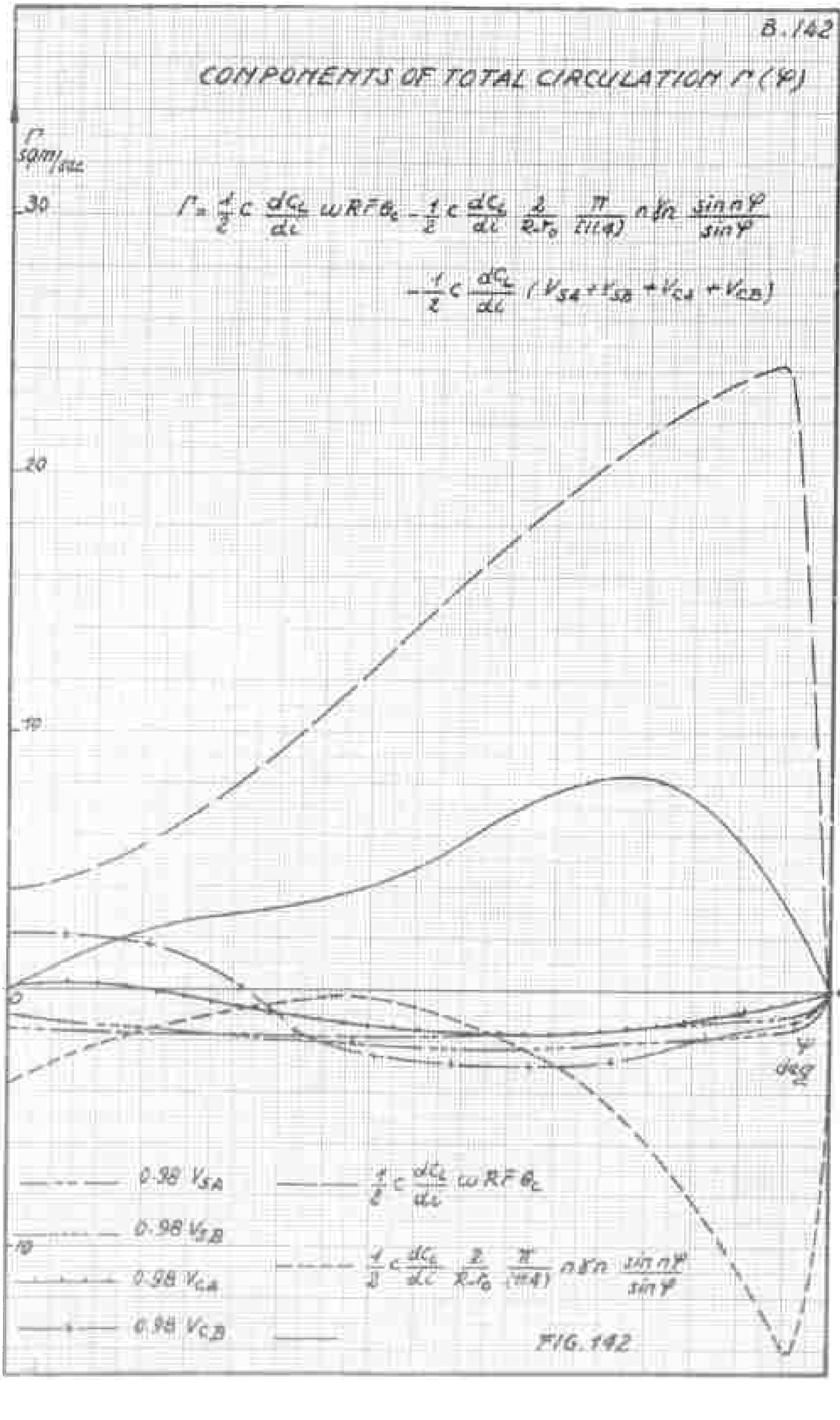
B.142
COMPONENTS OF TOTAL CIRCULATION Γ(ψ)
Γ sqm/sec
30
20
10
0
-10
ψ deg
0.98 V_SA
0.98 V_SB
0.98 V_CA
0.98 V_CB

FIG. 142

DETERMINING CIRCULATION BY TWO SIMPLIFIED METHODS AND COMPARISON WITH EXPERIMENTAL AND THEORETICAL RESULTS

FIG. 143

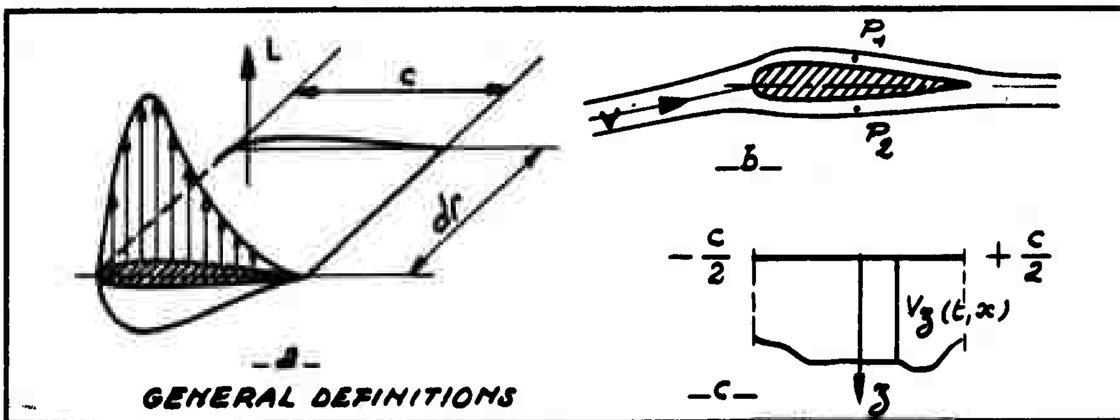

FIG. 144

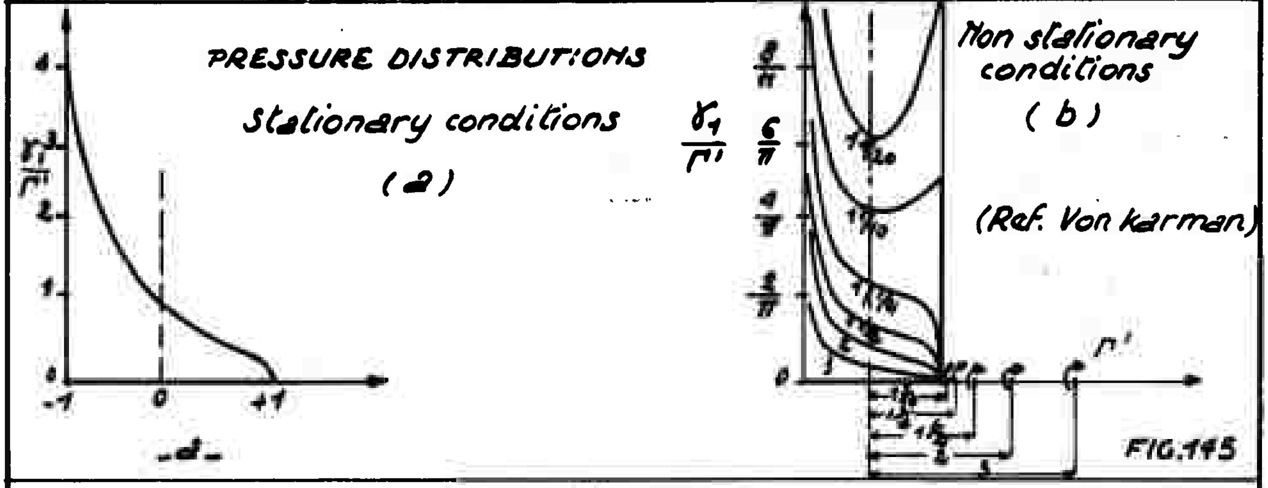

FIG. 145

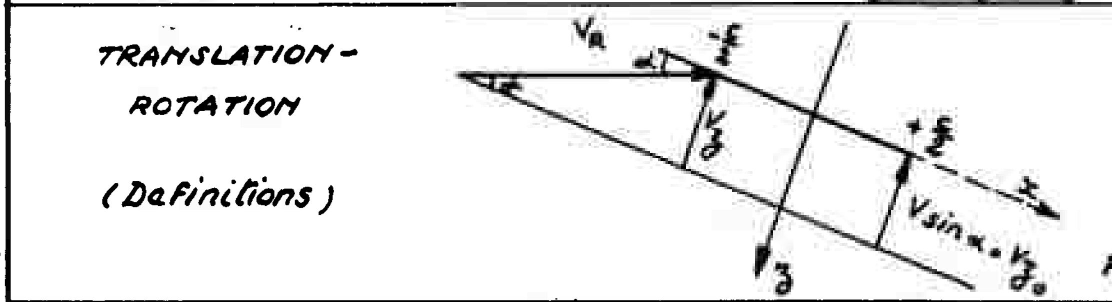

FIG. 146

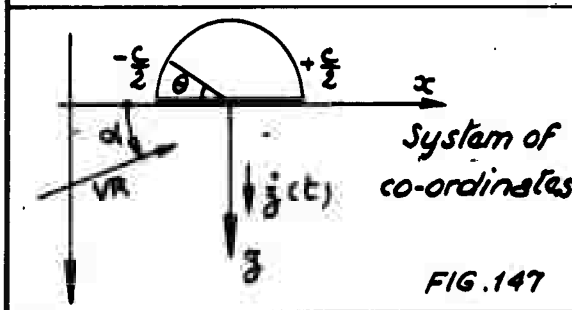

FIG. 147

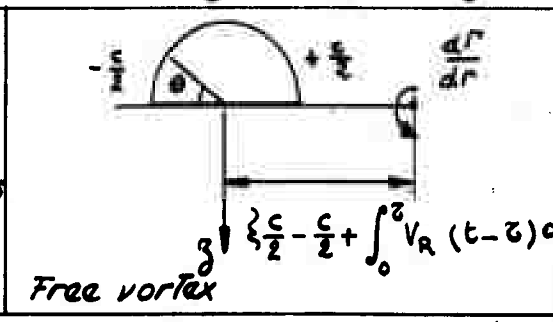

FIG. 148

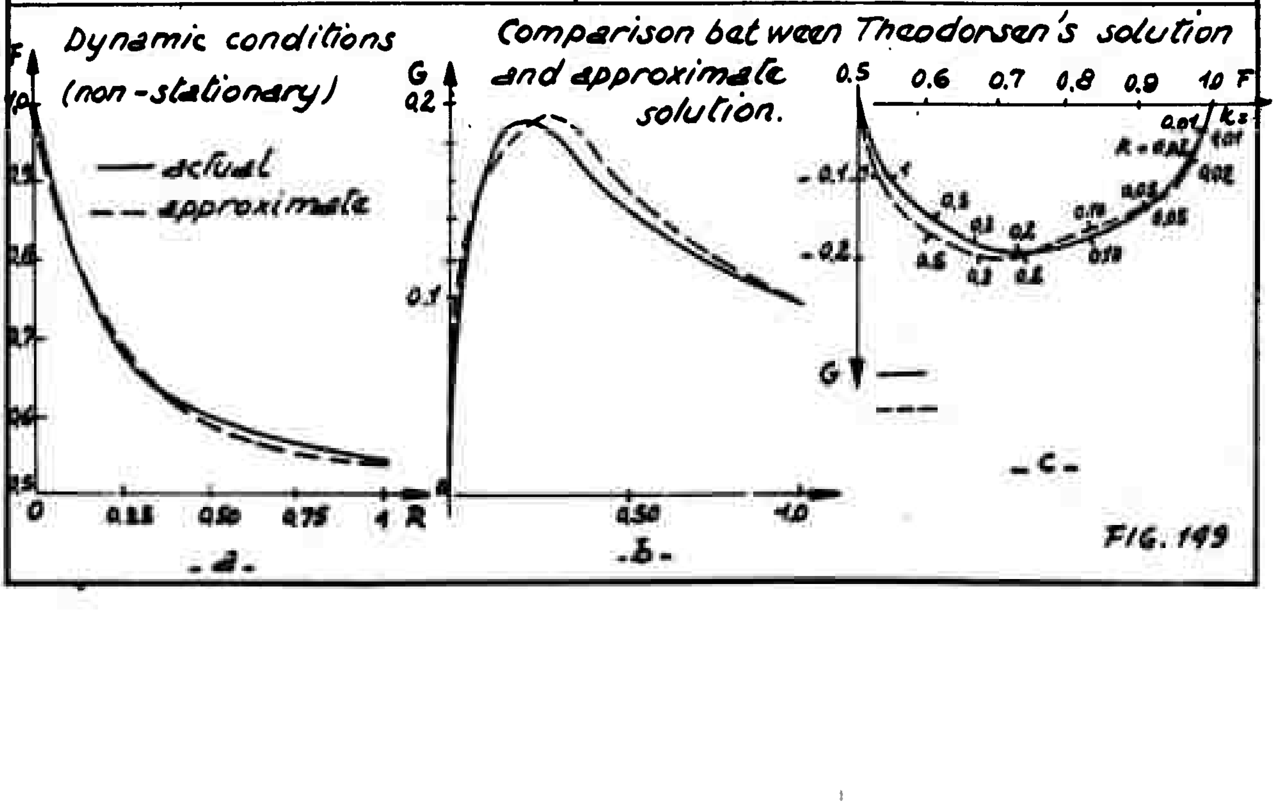

FIG. 149

UNCLASSIFIED

UNCLASSIFIED